NOTE TO USERS

Page(s) not included in the original manuscript and are unavailable from the author or university. The manuscript was scanned as received.

156

This reproduction is the best copy available.

UMI®

EXPLORING THE CONTROLS ON THE CYCLE OF CARBON IN THE ROSS SEA, ANTARCTICA

A DISSERTATION SUBMITTED TO THE DEPARTMENT OF GEOPHYSICS AND THE COMMITTEE ON GRADUATE STUDIES OF STANFORD UNIVERSITY IN PARTIAL FULFILLMENT OF THE REQUIREMENTS FOR THE DEGREE OF DOCTOR OF PHILOSOPHY

Alessandro Tagliabue

July 2006

I certify that I have read this dissertation and that, in my opinion, it is fully adequate in scope and quality as a dissertation for the degree of Doctor of Philosophy.

Kevin Arrigo (Principle Advisor)

I certify that I have read this dissertation and that, in my opinion, it is fully adequate in scope and quality as a dissertation for the degree of Doctor of Philosophy.

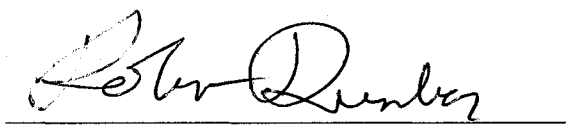

Robert Dunbar

I certify that I have read this dissertation and that, in my opinion, it is fully adequate in scope and quality as a dissertation for the degree of Doctor of Philosophy.

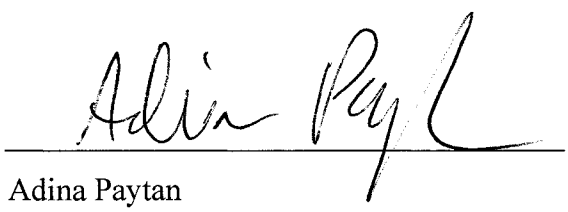

Adina Paytan

Approved for the University Committee on Graduate Studies

Abstract

Photosynthesis by surface-dwelling phytoplankton results in a disequilibrium in CO_2 with respect to the atmosphere, facilitating the oceanic uptake of atmospheric CO_2 (FCO_2). Despite only accounting for 10% of the global ocean, the Southern Ocean is responsible for 25% of global FCO_2. Moreover, this region is vulnerable to future changes in climate. The micronutrient iron is the predominant regulator of primary productivity (PP) across the modern Southern Ocean. Located on the Antarctic continental shelf, the southwestern Ross Sea (RS) sector of the Southern Ocean is typified by high rates of PP, multiple phytoplankton blooms, and spatially varying physiochemical characteristics. This makes the RS an ideal natural laboratory within which to examine the influence of biological, chemical, and physical factors on the oceanic carbon cycle. In this thesis, I use a combination of ecosystem modeling and laboratory experiments to examine the role of zooplankton grazing, phytoplankton species composition, upper ocean physics, and iron cycling on rates of PP and FCO_2.

The exaggerated boom/bust cycle that typifies RS phytoplankton blooms decouples them from zooplankton grazing resulting in low zooplankton biomass. Phytoplankton species composition controls the relative rate of macronutrient removal, while iron availability constrains the absolute magnitude of utilization. Shifts in phytoplankton species composition significantly alters both PP and FCO_2. Variability in wind speed, temperature, and sea-ice dynamics are also important in controlling FCO_2. Ultimately, PP and FCO_2 are limited by iron. Photoreduction governs the supply of bioavailable iron to the phytoplankton and is controlled by the

degree of organic complexation. As the speciation and bioavailability of iron depends on physiochemical factors, it is highly sensitive to mixed layer conditions. The efficiency with which iron fuels PP is greater in seasonal ice zones than in permanently ice-free waters. In general, shallow mixed layers are characterized by a greater supply of iron to phytoplankton via photoreduction, which is relatively insensitive to temperature. Variability in mixed layer characteristics in the geologic past or future would therefore impact the supply of bioavailable iron to the phytoplankton community, and FCO_2, independent of any change in exogenous iron inputs.

Acknowledgements

Firstly, I would like to acknowledge the continual support and advice of my Ph.D. advisor, Kevin R. Arrigo. Kevin is unstinting in this enthusiasm for science and has always provided great encouragement and perspective on my research ideas. There can be no doubt that I have learnt so much as a scientist and a person from Kevin's input. The ability of Kevin to maintain such a large research is testament to his science and people skills and I look forward to continuing our scientific relationship in the future.

Secondly, I would like to state my appreciation for all the help and assistance provided to me by Gert L. van Dijken. Gert is truly the means by which so much happens in our research group. Be it help with programming, server maintenance, ordering laboratory supplies, or assisting with experiments, Gert is always there helping to make things happen. I, for one, am highly indebted to Gert for his time, patience, good humor, and knowledge during my time at Stanford.

There have also been a number of people who have contributed to the work that I will present in the following pages that I would like to thank. At Stanford, Rochelle G. Labiosa, Andrew J. Hooper, Fabrizio Agosta, Scott D. Wankel, Cameron B. McDonald, Gaurav Misra, Paul Hagin, Matthew Mills, and Alessandro Airo have all proved to be highly effective sounding boards and their time and patience in listening to, and debating, my research is highly appreciated. Their passion for science is without doubt. I would like to thank Joseph Street and Elizabeth Morris for assistance with, as well as access to, their clean room for the laboratory experiments. Sudeshna Pabi provided useful advice on performing the remote sensing reflectance calculations in Chapter 7. Lastly, I would like to thank Robert B. Dunbar, Adina Paytan, and Dale Robinson (San Francisco State University) for forming my Ph.D. committee and their help, advice, and assistance over the years I have spent at Stanford.

Away from Stanford, Jean-Eric Tremblay (University of Laval, Canada) provided important assistance in the logistical design of my laboratory experiments. Andrew R.

Bowie (University of Tasmania, Australia) was an invaluable appraiser of my formulation of the oceanic cycle of iron presented in Chapters 5 and 6. I would also like to thank Laurent Bopp (Laboratoire des Sciences du Climat et de l'Environment, France), Tom Trull (University of Tasmania, Australia), Richard Matear (Commonwealth Scientific and Research Organization, Australia), and Mathew Maltrud (Los Alamos National Laboratory) for all their encouragement. Finally, Nicholas J. P. Owens deserves a mention for successfully firing my passions for oceanic biogeochemistry during my undergraduate studies at the University of Newcastle-upon-Tyne, United Kingdom.

Outside of science there is a numerous list of important people whose friendship I feel very lucky to have. Aside from those mentioned above, I would like to state my appreciation for Siraj Khaliq, Justin Rubinstein, Thomas Kohnstamm, Benjamin Mirus, Richard Gill, Marco Rolandi, Matthew Agard, Emma Stewart, Darren Runyon, Yasmine Wattebled and last, but by no means least, Anne Bernhardt. On longer timescales, Daniel Mayor, Alexander Newman, Leonie Robinson, Guy Connelley, Lee Plastow, Geoffrey M. Cheshire, Phillip Stubbs, Lawrence Carpenter, Claire Mahaffey, and Valerie Derolez should know why they are being mentioned. Finally, none of this would have been possible without the long-term support of my parents, Angelo and Janet, as well as my little sister, Lisa.

Table of Contents

List of Tables

Chapter 2

Chapter 3

List of Illustrations

Chapter 2

Chapter 3

Chapter 1

1.1 Introduction to the Problem

1.1.1 The role of the Southern Ocean in the global carbon cycle

Photosynthesis in oceanic surface waters by microscopic algae (phytoplankton) converts CO_2 into organic carbon [*Ruben et al.,* 1939; *Benson and Calvin,* 1947; *Calvin and Benson,* 1948] and results in a disequilibrium in CO_2 with respect to the atmosphere. As the surface dwelling phytoplankton die and sink, this carbon is effectively transported into the deep ocean for hundreds of years (the so-called biological pump). Globally, this results in the net influx of approximately 2 Pg of atmospheric CO_2 to surface waters each year [*Orr et al.,* 2001; *Takahashi et al.,* 2002; *Le Quere et al.,* 2003] to replace that which has been exported from surface waters. Herbivory by zooplankton will enhance this vertical flux by producing densely packaged fecal pellets [*Boyd and Newton,* 1995]. Bacterial remineralization in the deep ocean converts organic carbon back into CO_2 where it will remain until returned to the surface (where it can exchange with the atmosphere). Accordingly, the deep ocean is by far the largest (excluding sediments) global reservoir of carbon, accounting for around 40,000 Gt C [e.g. *Bolin et al.,* 1979].

The first and second Industrial Revolutions (between 1760 and 1830) heralded an explosion in human industrial activity and resulted in a significant anthropogenic signature on the partial pressure of atmospheric CO_2 (pCO_2). The increased burning of fossil fuels during industrial processes (primarily coal, but also petroleum and natural

gas during the mid to late 20th century) increased atmospheric pCO_2 from a pre-industrial value of 280 μatm to > 365 μatm by 1995 [*Petit et al.,* 1999; *Takahashi et al.,* 2002]. Rising CO_2 levels have resulted in increased atmospheric temperatures (due to increased radiative heating), also warming the ocean [REF]. Moreover, increasing ocean uptake of anthropogenic CO_2 will also cause fundamental changes in the carbonate chemistry (e.g. aragonite and calcite saturation states) and the *p*H of the ocean [*Bolin and Eriksson,* 1959; *Broecker et al.,* 1971; *Caldeira and Wickett,* 2003; 2005]. Model inversion studies have shown that the ocean has taken up around 50% of the anthropogenic pCO_2 emitted over the period 1880-1994 [*Sabine et al.,* 2004]. Unfortunately, it is not possible to measure the air-sea CO_2 flux directly and parameterization schemes based on solubility, wind speed, and the air-sea CO_2 disequilibrium are typically used [e.g. *Liss and Mervilat,* 1986; *Wanninkhof,* 1992].

The Southern Ocean is an important regulator of both atmospheric CO_2 and global climate [*Sarmiento et al.,* 1988; *Caldeira and Duffy,* 2000], as well as low latitude productivity [*Sarmeinto et al.,* 2004]. Polar waters are also proposed to be heavily impacted by any future changes in climate, such as increased sea ice melting or precipitation [*Sarmiento et al.,* 1998]. The recent analysis of *Takahashi et al.* [2002] found that waters south of 50 °S were responsible for 25% of the global air-sea CO_2 flux, despite only accounting for approximately 10% of the total oceanic area. Furthermore, the high rates of deepwater formation, driven by the extensive sea ice production [16 x 10^6 km^2 of ice annually, *Zwally et al.,* 1979], facilitate the direct exchange of climatically active gases (such as CO_2) between the atmosphere and the deep ocean [*Caldiera and Duffy,* 2000]. The cycle of sea ice is also important in

controlling surface albedo, providing a physical barrier to gas exchange, and impacting the physical structure of surface waters. Finally, the circumpolar distribution of the Southern Ocean allows Antarctic deep waters to exchange with all major ocean basins.

1.1.2 The importance of iron in governing Southern Ocean biogeochemistry

Net primary production (the amount of CO_2 converted into organic C minus that respired, NPP) in most of the global ocean is typically limited by the macronutrients nitrogen (N) and phosphorous (P), over different timescales [*Tyrell,* 1999]. However, the Southern Ocean is characterized by high, year round inventories of both nitrate and phosphate, yet low phytoplankton biomass (e.g. high Nutrient low chlorophyll, HNLC). It is now clear that the supply of iron (Fe) exerts a strong control upon NPP across the Southern Ocean where Fe inputs are low [*Hart,* 1934; *Martin et al.,* 1990; *De Baar et al.,* 1995; *Boyd et al.,* 2000; *Gervais et al.,* 2002; *Coale et al.,* 2004]. Other Fe limited HNLC regions are the Sub Arctic Pacific [*Tsuda et al.,* 2003; *Boyd et al.,* 2004] and the Equatorial Pacific [*Coale et al.,* 1996], but the Southern Ocean is by far the largest, both in terms of geographic area and inventory of unused macronutrients [*Conkright et al.,* 1994]. . As well as controlling modern NPP in HNLC regions, it is proposed that glacial-interglacial fluctuations in the supply of Fe to the Southern Ocean could be responsible for the change in atmospheric CO_2 observed from ice cores [*Petit et al.,* 1999], by alleviating Fe limitation [*Martin,* 1990; *Peng and Broecker,* 1991; *Bopp et al.,* 2003].

The trace metal Fe is essential to marine phytoplankton. Fe is a necessary component of photosystems I and II, photosynthetic proteins involved in the electron transport chain, as well as enzymes necessary for the intracellular reduction of nitrate, [e.g. *Raven,* 1988; 1990]. That said, assessing the role of Fe in structuring ecosystems and governing the regional C cycle is not straightforward [e.g. *Bowie et al.,* 2001]. Fe is a divalent trace metal and undergoes a complex cycle in seawater [*Morel and Price,* 2003; *Wells et al.,* 1995]. The free inorganic Fe pool is made up of Fe(II) and Fe(III), while Fe(III) can also be bound to a variety of organic ligands (with different photolability and bioavailability characteristics) and converted into solid inorganic particles via precipitation. Accordingly, phase transitions in the seawater Fe cycle are governed by a suite of physio-chemical processes, as well as by biological activity. Despite the potential for ecosystem models to better resolve the role of Fe in the Southern Ocean, the complexity of the seawater Fe cycle has resulted in relatively simplistic treatments of the Fe cycle within major ecosystem models [e.g. *Lancelot et al.* 2000; *Moore et al.,* 2002; *Aumont et al.,* 2003; *Parekh et al.,* 2003; *Arrigo et al.,* 2003a].

1.1.3 The southwestern Ross Sea

The southwestern Ross Sea is most productive region of the Southern Ocean and is an ideal natural laboratory within which to explore the variety of controls on the cycle of C. The British explorer James Clark Ross first discovered the Ross Sea (Figure 1) in 1841 [*Ross,* 1847] and phytoplankton blooms here are amongst the largest observed in the Southern Ocean [*Arrigo and McClain,* 1994; *Arrigo and Van Dijken,* 2003a].

Rates of NPP are typically > 120 gC m^{-2} yr^{-1} [*Arrigo and Van Dijken,* 2004] and result in some of the most CO_2 depleted surface waters in world [*Takahashi et al.,* 2002]. The large Ross Sea polynya (RSP) forms north of the Ross Ice Shelf, primarily by the northward advection of sea ice in October and supports a large bloom of the colonial prymnesiophyte *Phaeocystis antarctica* by late November/early December [*Arrigo and McClain,* 1994; *Smith and Gordon,* 1997; *Arrigo et al.,* 2000; *Smith et al.,* 2000; *Arrigo and Van Dijken,* 2004]. The RSP is characterized by relatively little sea ice melting and surface waters are only weakly stratified [*Arrigo et al.,* 2000]. Moreover, upwelling of warm circumpolar deep water (CDW) raises temperatures to between 1 and 2 °C during the austral summer [*Jacobs and Guilivi,* 1999]. In contrast, once the katabatic winds slacken in the late austral spring [*Arrigo et al.,* 1998a], the marginal ice zone (MIZ) and the persistent Terra Nova Bay polynya (TNBP) are strongly stratified by sea ice melting facilitates large blooms of diatoms (typically *Fragilariopsis and Nitzschia* spp.) by late January [*Arrigo et al.,* 2000; *Arrigo and Van Dijken,* 2004]. Phytoplankton species composition is thought to be controlled by the degree of stratification rather than Fe [*Arrigo et al.,* 2003a].

Distinct biogeochemical signatures and food web structure characterize the two discrete phytoplankton assemblages in the Ross Sea. For example, water column measurements over multiple field seasons have shown that each taxon exhibits unique nutrient uptake ratios, with *P. antarctica* taking up more than twice as much CO_2 per mole PO_4 removed than diatoms. This results in C/P uptake ratios (mol:mol) of approximately 133 and 63 for *P. antarctica* and diatoms, respectively [*Arrigo et al.,* 2002a. *P. antarctica* is also characterized by an NO_3/PO_4 uptake ratio (20 mol:mol)

that is greater than both the resident diatoms (<10 mol:mol) and the canonical Redfield ratio of 16:1 [*Redfield,* 1934; *Redfield et al.,* 1963]. An important inference from these unique N/P ratios is that in the absence of limitation by another nutrient (such as light or Fe), *P. antarctica* and diatoms should be driven to limitation by NO_3 and PO_4, respectively. High rates of sea ice melting in the TNBP and other MIZ regions, result in elevated Fe concentrations [*Sedwick and Di Tullio,* 1997; *Sedwick et al.,* 2000; *Coale et al.,* 2005], although ice derived Fe only appears to support around 10% of total NPP [*Edwards and Sedwick,* 2001]. Moreover, observations of phytoplankton degredation products [*Di Tullio and Smith,* 1996; *Goffart et al.,* 2000] and sediment trap data [*Dunbar et al.,* 1998; *Gowing et al.,* 2001] suggest that diatoms support a larger zooplankton abundance than do *P. antarctica*, which will impact the efficiency with which C is exported to depth.

1.2 Statement of problem and overall approach

Thus far the interactive roles of physics (e.g., sea ice, winds), chemistry (e.g., Fe cycling) and biology (e.g., grazing, phytoplankton species composition, non-Redfield nutrient stoichiometry) in regulating the cycle of C in the Ross Sea and other Southern Ocean regions are not well understood. For example, the impact of non-Redfield nutrient utilization and abiotic variability in Fe supply on NPP, as well as the interaction between biological activity and physical processes in dictating the air-sea CO_2 flux are poorly constrained.

To this end, mechanistic ecosystem models can be useful tools to examine how variability in a multitude of interactive processes act in concert to govern

biogeochemical cycles. The Coupled Ice-Atmosphere-Ocean (CIAO) model of the southwestern Ross Sea [*Arrigo et al.*, 2003a] is an ideal platform upon which to base such investigations. By improving the capacity of an ecosystem model to simulate the necessary tracers (PO_4, CO_2, carbonate system, O_2), and species specific biogeochemistry (non-Redfield nutrient stoichiometry), as well as including the physio-chemical processes pertinent to the cycle of Fe, I can fill a major gap in our knowledge of how variability in phytoplankton species composition, water column structure, and Fe supply interact to control the cycle of C in an Fe-limited, environmentally heterogeneous, and climatically significant region of the global ocean.

I propose that the processes controlling the cycle of C in the Ross Sea will be relevant to the greater Southern Ocean, where similar phytoplankton, as well as biogeochemical and physical processes, are found. The resident phytoplankton of the Ross Sea are also major components of phytoplankton blooms in the Antarctic Peninsula [*Kang et al.*, 2001], Prydz Bay [*Wright et al.*, 1996], Bransfield Straight [*Kang and Lee*, 1995], Mertz Glacier polynya [*Green and Sambrotto*, 2002], and East Antarctica [*Robinson et al.*, 1999]. All in situ Fe fertilization studies conducted in the Southern Ocean thus far have also elicited responses by the major components of Ross Sea phytoplankton assemblage [*De Baar et al.*, 2005 and references therein]. Furthermore, the heterogeneity in stratification between the RSP and MIZ regions such as the TNBP are useful analogues of the SIZ and POOZ regions of the greater Southern Ocean.

1.3 Synopsis

In Chapter 2, I provide a complete description of the CIAO ecosystem model, including all model equations added during this study. I include all new state variables, as well a new mechanistic Fe supply model. The remainder of this dissertation is written such that each individual chapter can be considered to be a stand-alone manuscript. In Chapter 3, I use CIAO to investigate the role of zooplankton grazing in the Ross Sea C cycle. Specifically, I provide an explanation as to why zooplankton biomass is anomalously low in the highly productive Ross Sea as well as why grazing rates are higher in regions dominated by diatoms. In Chapter 4, I explore carbon and nutrient biogeochemistry on local and regional spatial scales. I focus on examining variability in NPP and air-sea CO_2 exchange, as well as the significance of phytoplankton taxonomic composition and non-Redfield nutrient stoichiometry. The improved CIAO model is used to examine the increase in CO_2 uptake from the atmosphere under a complete and continual Fe fertilization (i.e. an upper limit). I then use the results obtained from the Ross Sea to examine the potential impact of a 100% efficient Fe fertilization of the entire Southern Ocean and put this into the context of fossil fuel emissions of CO_2. In Chapter 5, I describe a new complex Fe supply model that I parameterized for use within CIAO. This model includes all major aspects of Fe chemistry in seawater, and contains sufficient flexibility in its parameterizations for it to be used to examine the impact of stratification on Fe cycling and thus NPP across the diverse environmental conditions present in the Ross Sea. I show that variability in the physical structure of the water column can impact NPP independent of any change in Fe supply. In Chapter 6, I

decouple my Fe supply model from CIAO and examine the sensitivity of both abiotic and biotic Fe cycling to variability in mixed layer irradiance and temperature. Of particular interest was the role of photochemistry and the photolability of organically complexed Fe in dictating bioavailable Fe concentrations These results are used to draw broader conclusions as to the processes governing both the supply of Fe to phytoplankton and subsequent phytoplankton growth rates in a variety of HNLC regions of the global ocean. Chapter 7 contains the initial results from trace metal clean laboratory experiments conducted to examine the impact of reduced Fe upon phytoplankton bio-optical proportions

Chapter 2

Description of the ecosystem model

1.1 General Features

The coupled ice-atmosphere ocean model (CIAO) is a three dimensional ocean general circulation model with an embedded biological component that simulates the dynamics of the two dominant phytoplankton taxa (*P. antarctica* and diatoms), zooplankton, nitrate (NO_3), silicic acid ($Si(OH)_3$), phosphate (PO_4), iron (Fe), the full carbon system, oxygen (O_2), and three detrital pools (C, P, and Fe) within the southwestern Ross Sea, Antarctica [*Arrigo et al.*, 2003a; *Worthen and Arrigo,* 2003; *Tagliabue and Arrigo,* 2003; 2005; 2006, Figure 1]. The physics of CIAO are based on the Princeton Ocean Model (POM), a primitive equation ocean circulation model [*Blumberg and Mellor*, 1987] with vertical mixing calculated using the turbulence closure scheme of *Mellor and Yamada* [1982]. POM utilizes a terrain-following σ-coordinate system in the vertical and a curvilinear coordinate system in the horizontal and predicts the three dimensional fields of potential temperature, salinity, and velocity [*Arrigo et al.*, 2003a; *Worthen and Arrigo,* 2003].

The model domain for this study encompasses the Ross Sea sector of the Southern Ocean extending from 135°E to 60°W and from 58°S to 78°S (Figure 2). Nutrient concentrations at the open boundaries were specified using the annual climatologies of *Conkright et al.* [1994]. The horizontal grid spacing varies over the model domain, with the highest resolution on the continental shelf of the Ross Sea, south of Cape

Figure 1. A schematic representation of the ecosystem component of the CIAO model

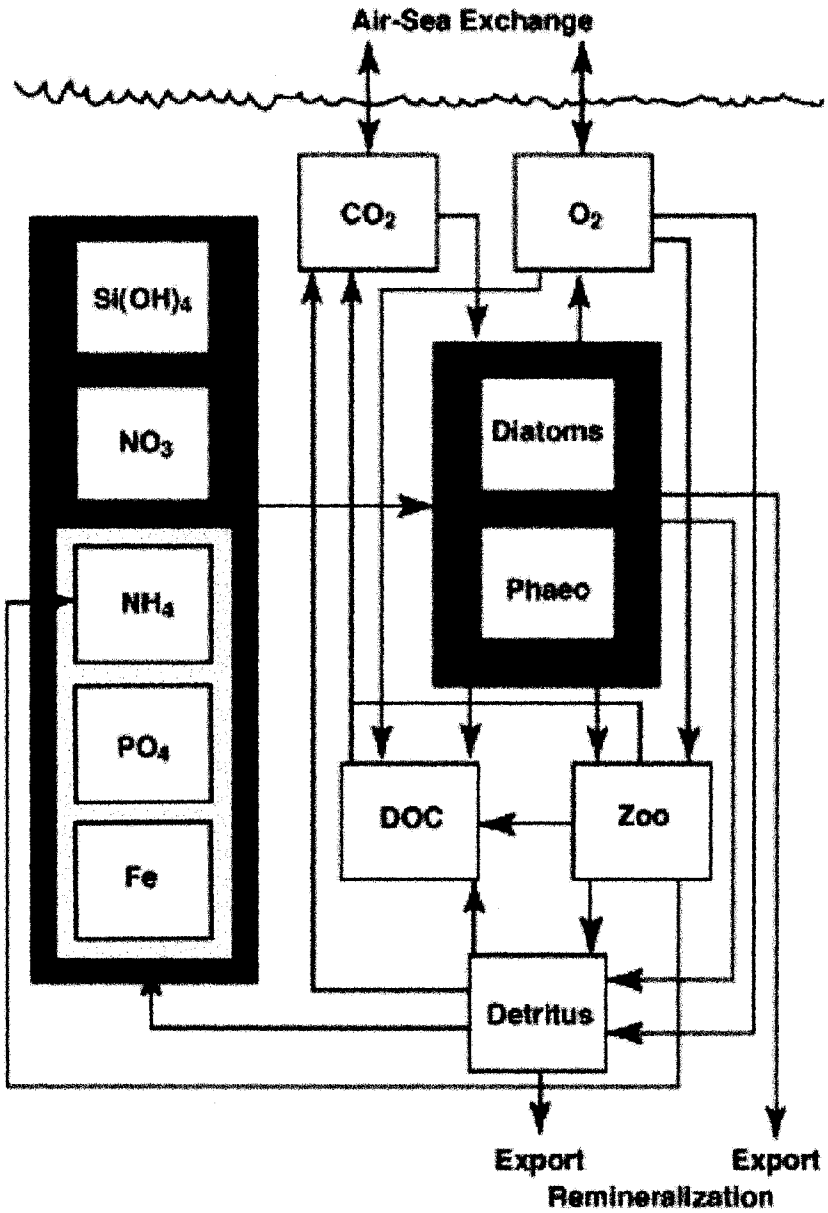

Figure 2. The CIAO model domain

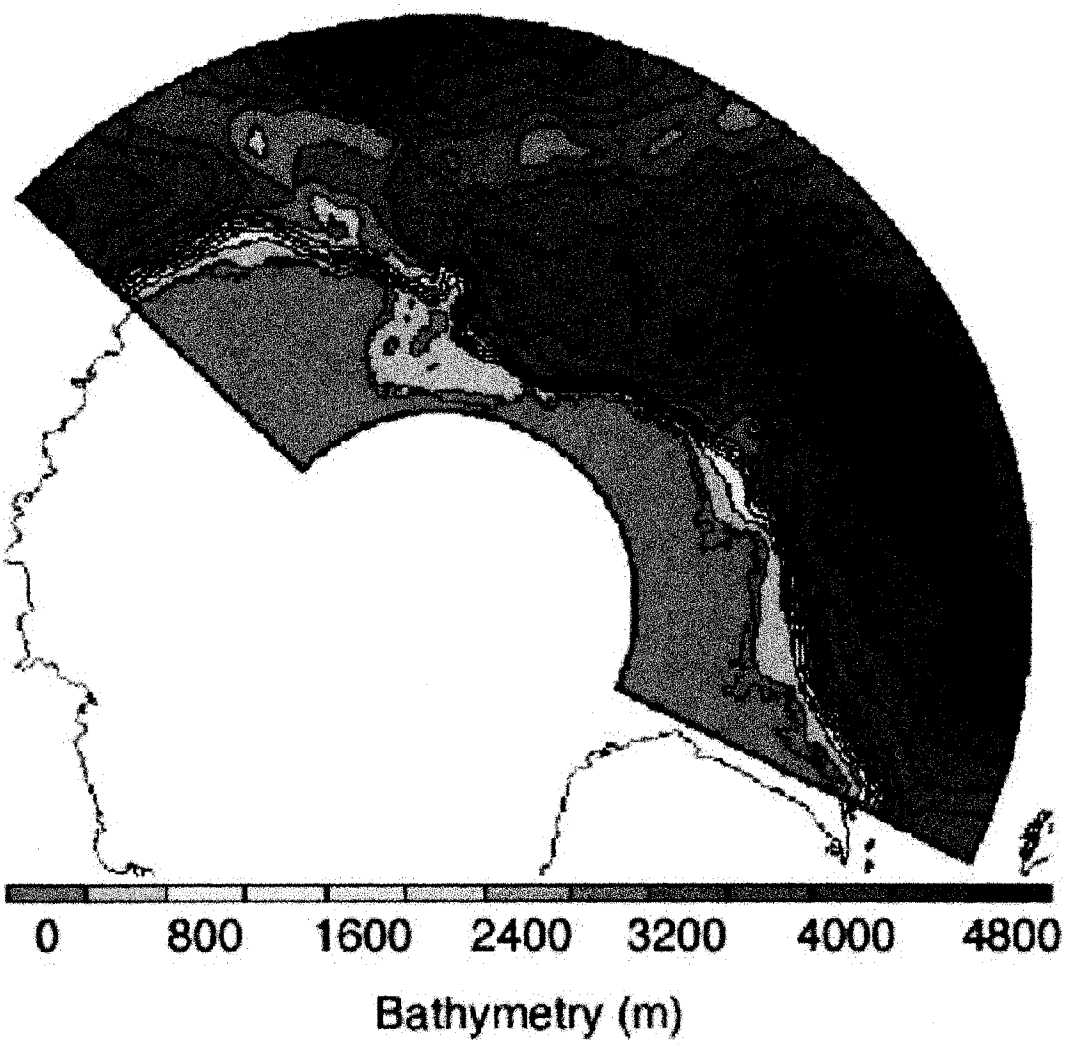

Adare and west of 150°W. The minimum grid spacing in the model is approximately $\Delta x = \Delta y = 25$ km at the southernmost reaches of the model, with a decrease in resolution to approximately $\Delta x = 180$ km and $\Delta y = 100$ km at the northern boundary. For the duration of this study I will focus on results from the southwestern portion of the Ross Sea (73 – 78 °S, 160 °E – 155 °W), which has the advantage of being well away from any model boundaries. The bottom topography for the model grid was interpolated from the TerrainBase5 data set (supplemented by GEBCO). The 23 σ-levels in the model, distributed smoothly in the vertical with an emphasis on resolution in the upper 200 m of the water column, are given by σ = (0.0, -0.0015, -0.0037, -0.0069, -0.0114, -0.0176, -0.0262, -0.0377, -0.0528, -0.0724, -0.0974, -0.1287, -0.1670, -0.2133, -0.2681, -0.3319, -0.4048, -0.4868, -0.5771, -0.6751, -0.7793, -0.8883, -1.0).

1.2 Forcing Fields

Atmospheric conditions required to force the model include downwelling spectral irradiance, total cloudiness, zonal and meridional winds at 10 m, sea-level pressure, and specific humidity and air temperature at 2 m. Clear sky downwelling irradiance between 400 and 700 nm was computed according to the radiative transfer model of *Gregg and Carder* [1990] and also corrected for fractional cloud cover. Irradiance was then propagated through the water column taking into account surface reflection, as well as attenuation by seawater, detritus and particles as per *Arrigo et al.* [1998b].

The surface forcing fields were obtained from the daily mean products from the National Centers for Environmental Prediction/National Center for Atmospheric

Research Reanalysis Project [*Kalnay et al.*, 1996] for the period 1979-1998 provided by the NOAA-CIRES Climate Diagnostics Center. The daily average values were further averaged over 5-day periods to create a long-term (1979-1998) mean 5-day surface forcing data set. Similarly, the ice concentrations for the period 1979-1998, calculated using the NASA Team algorithm [*Cavalieri et al.*, 1984; *Gloersen and Cavalieri*, 1986], were averaged into a long-term 5-day mean data set. Monthly mean snow cover for 1979-1998 [*Markus and Cavalieri*, 1998] was averaged to construct a long-term monthly climatology.

The specifications of surface fluxes applied to the POM are based on standard flux calculations and remotely sensed sea ice distributions [*Worthen and Arrigo,* 2003]. In brief, both the surface flux of heat and surface stresses are partitioned between ice and open water. The ocean-ice heat flux is a function of the difference between the water temperature and freezing temperature, as well as the frictional velocity (which is itself a function of the density and heat capacity of seawater). The air-water stress is governed by the wind speed and an approximation of the air-water drag. The relative velocity between the ice and water determines the ice-water stress and is proportional to the air-water stress [*Worthen and Arrigo,* 2003]. The ice-atmosphere heat flux is a function of the 2 m air temperature, snow cover, and ice thickness. The difference between the ocean-ice and the ice-atmosphere heat fluxes determines the net accumulation of sea ice, while melting is governed by the ocean-atmosphere heat flux (each divided by the latent heat of fusion of seawater and the density of ice). The surface salinity flux is a function of the net accumulation/melting of ice, as well as the

specified precipitation rate. Please see *Worthen and Arrigo* [2003] for more details on the physical parameterizations used in CIAO.

1.3 CIAO Ecosystem model

To simulate the ecosystem of the Ross Sea, an equation describing the advection, mixing, and sources and sinks for all state variables (see below) was added to the physical model. Following *Blumberg and Mellor* [1987], all state variables in the ecosystem model (Figure 1) are treated as passive tracers. The turbulent mixing coefficient is calculated in POM using a turbulence closure scheme [*Mellor and Yamada,* 1974; 1982] and is used to determine the degree of vertical mixing. Below, I describe the equations that govern the rate of change of all state variables in the ecosystem model. The initial values of both phytoplankton groups, zooplankton, and detritus are 2.5 mg C m^{-3}, 2 mg C m^{-3}, and 0.025 mg C m^{-3}, respectively. These values are fixed at the open boundaries, which is a reasonable approximation of such regions of low biomass and primary production. At the sea surface, there is a no-flux condition for all tracers, except CO_2 and O_2 (which can exchange with the atmosphere), and Fe and diatoms (which are supplied from melting sea ice). At the bottom boundary, the rate of change of all passive tracers is zero, except for Fe(II), which is supplied from sediments when the complex Fe supply model is employed.

1.3.1. Phytoplankton

CIAO includes the major components of the Ross Sea phytoplankton assemblage, namely the haptophyte *Phaeocystis antarctica* and a more generic 'diatom' group. All

parameters for the following equations can be found in Table 1; other parameter values are also given in tabular form within the pertinent chapter). The rate of change (Q_i, g C m^{-3} d^{-1}) in phytoplankton biomass (P_i, g C m^{-3}, where subscript i denotes either *P. antarctica* or diatoms) is

$$Q_i = \mu_i P_i - x_i P_i - \frac{\partial}{\partial z}(w_i P_i) - G_i Z \tag{1}$$

and is determined by phytoplankton specific growth (μ_i) and mortality (x_i) rates (d^{-1}), zooplankton grazing (G_i), and sinking (w_i). A maximum specific growth rate is calculated as a function of temperature [*Eppley*, 1972] and is then reduced by the most limiting resource (R_{lim}), yielding

$$\mu_i = [\mu_{0i} e^{r_i T}] R_{\lim i} \tag{2}$$

where μ_{0i} is the net growth rate at 0°C for phytoplankton i and r_i is a rate constant (0.0633 $°C^{-1}$) that determines the sensitivity of μ to temperature (T). The most limiting resource is the smaller of the nutrient and light limitation terms such that

$$R_{\lim i} = MIN[NO3\lim_i, PO4\lim_i, Si\lim_i, Fe\lim_i, L\lim_i]. \tag{3}$$

For all nutrients, the dimensionless limitation term $x_{\lim i}$ (where x is either NO_3, PO_4, Fe, or $Si(OH)_4$) is calculated as

$$x\lim_i = [x] / ([x] + K_{sxi}) \tag{4}$$

where [x] and K_{sxi} are the concentration and half saturation constant for growth, respectively, of nutrient x. Light limitation ($Llim_i$) is calculated as

$$L\lim_i = (1 - e^{(-PUR/Ek_i)}) Inhib_i \tag{5}$$

Table 1. Parameters values for the phytoplankton component of the CIAO model

Parameter	Description	Value
P_i	Concentration of phytoplankton group *i*	mg C m^{-3}
μ_i	Specific growth rate of phytoplankton group *i*	d^{-1}
$\mu 0_i$	Specific growth rate at 0 °C for phytoplankton group *i*	0.59/0.71 d^{-1}
Ek_{maxi}	Photoadaptation parameter for phytoplankton group *i*	30/90 μEin m^{-2} s^{-1}
x_i	Specific mortality rate of phytoplankton group *i*	0.025 d^{-1}
C/Chl_i	Carbon to Chlorophyll ratio	90/70 g:g
$Inhib_i$	Photoinhibition term	No units
PT_i	Threshold irradiance for photoinhibition for phytoplankton group *i*	100/∞ μEin m^{-2} s^{-1}
K	Rate constant for growth	0.0633 $°C^{-1}$
r_{limi}	Resource limitation term for phytoplankton group *i*	Dimensionless

Where two values are given (separated by '/'), the first is for *P. antarctica* and the second for diatoms.

where PUR is the photosynthetically usable radiation (μEin m^{-2} s^{-1}) [*Morel,* 1978], Ek_i is the photoadaptation parameter for phytoplankton group *i* [*Arrigo et al.,* 1998b] and $Inhib_i$ is the photoinhibition term defined as

$$Inhib_i = 1 - \frac{1 - e^{(-20 PUR_{ML}/PT_i)}}{1 + ae^{(-20 PUR_{ML}/PT_i)}} \quad (6)$$

where PUR_{ML} is the mean daily PUR for the mixed layer, a ($5x10^8$) determines the sensitivity of the photoinhibition term to PUR, and PT_i is the irradiance threshold above which photoinhibition begins for phytoplankton group *i*.

The vertical sinking flux of particles (phytoplankton, w_iC_i, and detritus, $w_{Det}D$) from the bottom of a given layer is determined by the vertical sinking flux into the top of that layer and the tracer concentration within the layer [*Arrigo et al.,* 2003a]. Sinking velocities of up to 10 m d^{-1} are predicted by the model, in agreement with rates reported in the literature. Higher sinking efficiencies in the model resulted in too rapid a flux of particulate material out of the surface layers and insufficient buildup of phytoplankton biomass [*Arrigo et al.,* 2003a].

1.3.2. Zooplankton

The rate of change in zooplankton abundance (Q_Z, mg C m^{-3} d^{-1}) is calculated as

$$Q_Z = (\gamma_P G_P + \gamma_D G_D)Z - x_Z Z - r_Z Z \quad (7)$$

where Z is the zooplankton concentration (mg C m^{-3}), γ_i is the assimilation efficiency of zooplankton grazing on phytoplankton species *i*, x_Z is the specific loss rate

(including natural mortality and higher predation, d^{-1}), and r_Z is respiration. A detailed comparison of zooplankton parameter values with the literature is undertaken in Chapter 3.

Grazing in CIAO is modeled as a simple Holling Type II function of phytoplankton abundance [*Holling*, 1959] such that

$$G_i = \frac{G_{\max}(P_i - h)}{K_z + (P_i - h)} \tag{8}$$

where G_i is the grazing rate (d^{-1}) on phytoplankton taxa i, G_{max} is the maximum grazing rate (d^{-1}), P_i is the concentration of phytoplankton group i (mg C m^{-3}), h is the feeding threshold below which G_i is zero (mg C m^{-3}), and K_z is the concentration of phytoplankton (mg C m^{-3}) at which G_i is half of G_{max}.

1.3.3. Detritus

The rate of change in the C detrital pool (Q_{Det}, mg C m^{-3} d^{-1}) is

$$Q_{Det} = (1-\beta)((1-\gamma_P)g_P Z + (1-\gamma_D)g_D Z + x_P P_P + x_D P_D + x_Z Z - r_{Det} D) - \frac{\partial}{\partial z}(w_{Det} D) \tag{9}$$

and is a function of the insoluble fraction (1-β) of unassimilated grazing products (γ_i), dead zooplankton ($x_Z Z$) and phytoplankton ($x_i C_i$), remineralization ($r_{Det} D$), and sinking. Due to the different taxon specific C/P and C/Fe uptake ratios exhibited by the phytoplankton of the Ross Sea [*Arrigo et al.*, 2002a], the P and Fe detrital pools must be computed independently by tracking the specific P and Fe content of

Table 2. Parameters values for the zooplankton and detrital components of the CIAO model

Parameter	Description	Value
Z	Concentration of zooplankton	mg C m^{-3}
G_{max}	Maximum grazing rate	0.4 d^{-1}
K_s	Grazing half saturation	85 mg C m^{-3}
H	Feeding threshold	9.5 mg C m^{-3}
x_Z	Specific zooplankton mortality rate	0.2 d^{-1}
r_Z	Zooplankton respiration rate	0.019 d^{-1}
γ	Assimilation efficiency	0.75
D	Concentration of detritus	mg C m^{-3}
PD	Concentration of phosphate detritus	mg P m^{-3}
FeD	Concentration of iron detritus	μg Fe m^{-3}
β	Soluble fraction of detritus	0.1
r_D	Remineralization rate for all detrital pools	0.03 d^{-1}

unassimilated grazing, zooplankton biomass, and phytoplankton biomass. As I assume a fixed C/N ratio [*Redfield,* 1934], I can readily compute the N content of detritus by dividing the C detritus concentration by the C/N ratio. The sources and sinks of both the P and Fe detrital pool are identical to the C detrital pool. All zooplankton and detrital parameters are given in Table 2. It should be noted that I assume remineralization of P detritus produces PO_4 and I do not include different remineralization depth scales for C, P, and Fe.

1.3.4. Dissolved macronutrients

Because biogeochemical processes responsible for remineralization of N and Si are not explicitly modeled, I utilize a weak restoring function to maintain appropriate concentrations of these tracers at depth. The restoring is calculated as

$$R_\zeta = \frac{1}{\tau}\sigma^6(\zeta_{clim} - \zeta) \tag{10}$$

where $\tau = 30$ days is the restoring time scale, ζ_{clim} is the climatological nutrient concentration, ζ is the concentration of the nutrient to be restored and σ is the vertical coordinate. The vertical coordinate σ is defined as $(z-\eta)/(H+\eta)$ where η is the surface elevation relative to the ocean depth, H_{tot}. Because the vertical coordinate σ varies from 0 at the surface to 1.0 at the model ocean bottom, the restoring is strongly confined to near-bottom layers. Although restoring violates the principal of mass balance, this process is restricted to autumn and winter months when deep convection mixes nutrient depleted surface waters to the bottom and when the bulk of

Table 3. Parameters values for the macronutrient component of the CIAO model

Parameter	Description	Value
C/N	Carbon to Nitrogen ratio	6.6 mol:mol
C/P_i	Carbon to Phosphorous ratio for phytoplankton group *i*	133.1/63.3 mol:mol
C/Si	Carbon to Silica ratio for diatoms	Variable mol:mol
ks_{NO3}	Half saturation constant for NO_3	0.5 μM
ks_{PO4}	Half saturation constant for PO_4	0.1 μM
$ks_{Si(OH)3}$	Half saturation constant for $Si(OH)_3$	5 μM

Where two values are given (separated by '/'), the first is for *P. anatarctica* and the second for diatoms.

the remineralization of particulate organic matter takes place. Therefore, nutrient restoring in the model is an effective substitute for the remineralization of NO_3 and $Si(OH)_4$, a process not currently included in the model. If not for nutrient restoring, the mass of N and Si contained in sinking organic matter would be lost from the system, and over time, N and Si would eventually become depleted [*Arrigo et al.*, 2003a]. See Table 3 for the parameter values for all macronutrients (NO_3, PO_4, and $Si(OH)_4$).

1.3.4.1 Nitrate

The rate of change in NO_3 (Q_{NO3}, mg m^{-3} d^{-1}) is

$$Q_{NO_3} = -N/C(\mu_i P_i) \tag{11}$$

and is simply a function of phytoplankton growth by taxon i ($\mu_i P_i$) adjusted by the N/C ratio (g:g).

1.3.4.2 Silicic acid

Silica is a vital component of diatom frustules and can be low in waters north of the Polar Front [*Conkright et al.*, 1994], and although $Si(OH)_4$ concentrations are typically above growth-limiting levels in the Ross Sea year round [e.g. *Arrigo et al.*, 2000], for completeness it is included in the model. The rate of change of $Si(OH)_4$ ($Q_{Si(OH)4}$, mg m^{-3} d^{-1}) is

$$Q_{Si(OH)4} = -(Si/C)_i(\mu_i P_i) \tag{12}$$

and is only a function of diatom growth (Si/C for *P. antarctica*=0), adjusted by their Si/C ratio. The Si/N uptake ratio of diatoms has been shown to increase as diatoms become Fe limited [e.g. *Takeda,* 1998]. Therefore Si/N (and thus Si/C, assuming a fixed C/N) is allowed to vary as a function of the bioavailable Fe concentration (bFe) using the following relationship based on the data of *Takeda* [1998]

$$Si/N = (1.322 + bFe)^{-0.27} \tag{13}$$

where bFe is the bioavailable Fe concentration (see later). Variability in the Si/N ratio ranges from 1 to 3 (mol:mol).

1. The rate of change in PO_4 (Q_{PO4}, mg m^{-3} d^{-1}) is computed as

$$\begin{aligned} Q_{PO4} &= (P/C)_P(e_P P_P + \beta[(1-\gamma_P)g_P Z + x_P P_P] - \mu_P P_P) \\ &+ (P/C)_D(e_D P_D + \beta[(1-\gamma_D)g_D Z + x_D P_D] - \mu_D P_D) + (P/C)_Z(x_Z Z + r_Z Z) + r_D PD \\ &+ (P/C)_D(e_D P_D + \beta[(1-\gamma_D)g_D Z + x_D P_D] - \mu_D P_D) + (P/C)_Z(x_Z Z + r_Z Z) + r_D PD \end{aligned} \tag{14}$$

where the subscripts *P* and *D* denote *P. antarctica* and diatoms, respectively. Changes in PO_4 are a function of phytoplankton growth (μ_i), taxon-specific exudation (e_i), and the soluble fraction (β) of unassimilated grazing products ($(1-\gamma_i)g_i Z$), dead phytoplankton ($x_i P_i$), and dead zooplankton ($x_Z Z$), as well as zooplankton excretion of P to balance the C respired while conserving the C/P ratio ($r_Z Z$), all scaled by the appropriate P/C ratio. The C/P ratio of detritus varies according to the relative contribution of each phytoplankton taxon to the detrital pool. Remineralization of the P detrital pool ($r_D PD$), is assumed to resupply PO_4. Non-particulate losses of P by

phytoplankton and zooplankton (e.g. exudation) are instantaneously allocated to the PO_4 pool. There is no restoring of PO_4.

1.3.5 The simple iron cycle model

During the subsequent investigations presented herein I will make use of two Fe cycle formulations (see Table 4 for parameter values), one simple and the other substantially more complex. In the simple parameterization, Fe is modeled in a fashion similar to other nutrient tracers and the rate of change in dissolved Fe (Q_{Fe}, umol m^{-3} s^{-1}) is

$$Q_{Fe} = r_{Det}FeD + icefe - (\mu_P P_P (Fe/C_P) + \mu_D P_D (Fe/C_D)) \quad (15)$$

and is a function of phytoplankton growth (μ_i), adjusted by the taxon specific C/Fe ratio, remineralization of the Fe detrital pool (r_{Det}), and the melting of sea ice (*icefe*). Sea ice melting is assumed to be a source of Fe with the prescribed concentration of 15 nM and a solubility of 40% [*Edwards and Sedwick,* 2001]. Planktonic C/Fe ratios can be highly plastic and the rationale behind the values ascribed to this parameter can be found in Chapter 4. In the simple parameterization scheme, I assume that all Fe is bioavailable (i.e. bFe = Fe) and do not include processes that could be important in governing the cycle of dissolved Fe is seawater (e.g. oxidation, precipitation, organic complexation, photochemistry). bFe is only lost by phytoplankton uptake.

1.3.6 The complex iron cycle model

To more accurately simulate the seawater Fe cycle, I replaced the simple Fe cycle used previously in CIAO with an Fe supply model that utilizes 4 dissolved (dFe, including Fe(II), Fe(III), Fe(III)La, and Fe(III)Lb) and 4 particulate (pFe, including inorganic particles >0.4 μm and Fe associated with detritus, phytoplankton and zooplankton) Fe pools. In this model (Figure 3), the two free inorganic Fe pools include Fe(II) and Fe(III). Fe(III) can be converted to solid inorganic Fe (Fe(III)s) and forms ligand complexes that can be either non-bioavailable (Fe(III)La) or bioavailable (Fe(III)Lb). Bioavailable forms of Fe (bFe) in the standard simulation are taken to be Fe(II), Fe(III), and Fe(III)Lb and total Fe (tFe) is simply the sum of the pFe and dFe pools.

1.3.6.1 Fe(II)

The rate of change in the Fe(II) pool ($Q_{Fe(II)}$, μmol m^{-3} s^{-1}) is

$$Q_{Fe(II)} = (1-A)Fe_{atm} + Fe_{sed} - \pi^{Fe(II)}{}_i(Fe/C_i)P_i - k_{ox}Fe(II) + k_{pr}Fe(III)La + e_z + icefe + r_{det}FeD \quad (16)$$

and is a function of oxidative loss ($k_{ox}Fe(II)$), photoreduction of Fe(III)La to Fe(II) ($k_{pr}Fe(III)La$), atmospheric deposition (Fe_{atm}), sedimentary resuspension (Fe_{sed}), sea ice melting ($icefe$), remineralization of detrital Fe ($r_{det}FeD$) and uptake by phytoplankton taxa i ($\pi^{Fe(II)}{}_i(Fe/C_i)P_i$, where i is either *P. antarctica* or diatoms). Fe(II) oxidation is modeled as a temperature-dependent (Table 4) pseudo first order rate constant (k_{ox}) [*Millero et al.*, 1987]. Data used to define the relationship between

Figure 3. A schematic of the complex Fe supply model

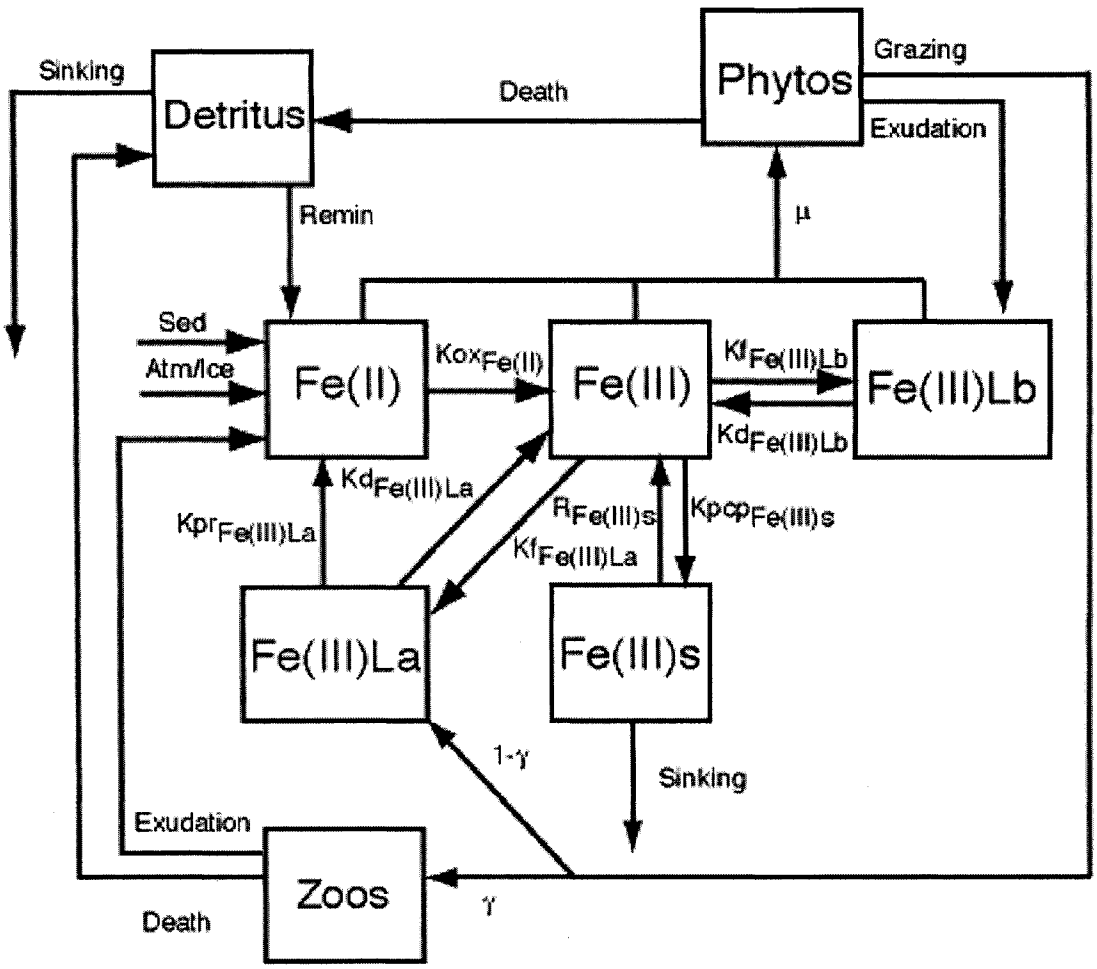

Table 4. Parameters values for the iron component of the CIAO model

Parameter	Description	Value
Fe(II)	Inorganic Fe(II)	nM
Fe(III)Lb	Bioavailable FeL	nM
Fe(III)	Inorganic Fe(III)	nM
Fe(III)La	Non-bioavailable FeL	nM
Fe(III)s	Solid inorganic Fe	nM
dFe	Dissolved Fe	Fe(II) + Fe(III) + Fe(III)La + Fe(III)Lb, nM
pFe	Particulate Fe	Fe(III)s + Det_{Fe} + Phyto, nM
bFe	Bioavailable Fe	Fe(II) + Fe(III) + Fe(III)Lb, nM
tFe	Total Fe	dFe+pFe, nM
Det_{Fe}	Detrital Fe	nM
L_a	Concentration of the non-bioavailable ligand	2 nM
L_b	Concentration of the bioavailable ligand	0.6 nM
k_{ox}	Fe(II) oxidation rate constant	$9x10^{-22}e^{(0.1455T(T))}$, s^{-1}
k_{pr}	Fe(III)La photoreduction rate constant	((PAR/4.16)*1.67x10^{-7})*(100/35), s^{-1}
$k_{fFe(III)Lb}$	Fe(III)Lb formation rate constant	19.6 x 10^5 M^{-1} s^{-1}
$k_{dFe(III)Lb}$	Fe(III)Lb dissociation constant	1.5 x10^{-6} s^{-1}
$k_{fFe(III)La}$	Fe(III)La formation rate constant	4.2 x10^4 M^{-1} s^{-1}
$k_{dFe(III)La}$	Fe(III)La dissociation constant	2 x10^{-7} s^{-1}
Log $K_{Fe(III)Lb}$	Conditional stability constant for Fe(III)Lb	23.11
Log $K_{Fe(III)La}$	Conditional stability constant for Fe(III)La	22.32
k_{pcp}	Fe(III)s precipitation rate constant	2.78 x10^{-5} s^{-1}
$R_{Fe(III)s}$	Remineralization rate of Fe(III)s	3.57 x10^{-8} s^{-1}
K_{sFe}	Half saturation constant for Fe uptake	0.01/0.1 nM
Fe/C_i	Fe to C uptake ratio for phytoplankton group *i*	2.22/10 μmol :mol
Fe/C_z	Zooplankton Fe to C ratio	5 μmol : mol
Fe_{atm}	Atmospheric deposition of Fe	0.1 μmol m^{-2} yr^{-1}
Fe_{sed}	Sedimentary input of Fe	15.7 μmol m^{-2} yr^{-1}
π^X_i	Proportion of total Fe uptake by species i satisfied by Fe(II), Fe(III) or Fe(III)Lb.	dimensionless

Where two values are given (separated by '/'), the first is for *P. antarctica* and the second for diatoms.

temperature and k_{ox} also include the low temperature Fe(II) half lives measured during the Southern Ocean Iron RElease Experiment (SOIREE) [*Bowie et al.,* 2001]. The rate constant for photoreduction (k_{pr}, Table 4) varies as a function of irradiance as per *Rijkenberg et al.* [2005]. The rate of atmospheric Fe deposition into open water (Fe_{atm}, 0.1 μmol Fe(II) m^{-2} yr^{-1}) is taken from estimates made during SOIREE [*Bowie et al.,* 2001] and adjusted to account for the proportion of each grid cell that is ice covered (A). As in the simple Fe cycle, atmospheric Fe accumulating on sea ice is assumed to reach concentrations of 15 nM, 40% of which is soluble [*Edwards and Sedwick,* 2001]. The rate of sedimentary Fe(II) input (Fe_{sed}) is assumed to be constant (15.7 μmol Fe(II) m^{-2} yr^{-1}) and is at the low end of total dissolved Fe flux (which include other Fe species) measured by *Elrod et al.* [2004] off the coast of California. While there are no sedimentary Fe(II) flux data for the Southern Ocean, the Fe(II) sedimentary flux estimates of *Elrod et al.* [2004] result in deep dissolved Fe concentrations that are consistent with in situ measurements for the southwestern Ross Sea [*Coale et al.,* 2005]. The Fe demand for phytoplankton taxa i per unit C fixed is Fe/C_i (2.22 and 10 μmol Fe : mol C for *P. antarctica* and diatoms, respectively), while the fraction of the total Fe demand by each taxa that is satisfied by Fe(II) is denoted $\pi^{Fe(II)}{}_i$ (see below). Phytoplankton demands for Fe are highly variable as a function of incident irradiance and Fe concentration [*Sunda and Huntsman,* 1997], and in the absence of information describing such variability for Ross Sea phytoplankton, I use the taxon specific-ratios sensu *Tagliabue and Arrigo* [2005]. If the Fe/C ratio of zooplankton food is greater than their cellular Fe/C_z quota [*Schmidt et al.*, 1999, Table 1], then the excess Fe consumed (e_z) is assumed to enter the Fe (II) pool.

1.3.6.2 Fe(III)

The rate of change in Fe(III) ($Q_{Fe(III)}$, μmol m^{-3} s^{-1}) is

$$Q_{Fe(III)} = k_{ox}Fe(II) - k_{fFe(III)La}Fe(III)[L_a] + k_{dFe(III)La}Fe(III)La - k_{fFe(III)Lb}Fe(III)[L_b] + k_{dFe(III)Lb}Fe(III)Lb - \pi^{Fe(III)}{}_i(Fe/C_i)P_i - k_{pcp}Fe(III) + R_{Fe(III)s}Fe(III)s \quad (17)$$

where oxidation of Fe(II) produces Fe(III) ($k_{ox}Fe(II)$). Fe(III) can be complexed by either L_a or L_b to form Fe(III)La and Fe(III)Lb, respectively, at a rate that is a function of the respective ligand concentration ([L_a] or [L_b]) and the complex formation rate constant ($k_{fFe(III)La}$ or $k_{fFe(III)Lb}$). I include dissociation of each complex in the absence of light as a first order process ($k_{dFe(III)La}$ or $k_{dFe(III)Lb}$), while Fe(III)La also can be photoreduced to Fe(II) ($k_{pr}Fe(III)La$). I do not model the two ligand pools dynamically; instead, the concentration of L_a is fixed at 2 nM [*Boye et al.,* 2001; *Croot et al.,* 2004] and the concentration of the strong chelator ([L_b]) is set to 0.6 nM [R*ue and Bruland,* 1997]. Rate constants for the formation and dissociation of Fe(III)La are taken from measurements of *Witter and Luther* [1998]. *Maldonado and Price* [1999] demonstrated significant phytoplankton uptake of Fe when complexed with desferroxamine (DFO) ligands, which have been shown to be present in seawater [*McCormack et al.,* 2003] and produced by marine bacteria [*Martinez et al.,* 2001]. I therefore ascribe rate constants for the formation ($k_{fFe(III)Lb}$) and dissociation ($k_{dFe(III)Lb}$) of Fe(III)Lb in accordance with the measured kinetics of DFO [*Witter et al.,* 2000]. Calculated log conditional stability constants for L_a and L_b ($K_{Fe(III)La}$ and $K_{Fe(III)Lb}$, Table 1) are consistent with values reported for the Southern Ocean [e.g. *Boye et al.,*

2001; *Croot et al.*, 2004], assuming that the coefficient for the inorganic side reaction for all inorganic Fe species ($\alpha_{Fe'}$) is 10^{10} [*Hudson et al.* 1992]. The proportion of total phytoplankton uptake of Fe that is satisfied by Fe(III) is denoted as $\pi^{Fe(III)}{}_i$. Fe(III) is lost to solid inorganic forms (Fe(III)s) via scavenging/precipitation [*Johnson et al.*, 1994] as a first order processes ($k_{pcp}Fe(III)$, 2.78 x 10^{-5} s^{-1}) and is remineralized to Fe(III) at the same rate as detritus ($R_{Fe(III)s}Fe(III)s$, 3.57 x 10^{-8} s^{-1}).

1.3.6.3 Fe(III)La

The rate of change in the Fe(III)La pool ($Q_{Fe(III)La}$, μmol m^{-3} s^{-1}) is

$$Q_{Fe(III)La} = k_{fFe(III)La}Fe(III)[L_a] - k_{dFe(III)La}Fe(III)La \\ -k_{pr}Fe(III)La + Fe/C_z[(1-\gamma_i)g_iZ] \quad (18)$$

where L_a complexes inorganic Fe(III) as described above to produce Fe(III)La ($k_{fFe(III)La}Fe(III)[L_a]$) and facilitates its photoreduction to Fe(II) via LMCT ($k_{pr}Fe(III)La$). In order to conserve particulate Fe/C ratios, I also assume that the Fe content of unassimilated grazing (on phytoplankton taxa *i*, $Fe/C_z[(1-\gamma_i)g_iZ]$) will liberate organically complexed Fe which is added to the Fe(III)La pool.

1.3.6.4 Fe(III)Lb

The rate of change in Fe(III)Lb ($Q_{Fe(III)Lb}$, μmol m^{-3} s^{-1}) is

$$Q_{Fe(III)Lb} = k_{fFe(III)Lb}Fe(III)[L_b] - k_{dFe(III)Lb}Fe(III)Lb \\ -\pi^{Fe(III)Lb}{}_i(Fe/C_i)P_i + Fe/C_i(e_iP_i) \quad (19)$$

where Fe(III)Lb is also produced from the organic complexation of Fe(III) ($k_{fFe(III)Lb}Fe(III)L_b$, see above), but is assumed to be non-photoreactive [*Barbeau et al.*, 2003] and bioavailable to the phytoplankton. The quantity $\pi^{Fe(III)Lb}{}_i$ is the fraction of the total Fe demand for phytoplankton taxa *i* satisfied by Fe(III)Lb (see below). To conserve planktonic Fe/C ratios, I assume that organic Fe is also lost as phytoplankton exude dissolved organic carbon ($Fe/C_i(e_iP_i)$) which is added to the Fe(III)Lb pool. Model results are insensitive to this process.

1.3.6.5 Fe(III)s

The rate of change in solid inorganic Fe species (not associated with either phytoplankton or detritus, $Q_{Fe(III)s}$, μmol Fe(III)s m^{-3} s^{-1}) is

$$Q_{Fe(III)s} = k_{pcp}Fe(III) - R_{Fes}Fe(III)s - snkFe(III)s. \quad (20)$$

where Fe(III)s is produced from the precipitation of Fe(III) ($k_{pcp}Fe(III)$) and is lost due to remineralization ($R_{Fes}Fe(III)s$) and sinking ($snkFe(III)s$).

1.3.6.6 Phytoplankton demand for Iron

The fraction of the total Fe demand ($\pi^X{}_i$) for taxa *i* that is satisfied by Fe species X (where X is either Fe(II), Fe(III), or Fe(III)Lb) is calculated as

$$\pi^X{}_i = \frac{X/(X + K_{sFe})}{Fe(II)/(Fe(II) + K_{sFe}) + Fe(III)/(Fe(III) + K_{sFe}) + Fe(III)Lb/(Fe(III)Lb + K_{sFe})} \quad (21)$$

and $\pi^{Fe(II)}_i + \pi^{Fe(III)}_i + \pi^{Fe(III)Lb}_i = 1$. The sensitivity of the model to the precise values ascribed to each parameter and the precise parameterization scheme employed can be found in Chapter 5.

1.3.7 Dissolved organic carbon

Carbon cycle dynamics (see Table 5) require knowledge of the dissolved organic carbon (DOC) concentration, whose rate of change (Q_{DOC}, mmol m^{-3} s^{-1}) is calculated as

$$Q_{DOC} = e_P P_P + e_D P_D + \beta[(1-\gamma_P)g_P Z + (1-\gamma_D)g_D Z + x_P P_P + x_D P_D + x_Z Z] - r_{DOC} DOC_{lab} \quad (22)$$

where DOC sources are phytoplankton exudation ($e_i P_i$), and the soluble fraction (β) of unassimilated grazing products ($(1-\gamma_i)g_i Z$), dead phytoplankton ($x_i P_i$), and dead zooplankton ($x_Z Z$). Changes in DOC are added to a background (minimum) DOC concentration (DOC_{min}) of 40 μM which represents the more stable refractory pool [*Carlson et al.*, 2000]. Losses of DOC are restricted to bacterial remineralization of the labile pool ($r_{DOC} DOC_{lab}$), where $DOC_{lab} = DOC - DOC_{min}$. Both β and r_{DOC} were tuned by matching model predictions to the observed cycle of DOC in the Ross Sea [*Carlson et al.*, 2000].

1.3.8 Total carbon dioxide

The formulation for the rate of change in TCO_2 (Q_{TCO2}, mmol m^{-3} s^{-1}) is

$$Q_{TCO2} = r_{DOC} DOC + r_D D + r_Z Z - (\mu_P P_P + \mu_D P_D) - FCO_2 \quad (23)$$

where changes in water column TCO_2 are controlled by sea-air CO_2 exchange (FCO_2), taxon-specific phytoplankton photosynthesis ($\mu_i P_i$), zooplankton respiration ($r_Z Z$), and the remineralization of detritus and DOC ($r_D D$ and $r_{DOC} DOC$, respectively). To determine the air-sea pCO_2 difference used to calculate the FCO_2 term, I first computed pCO_2 (μatm) for all surface grid cells as a function of TCO_2, alkalinity, temperature, and salinity using the iterative formulations described in the Ocean Carbon-Cycle Model Intercomparison Project (OCMIP) protocols [*Najjar and Orr,* 1998]. Alkalinity is set to 2330 μmol kg^{-1} [*Bates et al.,* 1998] and is normalized to a salinity of 35 psu. Atmospheric pCO_2 is set at 365 μatm [*Takahashi et al.,* 2002] and CO_2 solubility (α, mmol m^{-3} μatm^{-1}) is calculated as a function of temperature (T, Kelvin) and salinity (S, psu) [*Weiss and Price*, 1980].

$$\alpha = exp[-162.8301 + 218.2968(\frac{T}{100}) + 90.9241\ ln(\frac{T}{100}) - 1.47696(\frac{T}{100})^2 + S(0.025695 - 0.025225(\frac{T}{100}) + 0.0049867(\frac{T}{100})^2)] \quad (24)$$

The sea-air flux of CO_2 for each surface grid cell then becomes

$$FCO_2 = (1 - A)\, k_{CO2} \alpha \Delta pCO_2 \quad (25)$$

where ΔpCO_2 (μatm) is the sea-air pCO_2 difference, α is the solubility, A is the proportion of the grid cell that is ice covered (0 to 1, dimensionless), and k_{CO2} is the gas transfer velocity (for long term wind products, m d^{-1}) calculated via *Wanninkhof* [1992] as

$$k_{CO2} = 0.39 * W_{10}^2 (\frac{Sc_{CO2}}{660})^{-1/2} \quad (26)$$

Table 5. Parameters values for the carbon and oxygen components of the CIAO model

Parameter	Description	Value
Atm. pCO_2	Atmospheric pCO_2	365 µatm
Init_TCO_2	Initial TCO_2	2225 µM
TA	Total Alkalinity	2330 µeq
e_i	Proportion of primary production exuded as DOC for phytoplankton group *i*	0.09/0.19
DOC_{min}	Minimum DOC concentration	40 µM
r_{DOC}	Remineralization rate of DOC	0.05 d^{-1}
C/O	Carbon to oxygen ratio	0.66 mol:mol

where W_{10} is the wind speed (computed from U_{10m} and V_{10m} winds forcing fields) at 10 m above sea level (m d^{-1}) and Sc_{CO2} is the Schmidt number for CO_2, itself a function of temperature (T) [*Wanninkhof* 1992]

$$Sc_{CO2} = 2073.1 - 125.62T + 3.627T^2 - 0.043219T^3. \quad (27)$$

1.3.9. Oxygen

Oxygen (O_2) is produced by photosynthesis and consumed during respiration. I model O_2 within CIAO via a relatively simple parameterization scheme whereby the rate of change in O_2 (mmol m^{-3} s^{-1}) is

$$Q_{O2} = C/O^{-1}(\mu_P P_P + \mu_D P_D) - C/O(r_{DOC} DOC + r_D D) - FO_2 \quad (28)$$

where the rate of net primary production ($\mu_i P_i$) and remineralization of detritus and DOC are scaled by a C/O ratio [0.66 mol:mol, *Hedges et al.*, 2002]. The calculation of the sea-air flux term requires knowledge of the saturation of O_2 in seawater. I calculate O_2(sat) (mmol m^{-3}) via the OCMIP modeling protocols [*Najjar and Orr*, 1998] to ensure valid comparison with existing work. The sea-air O_2 flux is then

$$FO_2 = (1 - A)\, k_{O2}(O_2 - O_2(sat)) \quad (29)$$

where the piston velocity for O_2 (k_{O2}) is calculated in a similar fashion to k_{CO2} [*Wanninkhof*, 1992]

$$k_{O2} = 0.39 * W_{10}^2 \left(\frac{Sc_{O2}}{660}\right)^{-1/2} \quad (30)$$

where Sc_{O2} is the Schmidt number for O_2 [*Keeling et al.,* 1998],

$$Sc_{O2} = 1638 - 81.83T + 1.483T^2 - 0.008004T^3 \quad (31)$$

and is a function of T (°C). See Table 5 for the parameter values.

Chapter 3

Anomalously low zooplankton abundance in the Ross Sea: An alternative explanation

Abstract The southwestern Ross Sea (Antarctica) supports a large bloom of *Phaeocystis antarctica* in the Ross Sea polynya, which is impacted minimally by zooplankton, and a smaller diatom bloom in the adjacent Terra Nova Bay polynya, which are more readily grazed. This difference in grazing pressure between the two regions frequently has been explained by a reduced susceptibility of *P. antarctica* to grazing, despite conflicting evidence showing that *Phaeocystis* spp. are readily grazed by zooplankton. Using a 3-D ecosystem model of the Ross Sea, my goal was to determine if phytoplankton growth dynamics, rather than mechanical and/or chemical defenses, might explain 1) the relatively low zooplankton abundance observed in waters dominated by *P. antarctica*, and 2) the low overall zooplankton biomass in the Ross Sea. Although in the model, diatoms and *P. antarctica* were grazed with equal ease (i.e. no prey selectivity), the slower growth of phytoplankton in Terra Nova Bay resulted in a higher degree of phytoplankton-zooplankton coupling and greater zooplankton abundance. Conversely, the exaggerated boom/bust cycle of the *P. antarctica* bloom in the Ross Sea polynya resulted in greater decoupling from higher trophic levels and reduced zooplankton biomass. This indicates that the low zooplankton abundance observed in the Ross Sea polynya may be a consequence of their inability to match the high growth rates of *P. antarctica*. The different degrees of

zooplankton-phytoplankton coupling between Terra Nova Bay and the Ross Sea polynya may have important implications for food web structure and carbon export, especially under changing stratification.[1]

[1] Elements of this chapter appeared in: Tagliabue, A. and K. R. Arrigo. 2003. Anomalously low zooplankton abundance in the Ross Sea: An alternative explanation. Limnology and Oceanography, *48(2)*:686-699

1. Introduction

The Southern Ocean is a dynamic system, exhibiting large mesoscale variability in primary production and zooplankton biomass, mainly along frontal boundaries [*Deacon*, 1982]. Variation ranges from the low productivity High Nutrient Low Chlorophyll (HNLC) areas of the sub Antarctic zone [e.g. *Martin et al.*, 1990] to the high productivity marginal ice zone (MIZ) and coastal polynyas such as those found in the Ross Sea [*Arrigo and McClain,* 1994; *Smith and Gordon,* 1997; *Arrigo and Van Dijken*, 2003]. The Southern Ocean is an important component of the global ocean system, linking all major ocean basins and facilitating global distribution of its deep waters. Furthermore, it directly exchanges large amounts of CO_2 with the atmosphere [*Caldeira and Duffy,* 2000] and may have played a major role in past climate change [*Martin,* 1990]. Recent climate models [e.g. *Sarmiento et al.*, 1998] predict that the critical role of the Southern Ocean may continue in the future as rising atmospheric CO_2 is predicted to impact the carbon (C) cycle significantly.

A key component of the marine C cycle is the biological pump, whereby phytoplankton remove CO_2 from surface waters and convert it to particulate organic C (POC), of which about 1% is exported to depth. The biological pump can help to maintain a positive CO_2 gradient, allowing CO_2 to diffuse from the atmosphere into the ocean; mixing of dissolved organic carbon (DOC) across the pycnocline also contributes to the net C flux. Food web characteristics, such as phytoplankton cell size, the degree of micro versus meso or macrozooplankton grazing, and bacterial remineralization, determine the export potential of POC [*Boyd and Newton,* 1995]. Elevated zooplankton grazing leads to the increased flux of C to depth within highly

refractory and dense fecal pellets, and phaeopigment production (primarily phaeophorbide *a*) occurs via 'sloppy feeding' upon phytoplankton. An improved understanding of the processes that control the rates of zooplankton grazing and biomass levels would allow us to better assess the degree to which zooplankton impact the export flux of C.

The Ross Sea is one of the most productive ecosystems in the Southern Ocean [*Arrigo and Van Dijken*, 2003], yet data suggest that meso and macrozooplankton biomass there, relative to the high phytoplankton biomass, is anomalously low (see Table 1) compared to other Southern Ocean areas. Data collected by *Huntley and Zhou* [2000] during the AESOPS-JGOFS expeditions in the southwestern Ross Sea found a springtime zooplankton biomass of ~0.5 g C m^{-2}, which increased to around 0.7 g C m^{-2} during the austral summer. These values were obtained over a range of depths and then integrated at each station (n=20 and 22 stations during austral spring and summer respectively). Measurements by *Sertorio et al.* [2000] support these values, although they sampled slightly to the north of my study area; zooplankton biomass was found to be around 0.34 g C m^{-2} at the end of the austral spring (n=19). Krill also appeared to be scarce in this otherwise highly productive oceanic region [*Biggs,* 1982]. By comparison, zooplankton biomass in the vicinity of South Georgia Island (6 g C m^{-2}, *Ward et al.,* 1995) and at the Antarctic Polar Front (4 g C m^{-2}, *Fransz and Gonzalez,* 1997) is around an order of magnitude greater than in the Ross Sea. Historic measurements by *Foxton* [1956] during the Discovery cruises support this trend, finding the coastal areas (65-70°S) to have by far the lowest zooplankton biomass of the Southern Ocean region, especially when compared to the frontal zones

further north (~0.8 and 1.6 g C m^{-2} respectively; see Table 1). Even in the Croker Passage (1.1 g C m^{-2}, *Conover and Huntley,* 1991) and portions of the Weddell Sea (0.85 g C m^{-2}, *Boysenennen et al.,* 1991), both regions of low zooplankton abundance by Southern Ocean standards, zooplankton biomass is still greater than in the Ross Sea (Table 1).

In addition to its low abundance, the meso- and macrozooplankton community of the Ross Sea is of low diversity and exhibits low reproduction rates [*Knox,* 1994]. Herbivorous mesozooplankton are represented by the slower growing copepods *Calanus propinquus* and *Calanoides acutus*, while krill (*Euphausia superba*) and the mollusc *Limacina helicina* are the major macrozooplankton species [*Hecq et al.,* 2000]. Copepods such as *Metridia gerlachei* and *Oithona similis* make up the bulk of the remaining zooplankton [*Hecq et al.,* 2000].

Data from the southwestern Ross Sea also suggest that grazer populations vary spatially. For example, waters associated with the Ross Sea polynya (Figure 1) appear to support a significantly lower grazer population than those of the adjacent Terra Nova Bay (from phaeophorbide *a* variability [*Goffart et al.,* 2000], despite the fact that both regions exhibit similar maximum Chl *a* concentrations (> 7 mg Chl *a* m^{-3}) and annual rates of production (~140-200 g C m^{-2} yr^{-1}) [*Arrigo et al.,* 2000]. Seventy percent of the total mass flux measured in sediment traps located in Terra Nova Bay was composed of zooplankton fecal pellets (a byproduct of grazing), compared to only 38% in the Ross Sea polynya [*Dunbar et al.,* 1998] where the particulate flux was instead dominated by loose aggregates [*DeMaster et al.,* 1992] composed primarily of phytoplankton detritus. Pigment data also support the existence of higher grazing

Table 1. A summary of existing measurements of depth integrated zooplankton biomass for a range of Southern Ocean regions.

Location	Zooplankton Biomass	Notes	Source
*South Georgia	5.8 g C m^{-2}	Copepods (Jan)	Ward *et al.*, (1995)
*Polar Front (6°W)	3.7 g C m^{-2}	84-87% Copepods (Oct-Nov)	Fransz and Gonzalez (1997)
*Nr Polar front $^{\alpha}$	1.6 g C m^{-2}	All types (Nov - Apr)	Foxton (1956)
Croker Passage	1.1 g C m^{-2}	Copepods (Mar – Apr)	Conover & Huntley (1991)
*Antarctic Zone $^{\beta}$	1.04 g C m^{-2}	All types (Nov – Apr)	Foxton (1956)
*East Wind Drift $^{\gamma}$	0.81 g C m^{-2}	All types (Nov – Apr)	Foxton (1956)
NW Weddell Sea (NE shelf)	0.85 g C m^{-2}	Copepods (Feb)	Boysenennen *et al.*, (1991)
Ross Sea (Spring)	0.5±0.2 g C m^{-2}	All types (Oct/Nov)	Huntley and Zhou (2000)
Ross Sea (Summer)	0.7±0.3 g C m^{-2}	All types (Jan/Feb)	Huntley and Zhou (2000)
63-73°S, ~180°W	0.34±0.1 g C m^{-2}	Copepods (Dec),	Sertorio *et al.*, (2000)

* Taken from Atkinson *et al.*, (2001)
$^{\alpha}$Average of all sectors 50-55°S
$^{\beta}$ Average of all sectors 55-65°S
$^{\gamma}$ Average of all sectors 65-70°S
g Dry weight was converted to g C m^{-2} by assuming a 45% conversion to carbon units [*Conover and Huntley,* 1991].

Figure 1. Map of the southwestern Ross Sea (Antarctica), showing the location of the two study areas, A = Terra Nova Bay (74.5°S – 75.5°S, 165°E – the coast) and B = central Ross Sea polynya (75.5°S-77°S, 172°E - 177°E).

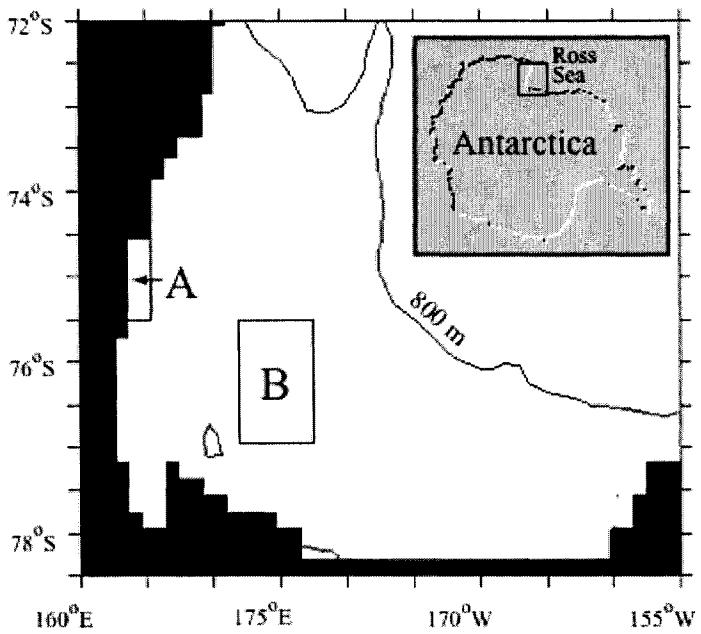

pressure in Terra Nova Bay than in the Ross Sea polynya. *DiTullio and Smith* [1996] found that phaeophytin:phaeophorbide *a* ratios in Terra Nova Bay were approximately 2-fold greater than in the waters of the Ross Sea polynya. Since phaeophorbide *a* is associated with copepod fecal pellets, relatively high levels of this compound in Terra Nova Bay suggest that mesozooplankton grazing rates there are enhanced relative to the Ross Sea polynya. This is supported by *Goffart et al.* [2000] who found phaeophorbide *a* levels of 190 mg m^{-2} during January 1990 in the diatom dominated Terra Nova Bay, compared to <50 mg m^{-2} within the Ross Sea Polynya. Earlier in the season (November 1994) phaeophorbide *a* levels in the Ross Sea polynya were even lower, barely reaching 25 mg m^{-2} [*Goffart et al.*, 2000].

Differences in phytoplankton community structure are thought to be responsible for the differences in grazing intensity between the Ross Sea polynya and Terra Nova Bay. The Ross Sea polynya is dominated by the colonial haptophyte *Phaeocystis antarctica* while diatoms (mostly *Fragilariopsis* spp.) are more commonly found in Terra Nova Bay. This contrast in taxonomic distribution is thought to be controlled by the timing and intensity of water column stratification [*Arrigo et al.*, 2000]. Although numerous studies have shown that diatoms are readily grazed, it has been suggested that *Phaeocystis* spp. may be more able to resist grazing by producing chemical deterrents such as mucopolysaccharides, and dimethylsulphoniopropionate (DMSP) [e.g. Bautista *et al.*, 1992], including *P. antarctica* in the Ross Sea [*DiTullio and Smith*, 1995]. DMSP is converted into acrylic acid and dimethylsulphate (DMS), compounds which have been proposed to reduce grazing pressure in and around colonies [*Turner and Tester*, 1997]. *Bautista et al.* [1992] measured lower copepod

ingestion rates, gut fluorescence, and abundance when waters of the English Channel were dominated by *Phaeocystis* sp. than during the subsequent diatom bloom in the same region. Studies have found [see *Liss et al.*, 1994 and references therein] that the production by *Phaeocystis* of DMS and acrylic acid from DMSP may deter chemosensory feeders such as copepods and that *Phaeocystis* may have been avoided by grazers due to it's 'unpalatability' or 'poor nutritional quality' [*Liss et al.*, 1994]. Consistent with reduced grazing on *P. antarctica*, *Gowing et al.* [2001] measured fecal pellet fluxes associated with *P. antarctica* that were only about 10% of those measured in waters dominated by diatoms (5 and 45 mg C m^{-2} d^{-1}, respectively).

In addition, *P. antarctica* colonies have a tough outer skin and can reach up to 2 mm in diameter [*Hamm,* 2000], allowing them to resist grazing by microzooplankton once the colonial stage is reached [*Bautista et al.,* 1992]. As a result, microzooplankton have a minimal grazing impact upon phytoplankton stocks in the Ross Sea [*Caron et al.,* 2000]. The combination of possible chemical and mechanical inhibition of zooplankton grazing led *Huntley et al.* [1987] to coin the phrase "the legend of *Phaeocystis* unpalatibilty". It is not surprising then that the presence of *P. antarctica* has been used as an explanation for low zooplankton biomass and grazing [e.g. *Asper and Smith,* 1999; *Moore et al.,* 2000] and in response, some ecosystem models of the Southern Ocean assume that *P. antarctica* are not grazed at all [e.g. *Hecq et al.,* 2000] or are grazed at a much lower rate than diatoms [e.g. *Lancelot et al.,* 2000].

However, there is contrary evidence showing that *Phaeocystis* spp. are indeed grazed by both meso and macrozooplankton. While the colonial habit of many

Phaeocystis species prevents grazing by the smaller microzooplankton, *Hansen et al.* [1994] suggests that meso and macrozooplankton, such as *L. helicina* and the raptorial feeder *M. gerlachei*, are able to actively graze large colonies of *P. antarctica. Hamm et al.* [2001] found that *Phaeocystis* colonies were a potentially valuable food source due to their high fatty acid composition. *Lebour* [1922] observed feeding on *Phaeocystis* sp. by calanoid copepods and experiments by *Huntley et al.* [1987] also found that *Calanus hyperborous* was capable of satisfying its metabolic and growth requirements by consuming *P. pouchetii.* Similarly, *Hansen et al.* [1994] showed that both calanoid copepods (*C. hyperborous* and *C. finmarchicus*) and euphausiids (*Thysanoessa* spp.) actively grazed both solitary and colonial *P. pouchetii*, which comprised up to 36% of their daily C ration [*Hansen et al.,* 1994]. Work in Norwegian waters by *Hamm et al.* [2001] showed that Arctic krill effectively grazed *P. pouchetii* colonies, with both the transfer of C to higher trophic levels and sedimentation of *Phaeocystis* sp. derived organic matter in fecal material being more effective than was commonly believed. Finally, laboratory experiments by *Verity* [2000] showed that calanoid copepods could readily graze both solitary cells and colonies of another closely related prymnesiophyte species, *P. globosa.*

This raises two key questions regarding the unusual meso and macrozooplankton dynamics in the Ross Sea. First, why is zooplankton abundance so much lower than elsewhere in the Southern Ocean, particularly in areas with similar levels of phytoplankton production? Second, considering the conflicting information concerning the ability of meso and macrozooplankton to graze *P. antarctica*, is there an alternative explanation that can explain the extremely low zooplankton abundance

in the *P. antarctica* dominated Ross Sea polynya? To address these questions, I employed a numerical modeling approach, utilizing the Coupled Ice And Ocean (CIAO) model [*Arrigo et al.*, 2003] to examine phytoplankton/zooplankton (P/Z) interactions throughout the spring and summer phytoplankton bloom in the Ross Sea. The CIAO model was chosen because it has been shown to be capable of accurately simulating the temporal dynamics of both the diatom bloom associated with Terra Nova Bay and the *P. antarctica* bloom in the Ross Sea polynya [Figure 2, *Arrigo et al.*, 2003], and is an ideal platform for investigating trophic interactions in these two distinct pelagic communities.

2. Methods

2.2 Model Description

For a complete description of the CIAO ecosystem model please see Chapter 2, in this particular study I utilized the 'simple' Fe parameterization and will focus hereafter on the zooplankton details (see Table 2 for coefficients and parameter values ascribed). In order to assess whether mechanical or chemical defenses by phytoplankton are required to accurately simulate meso and macrozooplankton distributions in the Ross Sea, I formulated CIAO without endowing phytoplankton with these characteristics. In the standard run of the model, a single zooplankton grazer was included that could consume both diatoms and *P. antarctica* without regard to taxa (e.g. no taxonomic preference due to size or possible defense mechanisms). My rationale was that if the model, using a generic zooplankter that feed equally well on both phytoplankton taxa, can successfully simulate both the generally low

Figure 2. a) Spatial comparison of species composition observed during the ROAVERRS cruise and predicted by the CIAO model. b) Time series comparison of Chl *a* predicted by CIAO and that observed via satellite (SeaWiFS) in the two study regions. Averages were calculated in both cases for the regions shown in Figure 1.

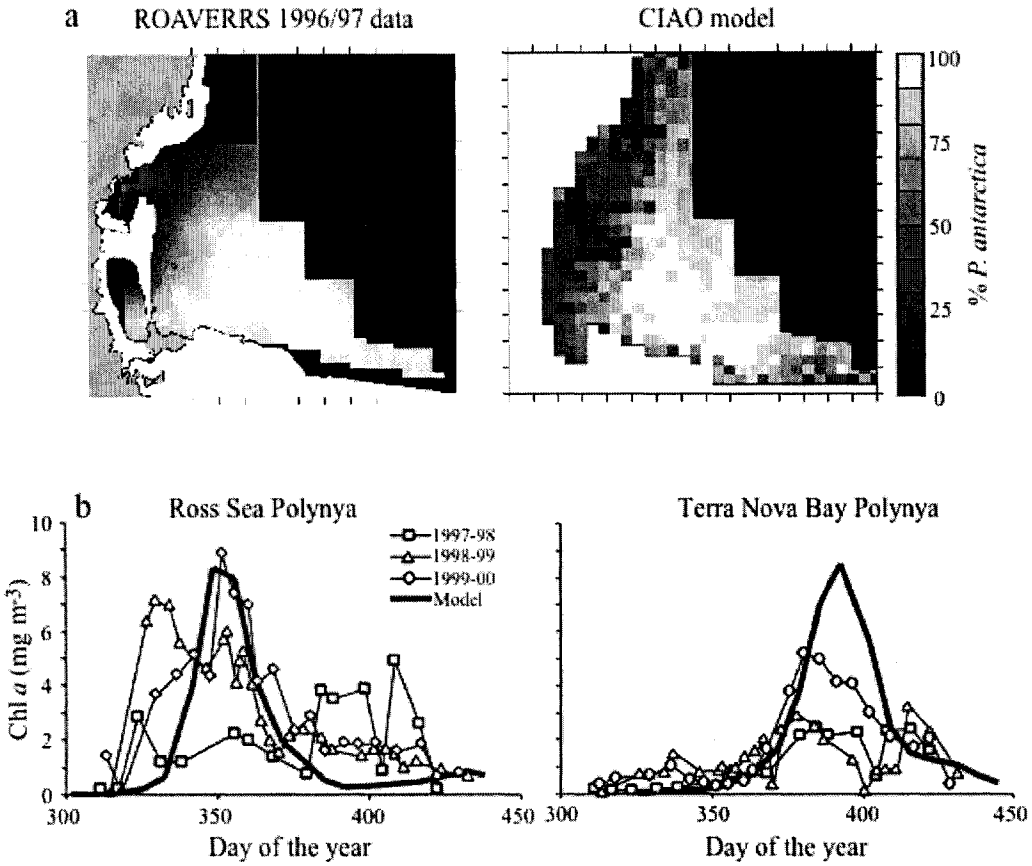

Table 2. A comparison of Zooplankton parameter values from the literature alongside those used in the CIAO model

Parameter	Description	Units	Value	Reference:
G_{max}	Maximum grazing rate	d^{-1}	0.2	*Hecq et al.* [2000]
			0.4	*Pitchford and Brindley* [1999]
			0.48	*Verity* [2000]
			0.4	*This study*
K_z	Grazing half saturation	mg C m^{-3}	60*	*Verity* [2000]
			79*	*Fasham* [1993]
			79*	*Pitchford and Brindley* [1999]
			87*	*Pondaven et al.* [1999]
			182*	*Pondaven et al.* [1999]
			200	*Hecq et al.* [2000]
			85	*This study*
h	Feeding threshold	mg C m^{-3}	7.9*	*Fasham* [1993]
			9.5*	*Verity* [2000]
			9.5	*This study*
x_Z	Specific zooplankton loss	d^{-1}	0.1	*Pondaven et al.* [1999]
			0.325	*Fasham* [1993]
			0.2	*This study*
γ	Assimilation efficiency	N/A	0.62	*Lancelot et al.* [2000]
			0.75	*Fasham* [1993]
			0.8	*Hecq et al.* [2000]
			0.75	*This study*
C:Chl *a*	Carbon:chlorophyll *a* ratio	N/A	50	*This study*

* = value converted from μM N assuming Redfield C/N ratio of 6.6 [*Redfield,* 1963].

zooplankton abundance in the Ross Sea and the higher grazing in Terra Nova Bay relative to the Ross Sea polynya (in addition to observed phytoplankton and nutrient dynamics), then mechanical and chemical defenses by *P. antarctica* are not required to explain the low meso and macrozooplankton abundance in the Ross Sea.

I have elected not to model microzooplankton dynamics because to do so would require simulation of the *P. antarctica* life cycle from small solitary cells to larger colonies in order to accurately simulate the variability in prey size encountered. Although solitary cells are available to microzooplankton grazers early in the *P. antarctica* bloom, the switch to the colonial form is rapid and likely explains the insignificant impact of microzooplankton on *P. antarctica* in the Ross Sea [Caron *et al.*, 2000].

Grazing in CIAO (see: Chapter 2 for detailed equations) is modeled as a simple Holling Type II function of phytoplankton abundance [*Holling,* 1959] such that the rate of grazing is a monod function of the food supply (above a feeding threshold, h) up to a maximum rate of grazing (d^{-1}). The relationship between rate of grazing and prey concentration is controlled by the parameter K_z (the prey concentration at which G_i is half of G_{max}). The rate of change in zooplankton abundance (Z) is a function of the net grazing flux (i.e. G_iZ) and the carbon specific losses (natural mortality, respiration, and higher predation, x_ZZ, see Chapter 2 for a full description). In the standard run, the assimilation efficiency of consumed food (γ) is the same for consumption of both diatoms and *P. antarctica* (see Table 2 for parameter values pertinent to this study). As most zooplankton data are collected via net hauls from depth and generally collect most, if not all, zooplankters present in the water column

(although net avoidance can occur), my results will be presented as depth integrated (throughout the whole water column) zooplankton biomass (g C m^{-2}).

3. Results

Sea ice concentrations in the Ross Sea polynya begin to decrease rapidly around early November, and shortly thereafter, *P. antarctica* is predicted to bloom profusely, with a net biomass accumulation rate of 0.10 d^{-1} between 7 November and its biomass peak on 21 December (Figure 3a). Northward advection of the sea ice prior to melting causes these waters to be weakly stratified, allowing *P. antarctica* to effectively compete with diatoms in this relatively low light environment (Figure 4b), consistent with observed photophysiological differences between the two taxa [*Moisan and Mitchell*, 1999]. Within 2 weeks of the Ross Sea polynya becoming ice free, *P. antarctica* biomass is predicted to reach mean levels of 4 g C m^{-2}, with values of >6 g C m^{-2} in some areas. Throughout the early stages of the *P. antarctica* bloom, zooplankton abundance remains near its winter minimum (~0.049 g C m^{-2}), and increases to only <0.1 g C m^{-2} when the *P. antarctica* bloom peaks in mid December (Figure 3a, 5b).

After mid December, predicted growth rates of *P. antarctica* in the Ross Sea polynya begin to decline due to Fe limitation [see also *Arrigo et al.*, 2003], consistent with field data which indicate that Fe concentrations drop to growth limiting levels in surface waters at this time [e.g. *Sedwick et al.*, 2000]. As the *P. antarctica* bloom begins to wane within the Ross Sea polynya, simulated zooplankton biomass increases, but never attains high levels (Figure 5), eventually peaking at only 0.15 g C

Figure 3. Modeled time series of depth integrated (full water column) phytoplankton and zooplankton biomass (mg C m^{-2}) in the a) Ross Sea and b) Terra Nova Bay Polynya regions. The region denoted 'Ice', and shaded white, is where modeled ice concentrations are ≥50% for each pixel.

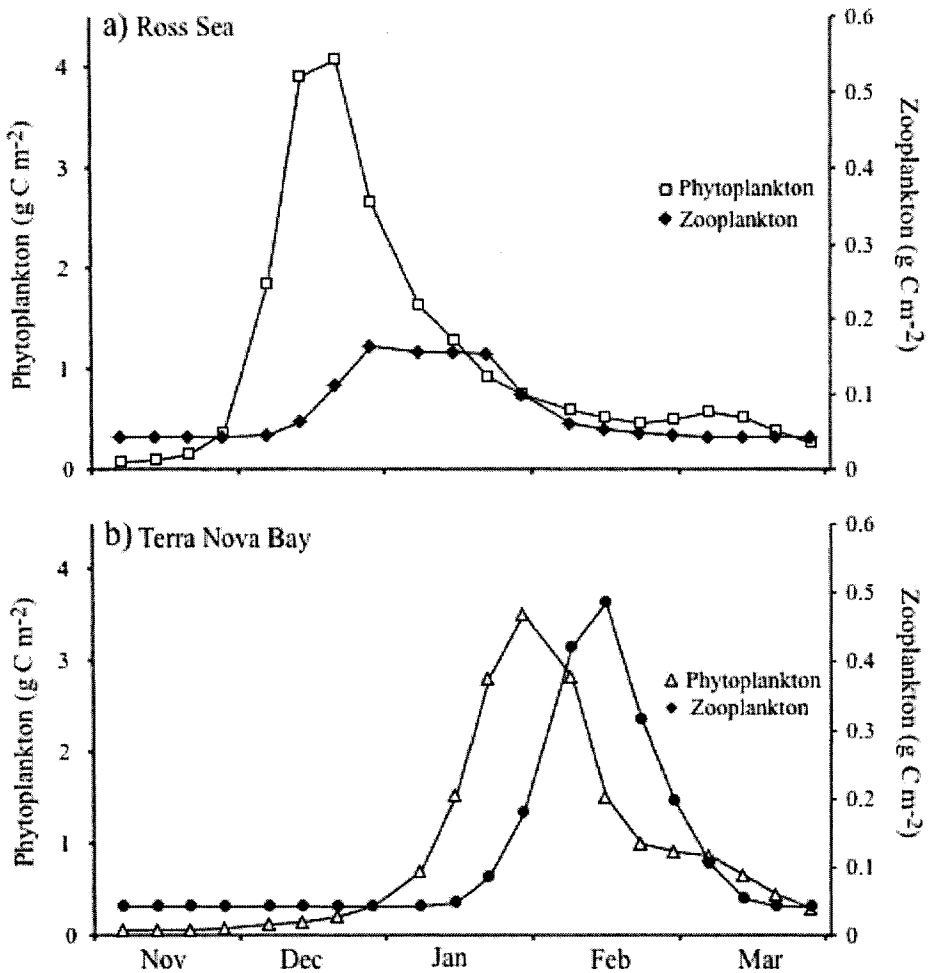

Figure 4. a-d) Modeled surface plots of depth integrated phytoplankton biomass (mg C m^{-2}) and e-h) taxonomic composition (% *P. antarctica*, or 100-%diatoms), at monthly intervals. The region denoted 'Ice', and shaded white, is where modeled ice concentrations are ≥50% for each pixel.

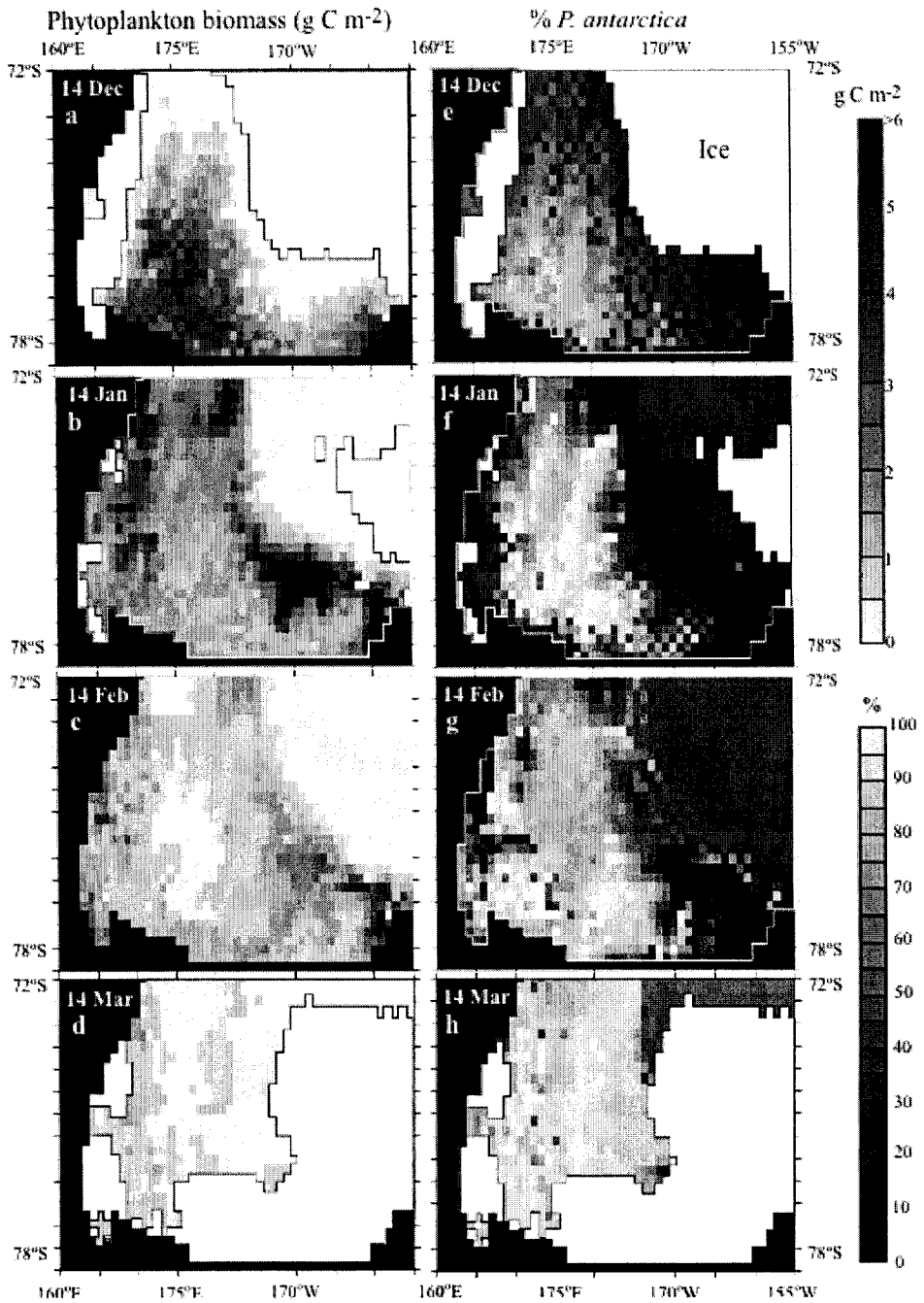

m^{-2} by 28 December (Figure 3a). By mid January, mean zooplankton abundance throughout the Ross Sea polynya is still unchanged [Figure 3a), but a striking spatial pattern emerges. Zooplankton abundance throughout much of the region increases markedly, with the exception of a large area in the center of the Ross Sea polynya that contains the lowest zooplankton biomass of the entire ice free Ross Sea (Figure 5d). This distinct low zooplankton zone is even more pronounced in mid February (Figure 5f) and is always associated with the most extreme *P. antarctica* dominated waters (e.g. Figure 4f). Comparison of the spatial distributions of phytoplankton (Figure 4) and zooplankton (Figure 5) show that the low zooplankton zone coincides with the region where *P. antarctica* had bloomed a month prior but had already dropped to low levels by January (Figure 4b) and February (Figure 4c). Populations of both *P. antarctica* and zooplankton in the Ross Sea polynya changed little during February, maintaining levels of <0.5 g C m^{-2} and <0.05 g C m^{-2}, respectively (Figure 3). Zooplankton exhibited little subsequent change in population size, while *P. antarctica* numbers dropped again in mid April, to <0.1 g C m^{-2}, where they remained for the duration of the simulation.

In contrast to the Ross Sea polynya, Terra Nova Bay remains at least partially ice free all year, and throughout the spring, its waters are mixed below the critical depth [*sensu* Sverdrup 1953] by offshore winds that are twice the frequency and three times the velocity of those associated with the Ross Sea polynya [*Arrigo et al.,* 1998a]. Consequentially, modeled phytoplankton accumulation rates in Terra Nova Bay are negligible in mid December (when *P. antarctica* peaks in the Ross Sea polynya) and diatom abundance remains low (Figs. 3b and 4a). Because development of the diatom

Figure 5. Modeled surface plots of the temporal evolution of depth integrated zooplankton biomass (mg C m^{-2}) at fortnightly intervals. The region denoted 'Ice', and shaded white, is where modeled ice concentrations are ≥50% for each pixel.

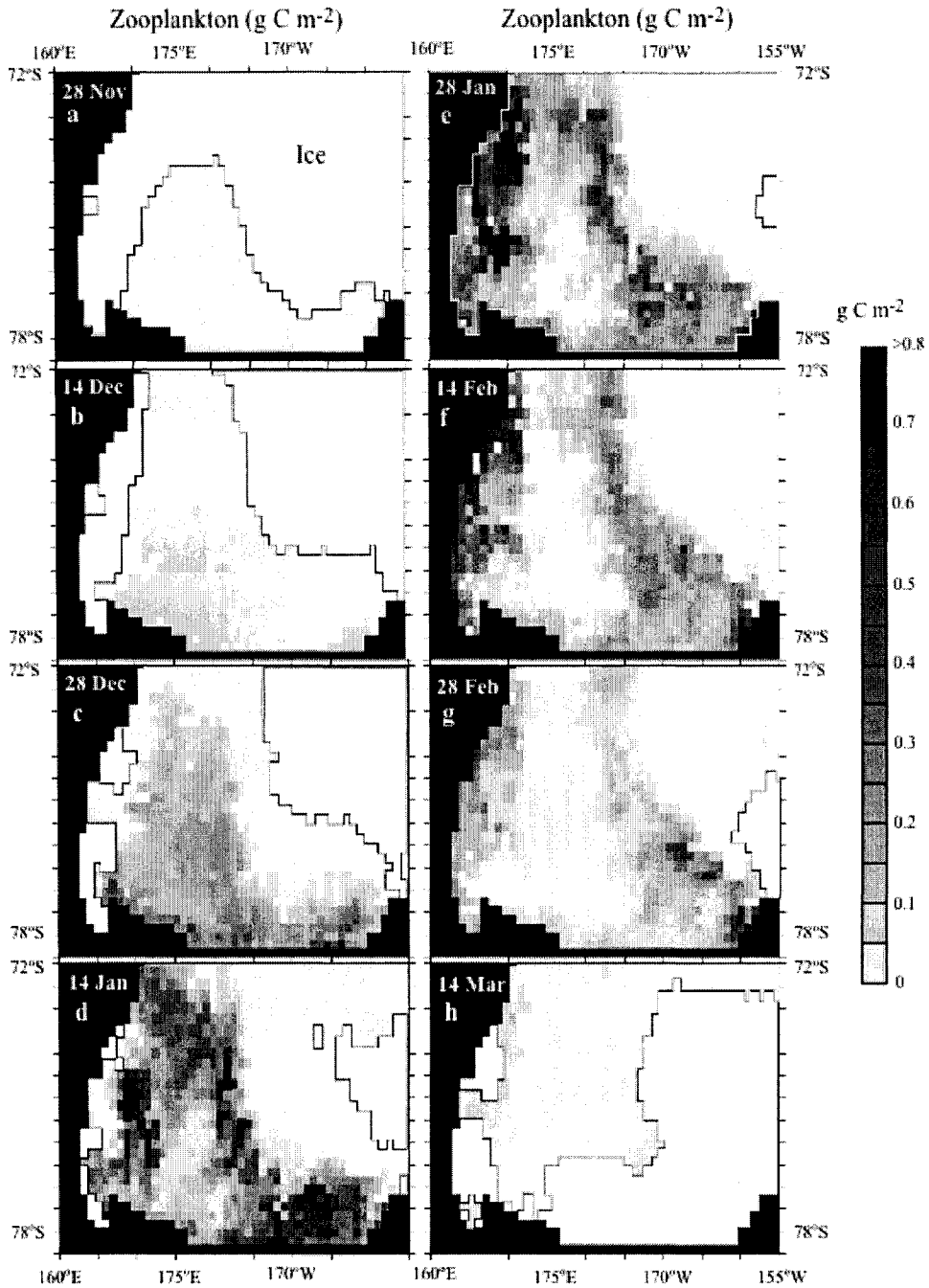

bloom in Terra Nova Bay and in the MIZ surrounding the Ross Sea polynya is slower than in the Ross Sea polynya (Figure 4b), with a biomass accumulation rate of only 0.05 d^{-1} between 7 November and the diatom peak on 28 January (Figure 3b), zooplankton in these diatom dominated waters remain at low levels throughout November and December (Figs. 3b and 5a and b).

Once sea ice in the Ross Sea begins to melt in late December, both in Terra Nova Bay and in the MIZ, surface waters begin to stratify, resulting in mixed layers as shallow as 10 m in depth. These high light environments favor the growth of diatoms, which begin to bloom in January (Figure 4b), with zooplankton biomass increasing soon after (Figs. 3b and 5d). The peak in mean zooplankton biomass in Terra Nova Bay (0.5 g C m^{-2}, Figure 3) lags by approximately 2 weeks the diatom peak in early February (3.5 g C m^{-2}, Figure 3b), with zooplankton abundance in mid February varying spatially from 0.3 to >0.8 g C m^{-2} (Figure 5) throughout Terra Nova Bay and the MIZ in mid February. After mid February, simulated Fe concentrations in Terra Nova Bay and the MIZ begin to fall to levels that limit diatom growth, resulting first in a decline in diatoms and then in zooplankton. By the beginning of March, Fe is almost fully depleted throughout the southwestern Ross Sea, which together with the return of seasonal sea ice, results in low phytoplankton and zooplankton biomass throughout the region.

Comparison of the maximum spatially averaged zooplankton biomass in Terra Nova Bay and the Ross Sea polynya (Figure 1) shows that the Ross Sea polynya reaches only 0.15 g C m^{-2} (Figure 3a), compared to 0.5 g C m^{-2} within Terra Nova Bay (Figure 3b). At individual grid points within the southwestern Ross Sea zooplankton

can reach biomass levels of as high as >0.8 g C m^{-2} (see Figure 5d and e), while the maximum depth integrated abundance predicted by CIAO over the entire southwestern Ross Sea (encompassing all open water up to the 800 m shelf break, see Figure 1) averaged 0.24±0.2 g C m^{-2}, the high standard deviation and lower value being due to the high spatial heterogeneity of the region (see Figure 5 all panels). Values from within my primary areas of interest, the Ross Sea Polynya and Terra Nova Bay Polynya, vary from ~0.1 to ~0.8 g C m^{-2}, in good agreement with the existing measurements of 0.3-0.7 g C m^{-2} (see Table 1). Accordingly, model results suggest that the Ross Sea appears to be at the low end of previously observed estimates of meso and macrozooplankton for the Southern Ocean (Table 1), especially considering its high phytoplankton biomass compared to other Southern Ocean regions [*Arrigo and McClain*, 1994; *Smith and Gordon*, 1997; *Arrigo and Van Dijken,* 2003].

4. Discussion

4.1 The Standard Run

The standard run of the model successfully simulates both the relatively low zooplankton abundance observed throughout the Ross Sea [*Biggs,* 1982, *Sertorio et al.,* 2000, *Huntley and Zhou,* 2000] and the difference in grazing pressure between the Ross Sea polynya and Terra Nova Bay inferred from sediment trap and pigment data [e.g. Dunbar *et al.,* 1998, Goffart *et al.,* 2000; Gowing *et al.,* 2001]. At the same time, the model results reproduce observed phytoplankton taxonomic distributions and population dynamics as well as nutrient dynamics of the region (Figure 2). Of particular importance, the unusually low zooplankton abundance characteristic of the

Ross Sea polynya was simulated without having to ascribe to the zooplankton a lower food preference for *P. antarctica* than for diatoms (e.g. reduced G_{max} or K_z), as has been done in previous studies [*Hecq et al.*, 2000; *Lancelot et al.*, 2000]. I consider the fact that the P/Z dynamics of the southwestern Ross Sea are simulated in the standard run without endowing *P. antarctica* with a uniquely high resistance to zooplankton grazing to be a compelling reason to question whether such resistance plays an important role in structuring phytoplankton community composition in the Ross Sea, as has been previously hypothesized. Note that I am not claiming that these model results prove that defense mechanisms by *P. antarctica* to resist grazing are unimportant, only that there may be an alternative, more significant and straightforward, explanation for the low zooplankton abundance in the Ross Sea.

If chemical and/or mechanical defenses of *P. antarctica* are not responsible for the low zooplankton levels either predicted by the model or observed within the Ross Sea polynya, there must be an alternative explanation. I propose that the low zooplankton abundance observed in the Ross Sea polynya is due simply to the difference in the degree of P/Z coupling between the Ross Sea polynya and Terra Nova Bay. Furthermore, I propose that the low zooplankton abundance in the Ross Sea compared to other regions of the Southern Ocean is due to the reduced P/Z coupling in the Ross Sea resulting from the high phytoplankton growth rates.

As a quantitative measure of the level of coupling between trophic levels, the ratio of the zooplankton specific grazing rate to the phytoplankton specific growth rate (G:μ, hereafter called the G-ratio) has been used [e.g. *Strom et al.*, 2001 and references therein]. A G-ratio that is constant and near unity indicates a high degree

of coupling between the phytoplankton population and their zooplankton grazers [*Strom et al.*, 2001]. This is because in a tightly coupled P/Z system, specific zooplankton grazing rates are able to keep pace with changing specific phytoplankton growth rates (i.e. a high proportion of new phytoplankton production is consumed by the grazing zooplankton). Within Terra Nova Bay (Figure 6b), the G-ratio during the summertime diatom bloom remains almost constant and averages approximately 0.6, indicating that a relatively high degree of P/Z coupling exists there. While not as high as the sub Arctic Pacific and the Antarctic Peninsula which exhibit G-ratios of 0.8 and 0.9, respectively [*Strom et al.*, 2001 and references therein], the degree of P/Z coupling in Terra Nova Bay was much greater than in the Ross Sea polynya, where the G-ratio during the *P. antarctica* bloom was more variable and far from unity, ranging from 0.10 to 35 (Figure 6a).

The relatively large departure in the G-ratio from unity within the Ross Sea polynya is due to the highly asynchronous dynamics of phytoplankton growth rates and zooplankton grazing rates predicted for these waters (Figure 6a and 6b). During the initial stages of the *P. antarctica* bloom in the Ross Sea polynya, zooplankton grazing is unable to keep pace with the rapidly increasing *P. antarctica* population, and the G-ratio is $<<1$ (Figure 6a). As the *P. antarctica* bloom progresses and Fe concentrations are drawn down to growth limiting levels, G begins to increase faster than μ and the G-ratio increases accordingly. Once the *P. antarctica* bloom peaks, the continued increase in G, combined with the Fe mediated decline in μ, yields values for the G-ratio that are $>>1$ (Figure 6a). Hence, the exaggerated boom/bust cycles for *P. antarctica* results in an almost complete decoupling from the zooplankton in the Ross

Figure 6. Temporal changes (every 4 hours) in the G-ratio (note log scale) over the 50 day period coinciding with the peak of the respective blooms in the a) Ross Sea polynya and b) Terra Nova Bay. Model results were taken from one discrete station within the Ross Sea polynya and Terra Nova Bay (76.5°S, 177°E and 75°S, 164°E, respectively).

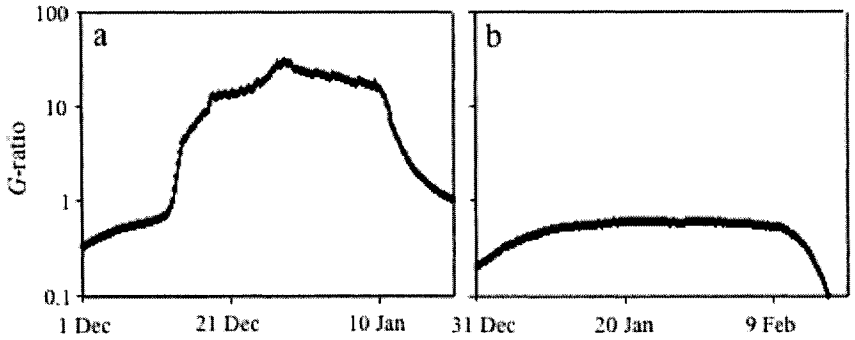

Sea polynya. In Terra Nova Bay, slower initial diatom accumulation rates allow G to increase along with μ and therefore the G-ratio remains stable and close to unity (Figure 6b). However, P/Z coupling is not perfect (G-ratio$\neq$1), and the zooplankton are unable to prevent a diatom bloom in mid summer. At the end of the season in both Terra Nova Bay and the Ross Sea polynya, the G-ratio falls quickly due to the declining zooplankton grazing rate in response to the lower phytoplankton biomass levels (Figure 6).

4.2 The role of shade acclimation

In theory, the reduced P/Z coupling predicted in the Ross Sea polynya could either be due to higher rates of *P. antarctica* biomass accumulation or too low initial zooplankton concentrations (Z_{min}), which would make it difficult for zooplankton to build up enough biomass to have an impact on phytoplankton abundance. It is straightforward to show that relative difference in zooplankton dynamics between the Ross Sea polynya and Terra Nova Bay are insensitive to the value of Z_{min} (see below). Therefore, the reduced P/Z coupling predicted in the Ross Sea polynya is due to the rapid early season rate of *P. antarctica* growth and accumulation. The high rate of biomass accumulation is a direct result of the fact that *P. antarctica*, both in the model and in nature [Cota *et al.*, 1994; Moisan and Mitchell 1999; Stuart *et al.*, 2000], are shade acclimated and therefore are able to achieve a positive net growth rate at lower light levels than are diatoms. Thus, as soon as waters of the Ross Sea polynya begin to be blown clear of ice by offshore winds, *P. antarctica* responds with extremely rapid growth, decoupling them from the still quiescent zooplankton population. This

prediction by the model is consistent with observed bloom dynamics of *P. antarctica* in the Ross Sea polynya, where concentrations in excess of 5 mg m^{-3} have been observed in waters where ice concentrations exceeded 50% [*Smith and Gordon,* 1997]. In Terra Nova Bay, early season mixing is very deep (>200 m) and exceeds the critical depth for both taxa. Once the ice in Terra Nova Bay begins to melt, strong vertical stratification and high solar elevation favors the growth of diatoms. Both populations exhibit different degrees of boom/bust dynamics, and although *P. antarctica* grows faster in the earlier stages of its bloom, once conditions become more favorable in Terra Nova Bay, diatom accumulation rates can also be high (even though early season rates are low). In fact, both taxa display similar maximal specific growth rates (0.5 d^{-1}).

Acclimation by phytoplankton to low light levels includes changes in cellular pigment content or composition [*Stuart et al.,* 2000] related to the number of photosynthetic units and reduction in the quantum yield of photosynthesis (ϕ). Consistent with shade acclimation, Moisan and Mitchell [1999] found high chlorophyll specific absorption (a^*_{ph}) and maximum quantum yield (ϕ_m) for *P. antarctica* under low light levels. Similarly, Stuart *et al.,* [2000] showed that prymnesiophytes had higher photosynthetic efficiency (α^*) and reached their theoretical maximum photosynthetic rate at lower irradiances (lower E_k) than diatoms under low light regimes, in agreement with work by *Cota et al.,* [1994] who also observed higher assimilation rates (P_m^*) and α^* by *Phaeocystis* sp. in the Greenland Sea. These changes in the photosynthetic apparatus require high ambient nutrient levels (including Fe), which are present early in season in the southwestern Ross Sea

[*Sedwick et al.,* 2000]. The colonial form of *P. antarctica* photoacclimates by storing excess photosynthate within its colonial matrix [*Lancelot and Rousseau,* 1994; *Robinson et al.,* 2003]. Utilization of the photosynthate stored under higher surface light levels when light levels decrease during deep mixing could allow *P. antarctica* to outcompete diatoms under the early season low light levels.

The ability to shade acclimate may be of major importance in decreasing P/Z coupling and promoting phytoplankton bloom development in other high latitude seas, where irradiance is the major determinant of photosynthetic and growth rates. For example, Boyd *et al.,* [1995] measured a high degree of shade acclimation for phytoplankton during the early spring bloom in the Bellingshausen Sea, Antarctica, where phytoplankton biomass reached 8 g C m^{-2} and production rates were approximately 0.75 g C m^{-2} d^{-1}. During this study, P^*_m (0.70±0.04 mg C mg Chl a^{-1} h^{-1}), E_k (<20 μmol quanta m^{-2} s^{-1}), and the C:Chl *a* ratio (33) were all low while α^* was high (0.048±0.009 mg C mg Chl a^{-1} h^{-1}/μmol quanta m^{-2} s^{-1}), all indicative of shade acclimation. Growth rates were 0.1 d^{-1}, similar to rates predicted by CIAO for the Ross Sea polynya, despite low irradiance due to ice cover and a mixed layer depth (MLD) of 70 m [Boyd *et al.,* 1995]. Calculation of the compensation irradiance put the critical depth at between 60 and 70 m [Boyd *et al.,* 1995], and consequently, the phytoplankton were sufficiently adapted to attain net growth in the low light environment [sensu *Sverdrup,* 1953]. Like in the Bellingshausen Sea, shade acclimation appears to be an important feature of the early season bloom in the Ross Sea, both structuring the phytoplankton community and allowing high primary production and biomass accumulation. Similar work by *Holm-Hansen and Mitchell*

[1991] during the RACER expedition near Gerlache Strait also found evidence of shade acclimation associated with the early stages of the phytoplankton bloom, including low P^*_m (1.1 mg C mg Chl a^{-1} h^{-1}), low E_k (~ 18 μmol quanta m^{-2} s^{-1}) and high α^* (0.06 mg C mg Chl a^{-1} h^{-1}/μmol quanta m^{-2} s^{-1}) .

In contrast, phytoplankton in the high latitude sub Arctic Pacific Ocean seldom bloom and the region is considered to be characteristically HNLC [*Banse and English*, 1999]. This lack of a bloom is typically explained by the dominance of smaller cells with a lower surface area to volume ratio in these Fe depleted waters which are readily grazed by the quickly responding microzooplankton community (i.e. the G-ratio is higher). However, the lack of Fe has also been shown to diminish the ability of the phytoplankton to shade acclimate, resulting in low growth rates, with Fe and light proposed to be co limiting [Maldonado *et al.*, 1999]. I hypothesize that it is the increased capacity for photoacclimation to lower irradiances that may structure the P/Z dynamics in high nutrient, high latitude waters. Nutrients (including Fe) play a controlling role in two ways: first, higher nutrients allow phytoplankton to synthesize the photosynthetic machinery required to photoacclimate, enabling early season growth rates that are sufficiently fast to decouple them from the meso and macrozooplankton grazers. Second, higher nutrients will favor larger cells (or the formation of colonies) which are more likely to become mechanically decoupled from the fast growing microzooplankton. Both mechanisms likely play a role during the *P. antarctica* bloom in the Ross Sea polynya where solitary *P. antarctica* cells are potentially susceptible to grazing by microzooplankton early in the bloom, albeit only a short period of time. This reduced opportunity for grazing likely explains the low

microzooplankton abundance in the Ross Sea and why my model, which does not explicitly include microzooplankton grazers, is still able to simulate the P/Z dynamics of the Ross Sea.

4.3 Sensitivity Analyses

Model predictions obviously depend on the coefficient values assigned, and although grazing coefficients used in CIAO are not always derived from experimental or field data from the Ross Sea, all values lie well within literature values (Table 2). Furthermore, observed distributions of nutrients, phytoplankton, zooplankton, fecal pellet fluxes, and pigments indicative of zooplankton grazing all provide constraints necessary to evaluate the response of the model to a given coefficient suite. Sensitivity of the CIAO model to changes in coefficients that control phytoplankton growth rates was tested previously and dynamics and distributions of both *P. antarctica* and diatoms were shown to be particularly sensitive to changes in photosynthetic parameters [*Arrigo et al.*, 2003].

Here I focus on the sensitivity of the model to changes in grazing related parameters (K_z, x_Z, G_{max}, Z_{min}, h) while fixing all other coefficients, including those controlling phytoplankton growth. The goal of this analysis is to assess the degree to which my conclusions depend on the coefficient values selected and to examine the relative control that grazing exerts upon the two different phytoplankton populations. Sensitivity of the model to changes in grazing coefficients (see below) was assessed by approximately halving and doubling the coefficients and subsequently comparing the results (Figure 7) to the standard run (Figure 3). The resulting range in coefficient

Table 3. Actual values used in the sensitivity tests presented in Figure 7.

Parameter	Description	Increase	Decrease	Standard	Units
K_z	Grazing half-sat constant	170	40	85	mg C m^{-3}
G_{max}	Maximum grazing rate	0.8	0.2	0.4	day^{-1}
h	Feeding threshold	20	5	9.5	mg C m^{-3}
x_Z	Specific zooplankton carbon losses.	0.4	0.1	0.2	day^{-1}
Z_{min}	Minimum zooplankton concentration	4	1	2	mg C m^{-3}

Figure 7. Sensitivity tests of phytoplankton and zooplankton biomass (mg C m^{-2}) from the Ross Sea polynya and Terra Nova Bay. Parameters were adjusted to be approximately twice and half the 'standard run' values (see Table 2). Adjustments were made to K_z, G_{max}, h, x_Z, and Z_{min}. See Table 3 for actual values assigned.

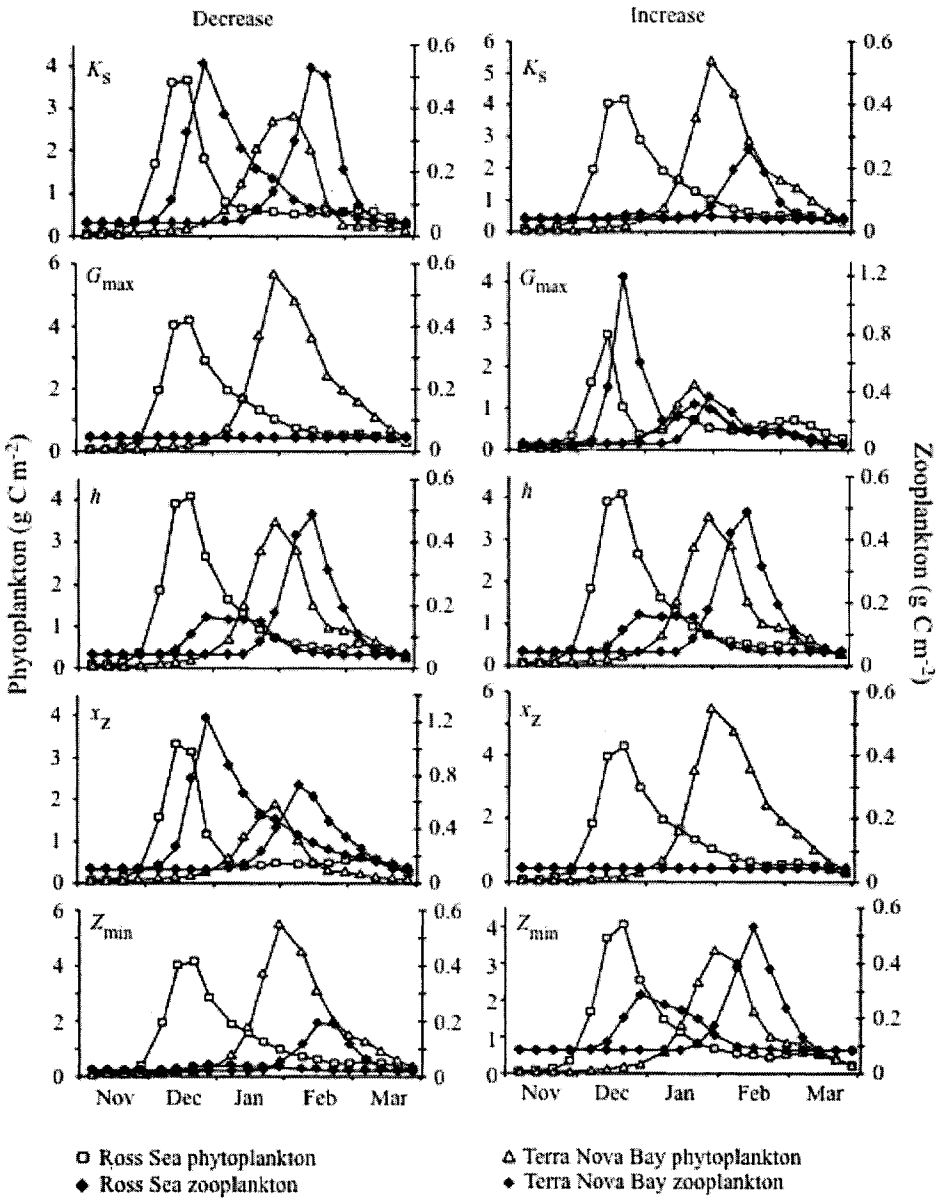

values tested was consistent with those found in the literature (Tables 2 and 3). Model sensitivity was evaluated and presented with respect to the ability of CIAO to reproduce phytoplankton and zooplankton distributions in Terra Nova Bay and the Ross Sea polynya.

Increasing K_z and x_Z and reducing G_{max} all resulted in reduced P/Z coupling and resulted in a significant, and hitherto unobserved, increase in phytoplankton and decrease in zooplankton abundance in Terra Nova Bay, with little change in the Ross Sea polynya (Figure 7). Zooplankton levels in the Ross Sea polynya and Terra Nova Bay were approximately equal when K_z was reduced (Figure 7), also contrary to existing observations. This parameter is the most important factor controlling the rate of response of the zooplankton to changes in the phytoplankton standing crop and the observed regional disparity in zooplankton biomass. CIAO also was sensitive to increases in G_{max} and reductions in x_Z (Figure 7), resulting in excessive P/Z coupling and leading to the unrealistic prediction of greater zooplankton abundance in the Ross Sea than in Terra Nova Bay and drastic reductions in phytoplankton in both regions. While a 50% reduction in Z_{min} leads to unrealistically high phytoplankton levels in both Terra Nova Bay and the Ross Sea polynya, increasing Z_{min} to 4 mg C m^{-3} results in satisfactory phytoplankton dynamics and regional differences in zooplankton abundance that are similar to the standard run. Finally, the rate of increase in the phytoplankton standing crop is far too great for any realistic value of the minimum grazing threshold, h, to impact the dynamics of the region, even when increased to 20 mg C m^{-3} (~ 0.4 mg Chl *a* m^{-3}) (Figure 7).

Results of all sensitivity analyses indicate that substantial changes in model coefficients controlling the degree of P/Z coupling generally result in phytoplankton and zooplankton dynamics that are inconsistent with observed patterns. The sensitivity analysis supports the initial conclusion from the standard run that the dynamics of phytoplankton and zooplankton are controlled strongly by the degree of P/Z coupling. Furthermore, the lack of zooplankton in the Ross Sea polynya is only simulated in those cases where phytoplankton and zooplankton populations were substantially decoupled. In all cases, the change in phytoplankton biomass when the P/Z coupling was perturbed was much greater in Terra Nova Bay than in the Ross Sea polynya (Figure 7, all panels). This supports observations which indicate that zooplankton play a greater role in controlling the phytoplankton populations of Terra Nova Bay than of the Ross Sea polynya.

5. Implications

Shade acclimation by *P. antarctica* explains its ability to become decoupled from the grazing zooplankton. Slower initial growth by diatoms allows the zooplankton to control phytoplankton biomass to a greater degree in Terra Nova Bay, but once conditions are optimal, diatoms also can bloom rapidly. Shade acclimation may be a feature of high latitude phytoplankton blooms, especially those which occur during the early spring and in association with relatively deep mixed layers. Moreover, the differing taxonomic capacities to shade acclimate may control the early spring phytoplankton community structure, and may lead to a species shift later in the summer when MLD depths are shallower and irradiance levels more suited to non low

light adapted species. It is also possible that Fe supply may be a controlling influence upon the degree of P/Z coupling, by either facilitating shade acclimation and higher growth rates at low light levels and/or altering the size structure of the phytoplankton community and its associated grazers. Likewise, zooplankton species specific life history traits, grazing parameters, and/or feeding adaptations could also have an impact on the degree of P/Z coupling observed. While not explicitly simulated, these effects are controlled by h, the feeding threshold, and as stated earlier (Figure 7), the model results and conclusions are insensitive to this parameter.

If much of the *P. antarctica* production is not grazed by the zooplankton, what is the fate of the high levels of C fixed during its growth? *P. antarctica* has been shown [Arrigo *et al.*, 2000] to fix >100% more C per mole phosphate (PO_4) consumed than diatoms, and thus the eventual fate of photosynthetically fixed C is of major interest, given the significant role of the Southern Ocean in oceanic C storage [Caldeira and Duffy 2000]. Generally, the bacterial community is most likely to utilize the C available at the termination of the *Phaeocystis* bloom, but in the Ross Sea, where bacterial numbers are low [Ducklow *et al.*, 2000], evidence from sediment traps [e.g. *DeMaster et al.*, 1992, *Dunbar et al.*, 1998] and *in situ* observations [e.g. *DiTullio et al.*, 2000] suggests that the senescent cells may sink intact out of the euphotic zone once Fe is exhausted in the surface waters. The contribution of zooplankton to the vertical C flux appears to be low in the Ross Sea polynya, and the fate of sinking *P. antarctica* cells relative to enhanced fecal pellet fluxes in Terra Nova Bay is as yet unknown. However, *DiTullio et al.* [2000] observed evidence of photosynthetically

active *P. antarctica* cells at depth, indicating rapid export from surface waters. This could be due to aggregation and subsequent rapid sinking, or extreme mixing events.

The impact of the simpler food web within the Ross Sea polynya may have implications for the efficiency of C flux to deep waters. Even if *P. antarctica* can fix more C per mole PO_4 than diatoms, the efficiency of its transport from the euphotic zone (i.e. the depth of remineralization) is crucial to its impact on atmospheric CO_2 levels. It is feasible that rising atmospheric CO_2 may induce changes in water column stratification, via increased precipitation or ice melt [*Sarmiento et al.,* 1998] and this may subsequently alter early season water column structure and irradiance. These physical changes could then lead to shifts in the taxonomic composition and growth rates of the spring phytoplankton, with possible implications for the ensuing food web structure (this study), nutrient uptake dynamics [*Arrigo et al.,* 2000] and C export [e.g. *this study; Boyd and Newton,* 1995] of the region. All these factors are of real importance in understanding the quantity and fate of CO_2 fixation in both the southwestern Ross Sea and the global ocean in general.

Examination of the CIAO model shows it is possible to accurately simulate the distribution of zooplankton and phytoplankton in the southwestern Ross Sea using model coefficients that are in agreement with literature values. Results suggest that the generally low zooplankton biomass in the Ross Sea can be explained simply by the reduced degree of P/Z coupling resulting from rapid phytoplankton growth at the early stages of the bloom. Furthermore, the lower zooplankton abundance in the Ross Sea polynya than in Terra Nova Bay can be explained without invoking mechanical or chemical defense strategies by *P. antarctica.* While model results cannot eliminate

the possibility that such strategies exist, I have shown that it is possible to accurately simulate zooplankton biomass without them.

Any defense strategy by *P. antarctica* is likely to be of lesser significance than its greater degree of shade acclimation, leading to higher growth rates and reduced P/Z coupling, relative to diatoms. Therefore, the true adaptation by *P. antarctica* to resist grazing may reside in its ability to attain net growth rates under low light conditions, rather than any other defense mechanisms previously introduced. It is reasonable to expect, therefore, that accumulation of *P. antarctica* in the Ross Sea polynya is under bottom up control (nutrients, Fe) while the diatom community in Terra Nova Bay is under both bottom up (nutrients, Fe) and top down (grazing) control.

The role of the different food webs in the Ross Sea on the fate of the high levels of organic C fixed at the end of the growing season is, as yet, unknown. Although C export should be more efficient in Terra Nova Bay than in the Ross Sea polynya, because of the enhanced contribution of zooplankton to the vertical C flux via fecal pellet fluxes, lack of significant bacterial remineralization may well elevate the sinking fluxes of senescent *P. antarctica* cells. Accordingly, the comparative lability of the variable forms of C export in controlling the fate of organic C in the Ross Sea requires further scrutiny. The Ross Sea may well provide an ideal natural laboratory for the study of two boom/bust populations with different nutrient drawdown ratios, food webs, life cycles, and photoacclimation capacities.

Chapter 4

The impact of iron, phytoplankton biogeochemistry and physical processes on CO_2 fluxes

Abstract. I present results examining nutrient and carbon biogeochemistry within the Ross Sea, focusing on the sensitivity of ecosystem dynamics to taxon-specific nutrient utilization parameters and the impact of alleviating Fe-limitation of phytoplankton growth. The CIAO model of the Ross Sea was modified to include air-sea CO_2 exchange and non-Redfield C/N/P uptake ratios for the dominant phytoplankton taxa. Results show that the Ross Sea was a substantial sink for atmospheric CO_2, driven by the high primary productivity prior to the onset of Fe limitation. Taxon-specific C/N/P uptake ratios controlled the relative rate of removal of each macronutrient, while Fe availability constrained the absolute magnitude of utilization. When Redfield C/N/P stoichiometry was applied to both phytoplankton taxa, net primary production (NPP) was overestimated in areas normally dominated by diatoms and underestimated in regions of *Phaeocystis antarctica* dominance, and macronutrient dynamics are misrepresented. Simulated shifts in phytoplankton taxonomic composition significantly altered uptake of atmospheric CO_2 when the phytoplankton were dominated by diatoms (-70%) or *P. antarctica* (+35%). The ability to bloom later in the season afforded *P. antarctica* a relatively greater role than diatoms in controlling the air-sea flux of CO_2 in the Ross Sea. In response to alleviation of Fe-limitation, both total Ross Sea NPP and CO_2 uptake increased by 30%. The response

of the carbon cycle to Fe fertilization was predicted to be complex and its magnitude and nature were dictated by patterns of macronutrient utilization.[1]

[1] Elements of this work were originally published as: Tagliabue, A. and K. R. Arrigo. 2005. Iron in the Ross Sea: 1. Impact on CO2 fluxes via variation in phytoplankton functional group and non-Redfield nutrient stoichiometry. Journal of Geophysical Research – Oceans. doi: 10.1029/2004JC002531

1. Introduction

The importance of iron (Fe) to phytoplankton growth and carbon dioxide (CO_2) uptake in the Southern Ocean has been established via both bottle enrichments [e.g. *Martin et al.,* 1990; *De Baar et al.,* 1995; *Sedwick et al.,* 2000] and four separate Southern Ocean *in situ* Fe release experiments [*Boyd et al.,* 2000; *Gervais et al.,* 2002; *Coale et al.,* 2004]. In this high nutrient-low chlorophyll (HNLC) region of the global ocean, phytoplankton fixation of CO_2 and biomass accumulation is limited by Fe availability in the surface ocean. This results in a large fraction of nitrate (NO_3), phosphate (PO_4), and silicic acid ($Si(OH)_4$) remaining unutilized at the end of the growing season. Box models suggest that Fe-mediated macronutrient exhaustion could increase uptake of atmospheric CO_2 in the Southern Ocean by 1-2 Pg C [*Sarmiento and Orr,* 1991] and reduce the partial pressure of atmospheric CO_2 (pCO_2) levels by as much as 100 ppm [*Peng and Broecker,* 1991]. Indeed, it has been proposed [*Martin,* 1990] that an increase in the Fe supply to the Southern Ocean could be the major component of glacial–interglacial CO_2 variability via a more efficient biological pump [*Watson et al.,* 2000]. Physical processes such as ocean stratification and ventilation of intermediate waters have also been proposed as drivers of CO_2 variability over glacial-interglacial timescales [e.g. *Toggweiler* 1999]. Nevertheless, oceanic Fe fertilization is being considered as a mechanism by which humankind might reverse the trend of ever-increasing atmospheric CO_2 levels [e.g. *Markels and Barber,* 2000]. In fact, as many as eight U.S. patents on this topic have been filed thus far to develop Fe-based CO_2 mitigation strategies [*Chisholm et al.*, 2001].

Located within the Southern Ocean, the Ross Sea (Figure 1) is an excellent location within which to investigate the role of Fe in regulating net primary production (NPP) and air-sea CO_2 exchange. Phytoplankton blooms here are among the largest observed in the Southern Ocean [*Arrigo and Van Dijken,* 2003a], resulting in some of the most CO_2 depleted surface waters in the world [*Takahashi et al.,* 2002]. There are usually two spatially separated blooms, characterized by distinct phytoplankton assemblages [*Arrigo and McClain,* 1994; *Smith and Gordon,* 1997; *Arrigo et al.,* 2000; *Arrigo and Van Dijken,* 2004]. A bloom of the colonial prymnesiophyte *Phaeocystis antarctica* becomes established in the weakly stratified waters of the Ross Sea polynya (RSP, Figure 1) by the end of November. Diatom blooms (primarily *Fragilariopsis* spp.) develop later, dominating areas of substantial ice melt, such as the persistent Terra Nova Bay polynya (TNBP, Figure 1), with algal biomass peaking by the end of January [*Arrigo et al.,* 1998; 2000; *Smith et al.,* 2000, *Arrigo and Van Dijken* 2004].

Previous studies in the Ross Sea [e.g. *Bates et al.,* 1998; *Gordon et al.,* 2000; *Sweeney et al.,* 2000b] have shown that biological activity in the RSP leads to large deficits in water column total CO_2 (TCO_2) and pCO_2. *Bates et al.* [1998] measured TCO_2 depletion relative to wintertime values of up to 200 μmol kg^{-1} in surface waters, which resulted in a 180 μatm drop in pCO_2. Alkalinity was virtually constant with changing TCO_2, indicating that calcification did not have a significant impact upon pCO_2 in the Ross Sea [*Bates et al.,* 1998]. *Carlson et al.* [2000] showed that the vast majority of total organic carbon (TOC) produced in the Ross Sea was partitioned into particulates, with little entering the dissolved organic carbon (DOC) pool (~11%).

Figure 1. A map of the southwestern Ross Sea, showing the locations of the two polynya regions. Inset shows locations where model output was extracted to represent the Terra Nova Bay polynya (A, 74.5°S–75.5°S, 165°E – the coast), the Ross Sea polynya (B, 75.5°S–77°S, 172°E–177°E), and the central Ross Sea (C, 76°S–77°S, 175°E to 180°). Spatial mean values for model output representing the southwestern Ross Sea were extracted from the region bounded by 73°S–78°S and 160°E–155°W.

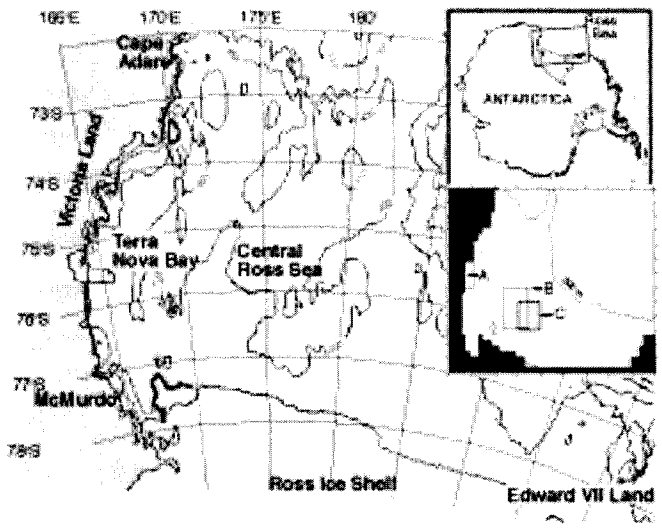

Furthermore, the proportion of TOC that entered the DOC pool was variable between taxa; 9% of TOC in the *P. antarctica*-dominated RSP and 19% of TOC in the diatom-dominated waters [*Sweeney et al.,* 2000a].

Water column measurements over multiple field seasons within these distinct bloom locales have shown that each taxon exhibits unique nutrient uptake ratios, with *P. antarctica* taking up more than twice as much CO_2 per mole of PO_4 removed than diatoms. C/P uptake ratios (mol:mol) of approximately 130 and 65 have been measured for *P. antarctica* and diatoms, respectively [*Arrigo et al.,* 2000; 2002a]. N/P uptake ratios of the two taxa are also significantly different, with values of 20 measured in *P. antarctica*-dominated waters and <10 in areas of diatom-dominance [*Arrigo et al.,* 2000; 2002a]. Both the C/P, and N/P uptake ratios are significantly different from the canonical 'Redfield ratio' of 106C:16N:1P [*Redfield,* 1934], a ratio that is used as a 'currency converter' by many ecosystem models. An important repercussion of these different taxon-specific ratios is that, in the absence of limitation by light or another nutrient (such as Fe), *P. antarctica* should be driven to NO_3 limitation and diatoms to PO_4 limitation. The causes of these taxonomic differences are, as yet, unknown, but importantly, they have been measured during multiple field programs [*Arrigo et al.,* 2002a] and appear to be conserved in the particulate matter exported to depth [*Arrigo et al.,* 2002a; *Dunbar et al.*, 2003]. High growth rates of *P. antarctica* in the RSP decouple these phytoplankton from their associated grazers to a greater degree than in the TNBP, suggesting that export of C from surface waters may be more efficient in diatom dominated waters [*Dunbar et al.,* 1998; *Tagliabue and Arrigo,* 2003]. Both blooms are terminated by exhaustion of Fe, with approximately

one third of the macronutrients remaining at the end of the growing season [*Sedwick et al.*, 2000; *Arrigo et al.*, 2000; *Coale et al.*, 2003].

Ecosystem dynamics in the Ross Sea have been successfully simulated using the CIAO model (see Chapter 2). Such regions are usually absent from the low spatial resolution domains of global ocean/climate models. It is therefore of major interest to examine how a higher resolution, regional ecosystem model with a more realistic representation of phytoplankton functional groups, Fe cycling, and taxon-specific biogeochemical characteristics responds to Fe perturbations.

In this study, I modified the existing CIAO model [*Arrigo et al.*, 2003a] by adding PO_4 and components of the carbonate system as new tracers and a formulation for air-sea CO_2 exchange. These new tracers allowed me to more accurately simulate the dynamics of a diverse phytoplankton assemblage where different taxa exhibit unique nutrient uptake ratios. Specifically, my goal during this study was to investigate how sensitive ocean biogeochemistry and air-sea CO_2 exchange is to non-Redfield nutrient utilization ratios, phytoplankton taxonomic composition, and alleviation of Fe-limitation (see Table 1 for more details). An analysis of more realistic Fe fertilization scenarios can be found in [*Arrigo and Tagliabue*, 2005]. Prior to including PO_4 in the model, CIAO had overestimated diatom production in waters with high Fe content. This is because, given their low N/P uptake ratios [*Arrigo et al.*, 2002a], these waters should have been driven to PO_4 limitation.

Table 1. Summary of the Different Experimental Conditions.

Experiment	Details	Fe fertilized?
standard	Parameters as per Table 2a	no
nobio	No biology	no
redfield	C/P = 106 and C/Fe = 250,000	no
alldia	All phytoplankton assumed to be diatoms*	no
allpha	All phytoplankton assumed to be *P. antarctica**	no
fefert	Fe limitation term set to 1.0 (no Fe limitation)	yes

*Species-specific values can be found in Table 2a.

2. Methods

2.1. New Tracers

A full description of the CIAO ecosystem model can be found in Chapter 2, hereafter I will provide a brief description of the parameterizations included for this particular study. All parameter values (Table 2a and b) are in carbon (C) units unless otherwise stated and this study utilized the 'simple' Fe cycle parameterization (i.e. only one Fe pool). The rate of change in PO_4 is a function of phytoplankton uptake and taxon-specific exudation, both scaled by the fixed taxon-specific P/C ratio, and of the soluble fraction of unassimilated grazing products, dead phytoplankton, and dead zooplankton, as well as zooplankton excretion of P to balance the C respired while conserving the C/P ratio. Due to the distinct C/P ratios exhibited by each phytoplankton taxa, the P detrital pool is computed explicitly. Remineralization of detritus is assumed to resupply PO_4 and non-particulate losses of P (e.g. exudation) are instantaneously allocated to the PO_4 pool.

Sources of DOC are phytoplankton exudation, and the soluble fraction of unassimilated grazing products, dead phytoplankton, and dead zooplankton. Changes in DOC are added to a background (minimum) DOC concentration (DOC_{min}) of 40 μM which represents the more stable refractory pool [*Carlson et al.*, 2000]. Losses of DOC are restricted to bacterial remineralization of the labile pool ($r_{DOC}DOC_{lab}$), where $DOC_{lab} = DOC - DOC_{min}$.

Changes in water column total carbon dioxide (TCO_2) are controlled by sea-air CO_2 exchange (FCO_2), taxon-specific phytoplankton photosynthesis, zooplankton respiration, and the remineralization of detritus and DOC. Alkalinity is set 2330 μmol

Table 2a. Parameter values used in the standard run.

Parameter	Value	Units	Source
Atm. pCO_2	365	μatm	*Takahashi et al.*, [2002]
Initial TCO_2	2225	μM	*Arrigo et al.*, [2000]
Total alkalinity	2330	μeq	*Bates et al.*, [1998]
C/P_i	133.1/63.3	mol mol^{-1}	*Arrigo et al.*, [2000]
C/Fe_i	$450x10^3/100x10^3$	mol mol^{-1}	This study
Ks_{Fei}	0.01/0,1	nM	*Arrigo et al.*, [2003a]
β	0.1	no units	This study
r_{DOC}	0.05	d^{-1}	This study
r_Z	0.019	d^{-1}	This study
e_i	0.09/0.19	no units	*Sweeney et al.*, [2000a]
DOC_{min}	40	μM	*Carlson et al.*, [2000]
Fe_{ice}	15	nM	*Edwards and Sedwick*, [2001]
Fe_{sol}	40	%	*Edwards and Sedwick*, [2001]

Where two values are given (separated by '/'), the first is for *P. antarctica* and the second is for diatoms. See methods for symbol details and Table 2b for additional parameters.

Table 2b. Additional parameter values used in the standard run.

Parameter	Description	Value	Units
C/Chl	Carbon to chlorophyll ratio	90/70	g g^{-1}
E_k	Photoadaptation parameter	30/90	μEin m^{-2} s^{-1}
N/C	Nitrogen:Carbon ratio of all phytoplankton	0.175	g g^{-1}
Ks_{NO3}	Half-saturation constant for NO_3 uptake	0.5	μM
$\mu 0_i$	Growth rate of phytoplankton group *i* at 0 °C	0.59/0.71	d^{-1}
x_i	Specific mortality rate of phytoplankton	0.025	d^{-1}
r_D	Detrital remineralization rate	0.03	d^{-1}
G_{max}	Maximum zooplankton specific grazing rate	0.4	d^{-1}
K_z	Concentration of phytoplankton at which $g = 0.5G_{max}$	85	mg C m^{-3}
γ	Zooplankton assimilation efficiency	0.75	no units
x_Z	Zooplankton specific mortality rate	0.2	d^{-1}

Where two values are given (separated by '/'), the first is for *P. antarctica* and the second is for diatoms

kg^{-1} [*Bates et al.,* 1998] and is normalized to a salinity of 35 psu. pCO_2 is calculated as described in Chapter 2, with atmospheric pCO_2 set to 365 μatm [*Takahashi et al.,* 2002] and CO_2 solubility an empirical function of temperature and salinity [*Weiss and Price,* 1980]. The sea-air flux of CO_2 (FCO_2) is a function of the sea-air difference in pCO_2, CO_2 solubility, ice coverage and the piston velocity, which is assumed to be a quadratic function of wind speed [*Wanninkhof,* 1992].

2.2. Setting of Fe Parameters

Considerable uncertainty exists with regard to phytoplankton Fe parameters, particularly the C/Fe uptake ratio. C/Fe ratios are thought to vary with phytoplankton taxa, Fe availability, and incident light [*Brand,* 1991; *Sunda and Hunstman,* 1995; 1997]. *Brand* [1991] examined numerous phytoplankton groups and found Fe demands to be highly variable. Fe/P molar ratios ranged from $<10^{-4}$ to 10^{-2} [*Brand,* 1991], which correspond to C/Fe molar ratios of ~10,000 to >100,000 (using a Redfield C/P of 106). *Sunda and Huntsman* [1995] found C/Fe ratios to vary from 140,000 to 500,000 in laboratory studies, consistent with the mean oceanic value of 250,000 reported by *Johnson et al.* [1997]. *Sunda* [1997] examined the relationship between dissolved Fe concentrations and apparent oxygen utilization (AOU) in the dataset of *Johnson et al.* [1997] and obtained C/Fe ratios of ~600,000 for the northern Ross Sea and ~450,000 for Drake Passage. These are some of the highest values observed, and since they were calculated using an AOU:Fe relationship, are good indicators of actual removal ratios from the water column [*Sunda,* 1997] and likely account for particle scavenging. Measurements made prior to Fe enrichment during the Southern Ocean Fertilization Experiment (SOFEX) found that diatoms in the

southern fertilized patch (~ 66°S) exhibited C/Fe ratios of <150,000 [*Twining et al.*, 2002].

Given the reported differences in the C/Fe ratios measured in laboratories and collected in the field, I derived appropriate values for the Ross Sea using a diagnostic approach, whereby the C/Fe uptake ratios for diatoms and *P. antarctica* were assigned based on their ability to allow accurate simulation of field measurements of chlorophyll *a* (Chl *a*), nutrients, and TCO_2. As a result of this analysis (data not shown), I assigned molar C/Fe uptake ratios of 450,000 and 100,000 to *P. antarctica* and diatoms, respectively. These values are well within the reported C/Fe ranges, both globally and for the Ross Sea [*Johnson et al.*, 1997; *Sunda*, 1997], and are consistent with observations that Fe demands are greatest for algae growing in high Fe waters [*Sunda*, 1997], such as diatoms that grow near melting ice-edges in the Ross Sea. For comparison, the recently published global ecosystem model of *Moore et al.* [2002] uses C/Fe ratios ranging from 140,000 to 1,000,000, while the model of *Aumont et al.* [2003] uses ~350,000.

2.3. Tracer Validation

In order to assess the performance of the model with the new tracers, it is important to compare model predictions of pCO_2 and PO_4 with field data collected from my study area (see *Arrigo et al.* [2003a] for validation analyses of other tracers). The southwestern Ross Sea is a logistically difficult area within which to sample and measurements of water column properties over a complete annual cycle do not exist. However, the Antarctic Environments Southern Ocean Process Study (AESOPS) and the Research on Ocean-Atmosphere Variability and Ecosystem Response in the Ross

Sea (ROAVERRS) field programs collected extensive nutrient and C system data that can be used, along with satellite derived Chl *a* (SeaWiFS), to assess model performance. To do so, a validation box was designated in my study area from 76-77°S and 175-180°E (denoted by C in Figure 1), the region of greatest field data density. AESOPS and ROAVERRS data collected within the validation box were binned spatially and the temporal dynamics of these data compared to CIAO output averaged over the same area. It should be noted that the validation box lies within the general location of the RSP (denoted by B in Figure 1). Unfortunately, much less data have been collected in the TNBP. In order to assess the accuracy of model predictions for the TNBP region (denoted by A in Figure 1), I used SeaWiFS Chl *a* measurements and reported literature values for pCO_2 and PO_4. Validation results are given throughout Section 3.

3. Results and Discussion

3.1. The Standard Run

3.1.1. Phytoplankton Biomass

As in earlier versions of CIAO [*Arrigo et al.*, 2003a], the RSP phytoplankton bloom begins by the end of November and is dominated by *P. antarctica*, reaching a peak biomass of ~8 mg Chl *a* m^{-3} by mid December (Figure 2). In the TNBP, phytoplankton growth rates at this time are low due to wind-driven deep mixing, consistent with observations by *Arrigo et al.* [1998a], and Chl *a* in CIAO increases slowly. Once the katabatic winds slacken in January, diatom biomass in the TNBP

increases substantially and reaches ~6 mg Chl *a* m^{-3} towards the end of January (Figure 2). The temporal

evolution of phytoplankton Chl *a* in both the RSP and TNBP is in good agreement with remotely sensed SeaWiFS retrievals (Figure 2) and with *in situ* measurements for the same regions [e.g. *Arrigo et al.*, 2000, *Smith et al.*, 2000].

3.1.2. Macronutrient Dynamics

CIAO is able to replicate major features of the *in situ* temporal variability of the newly added tracer PO_4 (Figure 3a), which declines from wintertime concentrations of 2.1 μM to a minimum of ~1 μM at the end of the growing season, returning to pre-bloom values by the end of the model year (Figure 3a). Significantly, the slope of the regression of NO_3 versus PO_4 (18.2) obtained from CIAO for the upper water column (within box C) agrees well with that determined *in situ* for *P. antarctica*-dominated waters (17.2). Note that the ratio of 18.2 produced by CIAO is lower than the prescribed N/P ratio of 20.2 for *P. antarctica*. This is because diatoms make up a small component of the phytoplankton population in the *P. antarctica*-dominated RSP and their lower N/P ratio brings the seasonal NO_3/PO_4 drawdown ratio below 20.2.

The seasonal utilization of macronutrients is markedly different between the RSP and the TNBP during the *standard* run. In the RSP, CIAO predicts that an average of 8.24 μM NO_3 and 0.88 μM PO_4 remains at the end of the growing season (Figure 4a, Table 3), while in the TNBP, NO_3 is drawn down to <5 μM and PO_4 to ~0.3 μM (Figure 4b, Table 3), despite both regions having the same pre-bloom concentrations of 31 μM NO_3 and 2.1 μM PO_4. Predictions of residual nutrients in the RSP agree well with AESOPS and ROAVERRS data collected within the same region [*Arrigo et*

Figure 2. Temporal changes in surface Chl *a* predicted by CIAO and measured by SeaWiFS for (a) the Ross Sea polynya and (b) the Terra Nova Bay polynya. Regions were assigned as per Figure 1. Data from the years 2000/01 and 2002/03 were not used since sea ice retreat was retarded and annual production depressed due to the influence of the icebergs B-15 and C-19 [*Arrigo et al.* 2002b, *Arrigo and Van Dijken,* 2003b].

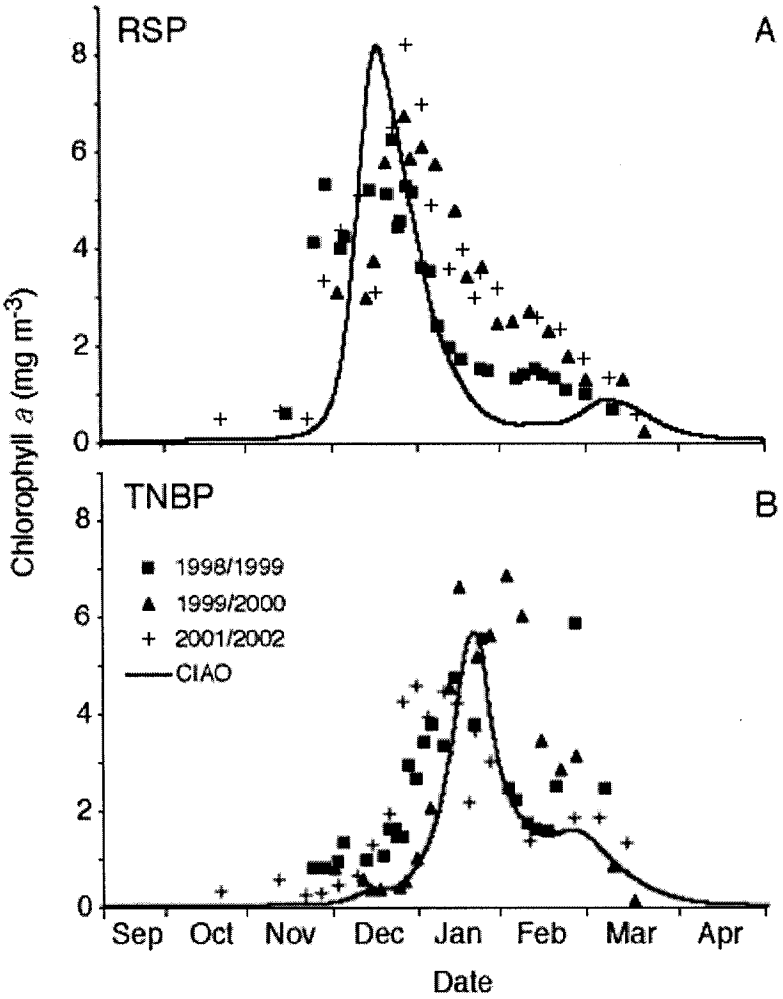

Figure 3. Comparison of CIAO predictions with *in situ* (a) PO_4 and (b) pCO_2 in the central Ross Sea (C in Figure 1).

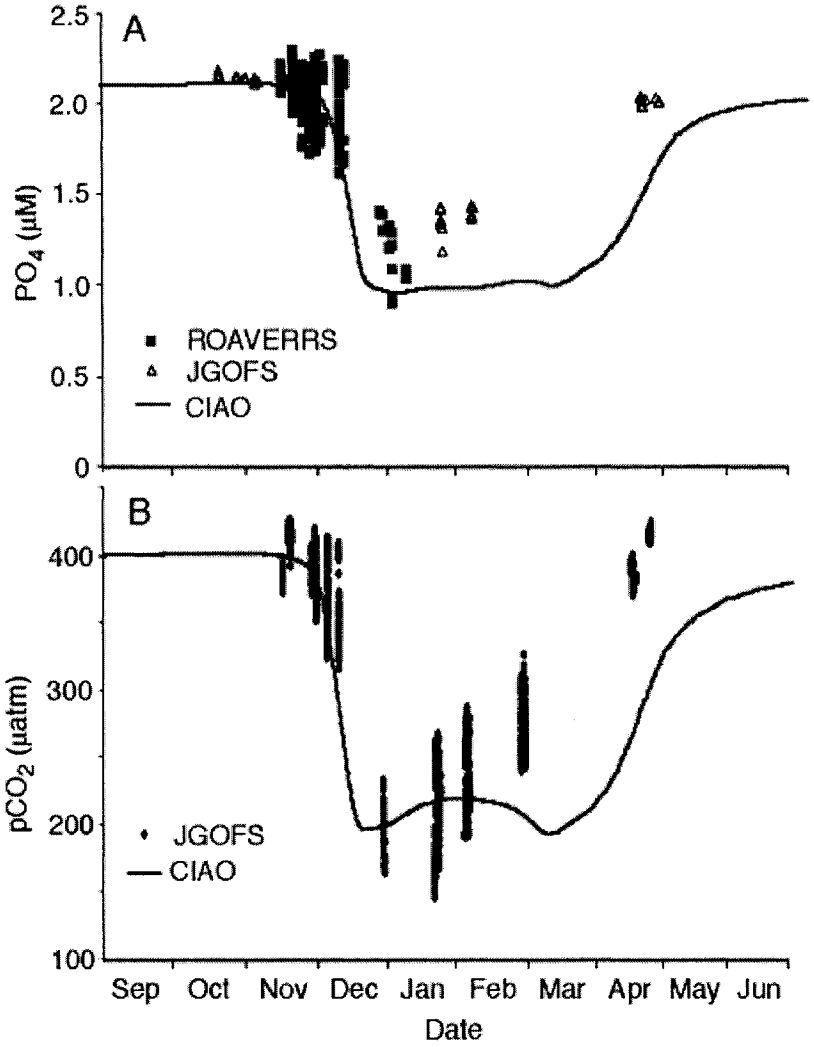

Figure 4. Temporal changes in surface (a) NO_3 and (b) PO_4 concentration in the RSP and the TNBP for the *standard* and *fefert* model runs.

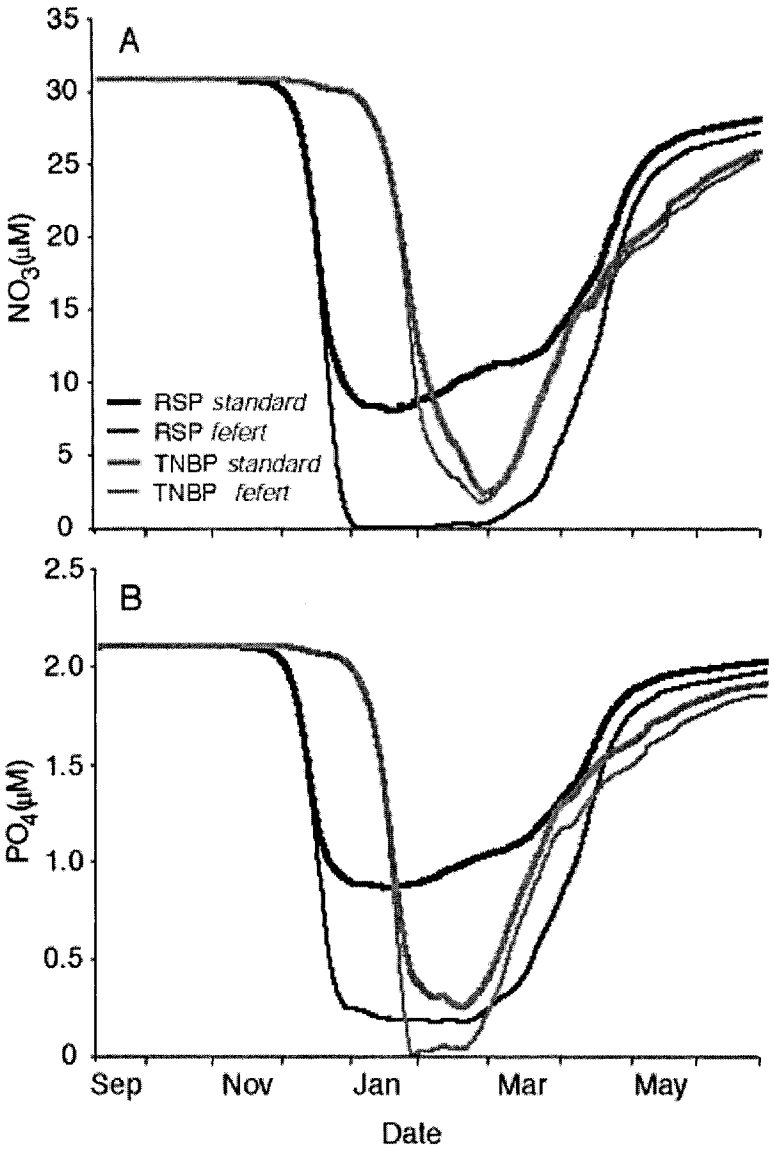

Table 3. Minimum nutrient concentrations.

			Experiment				
Variable	Units	Region	*standard*	*redfield*	*alldia*	*allpha*	*fefert*
NO_3	μM	RSP	8.24	7.49	23.65	0.81	0.02
		TNBP	2.43	0.23	15.76	0.13	1.67
PO_4	μM	RSP	0.88	0.91	1.42	0.62	0.18
		TNBP	0.26	0.34	0.59	0.46	0.01
Fe	nM	RSP	0.00	0.00	0.00	0.00	n/a
		TNBP	0.00	0.09	0.00	0.25	n/a

Values are averaged over either the RSP or the TNBP (see Figure 1 legend for locations).

al., 2000; *Smith et al.*, 2000]. Measurements are sparse in the TNBP, but the minimum PO_4 concentration predicted by CIAO (0.26 μM) agrees well with measurements by *Grotti et al.* [2001] within Terra Nova Bay (0.38 μM). Furthermore, *Fitzwater et al.* [2000] found the lowest PO_4 concentrations to be west of 170°E (~0.4 μM), consistent with regions of low PO_4 and high diatom dominance predicted by CIAO.

These regional differences in the fraction of initial macronutrients utilized during the growing season are due to both the taxon-specific macronutrient utilization ratios of the two dominant phytoplankton taxa and to the different Fe supply rates to each region. In the *P. antarctica* dominated RSP, little sea ice melts *in situ* and the primary route of Fe supply is from deep convection, whereas in the diatom dominated TNBP, local sea ice melting is a significant source of Fe that fuels extra macronutrient utilization. Differences in the N/P and C/P uptake ratios between the two major taxa in the Ross Sea control the rate of removal for each macronutrient, while the Fe concentration constrains the absolute magnitude of utilization. Because the N/P uptake ratio of *P. antarctica* more closely approximates the initial ratio of NO_3/PO_4 (15.5) in the water column (i.e. under Fe-replete conditions diatoms in the TNBP will exhaust PO_4 before *P. antarctica* in the RSP exhausts NO_3), and because the Fe supply is greater in the TNBP, the RSP likely has a much greater capacity for additional macronutrient utilization and CO_2 drawdown than the TNBP.

3.1.3. POC and DOC Production

NPP is relatively high within the RSP and lower in the TNBP, exhibiting annual rates of approximately 175 and 100 g C m^{-2} yr^{-1} (Table 4), respectively. This difference in annual NPP estimates between polynyas may seem counterintuitive given the higher Fe flux to the TNBP. It must be remembered, however, that diatoms have a higher Fe requirement than *P. antarctica*, which results in a lower rate of C uptake per unit Fe, thus offsetting the higher Fe availability in the TNBP.

Over the entire southwestern Ross Sea, spatially averaged annual NPP is only approximately 90 g C m^{-2} because of the low productivity in waters northeast of the continental shelf which are included in my study area. Over the course of a model year, CIAO predicts cumulative NPP over the entire study area to be 59 Tg C y^{r-1}, which is in agreement with satellite measurements over the same region [*Arrigo and van Dijken,* 2004]. CIAO predictions of NPP in the RSP compare well with estimates from the Ross Sea polynya derived from a number of sources, including satellite data (140-173 g C m^{-2}, *Arrigo and Van Dijken* [2004] and 156 g C m^{-2}, *Moore and Abbott,* [2000]), nutrient disappearance (200 g C m^{-2}, *Smith and Gordon* [1997]), and changes in algal biomass (91 to 216 g C m^{-2}, *Nelson et al.* [1996]).

The modeled accumulation of DOC associated with these blooms reached around 70 μM in the TNBP and around 60 μM in the RSP. These compare well with data collected by *Carlson et al.* [2000], who observed DOC concentrations increasing from a minimum of 40 μM to a maximum of >70 μM within the central Ross Sea. Over the course of the year, CIAO predicts that this labile fraction of DOC would be remineralized within the upper water column and concentrations would fall to a

Table 4. Net primary production (NPP), sea-air CO_2 exchange, and minimum pCO_2.

		Experiment				
Variable	Region	*standard*	*redfield*	*alldia*	*allpha*	*fefert*
PP	S.W. Ross	90.06	9	-50	33	30
	Sea					
(g C m^{-2} yr^{-1})	RSP	174.83	-18	-63	16	38
	TNBP	98.41	21	-42	19	4
FCO_2‡	S.W. Ross	-7.62	-5	-73	37	32
	Sea					
(g C m^{-2} yr^{-1})	RSP	-14.73	-14	-88	39	42
	TNBP	-22.04	-31	-88	14	9
Min pCO_2	S.W. Ross	223.06	-4	31	-22	-15
	Sea					
(μatm)	RSP	190.41	14	65	-24	-29
	TNBP	131.81	-4	57	-16	-5

Values are for the Standard run, and percent change from the Standard run for each experimental run (see Table 1), averaged over the RSP, the TNBP, and the southwestern Ross Sea (Figure 1 legend for locations).
‡ = defined as sea to air, such that a negative value implies ocean uptake. Positive percent changes are an increase in oceanic uptake.

minimum of 40 μM over the austral winter, representing the refractory component of the DOC pool.

3.1.4. TCO_2 and pCO_2

The annual cycle of TCO_2 mirrors that of Chl *a* (Figure 2) and NPP (data not shown), with the minimum TCO_2 concentration coinciding with maximum phytoplankton production. TCO_2 is reduced to a regional average of approximately 2100 μM in the RSP and to <2060 in the TNBP (Figure 5b). Again, these values compare well with values of 2150 μM observed in the RSP [*Gordon et al.*, 2000, converted from μmol kg^{-1} assuming a mean ocean density of 1024.5 kg^{-1}] and <2050 μM in the TNBP [*Arrigo et al.*, 2000]. CIAO predicts that the western continental shelf, where the TNBP is located, also experiences considerable TCO_2 depletion (to 2100 μM) and air-sea CO_2 exchange (Figure 5a, b, c), consistent with observations of large TCO_2 and NO_3 deficits west of 170°E [*Sweeney et al.*, 2000b; *Gordon et al.*, 2000]. After the phytoplankton blooms, TCO_2 concentrations trended toward pre-bloom levels in March due to both enhanced exchange with the atmosphere and mixing with high TCO_2 water from below.

The annual cycle of pCO_2 produced by CIAO (Figure 3b) resembles that of TCO_2 but is modified by variations in temperature and salinity. Upwelling of warm circumpolar deep water (CDW) in the central Ross Sea increases pCO_2 without a change in TCO_2, while input of cold fresh water from melting sea ice in the TNBP has the opposite, but smaller, effect. Early season pCO_2 levels of ~400 μatm are depleted to <200 μatm by the time of maximum PO_4 depletion, consistent with observations made during AESOPS (Figure 3b). There is substantial spatial heterogeneity in the

Figure 5. Spatial distribution of (a) minimum surface pCO_2 (b) minimum surface TCO_2, and (c) annual sea-air gas exchange. White areas are where the ice concentration is greater than 10% throughout the year.

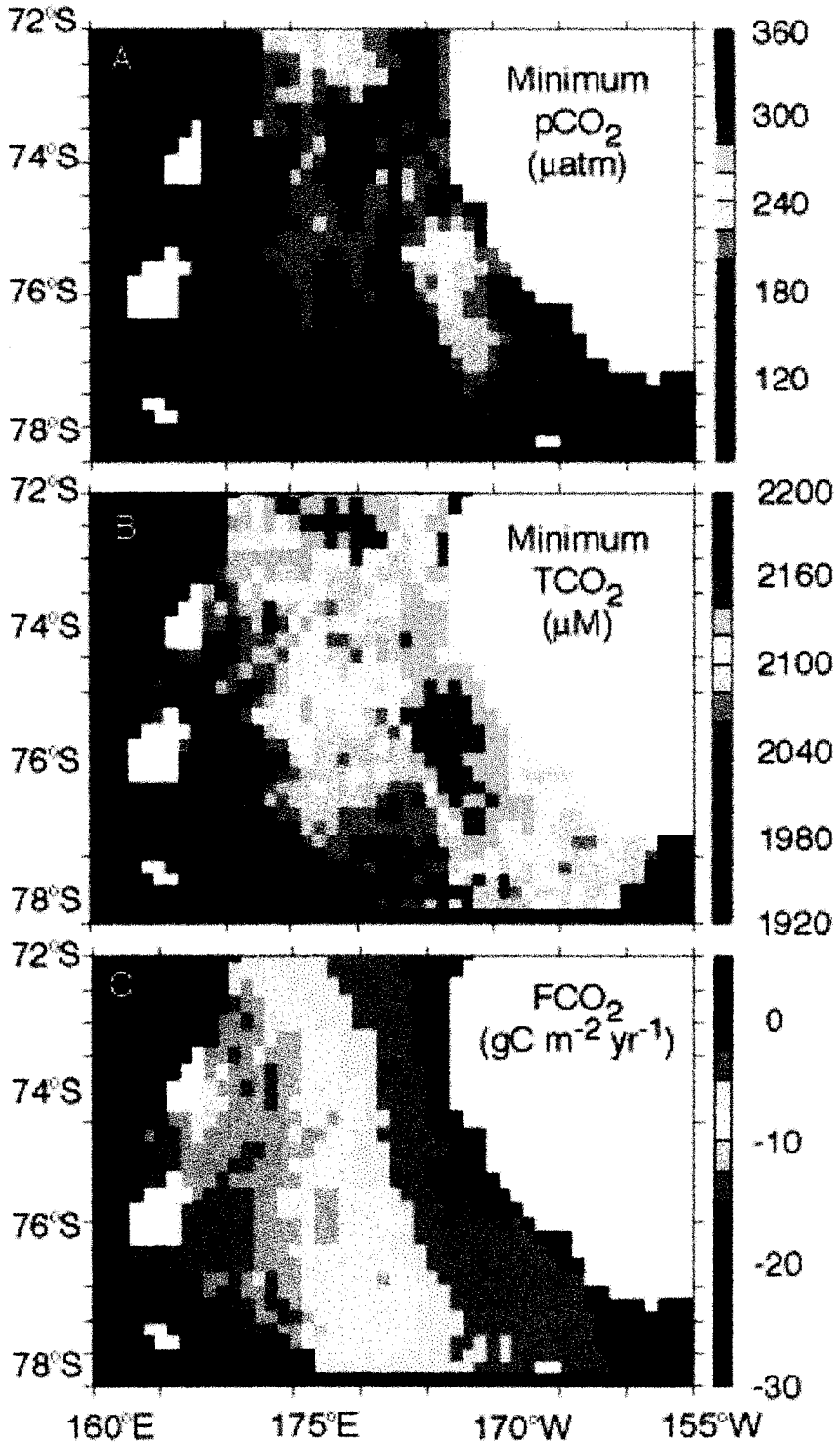

minimum pCO_2 values predicted by CIAO, with areas receiving elevated Fe fluxes along the ice edge showing the greatest depletion (to 100 - 140 μatm), and areas away from the ice melt (such as in the RSP) showing somewhat less depletion (to 120 - 200 μatm) (Figure 5a). Predictions for the RSP are in good agreement with data collected by *Bates et al.* [1998] and *Sweeney et al.* [2000b] who observed pCO_2 levels within the RSP area of ~150 and ~180 μatm, respectively.

3.1.5. Air-Sea CO_2 Exchange

The air-sea difference in pCO_2 results in 5.1 g C m^{-2} yr^{-1} of CO_2, or 3.43 Tg C yr^{-1}, being taken up by the southwestern Ross Sea, including the low productivity waters off the continental shelf (Figure 1). With CO_2 influx rates of 10.5 and 14 g C m^{-2} yr^{-1} in the relatively productive waters of the RSP and TNBP, respectively (Table 4), these values are in line with Ross Sea flux estimates of 12-24 g C m^{-2} yr^{-1} presented in *Takahashi et al.* [2002] (these values of *Takahashi et al.* [2002] may be slight overestimates due to their use of wind speeds measured at too high an altitude [*Takahashi*, personal communication]). In general, those areas near the western continental shelf exhibit the highest CO_2 uptake rates (Figure 5c) due to unusually high wind speeds [*Arrigo et al.*, 1998a] and lower sea ice coverage. Daily rates reach as high as 105 mg CO_2 m^{-2} d^{-1} by the beginning of March (Figure 6), which is coincident with the time of highest spring/summer wind speeds (Figure 7a). The flux of CO_2 from the atmosphere to the upper ocean amounted to around 7% of annual NPP in the RSP and 9% in the TNBP, consistent with the estimate of 10% measured for the Ross Sea [*Sweeney et al.*, 2000b].

3.1.6. Geographic Variability in Air-Sea CO_2 Exchange

The *standard* run of CIAO suggests that other geographic regions within the Ross Sea are also significant sites of reduced pCO_2/TCO_2 and high atmospheric CO_2 influx (Figure 5a, b, c). Specifically, large reductions in TCO_2 and pCO_2 are predicted along the ice edge close to Victoria Land and the Ross Ice Shelf (Figure 5a, b, compare with Figure 1). CIAO predicts surface water pCO_2 of 120-180 μatm in the McMurdo polynya (Figure 5b), in agreement with *Barbini et al.* [2003] who measured pCO_2 levels of <175 μatm at the same location. Model results suggest that this low pCO_2 water is advected into the McMurdo polynya region from the RSP (see Figure 1). These low pCO_2 waters produced in the RSP by the intense *P. antarctica* bloom are exposed to high winds in and around McMurdo Sound, and undergo a larger degree of gas exchange with the atmosphere than they would have had they remained in the RSP where wind speed is lower (Figure 7b).

It is also interesting that while the region off Edward VII land (~160 W) shows low pCO_2 and TCO_2 (Figure 5a, b) and high phytoplankton biomass [*Arrigo et al.*, 2003a], this area is only a weak sink for atmospheric CO_2 (Figure 5c). For example, pCO_2 is reduced to <200 μatm and TCO_2 to ~2100 μM, yet annual air-sea CO_2 exchange is only between 0 and 2.5 g C m^{-2} yr^{-1} (Figure 5 a, b, c). These relatively low values are due to the strong zonal gradient in wind speeds across the Ross Sea (Figure 7b). While the ΔpCO_2 in this region is large, lower wind speeds in the east promote little gas exchange. In general, FCO_2 exhibits a zonal decline from west to east (Figure 5c), with the highest rates predicted closest to Victoria Land, where wind speeds are highest. Meridonal changes in FCO_2 are relatively small, since meridonal

Figure 6. Temporal changes in sea-air CO_2 exchange (averaged over the Ross Sea) for the *standard*, the *nobio*, and the *fefert* run over the southwestern Ross Sea.

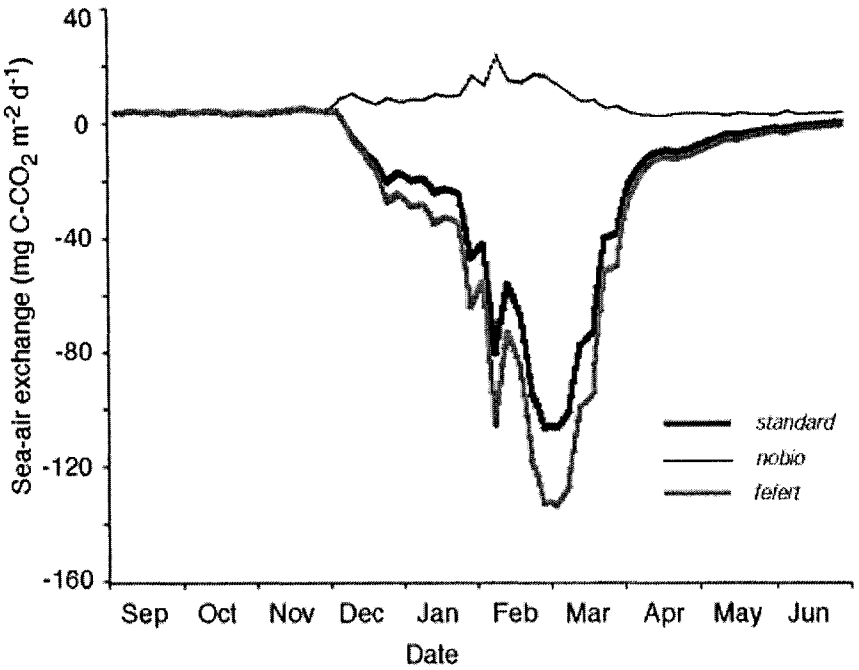

Figure 7. (a) Time series 5-day climatological squared winds (W_{10}^2, $m^2 s^{-2}$) averaged over the Ross Sea study area (see Figure 1 legend). (b) Variation in squared wind speed (W_{10}^2, $m^2 s^{-2}$) as a function of longitude and latitude, annually averaged.

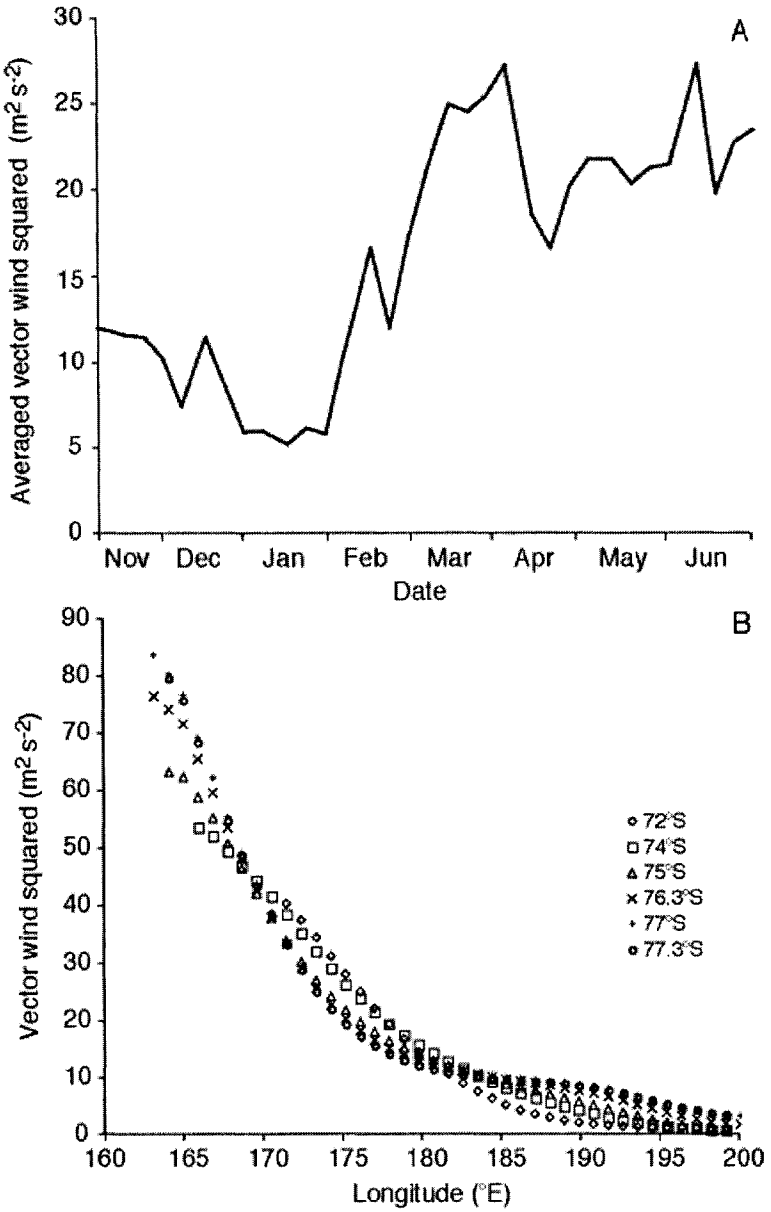

variability in wind speed is low, relative to the zonal gradient (Figure 7b). It should be noted that transient high wind events during the austral summer (prior to the elevation in winds and ice return), such as mesocyclones or katabatic wind surges, are probably important in controlling the sea-air flux of CO_2. Since the model forcing fields do not include such events, it is likely that I am underestimating air-sea gas exchange, particularly during periods of high ΔpCO_2 (ocean-atmosphere) during the austral summer. Short-term gas transfer events during the summer may facilitate enhanced CO_2 storage.

Previous studies have shown that annual phytoplankton production in the Ross Sea is regulated by Fe [*Sedwick and DiTullio,* 1997; *Arrigo et al.,* 2003a; *Coale et al.,* 2003]. CIAO suggests further that the spatial heterogeneity in TCO_2 depletion and absolute macronutrient utilization are a function of variability in Fe supply as well. The supply of Fe represents a balance between upwelling of Fe rich deep water and aeolian derived Fe from the melting of sea ice. While all regions within the Ross Sea are supplied by mixing of Fe from deep sources during the austral winter, those areas where this Fe supply is augmented by Fe fluxes from melting sea ice show a greater degree of nutrient utilization and TCO_2 depletion. However, it is not only the Fe flux that controls the degree of macronutrient utilization in the Ross Sea. Diatoms, with their higher P demand (low N/P uptake ratio), will deplete PO_4, relative to NO_3, to a greater degree than *P. antarctica*, resulting in residual NO_3 at the end of the growing season. The reverse is true for waters dominated by *P. antarctica*, which has a lower P requirement than diatoms and generally exhibit excess PO_4 post bloom. A further simulation where the concentration of Fe in ice was set to zero showed that ice derived

Fe supports only around 10% of annual NPP in the Ross Sea, consistent with an estimate of 5% for the seasonal sea ice zone by *Edwards and Sedwick* [2001] based on sea ice measurements in the Ross Sea.

3.2. Biological Versus Physical Control of Air-Sea CO_2 Exchange

To determine the extent to which biology, rather than physics or chemistry, controls air-sea CO_2 exchange, I performed a second simulation exactly like the *standard* run but with all biological parameterizations turned off (*nobio*, see Table 1). Field observations suggest that Ross Sea surface waters are generally supersaturated with CO_2, relative to the atmosphere (i.e. positive ΔpCO_2) at the end of the austral winter [*Sweeney et al.*, 2000b]. Consistent with these observations, the Ross Sea changes from a net CO_2 sink to a source of CO_2 to the atmosphere in the *nobio* model scenario, with as much as 21 mg C m^{-2} d^{-1} entering the atmosphere from Ross Sea surface waters, depending on temperature and wind speed (Figure 6). Integrated over the entire study area, as much as 1.23 Tg C would enter the atmosphere from oceanic surface waters over the course of a year in absence of biology. This is approximately 35% of the magnitude of the CO_2 sink during the *standard* run. The difference in air-sea CO_2 exchange between these two simulations (4.67 Tg C) represents the contribution of phytoplankton to the flux of CO_2 into surface waters of the Ross Sea.

Prominent CO_2 sources in the absence of biology are predicted along the western continental shelf and, to a lesser degree, in the central Ross Sea. Because there is a high degree of zonal heterogeneity in winds over the Ross Sea, locations such as those near the Victoria Land coast that experience high winds would become important sources of CO_2 to the atmosphere if it were not for the air-sea pCO_2 gradient created

by phytoplankton in surface waters. In the central Ross Sea, upwelling of warmer (by approximately 1°C) CDW onto the shelf reduces the solubility of CO_2, driving outgassing of CO_2 in the absence of biology. Although it is unlikely that NPP in the Ross Sea would ever fall to zero, annual NPP was reduced by 40% during 2000 [*Arrigo et al.,* 2002b] and by 75% in 2002 [*Arrigo and van Dijken,* 2003b]. This loss of production w as due to calving of large icebergs from the Ross Ice Shelf and the resulting build up of high concentrations of sea ice (which eventually dispersed late in the season) and had repercussions all the way up the food chain [*Arrigo et al.,* 2002b; *Arrigo and Van Dijken,* 2003b]. Results of the *nobio* run suggest that under these conditions of greatly reduced NPP in the Ross Sea, these waters would likely become a very weak sink, or possibly even a source, of CO_2 to the atmosphere.

3.3. Importance of Phytoplankton Biogeochemical Functional Groups

In order to assess the importance of including multiple phytoplankton groups (*P. antarctica* and diatoms), each with its own unique taxon-specific C/N/P/Fe uptake ratio, three additional model experiments were performed (see Table 1). Each of these experiments involved altering the taxon-specific C/N/P/Fe uptake ratios for diatoms and *P. antarctica.* In the *redfield* scenario, I assigned both phytoplankton taxa a C/N/P ratio consistent with *Redfield* [1934] and a C/Fe ratio of 250,000, which represents an oceanic mean [*Johnson et al.,* 1997]. In the *alldia* and *allpha* scenarios, both phytoplankton taxa were given C/N/P/Fe uptake ratios representative of either diatoms or *P. antarctica*, respectively (see Table 2a).

Redfield nutrient stoichiometry. Substituting a Redfield nutrient stoichiometry for the fixed taxon-specific values in the *standard* run caused CIAO to overestimate both

the annual NPP and the minimum pCO_2 in the TNBP and underestimate these quantities in the RSP, relative to the *standard* run (Table 4). The phytoplankton C/P and C/Fe ratios were higher in the TNBP during the *redfield* run (106 and 250,000) than during the *standard* run because diatoms, which normally dominate there, exhibit lower-than-Redfield C/P and C/Fe ratios (63 and 100,000 mol C:mol Fe). The higher C/P ratio in the *redfield* run permitted more C fixation by diatoms per mole PO_4 consumed, while the higher C/Fe ratio allowed more C fixation per mole Fe consumed. Because of the higher N/P ratio assigned to diatoms during the *redfield* run, utilization of NO_3 increased by around 7% in regions of diatoms dominance, while PO_4 utilization dropped by around 4% due to NO_3 limitation of phytoplankton in this high Fe environment. Annual NPP during the *redfield* run increased by 20% to 120 g C m^{-2} yr^{-1} in the TNBP. Despite the fact that both nutrient utilization and NPP increased during the *redfield* run, there was greater residual Fe at the end of the bloom, due to the reduced Fe requirements (increased C/Fe ratio) in diatoms. This resulted in a 30% decrease in the annual rate of air-sea exchange of CO_2, primarily caused by the early termination of the bloom which retarded late season gas exchange rates relative to the *standard* run.

The opposite is true in the *P. antarctica*-dominated RSP waters, where both the C/P and C/Fe ratios were lower during the *redfield* run than in the *standard* run. As a result, nutrient utilization and NPP decreased relative to the *standard* run (Tables 3 and 4). The decreased production in the RSP during the *redfield* run is more than compensated for by the increase in the TNBP, despite the smaller area of the TNBP. This is because the C/P ratios of *P. antarctica* (133), which dominate the RSP, are

closer to the values used during the *redfield* run (106) than those of diatoms (63), which dominate in the TNBP. Uptake of atmospheric CO_2 in the RSP dropped by 15% relative to the *standard* run under *redfield* conditions. Models using uniform Redfield nutrient parameters are thus predicted to show small, but potentially significant differences in the estimation of NPP, but exhibit much larger variability in the representation of FCO_2 and macronutrient dynamics in such Fe limited waters. It should be noted that disparities between the predictions of *standard* and *redfield* model runs are much greater over smaller areas, such as the RSP/TNBP, than over the whole region (see Tables 3 and 4).

Diatom only simulation. When all phytoplankton in the Ross Sea were assumed to have C/P and C/Fe ratios characteristic of diatoms (Table 2a), macronutrient utilization was altered significantly. This is particularly true of the RSP, where diatoms made up a small component of the phytoplankton assemblage during the *standard* run. Nutrient utilization in the RSP decreased, resulting in high residual NO_3 (23.65 μM) and PO_4 (1.42 μM) over the course of the growing season (Table 3). These high residual nutrients are a result of the higher Fe demand of diatoms (relative to *P. antarctica* that normally dominate in the RSP) and the lower Fe concentration in the RSP. The shift to diatoms in the RSP results in a 60% reduction in annual NPP, but a 90% decline in uptake of atmospheric CO_2 (Table 4). This is due to the elimination of a late season *P. antarctica* bloom in the RSP, which is fuelled by remineralization of particulate organic phosphate (POP) to PO_4 and occurs in phase with the higher wind speeds (Figure 7a), thereby enhancing gas exchange rates. This effect is also seen in the TNBP region, where late season growth of *P. antarctica* also

occurs under *standard* conditions. Over the entire Ross Sea, CIAO predicts a 50% reduction in annual NPP and a 70% drop in the uptake of atmospheric CO_2 if the Ross Sea were to be completely dominated by diatoms (Table 4).

P. antarctica *only simulation.* When simulating a floristic shift to *P. antarctica,* NO_3 utilization is increased in both the TNBP (by 8%) and, to a greater extent, the RSP (by 33%), relative to the *standard* run. Utilization of PO_4 also increases in the RSP (by 20%), but declines in the TNBP (by 11%), due to the much lower PO_4 requirement of *P. antarctica*, relative to diatoms (C/P = 133 and 63, respectively). The higher sensitivity of NO_3 utilization to a shift to *P. antarctica* in the RSP may seem counterintuitive, as the RSP is already dominated by *P. antarctica* during the *standard* run. However, in the *standard* run, diatoms make up approximately 25% of the phytoplankton population in the RSP and remove >4 times as much Fe per mole of CO_2 fixed as do *P. antarctica.* Therefore, when diatoms are replaced by *P. antarctica*, a greater pool of Fe is available to fuel additional macronutrient uptake. This effect is smaller in the TNBP where macronutrients are already drawn down to low levels during the *standard* run. Over the entire southwestern Ross Sea, rates of NPP and influx of CO_2 could be elevated by as much as 30% and 37%, respectively, relative to the *standard* run (see Table 4) with a complete switch to *P. antarctica* dominance.

These results could be significant if environmental change and/or anthropogenic activity resulted in changes in the phytoplankton community composition of the Southern Ocean. For example, global climate models predict that increases in precipitation and melting of sea ice will greatly impact the Southern Ocean [e.g. *Sarmiento et al.,* 1998]. In line with these predictions, a recent study has revealed

large decreases in shelf water salinity and surface salinity in the southwestern Ross Sea over the past four decades [*Jacobs et al.*, 2003]. If a more stable water column led to a phytoplankton taxonomic shift from *P. antarctica* to diatoms (in regions such as the RSP) and the potential for *P. antarctica* to bloom late was eliminated, then uptake of atmospheric CO_2 could be reduced by as much as 90%. The lower P and Fe demands and ability to achieve net growth in a more unstable water column of *P. antarctica,* relative to diatoms, does allows some degree of ecological succession in marginal ice zone waters under *standard* conditions. The ability to bloom later in the growing season, in phase with the elevated wind speeds (Figure 7a), thus affords *P. antarctica* an important role in controlling the air-sea flux of CO_2 in the Ross Sea.

3.4. Fe Fertilization

3.4.1. A Varied Response to Fe Fertilization

To investigate the impact of Fe fertilization on NPP, nutrient utilization, and air-sea CO_2 exchange in the Ross Sea, I parameterized CIAO such that Fe was non-limiting to phytoplankton growth over the entire southwestern Ross Sea for a complete annual cycle. Under these conditions, phytoplankton growth will continue until it becomes limited by one of the three macronutrients, or by light. This experiment represents the upper limit to what can be expected in the event of a large increase in Fe supply, either naturally, via increased dust input, as was seen during the Last Glacial Maximum, or artificially, via controlled Fe additions.

The most striking aspect of the Fe fertilization experiment (*fefert*, Table 1) was the marked heterogeneity in the phytoplankton response within the Ross Sea. *P.*

antarctica biomass increased dramatically in the RSP when Fe was added, with peak values increasing by almost 6 mg Chl *a* m^{-3} (Figure 8) over the *standard* run (60% increase). In contrast, Chl *a* in the diatom dominated TNBP increased by a maximum of only 2.5 mg Chl *a* m^{-3} over the standard run (Figure 8). Areas of *P. antarctica* dominance, such as the RSP, were completely stripped of surface NO_3, while an average of 0.2 μM PO_4 remained at the end of the growing season (Table 3, Figure 4). Regions dominated by diatoms, such as the TNBP, were eventually limited by PO_4, with a mean of 2 μM residual NO_3 (Table 3, Figure 4).

As with Chl *a*, there was a high degree of spatial variability in the response of the Ross Sea C cycle to simulated continuous Fe fertilization. Annual NPP was elevated by almost 40% in and around the RSP compared with increases of 10% throughout the TNBP region (Table 4). Averaged over the entire study area, annual NPP increased by approximately 30% (Table 4), to around 120 g C m^{-2} yr^{-1} or 71 Tg C yr^{-1} when integrated over my entire study area. In some areas of the Ross Sea, annual NPP increased by as much as 100 g C m^{-2} yr^{-1} (Figure 9a), while areas close to Edward VI land and along the ice shelf showed slight decreases in annual NPP during *fefert* (by as much as 60 g C m^{-2} (Figure 9a). Annual NPP in these waters declined because these areas were macronutrient limited under *standard* conditions and receive unused macronutrients from adjacent grid cells via advection. During *fefert*, these excess macronutrients are used *in situ* and therefore cannot support production in adjacent grid cells.

The RSP exhibited a large seasonal reduction in pCO_2 when continually fertilized with Fe, averaging an additional 60 to 80 μatm decrease over the *standard* run (Figure

Figure 8. Temporal changes in (a) surface Chl *a* in the standard and *fefert* model runs for the RSP and the TNBP, and (b) the difference in Chl *a* (ΔChl *a*) between the *standard* and *fefert* model runs for the RSP and the TNBP.

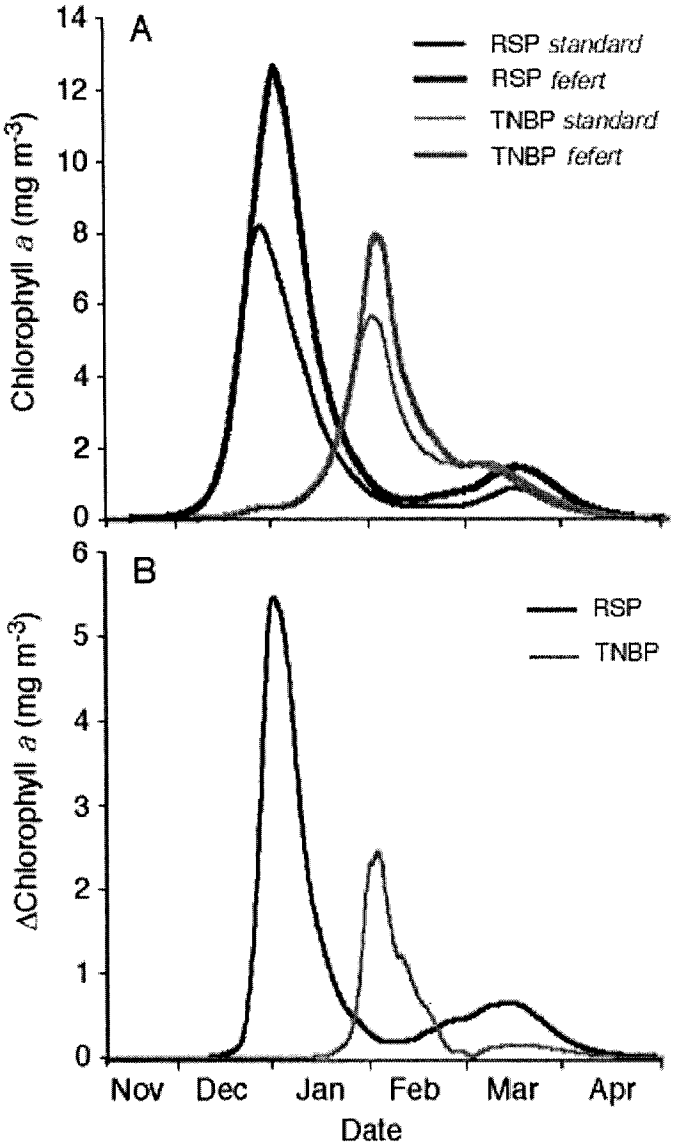

Figure 9. Absolute difference between the *standard* and *fefert* model runs for (a) annual primary production, (b) minimum pCO_2, and (c) annual air-sea CO_2 exchange. In panel (c) a positive change denotes an increase in the oceanic uptake of CO_2. White areas are where the ice concentration throughout the year is greater than 10%.

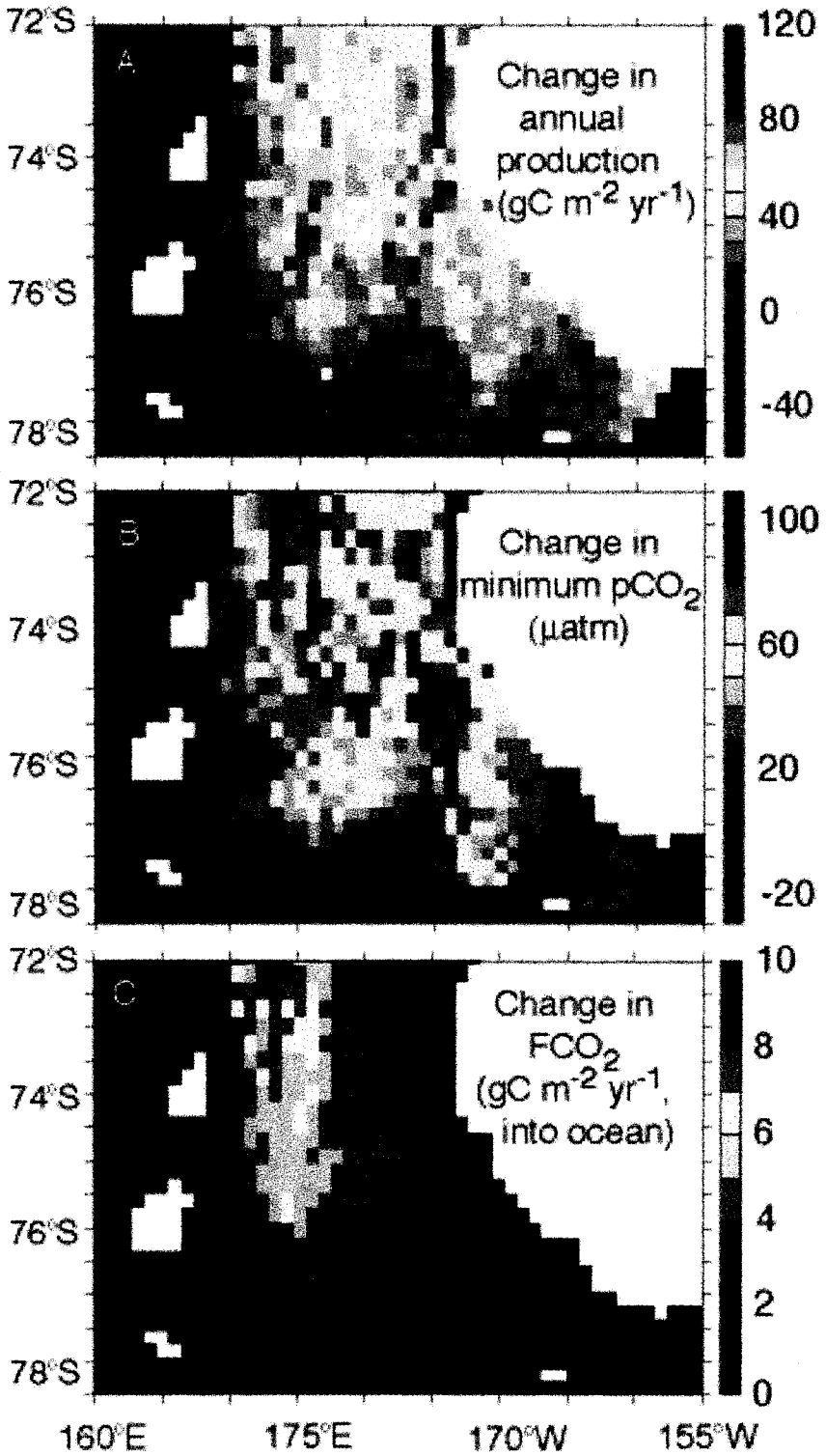

9b). In contrast, there was little impact of Fe fertilization on the seasonal decline in pCO_2 in and around the TNBP (<20 μatm, Table 4, Figure 9b), a region with a low capacity for additional growth due to the already high natural sources of Fe (e.g. ice melt). Indeed, seasonal pCO_2 changes in almost all areas bordering the ice shelf and Victoria Land coast were relatively unaffected by Fe fertilization (Figure 9b).

The greatest response to Fe in terms of both annual NPP, Chl *a* (Figure 8), and minimum pCO_2 is predicted in and around the RSP and extends northwards towards Cape Adare (Figures 9a, 9b) where CIAO predicts the largest increase in uptake of atmospheric CO_2 during *fefert* (Figure 9c). This region shows similar changes in annual NPP and minimum pCO_2 as the RSP, but wind speeds are much higher in this more westerly region (Figure 7b) and thus, gas exchange rates are higher.

The response in FCO_2 to Fe fertilization was similar to that of NPP and pCO_2 but was modified somewhat by the zonal variability in winds. Within the *P. antarctica* dominated RSP, oceanic CO_2 uptake in some locations increased by >100%, 0r 10 g C m^{-2} yr^{-1} (Table 4, Figure 9c). In line with the small changes predicted in annual NPP and seasonal pCO_2 decline, annual FCO_2 in the diatom-dominated regions rose by <4 g C m^{-2} yr^{-1}, an increase of <10% (Table 4, Figure 9c). The mean daily air-sea CO_2 exchange rate averaged over the southwestern Ross Sea increased by 25% to as much as 133 mg CO_2 m^{-2} d^{-1} (Figure 6). The *fefert* CO_2 exchange rate is always greater than in the *standard* run, with the difference greatest at the time of maximum wind speed and air-sea gas exchange (around the 6th of March, Figures 6, 7a). Overall, CO_2

uptake by the southwestern Ross Sea is increased from 3.43 Tg C yr^{-1} to 4.51 Tg C yr^{-1} in response to Fe fertilization.

3.4.2. Community Response to Fe Fertilization

Previous Southern Ocean Fe fertilization experiments have generally elicited floristic shifts from nanophytoplankton towards large diatoms [e.g. *De Baar et al.,* 1995; *Boyd et al.,* 2000, *Coale et al.,* 2004], although prymnesiophytes, such as *P. antarctica*, have also been observed to increase [*Boyd et al.,* 2000]. Consistent with these *in situ* experiments, CIAO predicted increases in both diatom and *P. antarctica* biomass after Fe fertilization. Over the entire model study area, diatom Chl *a* roughly doubled, whereas *P, antarctica* Chl *a* increased by 60% during *fefert*. Within the RSP, regionally averaged diatom Chl *a* increased by as much as 3-fold over the *standard* run, while *P. antarctica* Chl *a* increased by almost 2-fold. However, even though Fe was non-limiting, the less stable water column in the RSP precluded a large floristic shift to diatoms and *P. antarctica* still made up >75% of the phytoplankton biomass. Although the TNBP did not respond as strongly to Fe fertilization as the RSP, the increase in diatom Chl *a* was 5-fold greater than that of *P. antarctica*, consistent with most of the *in situ* Fe enrichment experiments conducted to date [e.g. *Boyd et al.,* 2000].

In addition to changes in phytoplankton community composition, CIAO predicted significant changes in the relationship between phytoplankton and their zooplankton grazers. In the *standard* run, phytoplankton growth and zooplankton grazing were temporally decoupled due to the high growth rates of phytoplankton, which the

zooplankton were unable to match. Phytoplankton/zooplankton (P/Z) coupling was markedly greater in the TNBP than the RSP, due to the slower development of the phytoplankton bloom in the TNBP [*Tagliabue and Arrigo,* 2003]. Complete coupling is achieved when *G*, the ratio of zooplankton specific grazing rate to phytoplankton specific growth rate, is equal to 1, such that phytoplankton growth exactly balances grazing losses. In the *standard* run, P/Z coupling (evaluated over a 10 day period at the peak of each respective bloom) was much tighter in the TNBP ($G = 1.11 \pm 0.69$) than in the RSP ($G = 5.89 \pm 5.84$), as shown previously by *Tagliabue and Arrigo* [2003]. Prolonging the *P. antarctica* bloom in the RSP via Fe fertilization resulted in more efficient coupling between phytoplankton and their zooplankton grazers ($G = 0.41 \pm 0.04$), intensifying 'top down' control of phytoplankton biomass [see *Tagliabue and Arrigo*, 2003]; little change in P/Z coupling was predicted within the TNBP ($G = 1.46 \pm 1.08$).

Increased P/Z coupling in the RSP via Fe fertilization should result in more efficient export of C from the euphotic zone because of the relatively refractory nature and rapid sinking speeds of zooplankton fecal pellets. On the other hand, aggregation of *P. antarctica* at the end of the RSP bloom has been shown to result in efficient C export in the Ross Sea [*DiTullio et al.,* 2000]. Although CIAO has shown that trophic interactions can be modified by addition of Fe, the relative importance of fecal pellet production versus aggregation cannot be addressed in the model at this stage due to insufficient mechanistic detail. As more information on particle aggregation, sinking speeds, and their rates of remineralization (labile versus refractory pools) become

available, it will be possible to implement a more realistic formulation of C export from the surface to the deep ocean.

3.4.3. Large-Scale Impact of Fe Fertilization

Overall, the strength of the Ross Sea C sink could be elevated by as much as 30% with Fe fertilization, with an extra 1.4 Tg C yr^{-1} being removed from the atmosphere. Annual NPP and air-sea CO_2 influx for the region could increase to 71 Tg C yr^{-1} and 6.3 Tg C yr^{-1}, respectively. I show that the effect of Fe fertilization will be greatest in those regions receiving little natural Fe input. In such regions, higher concentrations of macronutrients remain unused by the phytoplankton under normal conditions and the impact of alleviating Fe limitation will be greatest. This is seen in the RSP and other offshore regions, where the *fefert* run showed marked increases in both TCO_2 and pCO_2 depletion, Chl *a* concentration, and air-sea CO_2 exchange (Table 4, Figures 8 and 9) as the remaining macronutrients were utilized. Within the TNBP and other regions nearer the Ross Ice Shelf, lower concentrations of NO_3 and PO_4 remain naturally and therefore even when Fe becomes non-limiting, PO_4 is quickly exhausted and limits phytoplankton growth (Table 3); any further growth is controlled by the degree of POP remineralization. Late blooms of *P. antarctica,* during periods most conducive to gas exchange, will also have a large impact on uptake of atmospheric CO_2. Understanding the natural sources of Fe, the taxonomic composition of the phytoplankton, and the degree of macronutrient utilization and pCO_2 reduction under non-fertilized conditions are crucial to understanding how Fe fertilization, by anthropogenic or natural means, would impact the regional C cycle.

However, fertilization of the Southern Ocean would likely have only a minor mitigating impact on increasing atmospheric CO_2 concentrations. The global ocean is currently estimated to be a ~2 Pg C yr^{-1} sink for atmospheric CO_2 [*Orr et al.*, 2001; *Takahashi et al.*, 2002]. Regional analysis of the CO_2 fluxes by *Takahashi et al.* [2002], using a database of 940,000 global measurements, showed the Southern Ocean contributes around 25%, or 0.5 Pg C yr^{-1}, to this annual flux. If oceanic CO_2 uptake could be elevated to my regional maximum predicted rate (during *fefert*) of 24 g C m^{-2} yr^{-1} over the entire Southern Ocean (41 $x10^6$ km^2 south of 50°S), then C uptake would be increased to 0.98 Pg C yr^{-1}, which is in line with earlier estimates of 1-2 Pg C yr^{-1} by *Sarmiento and Orr* [1991]. The actual rate would likely be much lower, since it is unlikely that the combination of wind speed, ice coverage and ΔpCO_2 will result in such high gas exchange rates throughout the Southern Ocean. Indeed, if I utilize the regional average (over the whole study area) *fefert* rate of 7.42 g C m^{-2} yr^{-1}, then C uptake would be only 0.3 Pg C yr^{-1}. This range in C uptake, 0.3 to 0.98 Pg C yr^{-1}, would account for between 6% and 15% of the current global annual C emissions from fossil fuel burning of ~6.4 Pg C yr^{-1} [*IPCC*, 2001]. However, it is important to note that CO_2 emissions from fossil fuel burning currently increase atmospheric CO_2 each and every year and Fe fertilization will result in macronutrient (N, P, or Si) limitation of the phytoplankton. If the Southern Ocean were to be fertilized fully with Fe each year, then it is the rate of macronutrient renewal that will dictate the magnitude and sign of the C sink over interannual timescales.

4. Conclusions

Increased Fe supply to the Southern Ocean could result from climatically induced increases in the seasonal ice zone extent (which accumulates Fe during the winter), atmospheric dust input or by deliberate anthropogenic releases of Fe. I have shown that, in general, the magnitude of the response to Fe fertilization is dictated by the existing patterns of macronutrient utilization, driven by distinct phytoplankton taxon-specific nutrient utilization ratios and regional variability in Fe supply. I also found that physical processes modulate the role played by biology in controlling air-sea CO_2 exchange. For example, advection of low pCO_2 waters from the RSP to the McMurdo polynya results in enhanced CO_2 exchange in a location removed from the original site of primary production. Model results also show that the zonal, meridional, and temporal variability in wind speed is of significance in representing the sea-air CO_2 flux. In the eastern continental shelf region (~160°W), the low wind speeds significantly retard the exchange of CO_2 with the atmosphere, even though Chl *a* levels are high and TCO_2 and pCO_2 levels are low.

Perturbing the CIAO model has revealed a great deal about ecosystem processes in the Ross Sea, elucidating the varying significance of biological, chemical and physical processes. Species-specific nutrient utilization ratios are necessary to accurately represent NPP and macronutrient utilization. The application of Redfield nutrient stoichiometry resulted in small reductions in the predictions of annual NPP and gas exchange over the whole region, whereas variability between Redfield and non-Redfield models was much greater over smaller spatial scales. Alleviating Fe limitation leads to large increases in both NPP and uptake of atmospheric CO_2 by the

surface ocean. However, the response is complex and phytoplankton taxonomic composition will be crucial in dictating the nature of the relationship between Fe and the Southern Ocean C cycle. Indeed, a floristic shift in phytoplankton community composition (in the absence of any Fe fertilization) can have as great an impact on NPP, uptake of atmospheric CO_2, and food web structure as a complete and continual Fe fertilization. Field programs to these distinct regions could provide a unique opportunity to understand both the inter- and intra-specific variability in planktonic Fe demands and coupling of biogeochemical and physical processes. A better understanding of the drivers of species composition and Fe supply and demand in the Southern Ocean will prove to be fundamental in improving the accuracy of model predictions.

Chapter 5

Processes governing the supply of iron to phytoplankton in stratified seas

Abstract The impact of iron speciation on phytoplankton dynamics in the marine environment is currently not well understood. In this study, I modified the existing CIAO model of the Ross Sea to include major aspects of iron chemistry and examined the processes governing the supply of iron to phytoplankton. I suggest that the melting of sea ice and ensuing stratification dictates the speciation and bioavailability of iron. Photoreduction is the key process governing the supply of bioavailable Fe to the resident phytoplankton of the Ross Sea. Access to organically-complexed iron is of greater significance in strongly stratified waters dominated by diatoms than in weakly stratified waters dominated by *Phaeocystis antarctica*. Light may control phytoplankton taxonomic composition in the Ross Sea by impacting both photosynthetic performance and iron speciation. The efficiency with which iron fuels phytoplankton carbon incorporation is greater in seasonal ice zones than in permanently ice-free waters. Therefore, changes in the physical structure of the Southern Ocean could impact iron bioavailability, independent of any change in iron supply.[1]

[1] Elements of this work appeared in: Tagliabue, A. and K. R. Arrigo. 2006. Processes governing the supply of iron to phytoplankton in stratified seas. Journal of Geophysical Research – Oceans. doi:10.1029/2005JC003363.

1. Introduction

Measurements of macronutrient distributions and phytoplankton growth made during the *Discovery* cruises (1924-1939) suggested that the low primary productivity of the open Southern Ocean (SO), relative to the more productive shelf regions, could be attributed to reduced iron (Fe) availability [*Hart,* 1934]. The utilization of trace metal clean sampling techniques developed in the 1980's confirmed that Fe concentrations on the continental shelves are much higher than in the open SO [e.g. *Martin et al.,* 1990; *Johnson et al.,* 1997; *Sedwick and Di Tullio,* 1997; *Coale et al.,* 2005]. More recently, bottle enrichment and in situ mesoscale Fe addition experiments demonstrated that the availability of Fe does indeed limit primary productivity throughout much of the modern SO [*Martin et al.,* 1990; *De Baar et al.,* 1995; *Sedwick et al.,* 2000; *Boyd et al.,* 2000; *Gervais et al.,* 2002; *Coale et al.,* 2004].

Consistent with these observations, substantial rates of primary productivity are often associated with the numerous coastal polynyas (areas of open water surrounded by ice) located over the Antarctic continental shelf [*Arrigo and Van Dijken,* 2003a]. Although this enhanced production is primarily the result of higher light availability in waters with reduced sea ice cover, higher Fe availability also plays an important role. The most productive polynya is located in the Ross Sea (Figure 1), where phytoplankton blooms are large [*Arrigo and Van Dijken,* 2003a; *Arrigo et al.,* 2000; *Smith et al.,* 2000] and net primary production (NPP) commonly exceeds 150 g C m^{-2} yr^{-1} or 40 Tg C yr^{-1} [e.g. *Arrigo and Van Dijken,* 2004; *Tagliabue and Arrigo,* 2005]. The high rates of CO_2 fixation associated with the Ross Sea phytoplankton blooms drive large deficits in the oceanic partial pressure of CO_2 (pCO_2) [*Takahashi et al.,*

Figure 1. Map of the southwestern Ross Sea, showing the locations of the RSP (76.5 °S, and 177 °E) and TNBP (75 °S and 164 °E) stations. The whole southwestern Ross Sea study area is considered to be the region encompassed by 73 °S - 78°S and 160 °E – 155 °W.

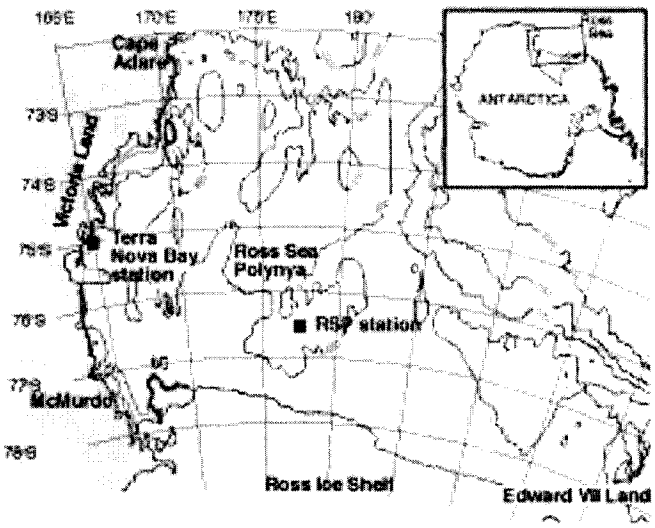

2002; Sweeney, 2003], resulting in the uptake of 5 Tg of atmospheric CO_2 each year [*Tagliabue and Arrigo,* 2005].

Phytoplankton blooms in the well-stratified marginal ice zones (MIZ) of the southwestern Ross Sea (such as the Terra Nova Bay Polynya, TNBP) are dominated by diatoms such as *Fragilariopsis curta*, *F. cylindrus,* and *Nitzschia subcurvata*, while the waters of the Ross Sea polynya (RSP) are only weakly stratified and the colonial haptophyte *Phaeocystis antarctica* blooms profusely [e.g. *Arrigo et al.,* 2000; *Smith et al.,* 2000]. Despite non-limiting dissolved Fe concentrations measured in the southwestern Ross Sea during the austral spring [*Fitzwater et al.,* 2000; *Coale et al.,* 2005], the annual accumulation of particulate organic carbon is eventually limited by Fe, with approximately one third of macronutrients remaining at the time of ice refreeze [*Sedwick et al.,* 2000; *Tagliabue and Arrigo,* 2005].

Because of its location on the continental shelf, concentrations of dissolved Fe in surface waters of the southwestern Ross Sea (0.5 nM) are greater than those measured in most other SO waters (< 0.2 nM) [e.g. *Martin et al.,* 1990; *Johnson et al.,* 1997; *Sedwick and Di Tullio,* 1997; *Fitzwater et al.,* 2000; *Sedwick et al.,* 2000; *Boye et al.,* 2001; *Grotti et al.,* 2001; *Croot et al.,* 2004; *Coale et al.,* 2005]. Concentrations are even greater in the vicinity of melting sea-ice (>1 nM) and near the seafloor (0.6-1.0 nM) [*Sedwick and Di Tullio,* 1997; *Coale et al.,* 2005]. Previous field work [*Edwards and Sedwick,* 2001] and modeling studies [*Tagliabue and Arrigo,* 2005] indicate that ice-derived Fe only supports approximately 10% of regional NPP. This suggests that Ross Sea phytoplankton are reliant upon water column or sedimentary sources of Fe

that persist over the winter. However, the processes governing the supply of bioavailable Fe to phytoplankton in such regions are not well understood.

Fe has a complicated cycle in seawater and the speciation of Fe is controlled by a suite of physical, chemical, and biological processes, including redox chemistry, organic complexation, precipitation, and photochemistry [*Wells et al.,* 1995; *Morel and Price,* 2003]. Most Fe in the oxidizing modern ocean exists in the trivalent oxidation state (Fe(III)), and while free inorganic dissolved Fe (Fe(II) and Fe(III)) can be utilized by phytoplankton [*Anderson and Morel,* 1982], over 99% of dissolved Fe(III) (generally defined as <0.2 μm) is complexed by one or more organic ligands [e.g. *Rue and Bruland,* 1997; *Witter and Luther,* 1998; *Nolting et al.,* 1998; *Wu et al.,* 2001; *Boye et al.,* 2001; *Croot et al.,* 2004]. Photoreduction can convert some ligand-bound Fe(III) species to Fe(II) via ligand-to-metal charge transfer (LMCT) [*Barbeau et al.,* 2003]. Fe is also present as particulates (typically > 0.2 μm) that are unavailable to the phytoplankton [*Rich and Morel,* 1990] and can coalesce and sink from surface waters.

Ligand concentrations in the SO typically range from 1–2 nM (Fe equivalents) [*Boye et al.,* 2001; *Croot et al.,* 2004] and are consistent with concentrations measured in other oceans [e.g. *Rue and Bruland,* 1997; *Witter and Luther,* 1998, but see *Wu et al.,* 2001]. Organic ligands are produced in seawater through exudation by heterotrophic bacteria [*Wilhelm and Trick,* 1994; *Martinez et al.,* 2001] and phytoplankton [*Geider,* 1999; *Morel and Price,* 2003], and are released during grazing by protozoa [*Barbeau et al.,* 1996] and zooplankton [*Hutchins et al.,* 1995], and during viral lysis [*Poorvin et al.,* 2004]. Each of these distinct release mechanisms

may produce ligands with unique moieties, kinetic characteristics, and functional forms. Studies utilizing competitive ligand exchange have shown that one or more ligands often are present in the SO [*Nolting et al.*, 1998; *Boye et al.*, 2001; *Croot et al.*, 2004], as they are in other ocean basins. Both *Rue and Bruland* [1997] and *Wu et al.* [2001] measured low concentrations of strongly complexing ligands, whereas weakly complexing ligands were found at much higher concentrations. *Wu et al.* [2001] also found significant concentrations of Fe ligands within the colloidal size range (0.03 – 0.40 μm) in both the oligotrophic North Atlantic and North Pacific. Unfortunately, the similar conditional stability constants measured for a wide-range of ligands [*Witter et al.*, 2000] may make it difficult to discern different species of ligands in situ.

The bioavailability of various Fe-ligand complexes for uptake by phytoplankton is currently uncertain. Experimental work using natural and model ligands suggests that at least some portion of the organically-complexed Fe pool is bioavailable to phytoplankton via cell surface reduction mechanisms [*Soria-Dengg and Horstmann,* 1995; *Hutchins et al.*, 1999; *Maldonado and Price,* 1999; *Shaked et al.*, 2005]. The bioavailability of Fe-ligand complexes for a given phytoplankton taxon appears to depend on the specific ligand in question [*Hutchins et al.*, 1999; *Maldonado and Price,* 1999].

In the frequently ice covered Ross Sea, ice melt-derived and atmospheric Fe only supports a small fraction of the high in situ NPP. Although most Fe likely will be organically complexed over the austral winter, a variety of mechanisms can supply enough Fe to phytoplankton during the spring ice melt. Phytoplankton may rely solely

on photochemical processes to mobilize inorganic dissolved Fe or they may need to access a portion of the organically complexed Fe pool directly. The efficiency of Fe recycling/retention may also differ between the well-stratified MIZ regions of the Ross Sea and the weakly stratified RSP, providing analogues to processes that are likely to be prevalent throughout the SO. To investigate the importance of Fe cycling on phytoplankton dynamics, I parameterized a complex Fe supply model (including the major aspects of seawater Fe chemistry) within the existing three-dimensional Coupled Ice-Atmosphere-Ocean (CIAO) ecosystem model of the Ross Sea. My Fe cycle model is similar in some respects to the model developed by *Weber et al.* [2005] to investigate the cycling of Fe at the Bermuda Atlantic Time Series (BATS). Unlike BATS, the Ross Sea is seasonally ice covered and Fe limited, and I would therefore expect ecosystem processes to exhibit a greater sensitivity to the Fe speciation and cycling represented within CIAO. My Fe supply model is also embedded within a realistic three dimensional ecosystem model and can therefore address questions related to spatial heterogeneity in environmental conditions or phytoplankton taxonomic composition. Specifically, my goal was to assess the role of the various physical (e.g. irradiance), chemical (e.g. organic complexation or photochemistry) and biological (e.g. Fe acquisition strategies) processes in dictating the supply of Fe to the resident phytoplankton across the diverse oceanic habitats present in the Ross Sea. In particular, I was interested in role of ligand-complexed Fe and whether an organically complexed bioavailable Fe pool was necessary to explain the observed phytoplankton dynamics.

2. Model description

Fe is an important nutrient for growth in several important oceanic regions, but is also a highly labile element in seawater due to its involvement in multiple physio-chemical reactions (see above). That said, contemporary models that include Fe biogeochemistry typically utilize relatively simple parameterizations. In this particular investigation I included a seawater Fe cycle that was as representative as permissible. Full details of this parameterization scheme are given in Chapter Two.

The speciation and concentration of Fe in seawater is determined in a variety of fashions that typically discriminate between dissolved (dFe, <0.2 μm) and particulate (pFe, >0.2 μm) phases (see *Bruland and Rue* [2001] for a discussion of the various methodologies). To more accurately simulate the complex Fe cycle in seawater, I replace the simple Fe cycle used previously in CIAO with an Fe supply model that utilizes 4 dFe (including Fe(II), Fe(III), Fe(III)La, and Fe(III)Lb) and 4 pFe (including inorganic particles >0.4 μm and Fe associated with detritus, phytoplankton and zooplankton) Fe pools (Figure 2). In this model, the two free inorganic Fe pools include Fe(II) and Fe(III). Fe(II) oxidation is a function of temperature, producing Fe(III) that can be converted to solid inorganic Fe species (Fe(III)s) and forms ligand complexes that can be either non-bioavailable (Fe(III)La) or bioavailable (Fe(III)Lb). Total Fe (tFe) is simply the sum of the pFe and dFe pools. Bioavailable forms of Fe (bFe) in the standard simulation are taken to be Fe(II), Fe(III), and Fe(III)Lb (see Table 1 for parameter definitions).

The standard run is detailed in Chapter Two, with parameter values ascribed as detailed in Table 1. To assess the role of photoreduction in supplying bioavailable Fe

Figure 2. Schematic of the Fe supply model

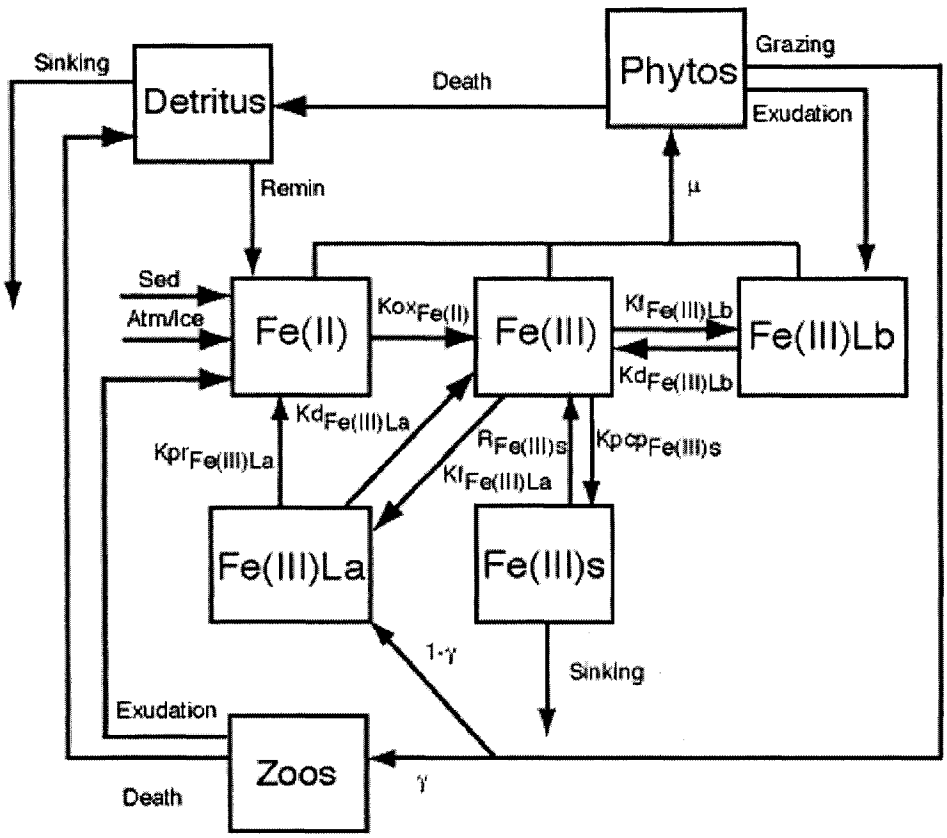

Table 1. Model parameters.

Parameter	Description	Value	Reference
Fe(II)	Inorganic Fe(II)	nM	-
Fe(III)Lb	Bioavailable FeL	nM	-
Fe(III)	Inorganic Fe(III)	nM	-
Fe(III)La	Non-bioavailable FeL	nM	-
Fe(III)s	Solid inorganic Fe	nM	-
dFe	Dissolved Fe	Fe(II) + Fe(III) + Fe(III)La + Fe(III)Lb, nM	-
pFe	Particulate Fe	Fe(III)s + Det_{Fe} + Phyto, nM	-
bFe	Bioavailable Fe	Fe(II) + Fe(III) + Fe(III)Lb, nM	-
tFe	Total Fe	dFe+pFe, nM	-
Det_{Fe}	Detrital Fe	nM	-
L_a	Concentration of the non-bioavailable ligand	2 nM	*Boye et al.*, 2001; *Croot et al.*, 2004
L_b	Concentration of the bioavailable ligand	0.6 nM	*Rue and Bruland*, 1997
k_{ox}	Fe(II) oxidation rate constant	$9x10^{-22}e^{(0.1455T(T))}$, s^{-1}	*Millero et al.*, 1987
k_{pr}	Fe(III)La photoreduction rate constant	((PAR/4.16)*1.67x10^{-7})*(100/35), s^{-1}	*Rijkenberg et al.*, 2005
$k_{fFe(III)Lb}$	Fe(III)Lb formation rate constant	19.6 x 10^5 M^{-1} s^{-1}	*Witter et al.*, 2000
$k_{dFe(III)Lb}$	Fe(III)Lb dissociation constant	1.5 x10^{-6} s^{-1}	*Witter et al.*, 2000
$k_{fFe(III)La}$	Fe(III)La formation rate constant	4.2 x10^4 M^{-1} s^{-1}	*Witter and Luther III*, 1998
$k_{dFe(III)La}$	Fe(III)La dissociation constant	2 x10^{-7} s^{-1}	*Witter and Luther III*, 1998
Log $K_{Fe(III)Lb}$	Conditional stability constant for Fe(III)Lb	23.11	Calculated
Log $K_{Fe(III)La}$	Conditional stability constant for Fe(III)La	22.32	Calculated
k_{pcp}	Fe(III)s precipitation rate constant	2.78 x10^{-5} s^{-1}	*Johnson et al.*, 1994
$R_{Fe(III)s}$	Remineralization rate of Fe(III)s	3.57 x10^{-8} s^{-1}	This Study
K_{sFe}	Half saturation	0.01/0.1 nM	*Arrigo et al.*,

	constant for Fe uptake		2003a
Fe/C_i	Fe to C uptake ratio for phytoplankton group *i*	2.22/10 μmol :mol	*Tagliabue and Arrigo*, 2005
Fe/C_z	Zooplankton Fe to C ratio	5 μmol : mol	*Schmidt et al.*, 1999
Fe_{atm}	Atmospheric deposition of Fe	0.1 μmol m^{-2} yr^{-1}	*Bowie et al.*, 2001
Fe_{sed}	Sedimentary input of Fe	15.7 μmol m^{-2} yr^{-1}	This study
π^X_i	Proportion of total Fe uptake by species i satisfied by Fe(II), Fe(III) or Fe(III)Lb.	unitless	calculated
e_i	Proportion of fixed carbon exuded	0.09/0.19	*Sweeney et al.*, 2000
e_z	Zooplankton exudation of Fe	nM	calculated
Ice_{Fe}	Ice melt flux of Fe(II)	nM	*Edwards and Sedwick*, 2001
R_{det}	Remineralization rate of detritus	3.57 $x10^{-8}$ s^{-1}	*Arrigo et al.*, 2003a

Where two values are given (separated by a backslash), the first is for *P. antarctica* and the second is for diatoms. See section 2 for symbol details.

to phytoplankton, I performed an additional run wherein the rate constant for photoreduction (k_{pr}) was set to zero. In order to address whether a bioavailable organically complexed Fe pool was necessary to replicate the observed phytoplankton dynamics, I also parameterized CIAO such that Fe(III)La was the only ligand present (i.e. no Fe(III)Lb). This run also allowed us to explore whether photoreduction of the Fe(III)La complex can supply enough bFe to sustain the observed phytoplankton blooms. The sensitivity of phytoplankton dynamics to the values ascribed to the rate constants for photoreduction (k_{pr}), formation of Fe(III)La ($k_{fFe(III)La}$), and dissociation of Fe(III)La ($k_{dFe(III)La}$), as well as the Fe pool assigned to recycled Fe, were also explored. In order to remove the effect of taxon-specific variability in phytoplankton demands for Fe, I also performed a simulation wherein both *P. antarctica* and diatoms were assigned the same Fe/C uptake ratio (10 μmol Fe : mol C).

3. Results and Discussion

3.1 Comparison with Observations

Dynamics of surface chlorophyll *a* (Chl *a*) using the new Fe supply model in CIAO are in excellent agreement with satellite retrievals of Chl *a* (Figure 3a and b). The phytoplankton bloom associated with the RSP begins at the end of November and rapidly reaches biomass levels of approximately 10 mg Chl *a* m^{-3}, 90% of which is associated with *P. antarctica* (Figure 3a). Strong katabatic winds and deep mixing in the TNBP delay the onset of the phytoplankton bloom (mostly diatoms) until the beginning of January [*Arrigo et al.*, 1998a]. Once the in situ ice melt begins and surface waters become stratified, phytoplankton in the TNBP reach a peak biomass of

Figure 3. Temporal variability in surface water Chl *a* (mg m^{-3}), the proportion of total Chl *a* associated with *P. antarctica* (phaeo, 0 to 1) and the proportional ice cover (ice, 0 to 1) predicted by CIAO (lines) and Chl *a* measured by SeaWiFS (open symbols) for (a) the RSP (b) the TNBP during the standard run and (c) the RSP and (d) the TNBP when the Fe(III)Lb pool was removed.

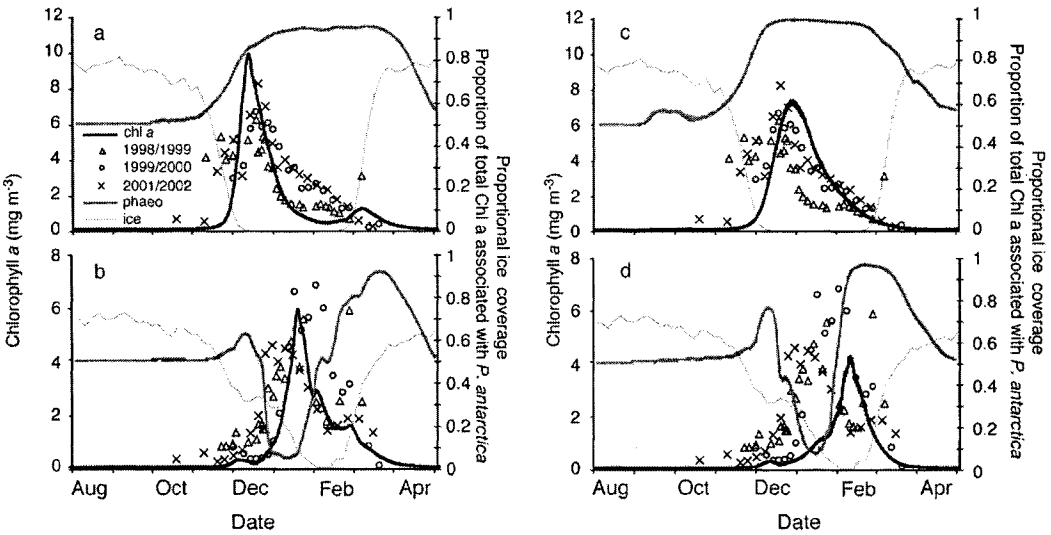

6 mg Chl *a* m^{-3} by mid January (Figure 3b). By mid February, Chl *a* levels are still relatively high (~2 mg m^{-3}), which is consistent with satellite data (Figure 3b). CIAO predicts that although diatoms dominate the initial bloom, *P. antarctica* makes up over half of the phytoplankton biomass during mid to late February (Figure 3b). For a more complete discussion of the significance of phytoplankton taxonomic composition, see *Arrigo et al.* [2003a] and *Tagliabue and Arrigo* [2005].

Annual NPP from CIAO over the whole southwestern Ross Sea is 65.1 Tg C, or 107 g C m^{-2} (including the low productivity waters northeast of the continental shelf break), with rates of 186 and 91 g C m^{-2} for RSP and TNBP, respectively. Model predictions of NPP are in line with the previous version of CIAO [*Tagliabue and Arrigo,* 2005] and both satellite-based and field estimates for the Ross Sea [e.g. *Arrigo and Van Dijken,* 2004; *Smith and Gordon,* 1997].

Vertical profiles of dFe from CIAO fall well within the range of in situ measurements made in the Ross Sea (Figure 4) [*Johnson et al.,* 1997; *Sedwick and DiTullio,* 1997; *Fitzwater et al.,* 2000; *Sedwick et al.,* 2000; *Grotti et al.,* 2001; *Coale et al.,* 2005]. It should be noted that the highest reported in situ dFe concentrations are somewhat atypical of much of the Ross Sea as they were from studies conducted in regions of high sea ice melt where large quantities of Fe were likely released into the water column [*Sedwick et al.,* 2000; *Grotti et al.,* 2001]. The mean dFe concentration from CIAO is approximately 0.4 nM throughout most of the water column, increasing slightly near the sea floor. This is close to the mean in situ dFe value of 0.53 nM, which excludes the upper and lower depth quartiles that are impacted by the atmosphere and sediments, respectively. Maximum dFe concentrations produced by CIAO are found in surface waters (~1.5 nM) and result from the release of Fe as sea ice melts in spring and summer (Figure 4). Concentrations are almost as high near the sea floor due to resuspension of sedimentary dFe. Minimum concentrations of dFe are

Figure 4. A comparison between the global average, minimum and maximum dFe (nM) predicted by CIAO over the course of the standard run (assessed over the entire southwestern Ross Sea, see Figure 1 legend) and in situ measurements of dFe (nM) from a variety of investigators [MLML World Iron Database, *Johnson et al.,* 1997; *Fitzwater et al.,* 2000; *Sedwick and Di Tullio,* 1997; *Sedwick et al.,* 2000; *Grotti et al.,* 2001; *Coale et al.,* 2005]. Note that in order to facilitate comparisons in the bathymetrically heterogeneous Ross Sea, all dFe measurements have been normalized by their maximum depth (0 to 1).

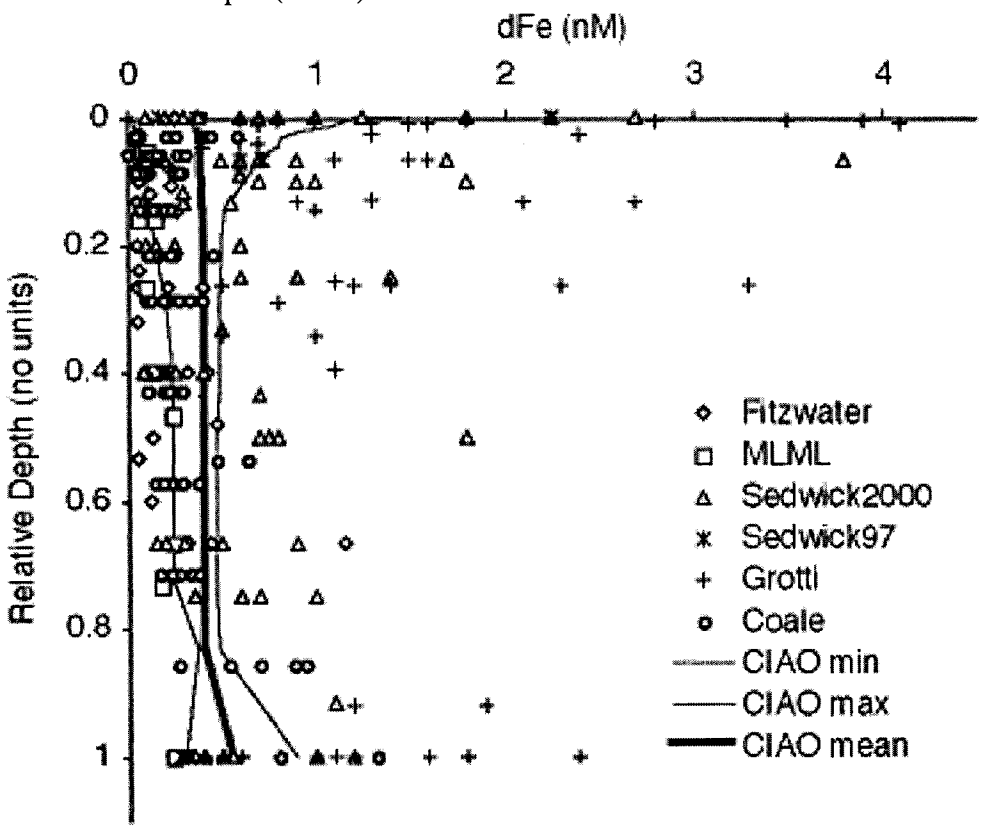

near zero in surface waters and increase with depth to approximately 0.3 nM throughout the rest of the water column, in good agreement with in situ measurements (Figure 4).

3.2 The annual cycle of Fe

Processes such as Fe release from melting sea ice and photoreduction of Fe(III)La to Fe(II) can greatly impact the amount of bioavailable Fe in surface waters. Therefore, it is of interest to contrast the annual cycles of Fe in waters of the Ross Sea where the role played by sea ice processes is large (e.g. the MIZ region near the TNBP) and where it is small (e.g. the RSP). During the ice covered austral winter, CIAO predicts dFe concentrations of approximately 0.4 nM in both the RSP and the TNBP (Figure 5a and b), with over 99% of the dFe pool being organically complexed (by either L_a or L_b). It should be noted that although these bulk dFe concentrations are high (relative to planktonic demands), the bioavailable fraction (bFe) remains low under sea ice (<0.1 nM, Figure 5a). As the system equilibrates (in the absence of light) over the long austral winter, the higher concentration of L_a (relative to L_b) results in Fe(III)La dominating the dFe pool. During spring in the RSP, katabatic winds blow sea ice to the north, and as irradiance levels subsequently increase, the Fe(III)La pool is rapidly photoreduced. This results in an increase in the concentration of the bFe pool, as the Fe(II) produced by photoreduction of Fe(III)La is oxidized to Fe(III) and rapidly complexed by L_b into Fe(III)Lb (Figure 2). Fe(II) is a transient species, with a maximum concentration in CIAO of around 40 pM during periods of enhanced photoreduction, in agreement with observations from the Australian sector of the SO

Figure 5. CIAO predictions of tFe, dFe, bFe and pFe for (a) the RSP and (b) the TNBP, (c) diurnal variability in Fe(III)La and Fe(II) from the 27th to the 29th of October in the RSP (all nM).

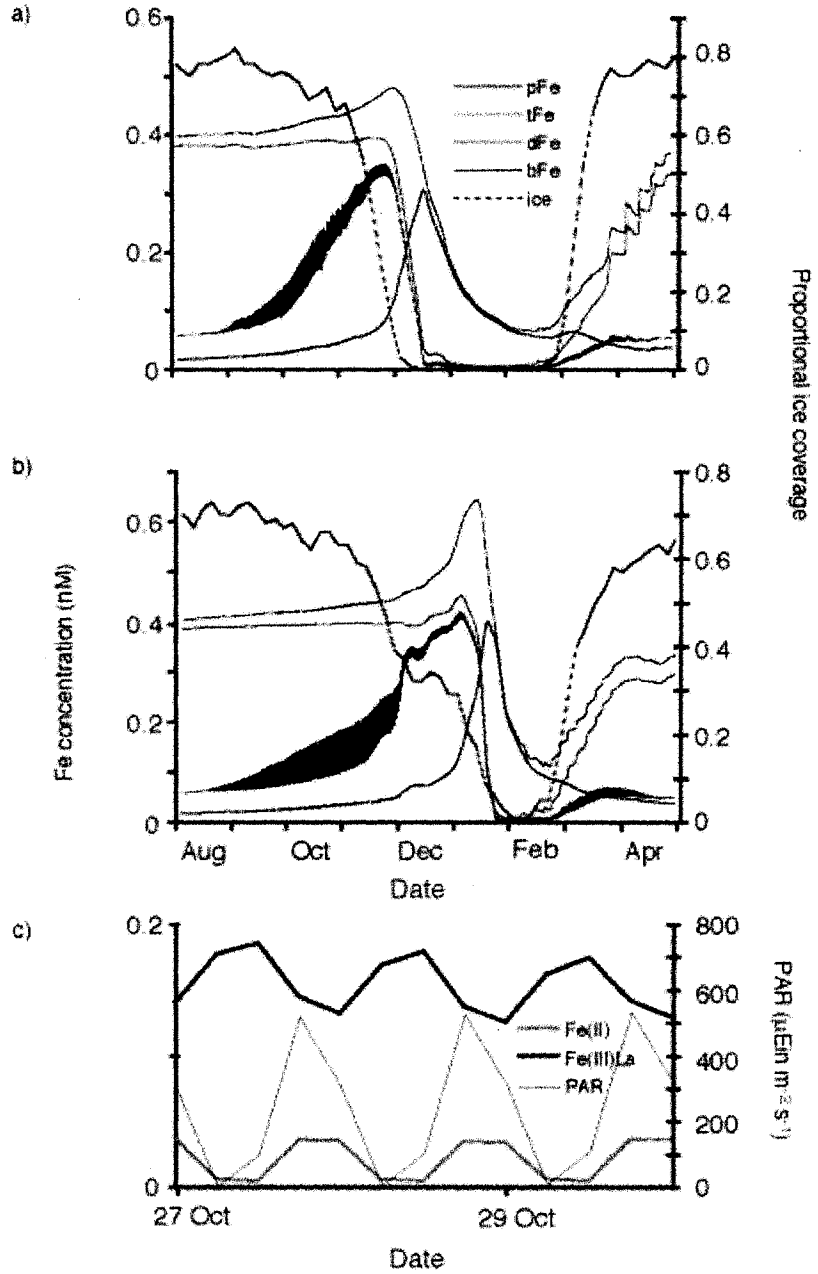

[*Bowie et al.*, 2002]. In contrast, Fe(III) is rarely predicted to exceed 1 pM. The high frequency variation in bFe (Figure 5a and b) is caused by changes in the relative rates of photoproduction and re-oxidation of Fe(II), driven by diurnal changes in irradiance (Figure 5c). The slight increase in tFe by mid November reflects atmospheric deposition onto ice-free surface waters.

Once bFe concentrations in the RSP increase above growth limiting levels in early October, *P. antarctica* begins to bloom and concentrations of dFe and bFe are reduced to zero by early December, with pFe (mostly phytoplankton Fe) dominating the bulk Fe pool (Figure 5a). The peak in pFe lags the Chl *a* peak in the RSP (Figure 3a) by approximately 5 days, reflecting the increased contribution of detrital Fe and Fe(III)s to pFe. Between the end of December and mid-February, almost all pFe sinks below the thermocline, resulting in the loss of ~0.4 nM from the tFe pool in surface waters. Deepening mixed layers in early March increase tFe concentrations in surface waters as relatively Fe-rich water is mixed up from below (Figure 5a). The return of sea ice during April precludes further photochemical conversion of Fe, and therefore tFe, dFe, bFe, and pFe begin to trend towards austral winter values.

While the annual cycle of Fe within the TNBP is generally the same as the RSP, there are some important differences (Figure 5b). As in the RSP, wintertime dFe is quite high in the TNBP, with most contained in organic complexes that are unavailable to the phytoplankton. However, high rates of ice melt in the TNBP increase tFe by 0.25 nM in January. Photoreduction of Fe(III)La also creates ample bFe in the TNBP by the beginning of December, but this remains unutilized until mid-January (Figure 5b) when the ice melt has completely stratified surface waters and

phytoplankton are no longer light limited. CIAO predicts that inorganic Fe(II) concentrations are also slightly higher in the TNBP (maximum of approximately 70 pM) than the RSP (40 pM, see below for discussion). In the current version of CIAO, appreciable Fe(II) can only be produced via photoreduction of Fe(III)La (atmospheric sources are negligible). However, in nature, oxidative reactions with hydrogen peroxide and back reactions between Fe(III) and superoxide are also important in dictating Fe(II) concentrations [e.g. *Croot et al.*, 2005]. That said, photoreduction rate constants that are derived from measuring Fe(II) evolution [e.g. *Rijkenberg et al.*, 2005] already account for these other processes that produce Fe(II). The accumulation and sinking of pFe is predicted to occur over a much shorter timescale in the TNBP (1 month) than the RSP (2 months); this is most likely to be due to the relative delay of the TNBP phytoplankton bloom. Consistent with the higher Fe demand of diatoms, there is a greater loss of Fe from TNBP surface waters (~0.6 nM).

The annual cycle of irradiance (modulated by sea-ice cover) also drives changes in Fe speciation with respect to depth. In deep water, the ratio of Fe(II)/dFe from CIAO is 0.04, whereas during photoreduction in surface waters the Fe(II)/dFe ratio increases to 0.2 in both the RSP and the TNBP, consistent with observations by *Bowie et al.* [2002]. Light attenuation by phytoplankton biomass will also affect Fe speciation. For example, CIAO shows that in waters characterized by large spring phytoplankton blooms (e.g. the RSP and TNBP), downwelling irradiance and photoreduction of Fe(III)La are retarded below the surface layers. This results in a delay in the photoreduction of Fe(III)La in subsurface waters (e.g. 25 m in the RSP, Figure 6). As the RSP spring phytoplankton bloom declines in late December, the concomitant

increase in subsurface irradiance results in photoreduction of Fe(III)La at 25 m (Figure 6). Deepening mixed layers during the late summer also exposes subpycnocline Fe(III)La to elevated light levels and subsequent photoreduction will increase bFe concentrations. Elevated bFe during the late austral summer stimulates increased phytoplankton biomass during mid March in both the RSP and the TNBP (Figure 3a and b).

Recycling of Fe via zooplankton grazing is of little consequence, due to the low zooplankton biomass and grazing rates within the Ross Sea [*Tagliabue and Arrigo,* 2003]. However, zooplankton-mediated Fe recycling will be significant in regions where large fractions of phytoplankton biomass are consumed by higher trophic levels, such as the Polar Front or near South Georgia [*Atkinson et al.,* 2001]. Microzooplankton and bacteria could also be acting as agents of Fe recycling [*Hutchins et al.,* 1995; *Barbeau et al.,* 1996], but while such processes are not explicitly included in CIAO at the present time, microzooplankton grazing rates and bacterial biomass are both low in the Ross Sea [*Caron et al.,* 2000; *Ducklow et al.,* 2000]. CIAO predictions of export compare well with in situ data [see: *Arrigo et al.,* 2003a] and it therefore appears reasonable to suggest that both the RSP and TNBP surface waters are net vertical exporters of Fe (alongside other nutrients), replenished each winter by convective mixing.

3.3 Significance of photoreduction and organic complexation

I performed tests to examine the importance of the process of photoreduction and

Figure 6. Time series of Fe(III)La, at the surface and 25m depth (nM), and phytoplankton chlorophyll *a* (mg m^{-3}) in the RSP.

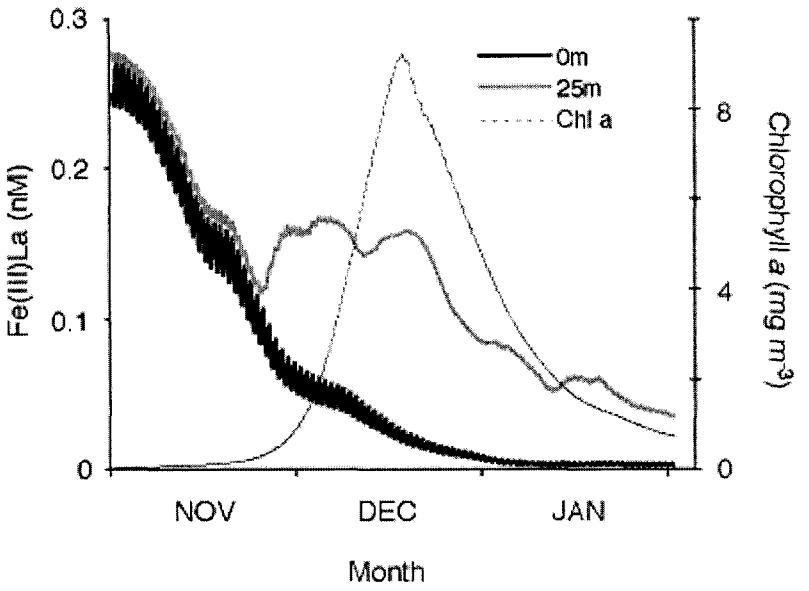

the presence of the Fe(III)Lb pool in predicting regional NPP and phytoplankton dynamics. Photoreduction of organically bound Fe is important in governing Fe speciation transitions and is posited to be responsible for the higher than expected Fe(II) concentrations measured during the later stages of SOIREE [*Croot et al.,* 2001]. By setting the rate constant for Fe(III)La photoreduction (k_{pr}) to zero, I was able to test the significance of photoreduction. Model results show that during the austral winter, almost all the Fe is complexed by ligands into forms unavailable to phytoplankton (Figure 5a and b). However, by retaining Fe within a photolabile organic complex, Fe(III)La can be rapidly mobilized into bioavailable phases once irradiance levels increase during the spring ice melt. Free Fe(II) produced by photolysis of Fe(III)La is then either consumed by phytoplankton, stabilized by L_b (and made available for uptake), or oxidized to Fe(III) and either taken up by phytoplankton, re-complexed by L_a, or lost to the refractory Fe(III)s pool. In the absence of photoreduction, regional cumulative NPP over the southwestern Ross Sea is reduced by >90% to 5 Tg C yr^{-1}, with appreciable production limited only to regions with substantial Fe(II) input from melting sea ice (data not shown).

In the southwestern Ross Sea, the cycling of Fe is predominately governed by photochemical processes, although in other regions, recycling by zooplankton and bacteria will also be important. Herbivory rates of meso- and microzooplankton are low in the Ross Sea [*Caron et al.,* 2000], likely due to the decoupling between primary and secondary production [*Tagliabue and Arrigo,* 2003]. Consequently, my findings are not sensitive to the precise Fe pool assigned to both the unassimilated grazing products and the products of detrital remineralization. In regions where secondary

production plays a more important role, e.g. the Antarctic Peninsula region, the speciation of Fe liberated by herbivory and remineralization will likely prove to be more important.

The characteristics of the ligands could prove to be of greater significance than recycling in the Ross Sea. *Maldonado et al.* [2005] suggest bioavailable Fe-organic complexes in the Sub-Antarctic region of the SO could well be photoreactive. Model results suggest that assigning photolability to Fe(III)Lb would result in only a slight increase in the Fe(III)s pool and little change in rates of phytoplankton primary production, especially in regions where cold surface waters retard rates of Fe(II) oxidation. Similarly, if I reduce the formation rate constant for Fe(III)La ($k_{fFe(III)La}$) by half, there is little impact on phytoplankton biomass accumulation and annual rates of photoreduction in the TNBP remain greater than those in the RSP. In the absence of photoreduction, the only scenario that results in phytoplankton biomass in accordance with observations is when the dissociation constant for Fe(III)La ($k_{dFe(III)La}$) is increased ten-fold, which approximates the role of photoreduction (i.e. breakdown of Fe(III)La complexes). However, unlike photoreduction, dissociation will also occur in dark, ice covered waters. Since there is no phytoplankton uptake under such conditions, there are increasing losses to the Fe(III)s pool and biomass at the peak of the RSP bloom is reduced by around 20%. In the TNBP, I predict a reduction in phytoplankton biomass of approximately 10% at the peak of the diatom bloom, and an increase of 20% during the later *P. antarctica* bloom. Rates of Fe(III)La dissociation in deep waters are elevated markedly during this scenario, resulting in increased deepwater bFe concentrations (by almost 0.25 nM). This extra Fe fuels additional biomass

accumulation by *P. antarctica* in the TNBP as mixed layers deepen in the late summer. Nevertheless, this suite of experiments suggest that photoreduction of Fe(III)La is the key process governing the supply of Fe to phytoplankton in regions of the SO where there is a substantial increase in irradiance resulting either from the loss of sea ice or from increased surface stratification as winds subside in spring.

The ability of phytoplankton to take up ligand-bound Fe has been demonstrated in culture experiments [e.g. *Soria-Dengg and Horstmann,* 1995; *Hutchins et al.,* 1999; *Shaked et al.,* 2005] and some field studies [*Maldonado and Price,* 1999; *Maldonado et al.,* 2005], but this may depend on the specific phytoplankton and ligand group in question *[Hutchins et al.,* 1999; *Blain et al.,* 2004]. In order to examine the potential importance of Fe(III)Lb complexes, I parameterized CIAO such that L_a was the only ligand present in seawater and the subsequent Fe(III)La complexes were unavailable to the phytoplankton. In the absence of the Fe(III)Lb, the resident phytoplankton rely on enhanced photochemical recycling of Fe(III)La to maintain bFe above growth limiting levels. This additional recycling results in a greater loss of Fe in the form of Fe(III)s, thus reducing the total bFe pool and further highlights the role Fe ligands play in the buffering of reactive Fe concentrations. As a result, cumulative regional NPP was reduced by 30%, from 61.7 Tg C yr^{-1} during the standard run to 43.7 Tg C yr^{-1}.

The reduction in NPP due to the absence of Fe(III)Lb was not uniform over the southwestern Ross Sea. Phytoplankton dynamics in the RSP change little, although the bloom is delayed somewhat relative to the standard run and is lower in magnitude (compare Figure 3c with Figure 3a). In line with the small changes in phytoplankton dynamics in the RSP, annual NPP is only predicted to fall by around 6%. The change

in phytoplankton dynamics resulting from the loss of the Fe(III)Lb pool is much more dramatic in the TNBP, where annual NPP is reduced by 45%. Furthermore, in the absence of Fe(III)Lb, the primary (mid January) diatom bloom never develops and only when mixed layers deepen during March does an appreciable bloom form (compare Figure 3d with Figure 3b). This later bloom has never been observed in SeaWiFS satellite retrievals and is predicted to be dominated by *P. antarctica* instead of the diatoms more commonly observed in such MIZ waters (Figure 3d).

The results of these simulations suggest that the ability to access some portion of the organically complexed Fe pool is of much greater significance in MIZ waters dominated by phytoplankton with a high Fe demand (such as diatoms), than in the weakly stratified, *P. antarctica* dominated RSP. This is consistent with culture experiments demonstrating the uptake of organically bound Fe by diatoms and other large phytoplankton via cell surface reduction mechanisms [e.g. *Soria-Dengg and Horstmann*, 1995; *Maldonado and Price,* 1999; *Shaked et al.,* 2005] and reduced rates of uptake by smaller phytoplankton [*Blain et al.,* 2004].

Previous CIAO simulations suggested that photosynthetic characteristics control species composition in the Ross Sea during spring [*Arrigo et al.,* 2003a]. However, if the resident phytoplankton exhibit taxon-specific uptake of organically bound Fe, then regional heterogeneity in environmental conditions and the subsequent speciation of Fe also may be important in determining species composition in the Ross Sea. It appears reasonable to suggest that although dFe concentrations are high during the austral spring, most dFe will be organically complexed, with low concentrations of inorganic Fe(II) and Fe(III). The results of these simulations suggest that it is possible

that *P. antarctica* and diatoms might employ different Fe acquisition strategies to sustain their high biomass levels. In the RSP, weak stratification results in low photoreduction rates of Fe(II), but the low Fe demand of *P. antarctica* allows this taxon to bloom profusely, despite the low bFe concentration. In the well-stratified TNBP, elevated rates of sea-ice melting and photoreduction of Fe(III)La supply a much higher bFe concentration. Diatoms, with their high Fe demand, might require these high Fe recycling rates, as well as an ability to access a portion of the organically complexed Fe pool, in order to reach high biomass. Therefore, light might control species composition in the Ross Sea by impacting both phytoplankton photosynthetic performance [*Arrigo et al.*, 2000] and Fe speciation. To address this possibility will require information about the kinetic characteristics and sources and sinks of such ligands in seawater and the subsequent bioavailability of organically bound Fe to specific phytoplankton taxa.

3.4 Efficient Fe cycling in MIZ waters

In the MIZ, melting sea ice creates a shallow (10-20 m) stratified surface layer that is well illuminated and often augmented with exogenous Fe and sea ice algae. As a result of the high light and high Fe conditions, there are often significant levels of both biological productivity [e.g. *Smith and Nelson,* 1986; *Arrigo et al.*, 1998b] and trophic transfer [e.g. *Hopkins et al.*, 1993] associated with the MIZ. Annual cumulative rates of photoreduction across the southwestern Ross Sea calculated from CIAO show that there is significantly more recycling of Fe within regions characterized by significant sea ice melt and shallow mixed layers (such as the TNBP) than in the weakly stratified

RSP (Figure 7a and b). Elevated annual photoreduction rates in the RSP are due to the greater number of ice-free days in this region, compared to the surrounding MIZ (Figure 8a). The highest annual rates of photoreduction occur where the minimum annual mixed layer depth is <10 m (Figure 9). Over the course of the year, the greater flux of Fe from sea ice melting and relatively shallow mixed layers close to Edward VII Land result in the highest cumulative rates of Fe photoreduction, even though the proportional sea-ice coverage does not fall below 0.4 (Figure 7a). CIAO produces rates of Fe(III)La photoreduction that average (December through January) 0.58×10^{-5} s^{-1} and 1.13×10^{-5} s^{-1} for the RSP and TNBP, respectively, both slightly lower than previously published estimates [e.g. *Miller et al., 1995; Barbeau et al.,* 2001; *Emmenegger et al.,* 2001]. Even if the calculated rate constant for Fe(III)La photoreduction is halved, annual photoreduction is only reduced by approximately 20% across the southwestern Ross Sea and the relationship between rates of Fe(III)La photoreduction and mixed layer depth is retained (data not shown).

Typically, MIZ waters are significantly colder than non-MIZ regions such as the RSP [*Arrigo et al.*, 2000], which will impact Fe(II) oxidation rates in CIAO by reducing the rate constant for Fe(II) oxidation (k_{ox}, Table 1). This is important because any decline in Fe(II) oxidation rate as temperature decreases [*Millero et al.,* 1987] will consequently increase the residence time of Fe(II) in the euphotic zone. Sea ice melting in the MIZ of the TNBP (and other MIZ regions) reduces surface water temperatures, whereas the upwelling of circumpolar deep water in the RSP raises temperatures by over 3°C [e.g. *Jacobs and Giulivi,* 1999]. Given the average rate

Figure 7. The spatial distribution of (a) annual photoreduction of Fe(III)La (nM), with proportional ice cover contoured (0 to 1, no units), (b) minimum mixed layer depth (m), and (c) the mean Fe(II) oxidation rate constant (between October and February, s^{-1}). In panels b and c, white areas are where the proportional ice coverage is greater than 0.1 throughout the year.

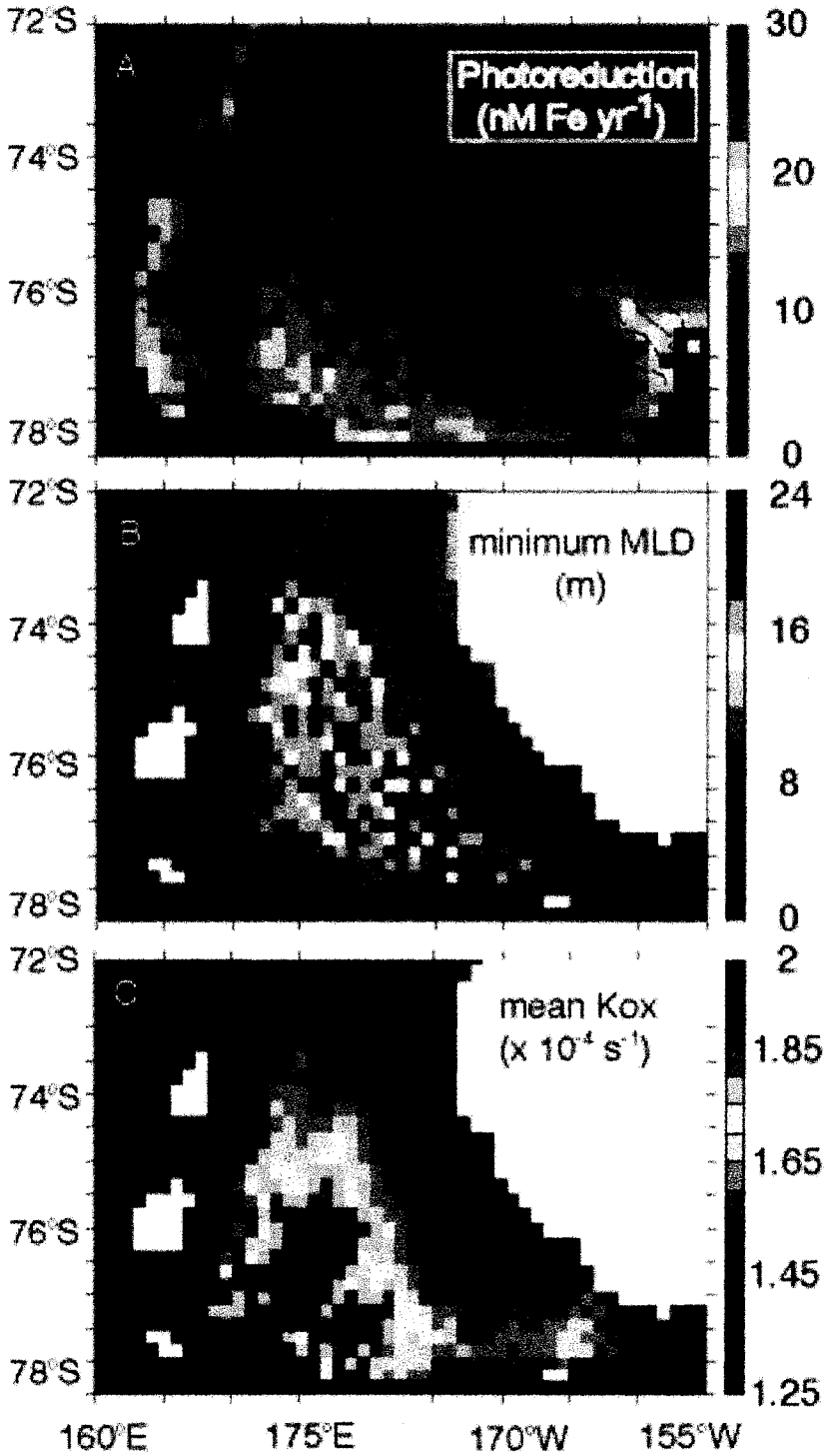

Figure 8. The spatial distribution (a) ice free days, where 'ice free' is considered a proportional ice coverage less than or equal to 0.2 and (b) annual photoreduction of Fe(III)La when the concentration of Fe in sea ice is set to zero (with proportional ice cover contoured, nM).

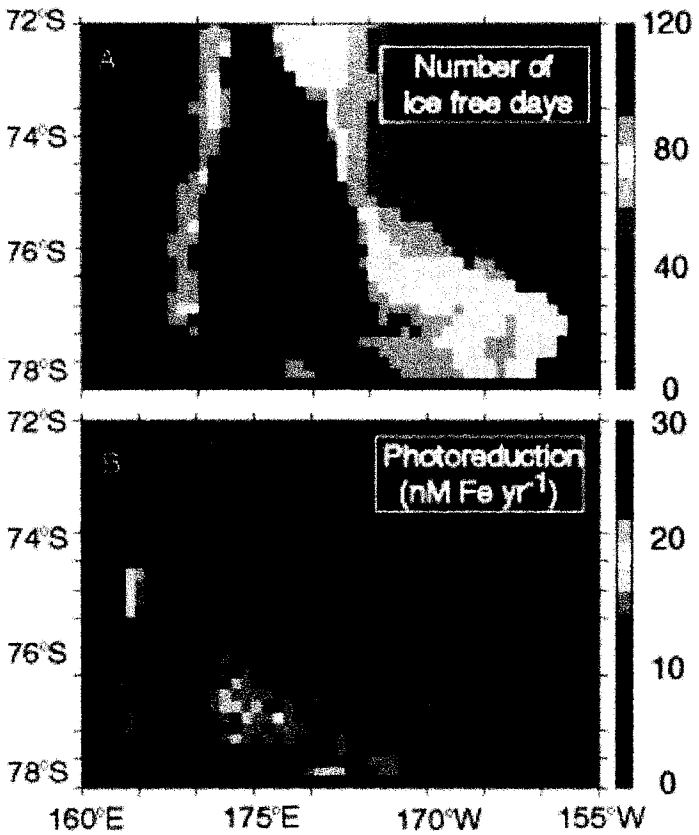

Figure 9. Annual photoreduction of Fe(III)La (nM Fe) as a function of minimum mixed later depth (m), evaluated the entire study area (see Figure 1).

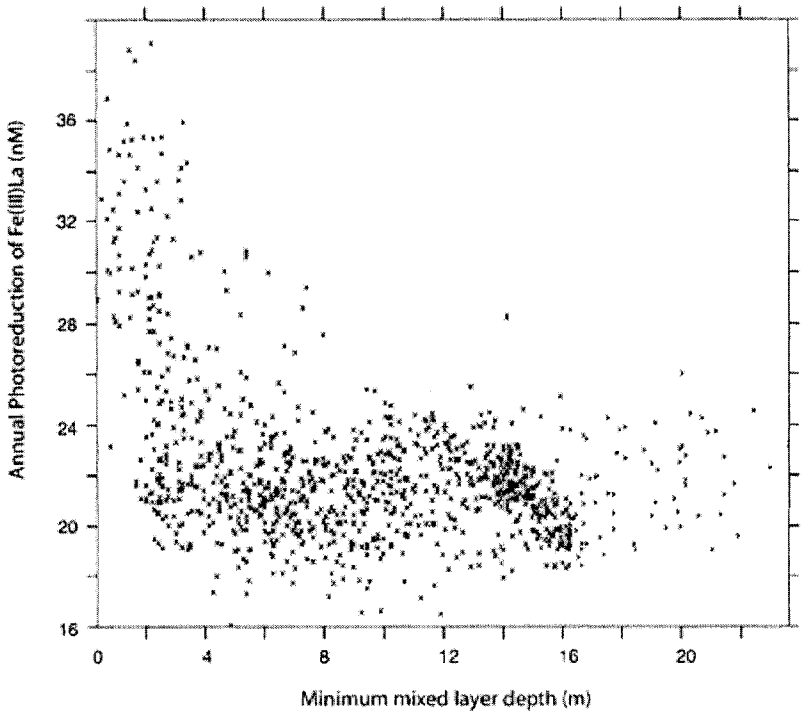

constant for Fe(II) oxidation (k_{ox}) for the growing season (between early December and early February), rates of Fe(II) oxidation are calculated to be much lower in the MIZ waters west of 170°E than within the RSP (Figure 7c). This is because the 3°C temperature difference between the TNBP and RSP yields a value for k_{ox} that is 55% greater in the RSP. Higher Fe(II) production rates (photoreduction) and lower loss rates (oxidation) likely explain why the maximal predicted Fe(II) concentration in the TNBP is higher than within the RSP.

Not only does melting sea ice usually provide an exogenous supply of Fe to surface waters, it also creates an environment that is highly favorable for efficient Fe recycling. Low vertical diffusivity in ice-melt stratified waters will retard the mixing losses of bFe to deeper waters that might be expected in a weakly stratified region such as the RSP. Furthermore, water column dFe, augmented by any Fe released from sea ice, will experience an environment that is both cold (low oxidation rates) and well illuminated (high photoreduction rates) during spring, resulting in effective Fe recycling and retention. In fact, even in the absence of an ice melt source of Fe, MIZ regions exhibit high rates of Fe recycling due to their shallow mixed layers. Daily rates of photoreduction within the MIZ only decrease by ~10% and remain approximately twice those of the RSP if the Fe concentration in melting sea ice is set to zero within CIAO (considering spatial heterogeneity in open water duration, Figure 8a and b). The unusually large reduction in cumulative photoreduction predicted in waters near Edward VII land was due to the large amount of ice melt and associated Fe release that typifies this region. My results suggest, however, that high Fe photoreduction rates in the MIZ are mostly a consequence of the physical environment

(e.g. high light, low temperature) and not simply due to additional Fe input from sea ice melting. This implies that interannual changes in sea ice dynamics, such as those observed in the Ross Sea during recent years [*Arrigo and Van Dijken*, 2004], could drive significant variability in Fe cycling and hence phytoplankton productivity in polar regions.

3.5 Utilization of Fe

In order to understand how changes in the supply of Fe (via natural or anthropogenic means) might impact the cycling of carbon, one must understand how efficiently dFe is converted into phytoplankton carbon via photosynthesis. The iron use efficiency (IUE, sensu *Raven,* [1988]) for a given habitat (referred to here as the apparent IUE) is a function of both biotic (e.g. Fe requirements of phytoplankton, remineralization) and abiotic (e.g. oxidation and photoreduction of Fe modulated by temperature and stratification, respectively) factors. For instance, waters conducive to Fe photoreduction and with phytoplankton having a low Fe requirement will exhibit a higher apparent IUE than waters with the opposite characteristics. In order to isolate the effect of abiotic factors on the apparent IUE, I assigned *P. antarctica* and diatoms the same cellular Fe/C requirement (10 μmol : mol) and examined differences in the ratio of depth integrated dFe depletion to depth integrated NPP between the RSP and the TNBP. Because the physical conditions of the RSP and TNBP change throughout the year, I evaluated the apparent IUE (NPP/ΔdFe) on a monthly basis during the growing season.

The apparent IUE is always highest when mixed layers are shallow and temperatures are low (see Table 2). During November, strong katabatic winds in the TNPB result in a significantly deeper mixed layer depth (MLD, >100 m) than in the RSP (33 m), whereas the average sea surface temperature (SST) is similar in both locations (-2°C). Increased photoreduction of Fe(III)La in the RSP results in a much higher apparent IUE than within the TNBP (by >90%). Once the katabatic winds begin to slacken in mid December, the average MLD in the TNBP becomes slightly less than in the RSP, while the RSP SST is almost 1°C warmer than in the TNBP. Decreased bioavailability of Fe due to increased oxidation of Fe(II) in the RSP results in a lower apparent IUE than in the TNBP. By January, the TNBP becomes much more stratified (22 m and 5 m for the RSP and TNBP, respectively) and upwelling of warm CDW in the RSP raises SST by almost 3°C above that of the TNBP. The combined effect of shallow mixed layers (high rates of photoreduction) and low temperatures (low oxidation rates) in the TNBP result in a much greater apparent IUE for this region in January, relative to the RSP. By February, MLD in the TNBP is again greater than in the RSP (31 m and 20 m, respectively), while average SSTs remain warmer in the RSP (by >2°C). These two conditions offset, resulting in similar apparent IUEs for both the RSP and the TNBP during this month. The role of MLD and SST upon the apparent IUE for the RSP and the TNBP is summarized in Table 2.

Non-biogenic losses of Fe will be more significant in the permanently open ocean zone (POOZ) than the seasonally ice covered zone (SIZ) of the SO. As for the RSP, surface waters of the POOZ are warmer and less stratified than the SIZ (i.e. elevated rates of oxidation, but low photoreduction rates) which result in less efficient Fe use

Table 2. General trends in monthly integrated apparent IUE and monthly averaged mixed layer depth (MLD, m) and sea surface temperature (SST, °C) for the RSP and the TNBP (when both *P, antarctica* and diatoms are endowed with an Fe/C ratio of 10 μmol : mol). Percentage values in parentheses are the % change relative to the RSP apparent IUE.

	Monthly Average		Monthly Integral
Month	MLD	SST	Apparent IUE
NOV	RSP << TNBP	RSP ≈ TNBP	RSP >> TNBP (+93%)
DEC	RSP > TNBP	RSP > TNBP	RSP < TNBP (-25%)
JAN	RSP >> TNBP	RSP >> TNBP	RSP << TNBP (-50%)
FEB	RSP < TNBP	RSP > TNBP	RSP ≈ TNBP (+5%)

(in terms of fueling NPP). I have shown that temporal changes in the physical environment greatly impact the rate of NPP per unit Fe removed (via the apparent IUE) in the Ross Sea. Moreover, I propose that regions of the SO that are characterized by relatively unstratified and warm surface waters (such as the POOZ) will exhibit less efficient dFe use (as a function of NPP) than those regions typified by well stratified, cold surface waters (such as the SIZ). My analysis shows that while apparent ratios of Fe/NPP measured in the field will be robust estimators of the ratio of depletion/accumulation of various elements in a given physical region (the apparent IUE), they are not likely to be accurate reflections of the actual planktonic demands for Fe (the planktonic IUE, moles carbon fixed per mole Fe taken up, *Raven* [1988]) that would be measured in a laboratory or parameterized in an ecosystem model. This will be especially true if the nutrient in question (e.g. Fe) undergoes cycling that is strongly affected by variability in environmental conditions (e.g. temperature).

4. Conclusions

The speciation of Fe in waters south of the Antarctic Circle (such as in the Ross Sea) is controlled primarily by photochemical processes, which are, in turn, driven by the annual cycle of solar irradiance, stratification, and sea-ice melt/refreeze. I have shown that the speciation of Fe can have profound impacts upon phytoplankton, particularly within MIZ waters dominated by taxa with a high Fe demand. Therefore, the nature of the spring ice-melt, and the degree of surface water stratification, will be crucial in dictating Fe speciation and ensuing Fe supply to phytoplankton. Although my Fe supply model was developed for the Ross Sea, it includes sufficient flexibility

in its parameterizations for my major conclusions to be applicable to the SO as a whole.

If distinct phytoplankton taxa such as *P. antarctica* and diatoms rely on different Fe acquisition strategies, then there may be a role for Fe in controlling species composition in the Ross Sea (and in other regions). Although dFe is above growth limiting levels at the time of the spring sea ice melt, it may be the chemical speciation, and in particular the nature of any organic complexation and subsequent bioavailability and/or photolability, that is of importance in understanding its impact upon phytoplankton. The Ross Sea is a region of net Fe export and depends on convective overturn to replenish surface waters with photolabile, organically complexed Fe during the austral winter. Further information on both the speciation of dissolved Fe and the bioavailability of such Fe species to phytoplankton is necessary to understand how changes in Fe supply might impact Antarctic phytoplankton and the regional carbon cycle. A better understanding of the plasticity in planktonic Fe demands, the bioavailability of in situ Fe-ligand complexes and the variability in sea ice Fe concentrations/speciation will aid future model improvement.

I propose that MIZ waters are regions of efficient Fe recycling and moreover, that this is primarily due to the physical environment created by the ice melt (stratification and temperature), rather than enhanced Fe supply. The ratio of dFe depletion to NPP in a given area (the apparent IUE) will depend upon the planktonic demand as well as the physical nature of the mixed layer and the extent of Fe recycling allowed therein. This could prove to be important in comparing the efficiency of Fe fertilization experiments conducted in locations characterized by different physical properties [*De*

Baar et al., 2005]. I have shown that the cycling of Fe (in terms of NPP) is more efficient in the SIZ regions of the SO, relative to the POOZ. If, as a consequence of future [e.g. *Sarmiento et al.*, 1998] or past [e.g. *Anderson et al.*, 2002] climatic change, a large proportion of the SO POOZ became more stratified during the austral spring/summer, then the enhanced recycling and retention of Fe (via an increased apparent IUE) should result in enhanced primary productivity, independent of any increase in Fe supply.

Chapter 6

The influence of mixed layer properties on Fe cycling

Abstract The cycle of Fe is governed by physical factors such as temperature and irradiance, as well as biological activity. Here I present results examining the role of abiotic and biotic processes in governing the cycling of Fe as a function of mixed layer temperature (MLT) and irradiance (MLI). This was achieved by formulating a relatively complex steady-state model of the seawater Fe cycle, both with and without a biological component. While phytoplankton biomass and Fe pools are highly sensitive to the MLI, I show that the MLT was of lesser importance if there was either a bioavailable organically complexed Fe pool or if phytoplankton were endowed with a very low requirement for Fe. Photochemistry was of particular importance in governing bioavailable Fe concentrations in cold mixed layers. In warmer waters, photochemistry was of a lesser importance and the presence of a bioavailable organically complexed Fe pool was of greater significance. However, an ability to access organically complexed Fe may be a common feature of all phytoplankton that have a high requirement for Fe, regardless of MLT. Fe limits primary productivity across the modern Southern Ocean. Therefore, any changes in mixed layer characteristics during the geologic past or future would drive variability in Fe cycling, and hence primary production and uptake of atmospheric CO_2.

1. Introduction

Sverdrup [1953] demonstrated that for phytoplankton to bloom, the mixed layer must be shallower than the depth at which vertically integrated photosynthesis is balanced by community respiration (the so-called critical depth). In temperate zones, the onset of stratification is driven by the springtime warming of surface waters, and if this follows a period of deep mixing, then ample macronutrients will be present in the mixed layer to fuel high rates of net primary production (NPP). In polar waters, the formation of sea ice during the austral autumn and winter will drive convective overturn, thus replenishing surface waters with dissolved nutrients. The springtime melting of seasonal sea ice results in the intense stratification of surface waters (due to freshwater input) and very cold, shallow mixed layers that are exposed to high light levels.

However, there are some areas of the worlds oceans where phytoplankton fail to bloom, even under well-stratified conditions with high macronutrient concentrations. Phytoplankton in these high nutrient low chlorophyll (HNLC) regions generally have been found to be limited by the availability of iron (Fe). Such regions include the Sub-Arctic Pacific [*Tsuda et al.,* 2003; *Boyd et al.,* 2004], the Equatorial Pacific [*Coale et al.,* 1996], and the Southern Ocean [*Boyd et al.,* 2000; *Coale et al.,* 2005]. The Southern Ocean is by far the largest HNLC region, both in terms of geographic area and the abundance of unused macronutrients [*Conkright et al.,* 1994]. Rates of NPP can be high in Southern Ocean Waters, but are restricted to locations with significant Fe supply, generally from deep waters [*De Baar et al.,* 1995]. Such regions include continental shelf polynyas and marginal ice zones (MIZ) [*Hart,* 1934;

Arrigo et al., 1998b; *Moore and Abbott,* 2000; *Arrigo and Van Dijken,* 2003a], island wakes in offshore waters (e.g. the Kerguelen Islands) [*Blain et al.,* 2001], and frontal zones [*Moore and Abbott,* 2000]. In the subarctic Pacific, the degree of Fe limitation shows a pronounced increase between the northwest and the northeast gyres, and is controlled by Fe deposition from Asian dust [*Harrison et al.,* 1999]. Episodic fluxes of Fe in the northeast gyre stimulate increases in small-celled phytoplankton, which become tightly coupled to micrograzers and regenerated nitrogen sources [*Harrison, et al.,* 1999; *Banse and English,* 1999]. In the Equatorial Pacific, Fe inputs from upwelling are too low for large diatoms to grow, but sufficient to stimulate small phytoplankton size classes. However, high rates of grazing by fast growing microzooplankton result in low overall biomass accumulation rates [*Landry et al.,* 1997]. Accordingly in the Equatorial Pacific, large phytoplankton are indeed limited by Fe, whereas small phytoplankton size classes are grazer controlled (although it has been shown that their photosynthetic competence is also reduced) [*Landry et al.,* 1997].

While the importance of Fe to phytoplankton metabolism and growth is now well established [e.g. *Raven,* 1988; *Sunda and Hunstman,* 1995], processes that control Fe availability and cycling are less well known. The transformation and cycling of Fe is governed by physical factors such as temperature and irradiance, as well as by biological activity. The cycle of Fe in seawater is complex and Fe exists in a variety of oxidation states and phases [*Morel and Price,* 2003; *Wells et al.,* 1995]. The dissolved Fe pool (dFe, passes through a 0.2 μm filter) contains free inorganic Fe(II) and Fe(III), with >99% bound to a variety of organic ligands [e.g. *Witter and Luther,*

1998; *Wu et al.,* 2001; *Croot et al.,* 2004]. Particulate Fe (pFe, captured by a 0.2 μm filter) is made up of inorganic particles and the Fe associated with phytoplankton, zooplankton, and bacteria. Fe(III) is lost to solid phases such as oxyhydroxides via precipitation/scavenging [*Johnson et al.,* 1994], which are unavailable to phytoplankton. However, phytoplankton can readily take up both free inorganic Fe(II) and Fe(III) [*Anderson and Morel*, 1982] and probably ligand-bound Fe as well [*Maldonado and Price,* 1999; *Maldonado et al.,* 2005], although this has not been demonstrated conclusively [e.g. *Hutchins et al.,* 1999; *Blain et al.*, 2004]. At oceanic pH, Fe(II) oxidation is a first order function of temperature [*Millero et al.,* 1987] and resupply of Fe(II) via photoreduction of the Fe-ligand complex is mediated by irradiance [*Miller et al.,* 1995; *Barbeau et al.,* 2001; *Emmenegger et al.,* 2001; *Rijkenberg et al.,* 2005], with the degree of photolability depending on the specific nature of the Fe-ligand complex [*Barbeau et al.,* 2003].

Variability in mixed layer depth will impact the mixed layer irradiance (MLI) and temperature (MLT), both of which directly influence phytoplankton growth rates [*Ryther,* 1956; *Eppley,* 1972] and determine phytoplankton bloom dynamics, as noted long ago by *Sverdrup* [1953]. However, because photoreduction of organically complexed Fe is a means by which Fe can be converted to bioavailable forms, the degree of surface stratification will also influence the cycling of Fe [*Tagliabue and Arrigo,* 2006]. This aspect of changing mixed layer depths has not been considered previously, yet may be critical in the regulation of phytoplankton growth rates, particularly in Fe-poor waters. In addition, changes in sea surface temperatures resulting from stratification will impact the residence time of bioavailable Fe via both

the temperature dependence of oxidation and phytoplankton growth rates. In light of recent field and laboratory studies on uptake of organically complexed Fe by phytoplankton [*Barbeau et al.,* 2003; *Maldonado et al.,* 2005; in press], it is also of interest to examine the significance of the degree of bioavailability and/or photolability of seawater Fe ligands to Fe cycling under different mixed layer conditions.

In this study, I investigated how the interplay between light and temperature in the upper mixed layer governs the cycling of Fe and phytoplankton growth in HNLC regions. Specifically, I formulated a relatively complex steady-state model of oceanic Fe cycling, both with and without biological activity. I was interested in appraising the impact of the photolability and bioavailability of organically complexed Fe on Fe cycling under different temperature and mixing regimes. The relative role of abiotic and biotic processes in controlling Fe cycling and phytoplankton growth as a function of MLI and MLT was also investigated. By adding an approximation of phytoplankton Fe uptake, I was able to examine how including a simple representation of the biogenic losses of bFe altered the conclusions of the abiotic model.

2. Methods

2.1. Fe Cycle Model

The standard abiotic Fe cycle model consists of five Fe pools, four dissolved (dFe) and one solid (Fe(III)s) (Figure 1a). The dFe pools consist of two free inorganic pools (Fe(II) and Fe(III)) and two ligand-bound Fe(III) pools, one of which is non-bioavailable, but photolabile (Fe(III)La) while the other is bioavailable, but

Figure 1. A schematic of the Fe supply model (a) with and (b) without a bioavailable organically complexed Fe pool (Fe(III)Lb). Pools with a white background are assumed to be bioavailable, while those that are shaded are non-bioavailable to phytoplankton. Photoreduction of Fe(III)Lb, as well as biological uptake and remineralization are not included in all models.

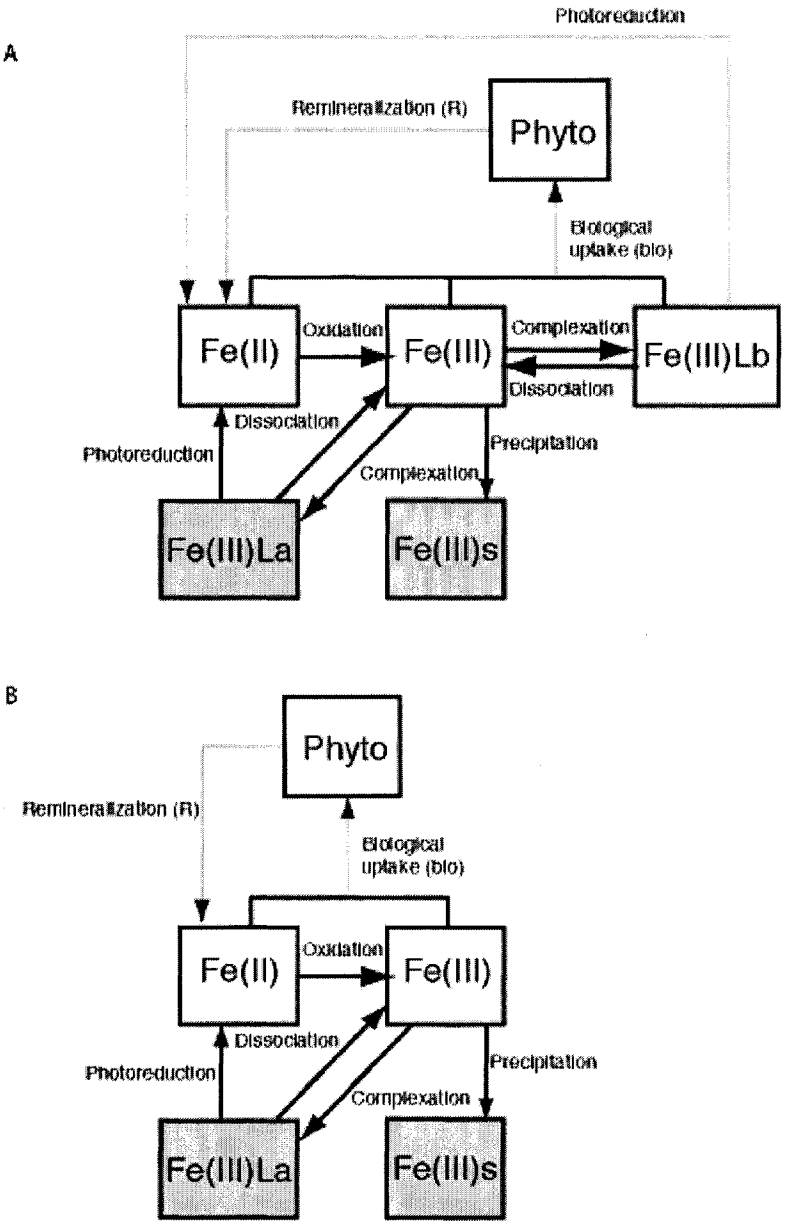

photostable (Fe(III)Lb) [*Tagliabue and Arrigo*, 2006]. The remaining Fe pool consists of Fe(III) that has precipitated to form solid Fe(III)s. When biotic processes are considered (see below), removal by phytoplankton (*bio*) and remineralization (*R*) of bFe are also included. In brief, phytoplankton take up Fe from the three bioavailable pools in proportion to the relative pools sizes. Remineralization (*R*) of Fe removed by phytoplankton enters the Fe(II) pool. The bioavailable Fe pool (bFe) is assumed to be made up of Fe(II), Fe(III) and Fe(III)Lb. During the abiotic scenario, I set both *bio* and *R* to zero. The standard simulation assumes that the bioavailable ligand (Lb) is photostable (i.e. cannot be photoreduced to Fe(II) and the term $k_{prLb}Fe(III)Lb$ is set to zero). In simulations where Lb is photolabile, then the rate constant for photoreduction is calculated in an identical fashion as described below for Fe(III)La.

Inorganic Fe(II) is oxidized to Fe(III) via a pseudo-first order rate constant (k_{ox}) that is a function of temperature [*Millero et al.,* 1987]. I assume that Fe(III)La complexes are photolabile and can be photoreduced to produce Fe(II), via ligand to metal charge transfer, as a function of the incident irradiance [*Rijkenberg et al.,* 2005]. If biotic processes are included, then phytoplankton uptake and remineralization, are sinks and sources, respectively, for Fe(II). The rate of change in Fe(II) (μmol m^{-3} s^{-1}) is therefore

$$Q_{Fe(II)} = -k_{ox}Fe(II) + k_{pr}Fe(III)La + k_{prLb}Fe(III)Lb - bio + R. \quad (1)$$

The rate of change in Fe(III) (μmol m^{-3} s^{-1}) is

$$Q_{Fe(III)} = k_{ox}Fe(II) - k_{fFe(III)La}Fe(III)[La] + k_{dFe(III)La}Fe(III)La - k_{fFe(III)Lb}Fe(III)[Lb] + k_{dFe(III)Lb}Fe(III)Lb - k_{pcp}Fe(III) + R_{Fe(III)s}Fe(III)s - bio \quad (2)$$

where Fe(III) is produced by oxidation of Fe(II) ($k_{ox}Fe(II)$) and is lost by precipitation to Fe(III)s (k_{pcp}Fe(III)), as well as by biological uptake (*bio*, if included). Rate constants for the formation (4.2 x10^4 M^{-1} s^{-1}) and dissociation (2 x10^{-7} s^{-1}) of Fe(III)La are taken from measurements of *Witter and Luther* [1998]. *Maldonado et al.* [2005] demonstrated significant in situ phytoplankton uptake of Fe-ligand complexes with kinetic characteristics that were similar to desferroxamine (DFO) ligands. I therefore ascribe rate constants for the formation (19.6 x 10^5 M^{-1} s^{-1}) and dissociation (1.5 x10^{-6} s^{-1}) of Fe(III)Lb in accordance with the measured kinetics of DFO [*Witter et al.,* 2000] and assume that Fe(III)Lb complexes are photostable [*Barbeau et al.,* 2003]. The concentrations of La and Lb are set to 2 nM and 1 nM (Fe equivalents), respectively.

The rate of change in Fe(III)La (μmol m^{-3} s^{-1}) is modeled as

$$Q_{Fe(III)La} = k_{fFe(III)La}Fe(III)[La] - k_{dFe(III)La}Fe(III)La - k_{pr}Fe(III)La \quad (3)$$

where Fe(III)La can be photoreduced ($k_{pr}Fe(III)La$) to form Fe(II) and thermodynamically dissociates to Fe(III) ($k_{dFe(III)La}Fe(III)La$). Fe(III)La complex formation is as described above.

The rate of change in Fe(III)Lb (μmol m^{-3} s^{-1}) is

$$Q_{Fe(III)Lb} = k_{fFe(III)Lb}Fe(III)[L_b] - k_{dFe(III)Lb}Fe(III)Lb - bio \quad (4a)$$

when Lb is photostable and

$$Q_{Fe(III)Lb} = k_{fFe(III)Lb}Fe(III)[L_b] - k_{dFe(III)Lb}Fe(III)Lb - k_{prLb}Fe(III)Lb - bio \quad (4b)$$

when Lb is photolabile. Fe(III)Lb is formed as described above and is lost via thermodynamic dissociation ($k_{dFe(III)Lb}Fe(III)Lb$). When Lb is photolabile (Eq. 4b), photoreduction ($k_{prLb}Fe(III)Lb$) is an additional loss of Fe(III)Lb. The rate constant

for photoreduction of Lb (k_{prLb}) is assumed to be the same as for La (in the absence of any ligand specific information).

Fe(III)s is produced via precipitation/scavenging of Fe(III) ($k_{pcp}Fe(III)$) and is remineralized back to Fe(III) at a rate of 0.05 d^{-1}. Therefore, the rate of change in Fe(III)s (μmol m^{-3} s^{-1}) is simply

$$Q_{Fe(III)s} = k_{pcp}Fe(III) - R_{Fe(III)s}Fe(III)s \quad (5)$$

and does not include sinking. It should be noted that this study is concerned with evaluating variability in Fe supply and for simplicity, I first use the Fe model to addresses variability in abiotic Fe cycling (the terms *bio* and *R* are fixed at zero). This configuration will be referred to as the 'abiotic' Fe supply model. For reference, I include the rate constants for Fe(II) oxidation and Fe(III)La photoreduction (k_{ox} and k_{pr}, respectively, s^{-1}) in Table 1.

In simulations that include biology, I added a simple approximation of phytoplankton uptake of bFe, as well allowing Fe recycled from dead phytoplankton (20% of the phytoplankton standing stock per day) to enter the Fe(II) pool. The steady-state phytoplankton growth rate was calculated as a function of temperature as well as nutrient and light limitation, as described in *Arrigo et al.* [2003a], assuming that Ek_{max} = 25 μEin m^{-2} s^{-1} and the half saturation constant for growth on bFe (kμ) is 0.01 nM. I calculate the steady-state daily phytoplankton growth rate (μ_{AVE}) during each simulation. Uptake of bFe was calculated assuming a C/Fe ratio is 250,000 (mol:mol). This model parameterization will be referred to as the 'biotic' Fe supply model.

Table 1. Values for the rate constants for Fe(II) oxidation (k_{ox}, s^{-1}) and Fe(III)La photoreduction (k_{pr}, s^{-1}) for the range of MLT (°C) and MLI (μEin m^{-2} s^{-1}) used in this study

MLT	k_{ox}	MLI	k_{pr}
-5	7.92×10^{-5}	25	2.87×10^{-6}
0	1.64×10^{-4}	50	5.73×10^{-6}
5	3.39×10^{-4}	100	1.15×10^{-5}
10	7.02×10^{-4}	150	1.72×10^{-5}
15	1.45×10^{-3}	200	2.29×10^{-5}
20	3.01×10^{-3}	300	3.44×10^{-5}
25	6.23×10^{-3}	350	4.01×10^{-5}

The most pertinent omission from this study is that phytoplankton grown at lower light levels have a greater demand for Fe [e.g. *Sunda and Hunstman,* 1997]. However, including such an effect in the context of this study would only serve to increase the sensitivity of phytoplankton growth to MLI-driven changes in Fe speciation and bFe concentrations. As the MLI increases, the increased supply of, and reduced demand for, Fe will act synergistically to elevate μ. In addition, the interactive impact of the photochemical cycling of hydrogen peroxide and superoxide, which can be involved in both the oxidation of Fe(II) and back reduction of Fe(III) [*King et al.,* 1995] could also prove to be of importance in governing bFe concentrations. Nevertheless, in the Southern Ocean at least, hydrogen peroxide concentrations are low and the major oxidant for Fe(II) is O_2 [*Sarthou et al.,* 1997].

Model simulations were conducted under a range of MLIs (0 to 350 μEin m^{-2} s^{-1}), which were held constant during the 12L:12D photoperiod, and a range of fixed MLTs (-5 to 25°C). The total Fe pool is fixed at 0.53 nM and reflects typical oceanic concentrations [e.g. *Jonhson et al.,* 1997; *Coale et al.,* 2005]. I evaluated the steady-state bFe concentration (nM), supply of Fe(II) by photoreduction (nM Fe(II) d^{-1}), as well as the degree of limitation of phytoplankton growth rates by Fe and MLI (where a higher value implies stronger control by either resource). The limitation terms are 1 minus the proportion of phytoplankton μ_{max} allowed by either light or Fe (Llim and Flim, respectively, dimensionless). Llim and Flim will always be between 0 and 1, where values of 0 and 1 yield growth rates of 100% and 0% of μmax, respectively.

I also conducted three model experiments during this investigation. The standard scenario (Figure 1a) assumes that Fe(III) can form Fe-ligand complexes that are

photostable (i.e. $k_{prLb}Fe(III)Lb$ is fixed at zero) and bioavailable to the phytoplankton (Fe(III)Lb) [*Maldonado and Price,* 1999; *Maldonado et al.,* 2005]. As Fe-specific ligands exhibit variability in their photolability [*Barbeau et al.,* 2003] and might well be photolabile in nature [*Maldonado et al.,* 2005], I first investigated the potential importance of a photolabile Fe(III)Lb pool to Fe cycling. This was performed by allowing Fe(III)Lb to be photoreduced in a manner identical to Fe(III)La. Second, uptake of organically-complexed Fe has not yet been demonstrated across a wide suite of phytoplankton taxa [*Hutchins et al.,* 1999; *Blain et al.,* 2004]. I therefore examined its potential significance by assuming that all ligand-bound Fe was non-bioavailable (i.e., no Fe(III)Lb, see Figure 1b). Third, because phytoplankton exhibit a wide range of half saturation constants for growth on Fe [e.g. *Blain et al.,* 2002; *Timmermans et al.,* 2004], I also conducted an experiment wherein the affinity for Fe was varied 100-fold (i.e., 0.001 to 0.1 nM bFe).

3. Results and Discussion

3.1 Impact of mixed layer conditions on Fe cycling

3.1.1 Abiotic Fe supply model

Fe(III)Lb photostable. Modifying MLI and MLT resulted in dramatic changes in Fe cycling, primarily via their impact on bFe concentrations. The largest changes in the concentrations of bFe stem from the interactive effect of increased rates of photoreduction of Fe(III)La to Fe(II) at increased light levels and complexation of Fe(III) by the photostable and bioavailable ligand Lb. Steady-state bFe concentrations increase with respect to MLI and exhibit little sensitivity to MLT (Figure 2a). Since

Figure 2. The (a) steady-state average daily bFe concentration (nM), (b) daily supply of Fe(II) due to photoreduction of Fe(III)La (nM d^{-1}), (c) concentrations of Fe(II), Fe(III)La, and Fe(III)Lb at 0°C (nM), and (d) steady-state daily photoreduction when the concentration of Lb was reduced 10 fold, as a function of MLI and MLT utilizing the abiotic Fe model.

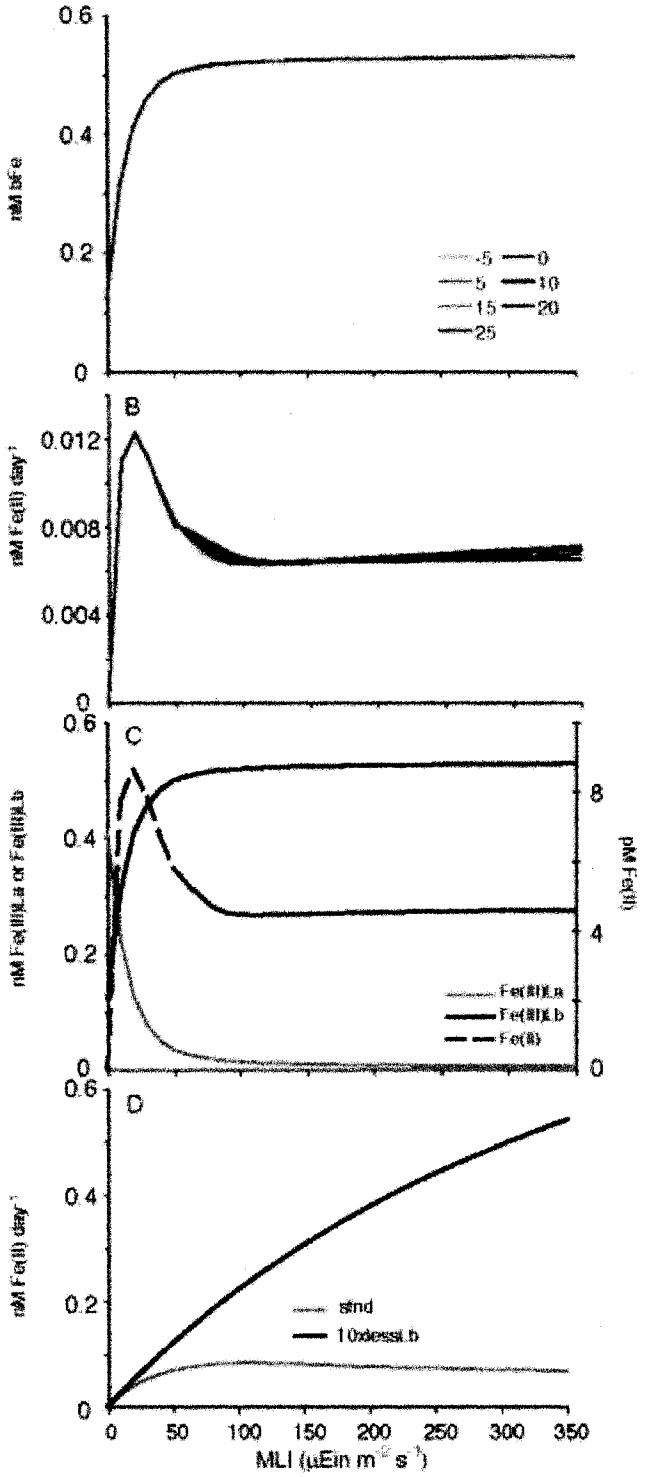

>75% of the total Fe pool is complexed as Fe(III)La in the dark, increased rates of Fe(III)La photoreduction at higher MLIs (Table 1) are essential for converting this Fe pool into bioavailable Fe species.

The relationship between steady-state photoreduction rate and MLI is not straightforward (Figure 2b). At low MLIs, photoreduction increases with increasing MLI (up to around 30 μEin m^{-2} s^{-1}). This is because the rate of complexation of Fe(III) by the photolabile La is much greater than by the photostable Lb. At higher MLIs, larger amounts of Fe(II) are produced photochemically (Figure 2c) and the rate of Fe(III) complexation by La becomes saturated. Under these conditions, more Fe(III) is complexed by the photostable ligand Lb and the concentration of Fe(III)Lb increases significantly, dominating the bFe pool (Figure 2c). Since Fe(III)Lb cannot be photoreduced, rates of photoreduction are lower at high MLIs, until the rate of complexation of Fe(III) by Lb becomes saturated (Figure 2b). Accordingly, if the concentration of Lb is reduced 10-fold, photoreduction increases markedly with MLI (Figure 2d). Overall, photoreduction of Fe(III)Lb exhibits little sensitivity to MLT.

Fe(III)Lb photolabile. Field evidence suggests that bioavailable organically-complexed Fe may be also be extremely photolabile, with light enhancing rates of phytoplankton Fe uptake 15-fold [*Maldonado et al.*, 2005]. Unsurprisingly, steady-state photoreduction rates increase markedly at all MLTs if Fe(III)Lb is assumed to be photolabile (Figure 3a). When Lb is photostable, Fe(III)Lb acts as a reservoir and reduces the turnover of bFe, thus reducing photoreduction of Fe(III)La at high MLIs (Figure 2b). However, when Fe(III)Lb is photolabile, photoreduction increases markedly, due to the additional photoreducible Fe pool.

Figure 3. The steady-state (a) daily supply of Fe(II) due to photoreduction of Fe(III)La (nM d^{-1}) and (b) steady-state average daily bFe concentration (nM), as a function of MLI and MLT when photolability is assigned to Fe(III)Lb in the abiotic Fe model.

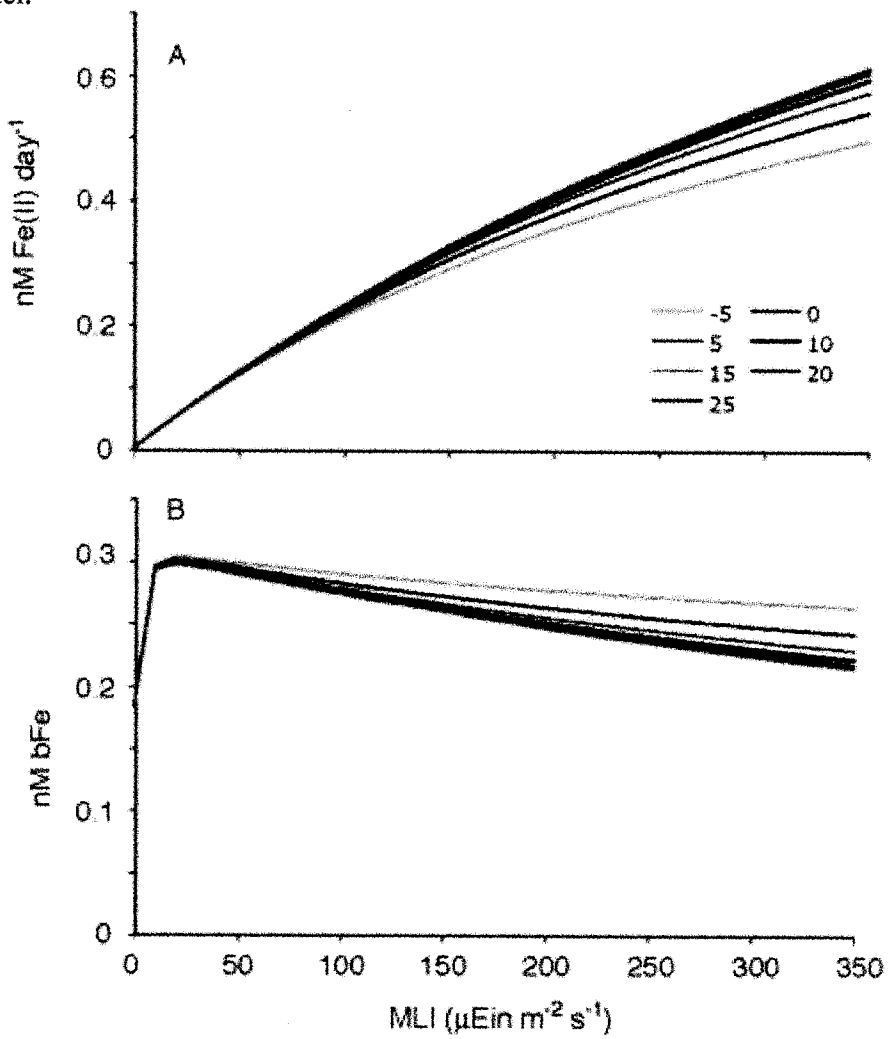

At MLIs <25 μEin m^{-2} s^{-1}, bFe concentrations increase with MLI at all MLTs, peaking at around 0.3 nM (Figure 3b). At higher MLIs, the increased turnover of dFe (due to photoreduction of both Fe(III)La and Fe(III)Lb) results in increasing losses of bFe as Fe(III)s since Lb is no longer able to buffer bFe concentrations. Therefore, bFe concentrations are slightly reduced at high MLIs, although the increased residence time of Fe(II) at lower MLTs does minimize losses of bFe (Figure 3b).

3.1.2 Biotic Fe supply model

3.1.2. Fe(III)Lb photostable

Impact of MLI. When biological processes are included, then the relationship between the various Fe pools and MLI becomes rather more complex than during the abiotic scenario, even when Fe(III)Lb is photostable. The dynamics of bFe provide a good example of this, exhibiting multiple transitions that correspond to shifts in the relative importance of biotic and abiotic processes as MLI increases (Figure 4).

At very low MLIs (the lowest light levels of region A in Figure 4), photoreduction supplies Fe at a greater rate than it is utilized by the biota (Figure 5b). This is because phytoplankton are light limited at these irradiances and are not yet a significant sink for bFe (Figure 5c). As a result, bFe begins to accumulate, much as it did in the abiotic scenario (Figure 2a). At higher MLIs, the rate constant for photoreduction (k_{pr}) becomes proportionally greater (Table 1). Light limitation of phytoplankton growth also is relaxed (Figure 5c), resulting in higher steady-state phytoplankton concentrations and enhanced uptake of bFe. However, at these relatively low MLIs, photoreduction of Fe(III)Lb to Fe(II) still exceeds the removal of bFe by

Figure 4. The relationship between bFe (nM) and MLI at 0 °C, is representative of the impact of including biological processes. The three regions (A, B, and C) are defined at low, moderate, and high MLI and referred to in the text.

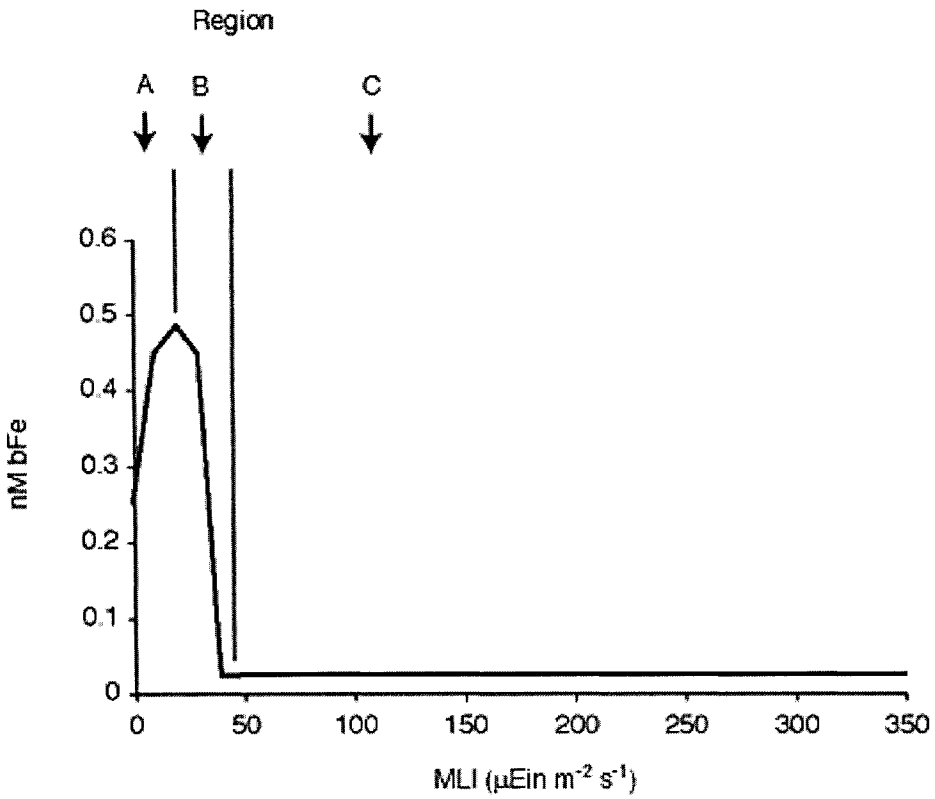

Figure 5. The steady-state (a) average daily bFe concentration (nM), (b) daily supply of Fe(II) due to photoreduction of Fe(III)La (nM d^{-1}), and ((c) light and Fe limitation terms (Llim and Flim, respectively) as a function of MLI and MLT when the biotic Fe model was employed and Lb was photostable.

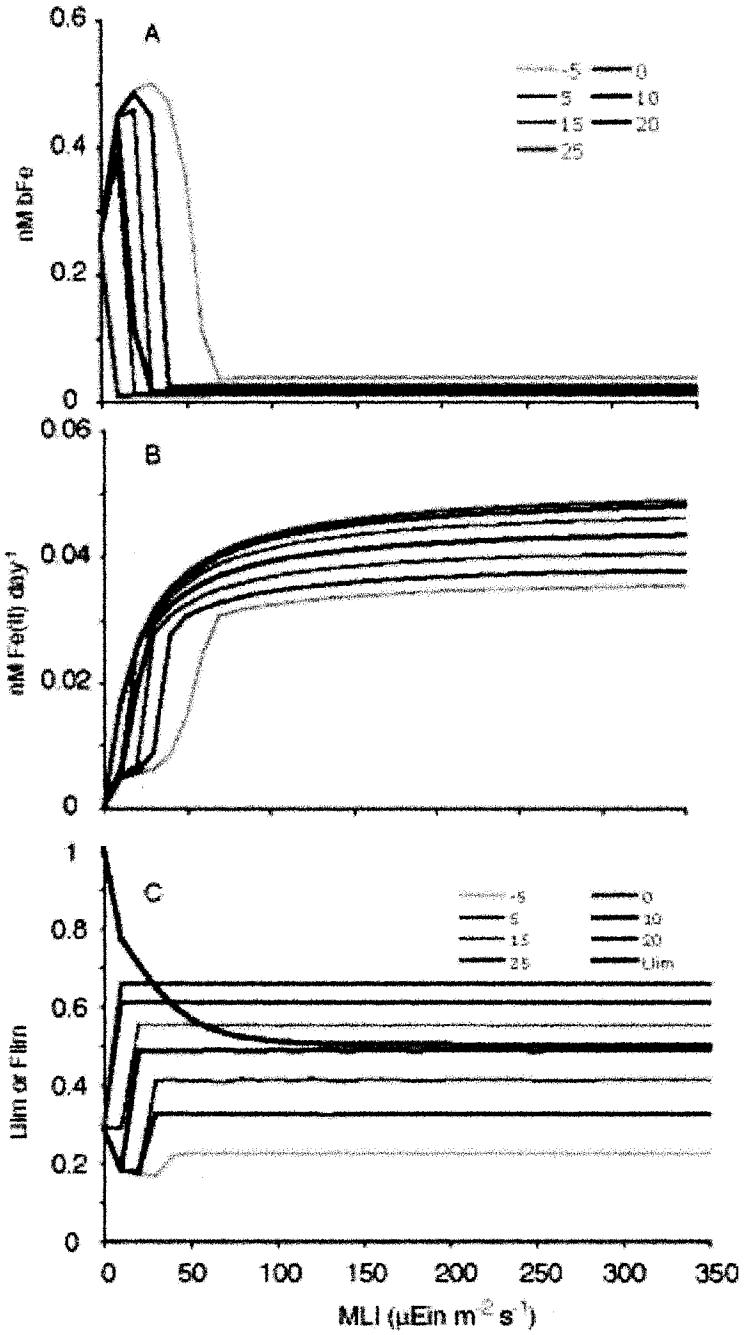

phytoplankton. Eventually, the bFe concentration reaches its peak (the boundary between regions A and B in Figure 4), representing the light level where the steady-state supply of bFe via photoreduction is balanced by phytoplankton uptake of bFe (and to a lesser extent, losses to Fe(III)s).

Further increases in MLI result in a smaller bFe pool as rates of photoreduction are exceeded by the phytoplankton growth rate and their associated uptake of bFe (region B in Figure 4). bFe continues to decline as MLI increases until the point is reached where losses of bFe via both phytoplankton uptake and precipitation of Fe(III)s are balanced by additions to the bFe pool from photoreduction and the remineralization of biogenic Fe (region C in Figure 4). When bFe concentrations reach their lowest levels, >80% of total Fe is in the phytoplankton pool.

Including phytoplankton uptake and release of Fe to the model increases the turnover rate of the dFe pool. Under such conditions, Fe(III)Lb is taken up by phytoplankton and is no longer the stable pool it was in the abiotic scenario (the only previous loss was the relatively low rate of dissociation). Higher turnover increases recomplexation of inorganic Fe by photolabile ligands, thereby minimizing the stabilizing impact of photostable ligands. Increased rates of photoreduction at higher MLIs only ensue once steady-state bFe concentrations begin to drop (Figure 5a and b).

Impact of MLT. Higher MLT results in elevated rates of both phytoplankton growth [*Eppley,* 1972] and Fe(II) oxidation [*Millero et al.,* 1987], affecting the rates of bFe turnover and losses of bFe as Fe(III)s, respectively. At higher MLTs, peak bFe concentrations (the boundary between region A and B in Figure 4) are shifted towards a lower MLI (Figure 5a). This is because phytoplankton growth rates are elevated at

higher temperatures, which results in both greater biomass levels and increased uptake of bFe at low light (within region A in Figure 4, relative to colder waters). In fact, at the highest temperatures considered (>15°C), there is no build up in bFe and the bFe concentration is maximal in the dark (Figure 5a). Greater biological turnover of the total Fe pool in warm waters also results in greater rates of photoreduction at higher MLTs, at any MLI (Figure 5b).

Elevated rates of oxidation at higher temperatures are also important in dictating the steady-state bFe concentration and rate of photoreduction. At a given MLI, the bFe concentration is always greatest at the lowest MLT (Figure 5a). This is because of both the increased residence time of Fe(II) in colder waters (due to lower oxidation rates) and slower phytoplankton growth rates (Figure 4a, regions A and B in Figure 4). This is particularly true at the highest MLIs (region C in Figure 4), where increased oxidation rates at the warmest MLTs result in 50% higher Fe(III)s concentrations at steady-state than at the lowest MLT. The lower bFe concentration in warmer water means that if the MLT is ≥15°C, Fe is more limiting than light at high MLI (region C of Figure 4) (Flim > Llim, Figure 5c).

3.1.2. Fe(III)Lb Photolabile

The additional phororeducible bFe pool (Fe(III)Lb) results in a slightly lower peak steady-state bFe concentration and an higher Fe(III)s concentration (at the boundary between region A and B in Figure 4) at any given MLI (Figure 6a), relative to the Fe(III)Lb photostable scenario. The transitions between regions A, B, and C illustrated in Figure 4 also span a smaller range of MLIs (Figure 6b). When

Figure 6. The steady-state (a) average daily bFe concentration (nM), (b) daily supply of Fe(II) due to photoreduction of Fe(III)La (nM d^{-1}), and (c) light and Fe limitation terms (Llim and Flim, respectively), as a function of MLI and MLT when the biotic Fe model was employed and Lb was photolabile.

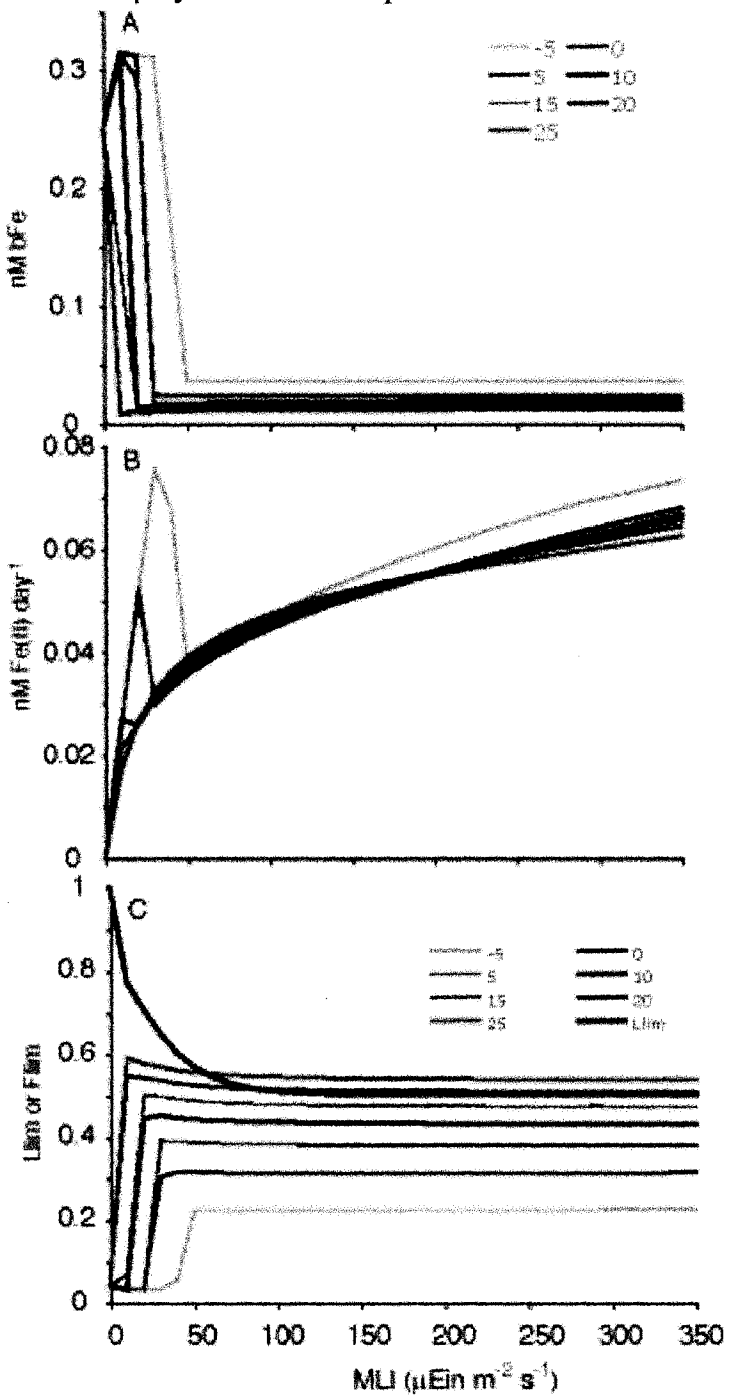

phytoplankton uptake of bFe is low (within region A in Figure 4) photoreduction is approximately 7-fold greater when both Fe(III)La and Fe(III)Lb can be photoreduced (at 0°C for example, Figure 6b). When MLI is sufficient for phytoplankton to reduce the bFe concentration (Figure 6a), photoreduction declines noticeably (Figure 6b). Photoreduction increases with MLI at MLIs above about 50 μEin m^{-2} s^{-1} (region C in Figure 4, Figure 6b), despite little change in bFe concentration (Figure 6a). As phytoplankton biomass is highest within this region, the greater steady-state remineralization of biogenic Fe increases the supply of Fe(III)Lb, which subsequently can be photoreduced.

At higher temperatures, both bFe concentrations and photoreduction are more sensitive to the photolability of Lb. Because phytoplankton uptake diminishes the size of the bFe pool when the MLT is >10°C (Figure 6a), there is also no peak in the rate of photoreduction, relative to colder waters (Figure 6b). At MLTs ≤10°C, photoreduction drops markedly once phytoplankton biomass is high enough to substantially reduce bFe concentrations (Figure 6a). If light is sufficiently high (i.e. within region C in Figure 4), the lower bFe concentration at warm MLTs means that Fe will control phytoplankton growth at MLTs ≥15°C (Flim > Llim, Figure 6c).

3.2 No bioavailable Fe(III) ligand pool

3.2.1 Abiotic Fe supply model

During this scenario, the supply of bioavailable Fe (Fe(II) and Fe(III)) is controlled solely by the photoreduction and dissociation of Fe(III)La (i.e. no Fe(III)Lb). In the absence of a competing photostable ligand, the steady-state photoreduction rate

increases approximately as a linear function of MLI (Figure 7a). The dFe pool undergoes a high rate of turnover at the highest MLIs and the increased loss of bFe as Fe(III)s reduces the steady-state rate of photoreduction. In general, steady-state bFe (Fe(II) and Fe(III)) concentrations increase as a function of MLI (at any given MLT, Figure 7b), but much less so than when Fe(III)Lb was included, despite higher photoreduction fluxes of Fe(II). This is due to the increased loss of bFe as Fe(III)s (by two orders of magnitude) when Lb is not present. Furthermore, Fe(III)La is the dominant form of Fe at all MLIs at steady-state during this abiotic scenario.

Photoreduction is greatest at the highest MLT and MLI, due to enhanced rates of oxidation and photoreduction (Figure 7a). Moreover, the reduction in the rate of Fe(II) oxidation at low MLTs (Table 1) reduces the loss of Fe(III) as Fe(III)s. Therefore both the residence time of Fe(II) and bFe concentrations are greater at lower MLTs (Figure 7b). Increased Fe(II) oxidation at the highest MLTs can result in significant steady-state losses of bFe as Fe(III)s (> 0.1 nM at the highest MLIs).

3.2.2 Biotic Fe supply model

Adding biology to the model in the absence of Fe(III)Lb has only a slight impact on model results since Fe pools are already highly dynamic. Within region A (in Figure 4), photoreduction supplies bFe at a greater rate than it can be taken up by light-limited phytoplankton and bFe concentrations increase (Figure 8b). As phytoplankton become a larger sink for Fe at moderate light levels, steady-state photoreduction peaks (Figure 8a). In fact, the limitation of phytoplankton growth rate by Fe can be as great as that by light at low to moderate MLIs, when phytoplankton

Figure 7. The steady-state (a) average daily bFe concentration (nM) and (b) daily supply of Fe(II) due to photoreduction of Fe(III)La (nM d^{-1}), as a function of MLI and MLT when the abiotic Fe model was employed and Lb was absent (Figure 1b).

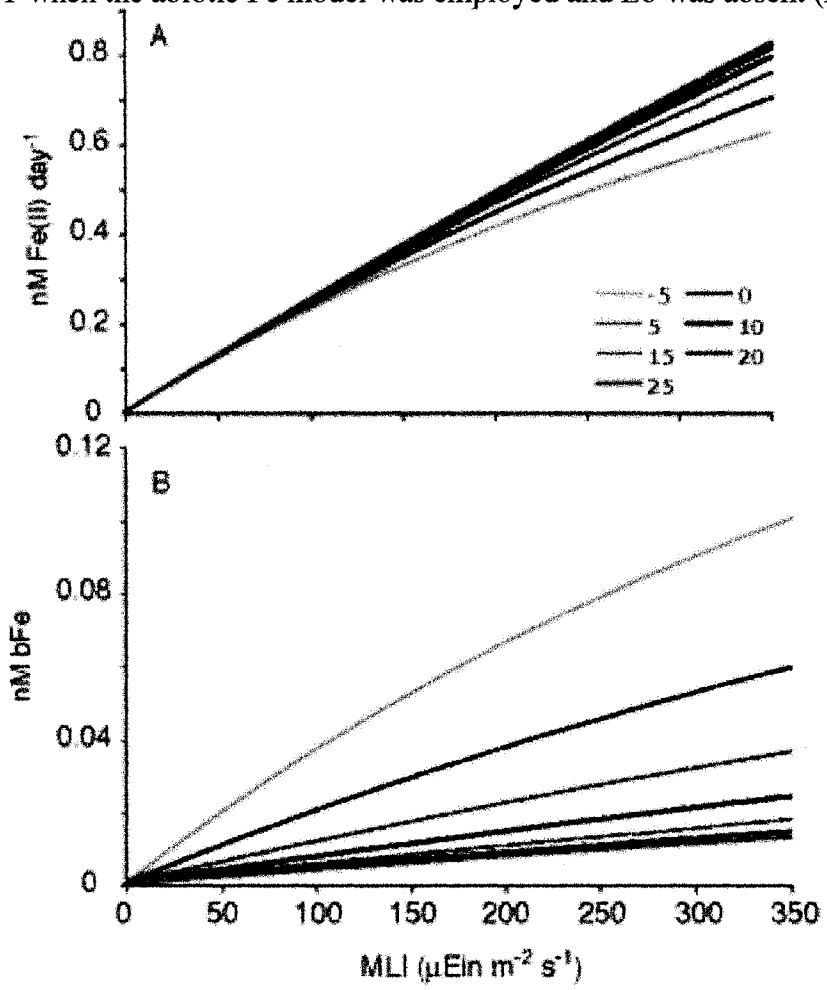

Figure 8. The steady-state (a) average daily bFe concentration (nM) and (b) daily supply of Fe(II) due to photoreduction of Fe(III)La (nM d^{-1}), as a function of MLI and MLT when the biotic Fe model was employed and Lb was absent (Figure 1b).

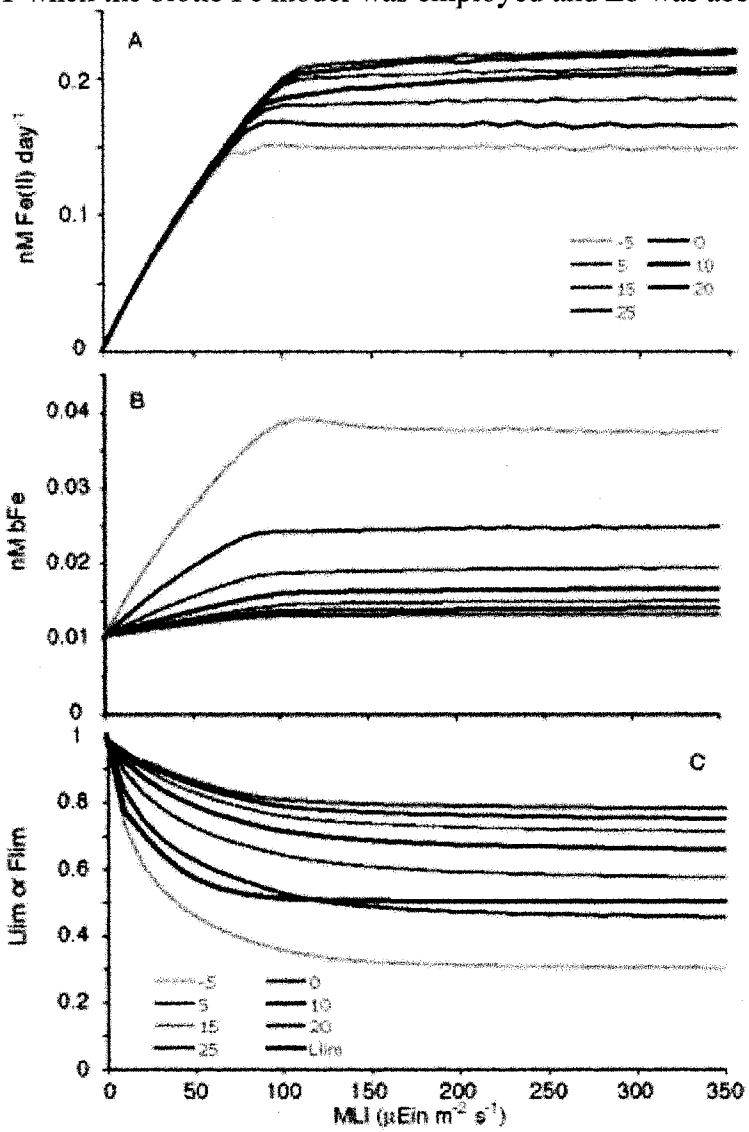

are reliant only on Fe(II) and Fe(III) (Figure 8c). At the highest MLIs, both the steady-state bFe concentration and rate of photoreduction reach a plateau that is maintained by the uptake and remineralization of Fe by the biota (Figure 8a and b).

The complimentary effect of the reduced phytoplankton uptake of bFe and the increased residence time of Fe(II) when MLT is low results in an inverse relationship between the steady-state bFe concentration and MLT (Figure 8b). Greater biologically-mediated turnover of dFe also results in the highest rate of photoreduction when the mixed layer is both warm and well lit (Figure 8a). Overall, phytoplankton Fe limitation declines as the MLI increases (for any given MLT, Figure 8c). At the highest MLIs, Flim is approximately 0.3 and 0.8 at -5 and 25 °C, respectively, whereas Llim is 0.5 (Figure 8c) and over 80% of total Fe is in the phytoplankton pool.

3.3 Phytoplankton requirement for bioavailable Fe

Because phytoplankton demands for Fe can be highly variable, I examine the sensitivity of biologically-mediated Fe cycling to changes in kμ (which will determine Flim). Simulations were performed both with and without an organically-complexed bioavailable Fe pool (Figure 1a and b) and with varying values assigned to the bFe half saturation constant for growth (kμ). The value for kμ used in the standard simulation is already at the low end of previously published estimates [*Blain et al.,* 2002; *Timmermans et al.,* 2004] so reducing kμ to 0.001 nM does not significantly alter the results. Therefore, I will focus on results obtained when kμ was increased to 0.1 nM bFe. Obviously, altering kμ has no impact in the abiotic system; the following results were obtained solely from the biotic Fe supply model.

3.3.1 With Fe(III)Lb

When Fe(III)Lb is included in the model (Figure 1a), raising kμ increases the sensitivity of both Fe cycling and phytoplankton Fe-limitation to increased MLT. This is because raising kμ will result in Fe exerting a greater influence on phytoplankton growth (via the Monod formulation of Flim). Just as in the standard scenario (where phytoplankton had a higher affinity for Fe), bFe concentrations increase with MLI at low to moderate MLIs and decline at higher MLIs (Figure 9a). However, when kμ is raised to 0.1 nM, the biologically-mediated decline in bFe is reduced (Figure 8a) due to increased Fe-limitation. Furthermore, the temperature threshold above which there is no accumulation in bFe (i.e. region A in Figure 4 is absent) is reduced from 20 to 15°C (Figure 9a). Despite Fe controlling phytoplankton growth rates when the MLT is >10°C (Figure 9b), phytoplankton dominate the total Fe pool for all MLTs at the highest MLI. This suggests that even phytoplankton with a high requirement for Fe can achieve high biomass (regardless of MLT) provided there is a bioavailable organically complexed Fe pool.

3.3.3.2 No Fe(III)Lb

When phytoplankton must subsist solely on free inorganic Fe(II) and Fe(III) (Figure 1b), a reduced Fe affinity results in low phytoplankton biomass and therefore a much lower impact of biology on Fe cycling than in previous scenarios. Compared to results obtained when Fe affinity was high (Figure 8b), bFe concentrations are greater across the entire range of MLIs in the absence of Fe(III)Lb (Figure 10a). At a higher kμ, Fe impacts phytoplankton growth at higher bFe concentrations and can control

Figure 9. The steady-state (a) average daily bFe concentration (nM) and (b) light and Fe limitation terms (Llim and Flim, respectively), as a function of MLI and MLT when the phytoplankton affinity for Fe was reduced to 0.1 nM bFe, utilizing the biotic Fe model (including Lb, Figure 1a).

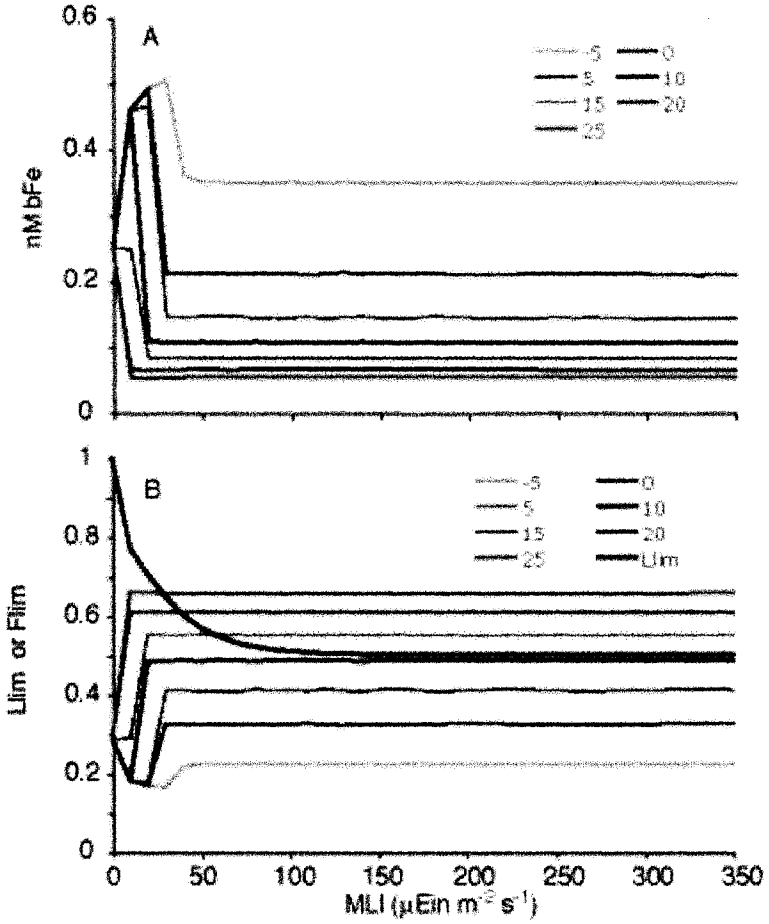

Figure 10. The steady-state (a) average daily bFe concentration (nM) and (b) light and Fe limitation terms (Llim and Flim, respectively), as a function of MLI and MLT when the phytoplankton affinity for Fe was reduced to 0.1 nM bFe, utilizing the biotic Fe model (without Lb, Figure 1b).

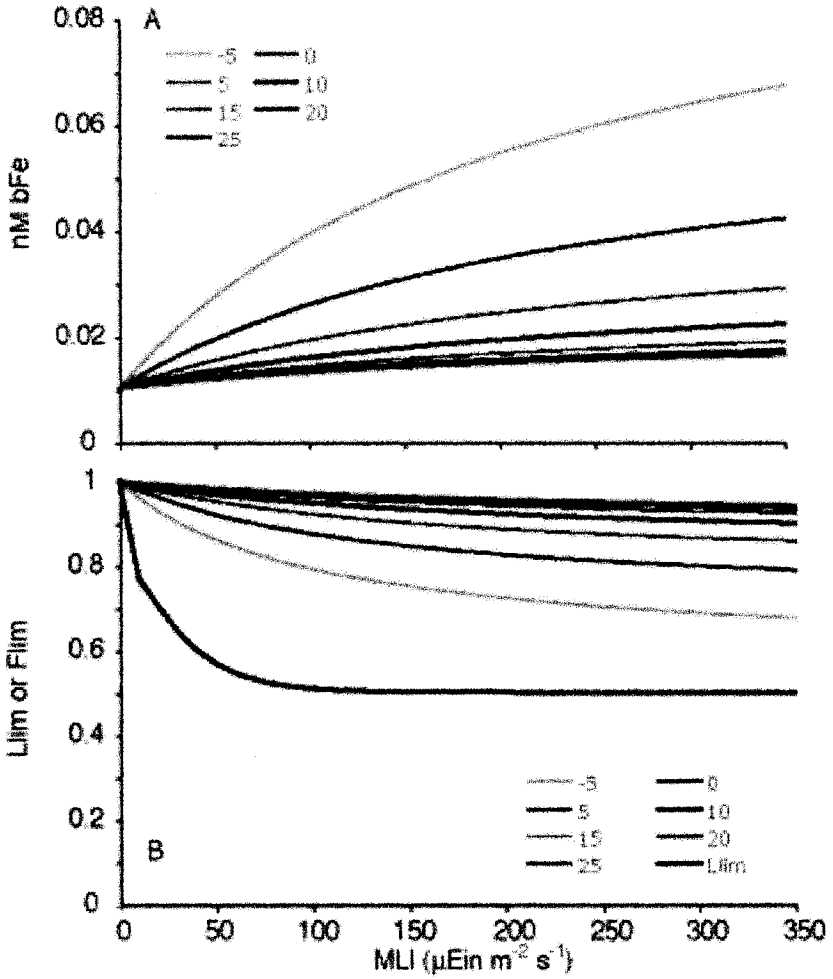

phytoplankton growth across the entire range of MLIs (Figure 10b). This results in low accumulation of phytoplankton biomass at all MLIs and greatly reduced biotic uptake of bFe. Phytoplankton with a high Fe requirement likely will need to access organically complexed Fe in order in achieve high biomass, even in cold mixed layers.

3.4 Implications of mixed layer temperature on Fe supply to phytoplankton

My study suggests that phytoplankton growing in cold HNLC waters can afford to be more discriminating in the forms of Fe they acquire. Because non-biogenic losses of Fe are enhanced in warm mixed layers (due to increased precipitation of Fe(III)s), phytoplankton may need to make up for this lost Fe by accessing organically complexed Fe to satisfy their Fe demand. In colder mixed layers, the loss of bFe as Fe(III)s is reduced, and therefore phytoplankton can satisfy the same demand using mostly inorganic Fe. The increased availability of inorganic Fe in cold mixed layers may reduce the need for phytoplankton to invest in the cellular machinery required to take up organically complexed Fe(III) (such as surface reductases and oxidases, *Maldonado et al.,* in press). While ligand production by phytoplankton has been observed following Fe enrichments [*Rue and Bruland,* 1997; *Bowie et al.,* 2001; *Croot et al.,* 2001], this need not necessarily reflect actual planktonic uptake of ligand bound Fe. Phytoplankton may be exploiting the photolability of ligand-bound Fe and/or the ability of ligands to buffer the free inorganic Fe concentration. In this sense, a bioavailable Fe-specific ligand can be thought of as a reservoir of bFe

An ability to access organically-complexed Fe may be a common feature of phytoplankton that have a high requirement for Fe, even in cold waters. Uptake of

organically-complexed Fe has been demonstrated in large diatoms from both the Sub-Arctic Pacific [*Maldonado and Price,* 1999] and the Southern Ocean [*Maldonado et al.,* 2005]. The requirement for Fe is typically a function of the cell surface area to volume ratio [e.g. *Timmermans et al.,* 2004]. It is therefore reasonable to suggest that large diatoms from the Sub-Arctic Pacific and Southern Ocean that take up organically-complexed Fe [*Maldonado and Price,* 1999; *Maldonado et al.,* 2005] likely also have a high requirement for Fe. Accordingly, work in the North Atlantic by *Blain et al.* [2004] demonstrated that the ability of phytoplankton to access organically-complexed Fe increased with increasing cell size.

4. General Implications

The results of Fe fertilization experiments, and in particular, the response of each particular HNLC location to the addition of Fe will be affected by mixed layer attributes. *De Baar et al.* [2005] show that the greatest response following Fe additions (in terms of a change in either dissolved inorganic carbon, maximum nitrate removal, maximum pCO_2 drawdown, or chlorophyll *a* production) is found in regions characterized by shallow mixed layers (see: Figures 11, 12 and Table 3, in *De Baar et al.* [2005]). By assuming that a shallow mixed layer is characterized by a higher MLI, these results were explained in terms of a lower phytoplankton demand for Fe within shallow mixed layers. Although a reduced Fe demand at higher MLIs is undoubtedly important [e.g. *Sunda and Hunstman,* 1995], I suggest that shallow mixed layers will also promote a greater supply of bFe to phytoplankton, as well as minimizing non-biogenic losses of Fe. Both processes will enhance phytoplankton growth rates when

mixed layers are shallow (independent of T) and will elevate the biogeochemical response to any Fe additions.

Similarly, an increase in the stratification of any Fe-limited system will result in increased bFe fluxes via photoreduction and therefore enhance NPP, without requiring an additional Fe supply. Models suggest that the degree of stratification in the Southern Ocean is likely to increase in the future, primarily due to greater sea ice melting and precipitation [e.g. *Sarmiento et al.,* 1998]. My study suggests that any increase in stratification will be accompanied by an increase in the photochemical supply of bFe, potentially increasing NPP across the Fe-limited Southern Ocean.

It has been proposed that greater Fe supply rates during the LGM could have increased NPP by alleviating Fe-limitation [*Martin,* 1990], although models have thus far struggled to account for the entire decline in atmospheric CO_2 via this mechanism [e.g. *Watson et al.,* 2000; *Bopp et al.,* 2003]. Sea ice dynamics probably also changed markedly at the LGM and may have impacted Fe availability. For example, reconstructions of glacial sea ice distributions suggest that there was an equatorward expansion in the winter sea ice extent, with a summer extent that was similar to modern times [*Anderson et al.,* 2002 and references therein]. This implies that large sections of the Southern Ocean permanently open ocean zone (POOZ) became seasonal ice zone waters during the LGM. Consistent with this, a number of investigators suggest elevated salinity stratification of the Southern Ocean during the LGM [e.g. *Francois et al.,* 1997; *Sigman and Boyle,* 2000]. If the POOZ of the Southern Ocean became more stratified at the LGM then the more efficient supply of Fe to phytoplankton would increase NPP without including any additional exogenous

Fe supply. Models that utilize simple parameterizations of seawater Fe chemistry will not account for this effect and could underestimate the change in NPP that results from elevated dust fluxes.

Chapter 7

Bio-optical properties of *Phaeocystis antarctica* and *Fragilariopsis cylindrus* under iron sufficient and deficient conditions

Abstract Phytoplankton bio-optical properties are important in understanding the absorption of light at different wavelengths (e.g. ultraviolet) by algae, as well as for parameterizing empirical algorithms that estimate phytoplankton pigment concentrations from space. The trace metal iron (Fe) is important for numerous cellular processes and regulates primary production across the modern Southern Ocean (where sampling often relies on remote observations). In this study I examine the absorption spectra of Fe sufficient and deficient laboratory cultures of *Phaeocystis antarctica* and *Fragilariopsis cylindrus*. Under Fe sufficient conditions, *P. antarctica* was typified by large absorption peaks at ultraviolet wavelengths, but reduced absorption in blue and red light, relative to *F. cylindrus*. When Fe deficient, the ultraviolet absorption peak for *P. antarctica* is eliminated, implying a reduced tolerance of ultraviolet radiation when Fe limited. The potential causes of this are explored in relation to the costs of producing ultraviolet absorbing compounds and changes in cell size. Marked differences in absorption at the wavelengths used for remote sensing algorithms were observed for both taxa when Fe deficient, especially for *P. antarctica*. This results in potentially significant errors in the estimation of chlorophyll concentrations from remote sensing reflectance when Fe limits phytoplankton.

1. Introduction

The micronutrient iron (Fe) is the primary determinant of net primary production (NPP) across much of the low productivity Southern Ocean [*Martin et al.,* 1990; *De Baar et al.,* 1995; *Boyd et al.,* 2000; *Gervais et al.,* 2002; *Coale et al.,* 2004]. Phytoplankton growth is also regulated by Fe in the highly productive continental shelf ecosystems of the Southern Ocean [*Arrigo and Van Dijken,* 2003a], such as the southwestern Ross Sea [*Martin et al.,* 1990; *Sedwick et al.,* 2000; *Arrigo et al.,* 2003a, *Tagliabue and Arrigo,* 2005]. Fluctuations in the supply of Fe to the Southern Ocean can have important ramifications for the global carbon cycle [*Martin,* 1990; *Watson et al.,* 2000; *Bopp et al.,* 2003]. As phytoplankton require Fe for numerous cellular processes, including photosynthesis, respiration, and nitrate (NO_3) reduction [*Raven,* 1988; 1990 and references therein], their requirements vary as a function of cell size, light intensity and nitrogen source [*Raven,* 1988; 1990; *Sunda and Hunstman,* 1995; 1997; *Timmermans et al.,* 2001; 2004].

Satellite remote sensing has been of overwhelming importance in providing quantitative information on phytoplankton biomass from the remote regions of the Southern Ocean [e.g. *Arrigo and McClain,* 1994]. Such datasets are critical to the analysis of interannual variability in NPP and phytoplankton biomass [*Arrigo and Van Dijken,* 2004], as well as providing the basis for the validation of regional ecosystem models [*Arrigo et al.,* 2003a; *Tagliabue and Arrigo,* 2005; 2006]. Remote sensing has shown that the Ross Sea typically accounts for over 25% of total Southern Ocean NPP [*Arrigo et al.,* 1998b, *Bushinsky,* pers comm] and in situ rates of NPP can be as high

as 150 to 200 g C m^{-2} yr^{-1} [*Smith and Gordon,* 1997; *Arrigo et al.,* 2000]. Phytoplankton blooms in the Ross Sea are typically dominated by either the prymnesiophyte *Phaeocystis antarctica,* or diatoms such as *Fragilariopsis cylindrus, F. curta*, and *Nitzschia subcurvata* [*Arrigo et al.,* 1998c; 2000; *Smith et al.,* 2000]. It is also noteworthy that *P. antarctica* exhibits a distinct life cycle, and can exist as either solitary cells or, more commonly, as a colonial form [*Rousseau et al.,* 1994].

Phytoplankton absorption influences estimates of remote sensing reflection, which is the basis for empirical algorithms that estimate phytoplankton pigment concentrations from space [e.g. *Sullivan et al.,* 1993; *Arrigo et al.,* 1998b; 1998c, *O'Reilly et al.,* 1998]. *Arrigo et al.* [1998c] have already noted marked inter-specific differences in the absorption spectra of Ross Sea phytoplankton; highlighting the need for regional remote sensing algorithms for the Southern Ocean. Phytoplankton absorption spectra are primarily determined by cell size and pigment composition [*Morel and Bricaud*, 1981; *Sathyendranath et al.,* 1987; *Kirk,* 1994]. Since cell size varies markedly as a function of Fe [*Sunda and Hunstman,* 1997; *Timmermans et al.,* 2001; *De Baar et al.,* 2005], the paucity of data concerning the impact of Fe on phytoplankton absorption spectra constitutes a major data gap.

In this study, I investigated the phytoplankton absorption spectra of Fe sufficient and Fe deficient *P. antarctica* and *F. cylindrus.* Fe is the limiting nutrient for phytoplankton in the globally important Southern Ocean and sampling often also relies on remote observations that depend on their photophysiology. Here I examine the impact of Fe upon the bio-optical properties of phytoplankton, as well as the

implications for remote sensing reflectance and satellite-based estimates of chlorophyll.

2. Methods

2.1 Study organisms

An isolate of the colonial prymnesiophyte *Phaeocystis antarctica* (Karsten) (CCMP 1871), the primary component of the Ross Sea polynya phytoplankton bloom, and an isolate of the diatom *Fragilariopsis cylindrus* (Grun.) that is typical of sea ice and marginal ice zone algal communities (CCMP1102) were examined in this study. The *P. antarctica* isolate from the CCMP was originally obtained from Palmer station in the Bellingshausen Sea, while *F. cylindrus* was isolated from the vicinity of the Islas Orcadas in the Weddell Sea.

2.2 Culture media

Each phytoplankton isolate was grown in the artificial seawater medium Aquil [*Price et al.*, 1988/1989]. Aquil is made up of a synthetic ocean water salt mixture (SOW) that is augmented with phosphate (PO_4, 10 μM) and silicic acid ($Si(OH)_3$, 100 μM). The SOW-P-Si mixture is then passed through a chelex exchange column to remove all metals. Chelex was prepared according to the protocol of *Price et al.* [1988/1989] and following chelation, all subsequent manipulations of the media were conducted in a Class-100 laminar flow hood. The media was heat sterilized by microwave in 5 minute intervals for a total of 15 minutes, to avoid boiling. To minimize any biological activity in the chelexed SOW-PO_4-Si mixture, a NO_3 stock

(300 μM) was chelexed and sterilized separately, but in an identical fashion to the SOW-PO_4-Si mixture. Trace metal and vitamin stocks were prepared individually in a class-100 clean laboratory. The trace elements Mn, Zn, Co, Mo, Se, and Cu were made up as individual stocks in 0.01M ultra pure HCl and precomplexed with ethylenediaminetetra-acetate (EDTA) to produce a mixed trace metal solution with a final EDTA concentration of 100 μM. The Fe stock was made in ultra pure 0.01M HCl and pre-complexed with EDTA in a 1:1 molar ratio (45 nM). The mixed trace metal and Fe-EDTA solutions were filter sterilized under trace metal clean conditions prior to addition to the media. The vitamins B_{12}, biotin, and thiamine were made up in milli-q water (MQ), filter sterilized and added to the media to achieve final concentrations of 5.5×10^{-7}, 5×10^{-7}, and 1×10^{-4} g L^{-1}, respectively. The metal - EDTA reactions were allowed to equilibrate overnight prior to any use of the media. The precise composition of Aquil is described in Table 1.

2.2 Washing protocol

In order to minimize any Fe contamination, all equipment used in all experiments was subjected to a rigorous cleaning protocol [*Achterberg et al.,* 2001]. Firstly, this involved an initial scrub and soak in non-phosphate soap for approximately 2 weeks. Following a MQ rinse, each item was then soaked in a 10% HCl solution (trace metal grade) for at least 2 weeks. Finally, equipment was filled with MQ, double bagged, and stored in a closed box, where it remained unopened until use.

Table 1. The composition of the growth medium Aquil [*Price et al.*, 1988/1989]

Substance	Final Concentration (M)
Aquil salts	
NaCl	4.20×10^{-1}
Na_2SO_4	2.88×10^{-2}
KCl	9.39×10^{-3}
$NaHCO_3$	2.38×10^{-3}
KBr	8.40×10^{-4}
H_3BO_3	4.85×10^{-4}
NaF	7.14×10^{-5}
$MgCl_2.6H_2O$	5.46×10^{-2}
$CaCl_2.2H_2O$	1.05×10^{-2}
$SrCl_2.6H_2O$	6.38×10^{-5}
Nutrients	
$NaH_2PO_4.H_2O$	1.00×10^{-5}
$NaNO_3$	3.00×10^{-4}
$Na_2SiO_3.9H_2O$	1.00×10^{-4}
Trace Metals	
Na_2EDTA	5.00×10^{-6}
$FeCl_3.6H_2O$	4.51×10^{-7}
$ZnSO_4.7H_2O$	4.00×10^{-9}
$MnCl_2.4H_2O$	2.30×10^{-8}
$CoCl_2.6H_2O$	2.50×10^{-9}
$CuSO_4.5H_2O$	9.97×10^{-10}
$Na_2MoO_4.2H_2O$	1.00×10^{-7}
Na_2SeO3	1.00×10^{-8}
Vitamins	
B_{12}	5.50×10^{-7} g L^{-1}
Biotin	5.00×10^{-7} g L^{-1}
Thiamine HCl	1.00×10^{-4} g L^{-1}

Figure 1. Lamp spectrum used to illuminate all cultures, as a function of wavelength (taken from inside a culture flask).

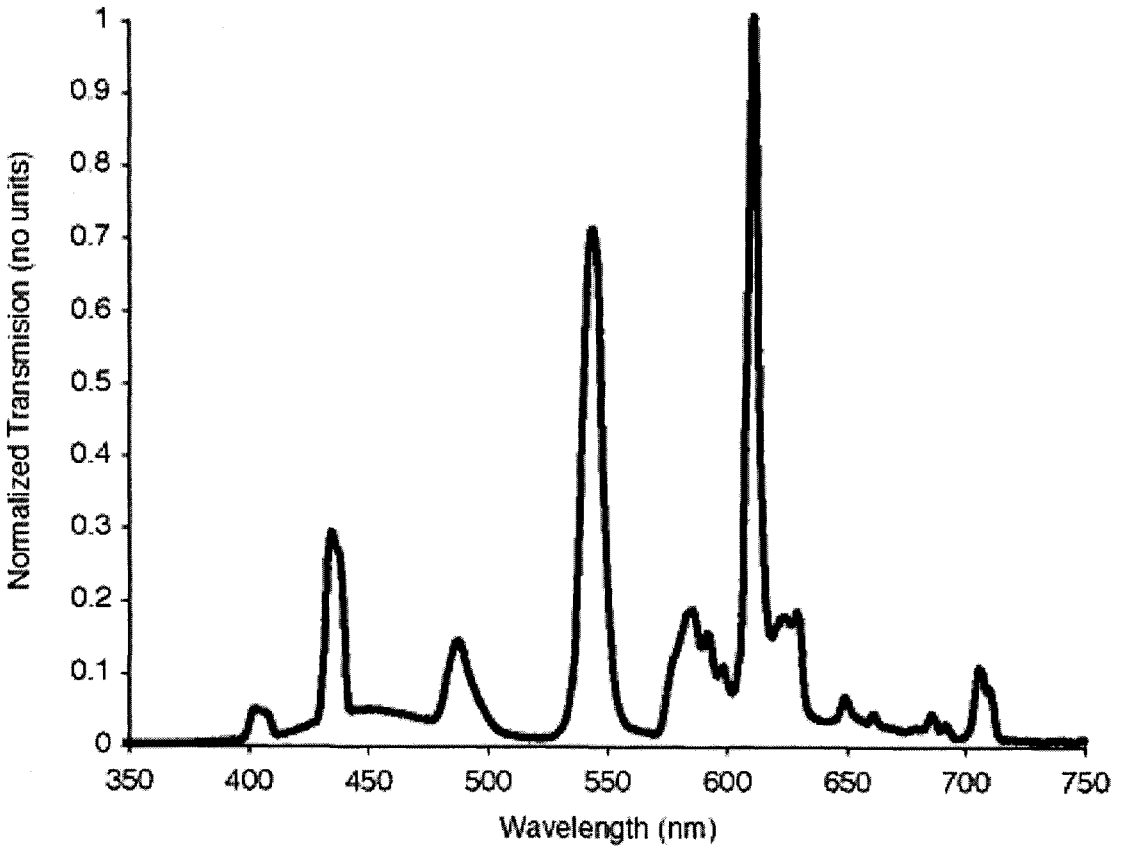

2.4 Approach

There are two separate treatments where Aquil is made according to the above protocol either with (F) or without (N) addition of the Fe-EDTA solution. Both phytoplankton species (under both treatments, where P and D denote *P. antarctica* and *F. cylindrus*, respectively) are grown at 2°C under continuous visible (i.e. no UV) illumination (65 μEin m^{-2} s^{-1}).

Phytoplankton cultures were grown in semi-continuous culture in trace metal clean 1L polycarbonate flasks (see above). Culture vessels were also augmented with a trace metal clean Teflon line sampling port to minimize contamination during sampling. All cultures were swirled gently each day and periodically sampled via trace metal clean syringes to determine the in vivo fluorescence and Fv/Fm. As each culture approached stationary phase (defined by a drop in Fv/Fm), cells were harvested for measurement and a small inoculum was used to initiate the new culture (approximately 10% by volume). Sterile, trace metal clean techniques were used in all manipulations.

2.5 Measurements

In vivo fluorescence is used as a qualitative index of culture biomass and was measured using a Turner Designs 10-AU fluorometer. The concentration of chlorophyll *a* was determined by filtering a 5 mL sample onto a 0.4 μm glass fiber filter (Whatmann GF/F), which was extracted overnight in 10 mL of 90% acetone at 4 °C. Chlorophyll *a* was then quantified fluorometrically using the method of *Evans et al.* [1987]. The photochemical conversion efficiency of photosystem II (ϕ_{II}, or Fv/Fm)

was measured using a pulse amplitude modulated fluorometer after cells had been dark adapted for at least 15 minutes.

Algal absorption spectra were determined by gently filtering phytoplankton and associated particles onto a 0.4 μm glass fiber filter under low vacuum pressure. For each filter, the absorption spectrum for the collected particles (a_p, m^{-1}) was measured from 300 to 800 nm using a Perkin-Elmer Lambda 35 spectrophotometer fitted with an integrating sphere. All spectra were corrected for optical path length amplification using the procedure of *Mitchell and Kiefer* [1988] and the coefficients of *Bricaud and Stramski* [1990]. Each filter was then extracted with 80% methanol and re-measured to obtain the absorption spectrum of non-extracted (detrital, a_d, m^{-1}) material remaining on the filter [*Kishino et al.,* 1985]. Phytoplankton absorption spectra (a_{ph}, m^{-1}) were determined by subtracting the detrital absorption spectra (a_d, m^{-1}) from the a_p spectra. Finally, a_{ph} was normalized by the concentration of chlorophyll *a* (the mean of 3 replicates) to obtain the chlorophyll *a*-specific absorption coefficient (a_{ph}*, m^2 mg Chl a^{-1}). I denote the maximum a_{ph}* within the narrow 660-675 nm, 435-445 nm, and 305-340 nm wavelength bands as red, blue, and UV absorption, respectively.

Phytoplankton specific growth rates (d^{-1}) were estimated from the slope of the log-transformed change in PO_4 concentration over time.

3. Results

3.1 Growth and physiological state

Growth rates were similar for *P. antarctica* and *F. cylindrus* under Fe sufficient conditions and averaged 0.156 day^{-1} and 0.142 day^{-1}, respectively (Table 2). Under Fe

deficient conditions, the rate of growth was depressed for both taxa, albeit more so in *F. cylindrus*. The growth rate of *P. antarctica* averaged 0.085 day^{-1} under Fe deficient conditions, whereas the growth rate of *F. cylindrus* was only 0.053 day^{-1}. This represented a reduction in average daily growth rate when Fe deficient of 45% and 60% for *P. antarctica* and *F. cylindrus*, respectively.

Unsurprisingly, measures of photophysiology also demonstrate an effect of the Fe deficient treatment. The average maximum Fv/Fm is high for both *P. antarctica* (0.556) and *F. cylindrus* (0.517) when grown under Fe sufficient conditions, which represents a high photochemical efficiency of photosystem II. Under Fe deficient conditions, maximum Fv/Fm was reduced by 30% (to 0.389) and 60% (to 0.203) for *P. antarctica* and *F. cylindrus*, respectively (Table 2).

3.2 Absorption spectra

3.2.1 Fe sufficient

Absorption spectra highlight important interspecific differences under Fe sufficient conditions (Figure 2). *F. cylindrus* exhibited values for a_{ph}*(b) that are almost 2-fold greater than for *P. antarctica* (0.023±0.006 and 0.013±0.003 m^2 mg Chl a^{-1}, respectively, Table 3). The caroteniod pigment fucoxanthin and chlorophylls *a* and *c*, are likely to be responsible for the increased absorption of *F. cylindrus*, relative to *P. antarctica*, in the 480-500 nm and 400 and 480 nm ranges, respectively (Figure 3).

The ratio of the blue to red peak is virtually identical for both taxa and suggests a similar degree of pigment packaging (Table 3, Figure 2) [sensu *Morel and Bricaud,* 1981], despite the markedly different cell morphologies. Although *F. cylindrus* does

Table 2. Growth rate (μ_{ave}, day^{-1}), maximum photochemical efficiency of photosystem II (Fv/Fm max, no units), chlorophyll specific absorption (a*, m^2 mg Chl a^{-1}), and chlorophyll per cell ($x10^{-7}$ µg chl $cell^{-1}$) for each treatment. Values are averages of all data at each treatment ± the standard deviation.

	P. antarctica Fe sufficient	*F. cylindrus* Fe sufficient	*P. antarctica* Fe deficient	*F. cylindrus* Fe deficient
μ_{ave}	0.156	0.142	0.085	0.053
	±0.022	±0.039	±0.004	±0.003
Fv/Fm	0.556	0.517	0.389	0.203
	±0.036	±0.074	±0.026	±0.068
a*	0.0085	0.015	0.0131	0.0354
	±0.0006	±0.003	±0.001	±0.006
Chl	3.48	2.42	4.92	2.38
$cell^{-1}$	±0.26	±0.24	±0.94	±0.32

Figure 2. Absorption spectra for phytoplankton (a_{ph}*, m^2 mg Chl a^{-1}) for *P. antarctica* (A), *F. cylindrus (B)*, and the average spectra (C) for *P. antarctica (PF) and F. cylindrus* (DF), all under Fe sufficient conditions.

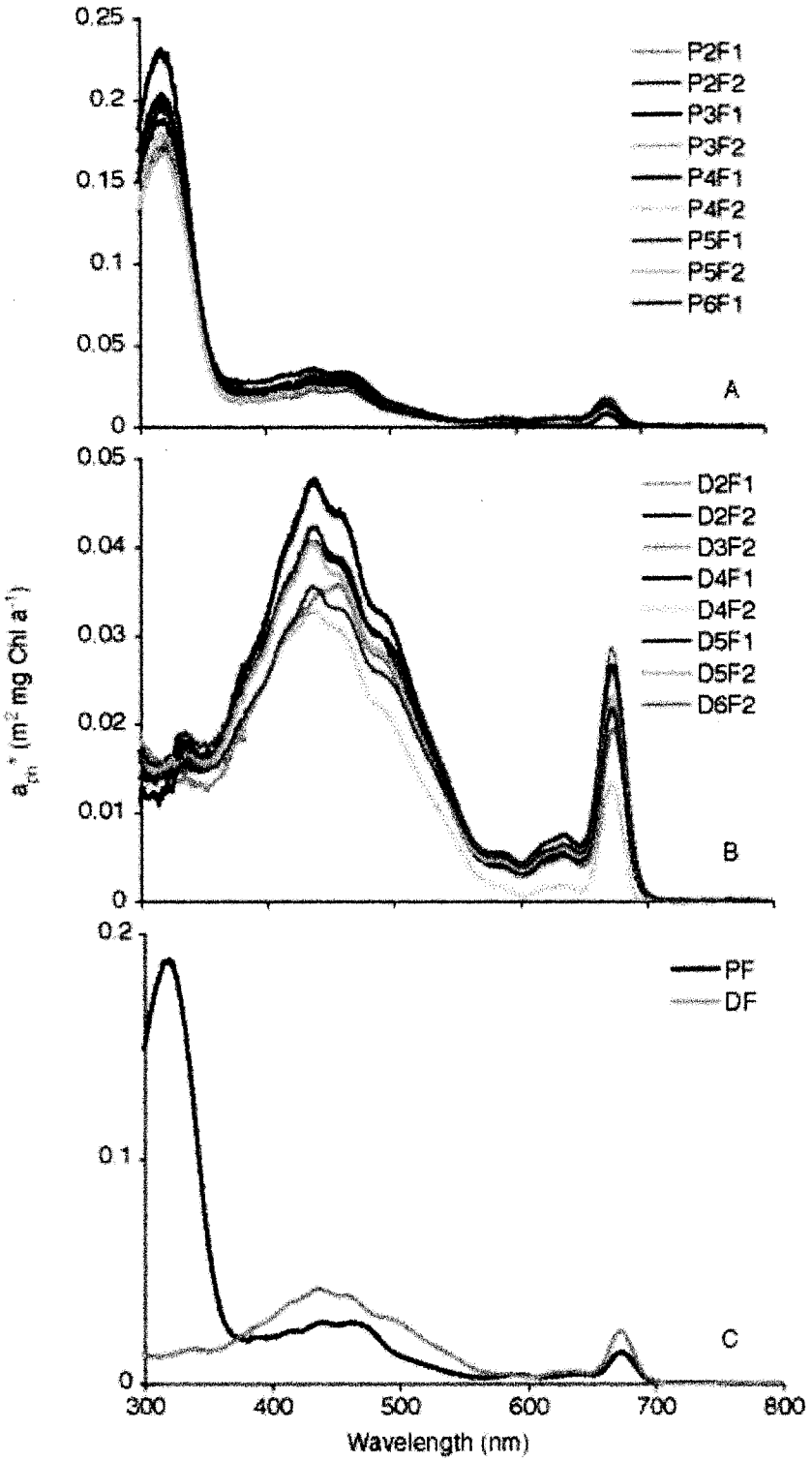

Table 3. Chlorophyll *a* normalized absorption (a_{ph}*, m^2 mg Chl a^{-1}) at red (r, 660 nm), blue (b, 440 nm) and UV (UV, 320nm) wavelengths, as well as the ratio of the blue to red (a_{ph}*(b)/a_{ph}*(r), no units) and UV to red (a_{ph}*(UV)/a_{ph}*(r), no units) peaks for all treatments. Also included are chlorophyll *a* normalized absorption at specific wavelengths used for remote sensing algorithms (443, 490 and 555 nm, m^2 mg Chl a^{-1}). All values are averages ± the standard deviation.

	P. antarctica Fe sufficient	*F. cylindrus* Fe sufficient	*P. antarctica* Fe deficient	*F. cylindrus* Fe deficient
a_{ph}*(r)	0.013	0.023	0.015	0.019
	±0.003	±0.006	±0.0008	±0.0017
a_{ph}*(b)	0.026	0.040	0.040	0.030
	±0.0046	±0.007	±0.004	±0.0050
a_{ph}*(UV)	0.188	0.017	0.022	0.010
	±0.020	±0.0017	±0.011	±0,0017
a_{ph}*(b):a_{ph}*(r)	1.8	1.8	2.7	1.5
	±0.0912	±0.114	±0.148	±0.180
a_{ph}*(UV):a_{ph}*(r)	14.9	0.8	1.5	0.5
	±4.89	±0.227	±0.790	±0.076
a_{ph}*(443)	0.026	0.040	0.041	0.030
	±0.004	±0.006	±0.0041	±0.0038
a_{ph}*(490)	0.016	0.028	0.032	0.023
	±0.0028	±0.004	±0.0041	±0.0025
a_{ph}*(555)	0.003	0.009	0.004	0.007
	±0.0004	±0.0006	±0.0043	±0.0009
a_{ph}*(443):a_{ph}*(555)	10.4	5.0	12.3	4.3
	±2.66	±0.62	±2.65	±0.99
a_{ph}*(490):a_{ph}*(555)	6.3	3.6	9.3	3.2
	±1.40	±0.33	±1.67	±0.64

show greater absorption in the blue, this is counteracted by a complimentary increase in absorption at red wavelengths (Table 3). In fact, $a_{ph}^*(r)$ for *F. cylindrus* (0.0231 m^2 mg Chl a^{-1}) is within the range of 0.023-0.029 m^2 mg Chl a^{-1} measured for unpackaged in vivo absorption of Chl *a-c* phytoplankton [*Johnsen et al.,* 1994; *Moisan and Mitchell,* 1999], suggesting little pigment packaging by *F. cylindrus* under Fe replete conditions. Furthermore a* increased by almost 50% when *P. antarctica* was Fe deficient (Table 2), suggestive of a reduction in pigment packaging by *P. antarctica* cultures during this treatment and more efficient light capture, per unit chlorophyll *a*.

Algorithms that estimate pigment concentrations from remote sensing reflectance (R_{rs}) typically exploit the differential absorption of blue (443 and 490 nm) and green (555 nm) light by phytoplankton. Under Fe replete conditions, $a_{ph}^*(443)$, $a_{ph}^*(490)$ and $a_{ph}^*(555)$ are all greater for *F. cylindrus*, relative to *P. antarctica* (Table 3). Additionally, both $a_{ph}^*(423)$: $a_{ph}^*(555)$ and $a_{ph}^*(490)$: $a_{ph}^*(555)$ are > 2 fold greater for *P. antarctica* than for *F. cylindrus* (Table 3).

The most striking difference between *P. antarctica* and diatoms is at the UV portion of the light spectrum. At wavelengths < 350 nm, the chlorophyll-normalized absorption of *P. antarctica* (0.188±0.020 m^2 mg Chl a^{-1}) is 10-fold greater than that of *F. cylindrus* (0.017±0.002 m^2 mg Chl a^{-1}) (Figure 2). This is likely to be due to the production of mycosporine like amino acids (MAAs) by *P. antarctica,* which absorb strongly in the UV [*Karentz et al.,* 1991]. Accordingly, the average $a_{ph}^*(UV)$: $a_{ph}^*(r)$

ratio for *P. antarctica* is over 18 times greater than for *F. cylindrus* (Figure 2, Table 3).

3.2.2. Fe deficient

All Fe deficient *P. antarctica* cultures showed significant changes in their absorption spectra. There was little change in the red peak, but increased absorption in the Soret band (400 – 555 nm, Figure 3, Table 3). Fe deficiency in *P. antarctica* resulted in a 50% increase in the average a_{ph}*(b): a_{ph}*(r) (to 2.67±0.148, Table 3), suggesting a decrease in pigment packaging when Fe is low. Nevertheless, a_{ph}*(r) remained lower than the range measured (0.023-0.029 m^2 mg Chl a^{-1}) for unpackaged Chl *a-c* [*Johnsen et al.,* 1994; *Moisan and Mitchell,* 1999], which would suggest that any reduction in pigment packaging by Fe deficient *P. antarctica* was only slight.

There were even more conspicuous changes in the absorption spectrum of Fe deficient *P. antarctica* at the UV end of the light spectrum. At wavelengths < 350nm, the UV peak that is characteristic of Fe sufficient *P. antarctica* is completely absent under low Fe concentrations (Figure 3). The average a_{ph}*(UV) decreased from 0.188±0.020 to 0.022±0.011 between Fe sufficient and Fe deficient treatments (Table 3). As there was only a small change in a_{ph}*(r), this resulted in a large change in a_{ph}*(UV): a_{ph}*(r) from 14.9±4.89 to only 0.767±0.227 when *P. antarctica* was Fe deficient (Table 3). Although some cultures did display a slight absorption signal in the UV, a_{ph}*(UV): a_{ph}*(r) fell by a minimum of 80%, relative to the Fe sufficient treatment (Figure 3).

Figure 3. Absorption spectra for phytoplankton (a_{ph}*, m^2 mg Chl a^{-1}) for a) *P. antarctica* and b) *F. cylindrus*, under Fe deficient conditions. For reference, the average absorption spectra of Fe sufficient *P. antarctica* (AVE PF) and *F. cylindrus* (AVE DF) are also included.

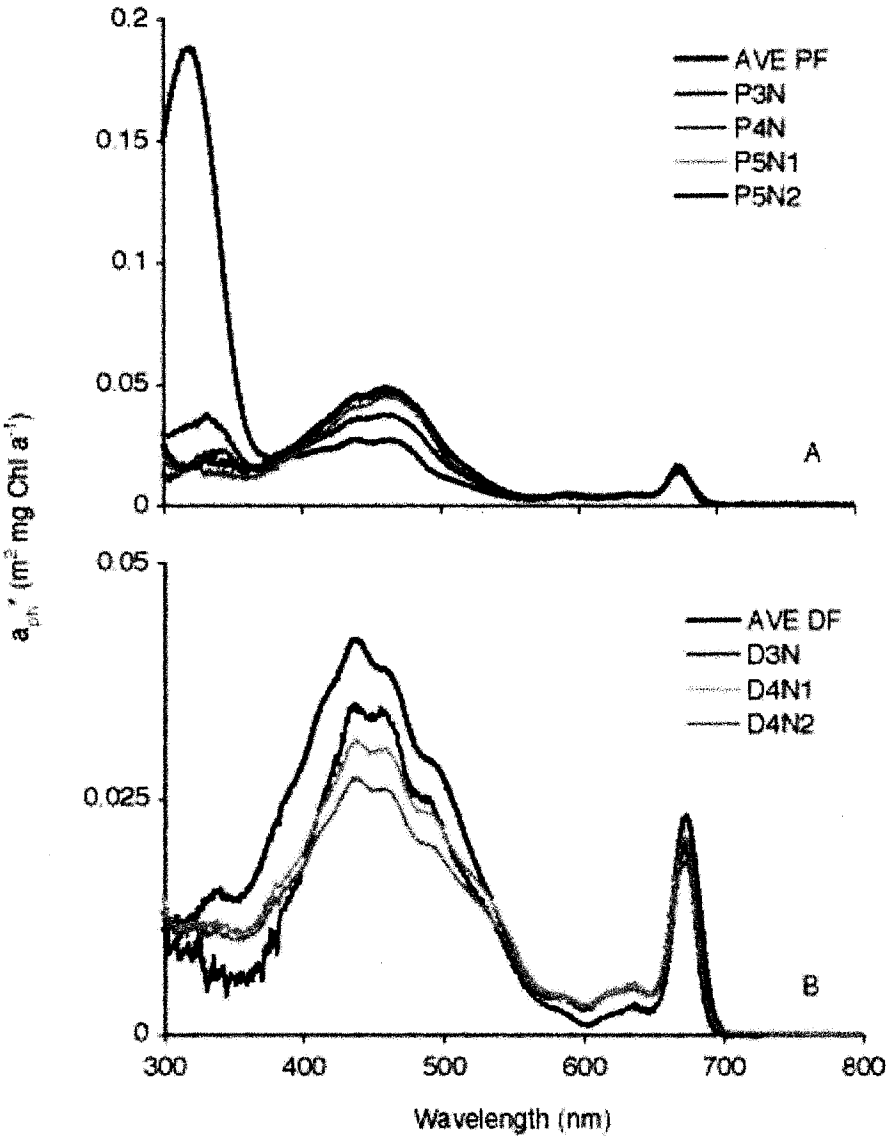

There were also changes in the absorption spectra of Fe deficient *F. cylindrus.* On average a_{ph}* from Fe deficient *F .cylindrus* is consistently reduced, with a_{ph}*(b) and a_{ph}*(r) being 25% and 16% lower respectively, than the Fe sufficient treatment (Figure 3, Table 3). Nevertheless, a_{ph}*(b): a_{ph}*(r) was within the range of measurements from Fe sufficient *F. cylindrus* (Table 3), suggesting little change in pigment packaging [sensu *Morel and Bricaud,* 1981]. The impact of Fe was more apparent at the UV end of the light spectrum and a_{ph}*(UV) declined by around 40% (Table 3). Notwithstanding, it is clear that the absolute change in the chlorophyll-specific absorption of *F. cylindrus* under Fe deficient conditions is much lower than was observed for *P. antarctica* (Figure 3).

Fe deficiency resulted in large difference in a_{ph}* at the wavelengths used for remote sensing (443, 490, and 555 nm). On average, a_{ph}*(490):a_{ph}*(555) was almost 50% greater for Fe deficient *P. antarctica*, whereas a_{ph}*(443):a_{ph}*(555) was only increased by 18% (Table 3). At specific wavelengths, the average a_{ph}* increased by 58%, 102%, and 43%, for 443, 490, and 555 nm, respectively when *P. antarctica* was Fe deficient (Table 3). The difference in a_{ph}*(443):a_{ph}*(555) and a_{ph}*(490):a_{ph}*(555) for Fe deficient *F. cylindrus* was not as great (≤10%), relative to Fe sufficient cultures (Table 3).

4. Discussion

4.1 Comparison with previous observations

4.1.1 Laboratory cultures

The suite of absorption spectra measured during this study compare well to previous measurements made on Fe-replete laboratory cultures of *P. antarctica* (this is the first such examination of absorbance by Fe-deficient *P. antarctica*). Firstly, the large absorption peaks at UV wavelengths that typify *P. antarctica* grown under Fe sufficient conditions are consistent with numerous other laboratory investigations [*Marchant et al.,* 1991; *Riegger and Robinson,* 1997; *Moisan and Mitchell,* 2001]. For example, *Moisan and Mitchell* [1999] report values for $a_{ph}^*(b):a_{ph}^*(r)$ of 1.5 and 3.3, for growth irradiances of 37 and 84 μEin m^{-2} s^{-1}, respectively, which compare well to my results (a range of 1.66 to 1.93 m^2 mg Chl a^{-1}, Table 3). Additionally, the mean $a_{ph}^*(UV):a_{ph}^*(r)$ for all Fe replete *P. antarctica* was 14.92 (Table 3), ranging from 9.94-26.5, which is consistent with the range of measurements previously reported from laboratory cultures [3-48.3, *Marchant et al.,* 1991; *Riegger and Robinson,* 1997; *Moisan and Mitchell,* 2001].

The higher $a_{ph}^*(b)$ and lower $a_{ph}^*(UV)$ for Fe sufficient *F. cylindrus*, relative to *P. antarctica,* measured during this study is consistent with previous data from *F. cylindrus* [*Riegger and Robinson,* 1997] and other Southern Ocean diatoms [*Davidson et al.,* 1994; *Riegger and Robinson*, 1997]. *Riegger and Robinson* [1997] observe little UV absorbance by *F. cylindrus* illuminated at similar light intensities to those used in this study, as well as increased absorption between approximately 400 to 500

nm, relative to *P. antarctica*. Nevertheless, enhanced UV absorbance was induced in their study for several other larger diatom species, although the magnitude of a_{ph}*(UV) was always >50% less than for *P. antarctica* [*Riegger and Robinson,* 1997]. In contrast, all diatoms investigated by *Davidson et al.* [1994] (including many also studied by *Riegger and Robinson,* [1997]) exhibited lower UV and increased blue absorbance than *P. antarctica* [*Marchant et al.,* 1991].

It is noteworthy that *P. antarctica* had high absorption in the UV despite the fact that the light spectra used to illuminate the algal cultures does not include UV wavelengths. This would imply that *P. antarctica* can be induced to produce UV absorbing compounds by visible light, as noted by *Riegger and Robinson* [1997]. The lack of a UV peak from *F. cylindrus* may be due to the absence of UV radiation from the lamp spectrum used (Figure 1), suggesting that UV wavelengths are required for induction of MAAs in this species.

4.1.2 Field measurements from the southwestern Ross Sea

At UV wavelengths, the data collected during this study differ somewhat from previous measurements made on *P. antarctica* and diatoms in the southwestern Ross Sea. The average ratio of a_{ph}* at 320 nm to a_{ph}* at 435 nm for *P. antarctica* during this study (7.39±1.29) is higher than the value of 4.03±1.85 measured in situ by *Arrigo et al.* [1998c]. Moreover, the overall mean a_{ph}* at 667 nm in the field [0.023 m^2 mg Chl a^{-1}, *Arrigo et al.,* 1998c] is almost twice as high as that measured for *P. antarctica* during this study (0.013 m^2 mg Chl a^{-1}, Table 3). For *F. cylindrus*, the ratio of a_{ph}*(320): a_{ph}*(435) is much lower (0.37±0.053) than that observed in situ for diatoms

(4.03±1.85) by *Arrigo et al.* [1998c]. The discrepancies between field and laboratory data at UV wavelengths may be due to the light spectrum used in the laboratory. However, it should also be noted that field samples were dominated by *N. subcurvata*, rather than *F. cylindrus* [*Arrigo et al.,* 1998c], which may have different absorption properties [*Morel and Bricaud,* 1981; *Sathyendranath et al.,* 1987].

At visible wavelengths, there is much better agreement between field and laboratory measurements. The ratio of a_{ph}*(443):a_{ph}*(555) measured during this study under Fe sufficient conditions (10.38±2.66) is within the overall range of field measurements on *P. antarctica* [8.03±3.10, *Arrigo et al.,* 1998c]. Likewise, the mean a_{ph}*(435):a_{ph}*(555) for *F. cylindrus* is within 20% of values measured in situ (6.24±2.11, *Arrigo et al.* [1998c]). Between 490 and 550 nm, the mean a_{ph}* ratio for both *P. antarctica* and *F. cylindrus* (6.27±1.40 and 3.56±0.33 m^2 mg Chl a^{-1}, respectively) compare well with measurements made in the Ross Sea by *Arrigo et al.* [1998c] (5.26±1.93 and 4.03±1.19 m^2 mg Chl a^{-1}). Overall, the data collected during this study support the higher a_{ph}*(443): a_{ph}*(555) and a_{ph}*(490): a_{ph}*(555) for *P. antarctica*, relative to diatoms, previously observed in the Ross Sea [*Arrigo et al.,* 1998c].

4.2 Impact of Fe on UV absorbance

The presence of UV absorbing compounds (typically MAAs) has been well documented for eukaryotic algae, cyanobacteria, and dinoflagellates, as well as algal-invertebrate symbionts and higher trophic levels [*Shick and Dunlap,* 2002 and references therein]. I believe my results are unique in demonstrating an Fe mediated

decline in UV absorbance (presumably by MAAs) for *P. antarctica*. MAAs are postulated to be formed via a branch point in the Shikimate pathway that produces aromatic amino acids from Ethyrose-4-phosphate (E4P) and phosphoenolpyruvate (PEP) [*Favre-Bonvin et al.,* 1987; *Shick et al.,* 1999]. Synthesis of MAAs in marine organisms appears to proceed from 3-dehydroquinate (DHQ) and MAA production can be arrested when the enzyme DHQ-synthetase is inhibited with millimolar concentrations of glycophosphate [*Shick et al.,* 1999]. Although both DHQ-synthetase and the enzyme responsible for the condensation of E4P and PEP have a requirement for a cobalt cofactor, there does not appear to be any evidence as of yet that Fe is directly involved in MAA synthesis.

This suggests that the relationship between low UV absorption and Fe deficiency may be more indirect. The de novo synthesis of MAAs can be costly for phytoplankton and might be down regulated under Fe stress. *Haslam* [1993] used stoichiometry and ATP-coupling coefficients to obtain a cost of 60 ATP equivalents for synthesizing one mole of chorismate, which is the final aromatic formed during the Shikimate pathway. *Shick and Dunlap* [2002] note that if the formation of MAAs does indeed proceed from the DHQ branch point, then the ATP cost should be similar and is almost double the cost of producing non-aromatic amino acids. Moreover, *Raven* [1984] calculates that an algal cell would require 300 moles of photons to be captured during photosynthesis for the synthesis of one mole of MAA, which is as much as 19% of the total energy cost of cell production [*Raven,* 1991]. I observe a consistent reduction in the average Fv/Fm, the growth rate, and total absorption when *P. antarctica* is Fe deficient. Given the relatively high cost of MAA synthesis, an Fe

mediated decline in the efficiency of photosynthesis might swing the cost/benefit away from MAA synthesis when phytoplankton are Fe deficient.

Cell size has been shown to be of particular significance in determining the effectiveness of MAA production as a strategy to mitigate against UV damage [e.g., *Raven,* 1984; *Garcia-Pichel,* 1994; *Riegger and Robinson,* 1997]. *Raven* [1984] estimates that the screening of sensitive organelles (especially DNA) from UV radiation was possible, despite the large metabolic cost, in a 5 μm radius cell, but was much less effective in a 0.5 μm radius cell [*Raven,* 1984]. Similarly, *Garcia-Pichel* [1994] estimates that for MAAs to be effective sunscreens a cellular radius of > 10μm is required, and 'powerful and efficient' sunscreening is only possible if the cell radius is > 200 μm [*Garcia-Pichel,* 1994]. This explains why the potential sunscreening effect of MAAs has been observed to increase with respect to cell size [*Riegger and Robinson,* 1997].

It is possible that the morphological shift towards single cells by Fe deficient *P. antarctica* is responsible for the decline in UV absorbance. *Marchant et al.* [1991] reported that *P. pouchetii* (sensu *antarctica*) exhibited reduced production of UV absorbing compounds when in the single cell stage. Both *Riegger and Robinson* [1997] and *Marchant et al.* [1991] suggest that MAAs are likely to be located extracellularly when *P. antarctica* is in the colonial form. Although MAAs typically contribute at most 1% to the total dry cell biomass [*Karentz et al.,* 1991], *Riegger and Robinson* [1997] estimate that at thhe concentrations they measured, MAAs would comprise up to 40% of total dry mass if they were located intracellularly. However, if

the colony, rather than the individual cell, was the optical unit, then MAAs were a more realistic proportion of the colony dry weight (<1%), supportive of an extracellular accumulation of UV absorbing compounds [*Riegger and Robinson,* 1997].

If MAAs are located extracellularly in *P. antarctica*, then their effectiveness at screening cellular organelles from UV radiation is questionable. This would suggest that MAAs might also be important for the chemical regulation of other physiological processes when *P. antarctica* is in the colonial form, such as osmoregulation [*Shick and Dunlap* 2002 and references therein].

4.3 Implications for remote sensing algorithms

An Fe mediated change in the absorption characteristics of *P. antarctica* at wavelengths used for bio-optical algorithms will impact the estimation of pigment concentrations via measurements of remote sensing reflectance. Several studies have already shown that different bio-optical algorithms should be used for polar regions [*Sullivan et al.,* 1993; *Arrigo et al.,* 1998c] and this study corroborates the inter specific variability in absorbance at 443, 490 and 555 nm observed for Ross Sea phytoplankton [*Arrigo et al.,* 1998c]. However, this study also demonstrates potentially significant variability in a_{ph}* within one phytoplankton group (*P. antarctica*) mediated by the lack of Fe. The differences in a_{ph}* between Fe deficient and Fe replete *P. antarctica* are as great as the inter-specific differences measured by *Arrigo et al.* [1998c] for *P. antarctica* and diatoms in the Ross Sea.

To test the potential impact of Fe-mediated changes in a_{ph}* on satellite-based retrievals of chlorophyll, I used the Southern Ocean semi-analytical reflectance model of *Reynolds et al.* [2001] to derive $R_{rs}(490)$ and $R_{rs}(555)$ from the phytoplankton absorbance data collected during this study. Empirical relationships and parameter values derived from data collected in the Ross Sea, as described by *Arrigo et al.* [1998c] and *Reynolds et al.* [2001], were used to estimate the total backscatter, absorption by chromophoric dissolved organic matter, and *f/Q*. The a_{ph}*(490) and a_{ph}*(555) from this study can then be used, alongside chlorophyll *a*, to determine if $R_{rs}(490)$ and $R_{rs}(555)$ for *P. antarctica* (and *F. cylindrus*) would differ under Fe sufficient and deficient conditions.

This analysis suggests that existing remote sensing algorithms derived from in situ data will overestimate chlorophyll *a* concentrations when *P. antarctica* experiences Fe stress. The algorithm of *Arrigo et al.* [1998c] relating chlorophyll to $R_{rs}(490):R_{rs}(555)$ was parameterized using data collected in the Ross Sea during December and January and is consistent with the $R_{rs}(490):R_{rs}(555)$ estimated here for Fe replete *P. antarctica* and *F. cylindrus* treatments (Figure 4). However, the increased a_{ph}*(490): a_{ph}*(555) of Fe deficient *P. antarctica* (Table 3) results in a reduction in $R_{rs}(490):R_{rs}(555)$ per unit chlorophyll *a* (Figure 4). Moreover, Fe deficient *F. cylindrus* show an increase $R_{rs}(490):R_{rs}(555)$ per unit chlorophyll *a* (Figure 4). This means that remotely sensed chlorophyll *a* concentrations based on $R_{rs}(490):R_{rs}(555)$ will be overestimated and slightly underestimated, respectively when waters dominated by *P. antarctica* and *F. cylindrus* experience Fe stress.

Figure 4. Remote sensing reflectance 490-555nm versus chlorophyll *a* (mg m^{-3}) for each treatment (averages, with error bars representing the standard deviation). Also included is the algorithm for predicting chlorophyll *a* from $R_{rs}(490):R_{rs}(555)$ of *Arrigo et al.* [1998c].

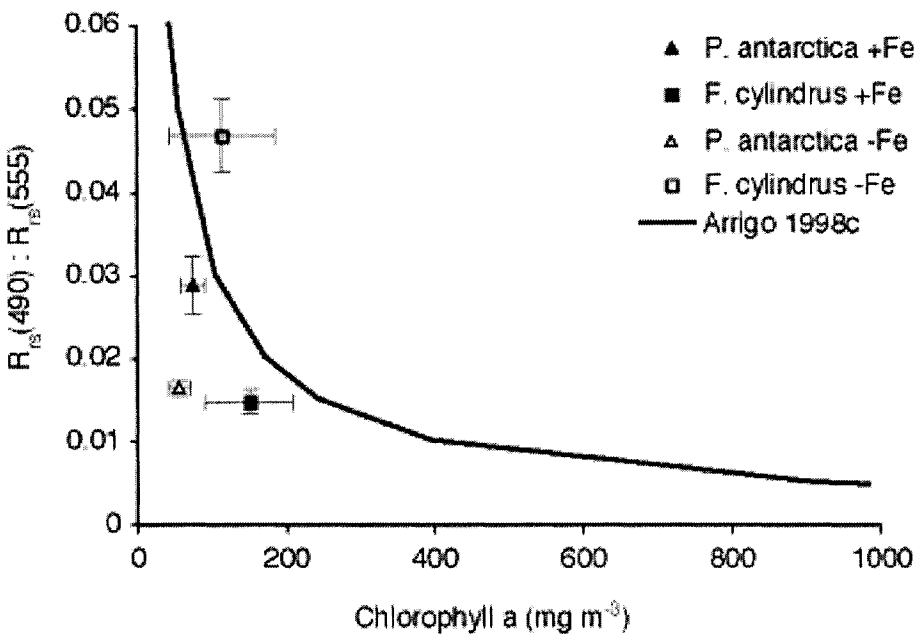

These results imply that changes in phytoplankton bio-optical parameters that are driven by Fe stress might be measurable via remote sensing. At the very least, this study suggests that intra-specific variability in absorption characteristics that is driven by nutrient stress (Fe in this case) could prove to be of importance in the interpretation of remotely sensed reflectance, especially at 490 nm. If remotely sensed chlorophyll *a* concentrations are erroneously high when *P. antarctica* is Fe limited, then both the magnitude and duration of the Ross Sea polynya *P. antarctica* bloom might have been overestimated. This will be mitigated by the fact that Fe limitation will manifest later in the growing season, when chlorophyll *a* levels begin to drop [*Tagliabue and Arrigo,* 2005; 2006]. Nevertheless, given the importance of remotely sensed chlorophyll *a* concentrations (especially for inaccessible regions such as the Ross Sea), an investigation of the *P. antarctica* R_{rs} to chlorophyll *a* relationship during the onset of Fe limitation is necessary.

Literature Cited

Achterberg, E. P., T. W. Holland, A. R. Bowie, R. Fauzi, C. Mantoura, and P. J. Worsfield, Determination of iron in seawater, Anal. Chem. Acta, 442, 1-14, 2001.

Anderson, M. A. and F. M. M. Morel, The influence of aqueous iron chemistry on the uptake of iron by the coastal diatom Thalassiosira weissfogii, Limnol. Oceangr., 27, 789-813, 1982

Anderson, R. F., Z. Chase, M. Q. Fleisher, and J. Sachs, The Southern Ocean's biological pump during the Last Glacial Maximum, Deep Sea Res. Part II, 49, 1909-1938, 2002.

Arrigo K. R. and C. R. McClain, Spring phytoplankton production in the western Ross Sea, Science, 266, 261-263, 1994.

Arrigo, K. R., A. M. Weiss, and W. O. Smith, Jr., Physical forcing of phytoplankton dynamics in the western Ross Sea, J. Geophys. Res., 103, 1007-1021, 1998a.

Arrigo, K. R., D. Worthern, A. Schnell, and M. P. Lizotte, Primary production in Southern Ocean waters, J. Geophys. Res., 103, 15587-15600, 1998b.

Arrigo, K. R., D. H. Robinson, D. L. Worthen, B. Schieber, and M. P. Lizotte, Bio-optical properties of the southwestern Ross Sea, J. Geophys. Res., 103, 21683-21695, 1998c.

Arrigo, K. R., G. R. DiTullio, R. B. Dunbar, M. P. Lizotte, D. H. Robinson, M. VanWoert, and D. L. Worthen, Phytoplankton taxonomic variability and nutrient utilization and primary production in the Ross Sea, J. Geophys. Res., 105, 8827-8846, 2000.

Arrigo, K. R., R. B. Dunbar, M. P. Lizotte, and D. H. Robinson, Taxon-specific differences in C/P and N/P drawdown for phytoplankton in the Ross Sea, Antarctica, Geophys. Res. Lett., 29, 1938-1938, 2002a.

Arrigo, K. R., G. L. van Dijken, D. G. Ainley, M. Fahnestock, and T. Markus, Ecological impact of a large Antarctic iceberg, Geophys. Res. Lett., 29, doi:10.1029/2001GL014160, 2002b.

Arrigo, K. R., D. L. Worthen, and D. H. Robinson, A coupled ocean-ecosystem model of the Ross Sea: 2. Iron regulation of phytoplankton taxonomic variability and primary production, J. Geophys. Res., 108, 3231, 2003a.

Arrigo, K. R., D. H. Robinson, R. B. Dunbar, A. R. Leventer, and M. P. Lizotte. Physical control of chlorophyll *a*, POC, and TPN distributions in the pack ice of the Ross Sea, Antarctica. J. Geophys. Res. 108, 3316. 2003b

Arrigo, K. R., and G. L. van Dijken. Phytoplankton dynamics within 37 Antarctic coastal polynya systems. J. Geophys. Res., 108, doi:10.1029/2002JC001739, 2003a.

Arrigo, K. R., and G. L. van Dijken, Impact of iceberg C-19 on Ross Sea primary production, Geophys. Res. Lett., 30, 1856, 2003b.

Arrigo, K. R., and G. L. van Dijken, Annual changes in sea ice, chlorophyll a, and primary production in the Ross Sea, Antarctica, Deep-Sea Res. Part II, 2004.

Arrigo, K. R., and A. Tagliabue, Iron in the Ross Sea, Part 2: Impact of discrete fertilization strategies, J. Geophys. Res., 110, C03009. 2005.

Asper, V. L., and W. O. Smith. Jr. Particle fluxes during austral spring and summer in the southern Ross Sea (Antarctica). J. Geophys. Res., 104, 5345-5359, 1999.

Atkinson, A. J., M. J. Whitehouse, J. Priddle, G. C. Cripps, P. Ward, and M. A. Brandon, South Georgia, Antarctica: a productive, cold water, pelagic ecosystem. Mar. Ecol. Prog. Ser. 216, 279-308, 2001.

Aumont, O., E. Max-Reimer, S. Blain, and P. Monfray, An ecosystem model of the global ocean including Fe, Si, P co-limitations, Global Biogeochem. Cycles, 17, 1060, 2003.

Baar, H. J. W. de, J. T. M. de Jong, R. F. Notling, K. R. Timmermans, M. A. van Leeuwe, U. Bathmann, M. R. van der Loeff and J. Sildam, Low dissolved Fe and the absence of diatom blooms in remote Pacific waters of the Southern Ocean, Mar. Chem., 66, 1-34, 1995.

Baar, H. J. W., J. T. M. de Jong, D. C. E. Bakker, B. M. Loscher, C. Veth, U. Bathmann, and V. Smetacek. Importance of iron for plankton blooms and carbon dioxide drawdown in the Southern Ocean. Nature. 373, 412-415, 1995.

Baar, H. J. W. et al, Synthesis of iron fertilization experiments: From the iron age in the age of enlightenment. J. Geophys. Res. 110, C09S16, 2005.

Banse, K. and D. C. English. Comparing phytoplankton seasonality in the eastern and western subarctic Pacific and the western Bering Sea. Prog. Oceanogr., 43, 235-288, 1999.

Bautista, B., R. P. Harris, P. R. G. Tranter, and D. Harbour. In situ copepod feeding and grazing rates during a spring bloom dominated by Phaeocystis spp. in the English Channel. J. Plankton Res., 14, 691-703, 1992.

Barbeau, K., E. L. Rue, C. G. Trick, K. W. Bruland, and A. Butler, Photochemical reactivity of siderophores produced by marine heterotrophic bacteria and cyanobacteria based on characteristic Fe(III) binding groups, Limnol. Oceanogr., 48, 1069-1078, 2003.

Barbini, R., R. Fantoni, A. Palucci, F. Colao, S. Sandrini, S. Ceradini, L. Tositti, O. Tubertini, and G.M. Ferrari, Simultaneous measurements of remote lidar chlorophyll and surface CO2 distributions in the Ross Sea. Int. J. Rem. Sens., 24, 3807-3819, 2003.

Bates, N. R., D. A. Hansell and C. A. Carlson, Distribution of CO2 species, estimates of net community production, and air-sea CO2 exchange in the Ross Sea polynya, J. Geophys. Res., 103, 2883-2896, 1998.

Behrenfeld, M. J. and P. G. Falkowski, Photosynthetic rates derived from satellite-based chlorophyll concentration, Limnol. Oceanogr., 42, 1-20. 1997

Benson, A. A., and M. Calvin, The dark reductions of photosynthesis, Science, 105, 648-649, 1947.

Biggs, D. C. Scarcity of E. superba in Ross Sea zooplankton excretion and NH4+ cycling in near surface waters of the Southern Ocean, I, Ross Sea, austral summer 1977-78. Polar Biol., 1, 55-67.

Bolin, B., and E. Eriksson. Changes in the carbon dioxide content of the atmosphere and the sea due to fossil fuel combustion, in The Atmosphere and the Sea in Motion, pp. 130-142, Rockefeller Inst. Press, New York. 1959.

Bolin, B., E. T. Degens, P. Duvigneaud, and S. Kempe, The Global Carbon Cycle, in Scope 13, The Global Carbon Cycle, B. Bolin, E. T. Degens, S. Kempe, and P. Ketner [eds], 491pp, Wiley. U,K. 1979.

Blain, S., et al., A biogeochemical study of the island mass effect in the context of the iron hypothesis: Kerguelen Islands, Southern Ocean. Deep. Sea. Res., Part I., 48, 163-187.

Blain, S., P. N. Sedwick, F. B. Griffiths, B. Queguiner, E. Bucciarelli, M. Fiala, P. Pondaven, and P. Treguer. Quantification of algal iron requirements in the subantarctic Southern Ocean (Indian Sector), Deep Sea Res. Part II, 49, 3255-3273, 2002.

Blain, S., C. Guieu, H. Claustre, K. Leblanc, T. Moutin, B. Queguiner, J. Ras, and G. Sarthou. Availability of iron and major macronutrients for phytoplankton in the northeast Atlantic Ocean. Limnol. Oceanogr. 49, 2095-2104, 2004.

Blumberg, A. F., and G. L. Mellor, A description of a three-dimensional coastal ocean circulation model, in Three Dimensional Coastal Ocean Models, Coastal Estuarine Sci., vol. 4, edited by N. S. Heaps, pp. 1-16, AGU, Washington, D.C, 1987.

Bopp, L, K. E. Kohlfield, C. Le Quere, and O. Aumont. Dust impact on marine biota and atmospheric CO_2 during glacial periods. Paleoceanography. 18, 1046. 2003.

Boyd, P. W., A. J. Watson, C. S. Law, E. R. Abraham, T. Trull, R. Murdoch, D. C. E. Bakker, A. R. Bowie, K. O. Buesseler, H. Chang, and M. Charette, A mesoscale phytoplankton bloom in the polar Southern Ocean stimulated by iron fertilization. Nature. 407: 695-702, 2000.

Boyd, P. W., *et al* The decline and fate of an iron-induced phytoplankton bloom. Nature. 428, 549-553. 2004.

Boye, M., C. M. G. van den Berg, J. T. M. de Jong, H. Leach, P. Croot, and H. J. W. de Baar, Organic complexation of iron in the Southern Ocean. Deep Sea Res. Part I, 48 1477-1497, 2001.

Bowie, A. R. et al., The fate of added iron during a mesoscale fertilization experiment in the Southern Ocean. Deep Sea Res, Part II, 48, 2703-2743, 2001.

Bowie, A. R., E. P. Achterberg, P. N. Sedwick, S. Ussher, and P. J. Worsfold, Real-time monitoring of picomolar concentrations of iron(II) in marine waters using automated flow injection-chemiluminescence instrumentation, Environ. Sci. Tech., 36, 4600-4607, 2002.

Brand, L. E., Minimum iron requirements of marine phytoplankton and the implications for the biogeochemical control of new production, Limnol. Oceanogr., 36, 1756-1771, 1991.

Bricaud, A., and D. Stramski, Spectral absorption coefficients of living phytoplankton and non algal biogenous matter: A comparison between the Peru upwelling area and the Sargasso Sea, Limnol. Oceanogr., 35, 69-75, 1990.

Broecker, W. S., Y-H Li, and T-H Peng. Carbon dioxide: Man's unseen artifact, in Impingement of Man on the Oceans, D. W. Hood [ed], Wiley Intersci., Hoboken, New York. 1971.

Bruland, K. W. and E. L. Rue, Analytical methods for determination of concentrations and speciation of iron, in The Biogeochemistry of Iron in Seawater, Chapter 6, edited by D. R. Turner and K. A. Hunter, John Wiley and Sons Ltd, 2001.

Caldeira, K. and P. B. Duffy. The role of the Southern Ocean in uptake and storage of anthropogenic carbon dioxide. Science. 287, 620-622, 2000.

Calderia, K., and M. E. Wickett. Anthropogenic carbon and ocean pH, Nature, 425, 365-365. 2003.

Calderia, K., and M. E. Wickett. Ocean model predictions of chemistry changes from carbon dioxide emissions to the atmosphere and ocean. J. Geophys. Res., 110, doi:10.1029/2004JC002671, 2005.

Calvin, M., and A. A. Benson, The path of carbon in photosynthesis, Science, 107, 476-480, 1948.

Carlson, C. A., D. A. Hansell, E. T. Peltzer and W. O. Smith, Stocks and dynamics of dissolved and particulate organic matter in the southern Ross Sea, Antarctica, Deep-Sea Res., Part II, 47, 3201-3225, 2000.

Caron, D.A., M.R. Dennett, D.J. Lonsdale, D.M. Moran, and L. Shalapyonok, Microzooplankton herbivory in the Ross Sea, Antarctica, during the U.S. JGOFS Program (October, 1996 - December, 1997). Deep Sea Res. Part II 47, 3249-3272, 2000.

Chisholm, S. W., P. G. Falkowski, and J. J. Cullen, Oceans - Dis-crediting ocean fertilization, Science, 294(5541), 309-310, 2001.

Coale, K. H., X. Wang, S. J. Tanner and K. S. Johnson, Phytoplankton growth and biological response to iron and zinc addition in the Ross Sea and Antarctic Circumpolar Current along 170°W, Deep-Sea Res., Part II, 50, 635-653, 2003.

Coale, K. H., et al., Southern Ocean iron enrichment experiment: carbon cycling in high- and low-Si waters. Science, 304, 408-414. 2004.

Coale, K. H., R. M. Gordon, and X. Wang,, The distribution and behavior of dissolved and particulate iron and zinc in the Ross Sea and Antarctic circumpolar current along 170°W, Deep Sea Res, Part I, 52, 295-318, 2005.

Conkright, M. E., S. Levitus, and T. P. Boyer, World Ocean Atlas 1994, Volume 1: Nutrients, in NOAA Atlas NESDIS 1, 150 pp., US Dep. Of Commer., Washington, D.C., 1994.

Conover, R. J., and M. Huntley. Copepods in ice-covered seas – Distribution, adaptations to seasonally limited food, metabolism, growth patterns and life cycle strategies in Polar seas. J. Mar. Sys., 2, 1-41, 1991.

Cota, G. F., W. O. Smith Jr., B. G. Mitchell. Photosynthesis of Phaeocystis in the Greenland Sea. Limnol. Oceanogr., 39, 948-953, 1994.

Croot, P. L., A. R. Bowie, R. D. Frew, M. T. Maldonado, J. A. Hall, K. A. Safi, J. La Roche, P. W. Boyd, and C. S. Law, Retention of dissolved iron and Fe(II) in an iron induced Southern Ocean phytoplankton bloom, Geophys. Res. Lett., 28, 3425-2428, 2001.

Croot, P. L., K. Andersson, M. Ozturk, and D. R. Turner, The distribution and speciation of iron along 6°E in the Southern Ocean, Deep Sea Res. Part II, 51, 2857-2879, 2004.

Croot, P. L., et al., Spatial and temporal distribution of Fe(II) and H2O2 during EisenEx, an open ocean mesoscale iron enrichment, Mar. Chem., 95, 65-88, 2005.

Davidson, A. T., D. Bramich, H. J. Marchant, and A. McMinn, Effects of UV-B irradiation on growth and survival of Antarctic marine diatoms, Mar. Biol., 119, 507-515, 1994.

DiTullio, G. R., and W. O. Smith. Jr. Relationship between Dimethylsulfide and Phytoplankton pigment concentrations in the Ross Sea, Antarctica. Deep-Sea Res. Pt. I. 42, 373-392, 1995.

DiTullio, G. R., and W. O. Smith. Jr. Spatial patterns in phytoplankton biomass and pigment distributions in the Ross Sea. J. Geophys. Res., **101**, 18467-18477, 1996.

DiTullio, G. R., J. Grebmeier, K. R. Arrigo, M. P. Lizotte, D. H. Robinson, A. Leventer, J. Barry, M. VanWoert, and R. B. Dunbar, Rapid and early export of Phaeocystis antarctica blooms in the Ross Sea, Antarctica, Nature, 404, 595-598, 2000.

Ducklow, H. W., M. L. Dickson, D. L. Kirchman, G. Steward, J. Orchardo, J. Marra, F. Azam, Constraining bacterial production, conversion efficiency and respiration in the Ross Sea, Antarctica, January-February, 1997. Deep Sea Res. Part II, 47, 3227-3247, 2000.

Dunbar, R. B., A. R. Leventer, and D. A. Mucciarone, Water column sediment fluxes in the Ross Sea, Antarctica: Atmospheric and sea ice forcing, J. Geophys. Res., 103, 30741-30759, 1998.

Dunbar, R. B., K. R. Arrigo, M. Lutz, G. D. DiTullio, A. R. Leventer, M. P. Lizotte, M. P. Van Woert, and D. H. Robinson, Non-Redfield production and export of marine organic matter: A recurrent part of the annual cycle in the Ross Sea, Antarctica, In Biogeochemistry of the Ross Sea, G. R. DiTullio and R. B. Dunbar (Eds.). Ant. Res. Ser., 78, 179-195, 2003.

Edwards, R., and P. N. Sedwick, Iron in East Antarctic snow: Implications for atmospheric iron deposition and algal production in Antarctic waters, Geophys. Res. Lett., 28, 3907-3910, 2001.

Elrod, V. A., W. M. Berelson, K. H. Coale, and K. S. Johnson, The flux of iron from continental shelf sediments: a missing source for global budgets, Geophys. Res. Lett., 31, 12307, 2004.

Emmenegger, L., R. Schonenberger, L. Sigg, and B. Schulzberger, , Light-induced redox cycling of iron in circumneutral lakes. Limnol. Oceanogr. 46, 49-61, 2001.

Eppley, R. W. Temperature and phytoplankton growth in the sea. Fishery Bull., 70, 1063-1085. 1972

Fasham, M. J. R. Modeling the marine biota. p. 457-504. In M. Heimann [ed.], The Global Carbon cycle. Springer, 1993.

Favre-Bonvin, J., J. Bernillon, N. Salin, and N. Arpin, Biosynthesis of mycosporines: mycosporine glutaminol in *Trichothecium roseum*, Photochemistry, 29, 2509-2514, 1987.

Foxton, P. The distribution of the standing stock of zooplankton in the Southern Ocean. Discovery Rep., 34, 1-116, 1956.

Fiztwater, S. E., K.S. Johnson, R. M. Gordon, K. H. Coale, and W.O. Smith, Trace metal concentrations in the Ross Sea and their relationship with nutrients and phytoplankton growth, Deep-Sea Res., Part II, 47, 3159-3179, 2000.

Fransz, H. G., and S. R. Gonzalez. Latitudinal metazoan plankton zones in the Antarctic Circumpolar current along 6°W during austral spring 1992. Deep-Sea Res. Pt. II. 44, 395-414, 1997.

Garcia-Pichel, F., A model for internal self shading in planktonic organisms and its implications for the usefulness of ultraviolet sunscreens, Limnol. Oceanogr., 39, 1704-1717, 1994.

Geider, R. J. 1999. Complex lessons of iron uptake. Nature. 400, 815-816.

Gervais, F., U. Riebesell, and M. Y. Gorbunov, Changes in primary productivity and chlorophyll a in response too iron fertilization in the Southern Polar Frontal Zone, Limnol. Oceangr., 47, 1324-1335, 2002.

Goffart A., G. Catalano, J. H. Hecq. Factors controlling the distribution of diatoms and Phaeocystis in the Ross Sea. J. Mar. Sys., 27, 161-175, 2000.

Gordon, L. I., L. A. Codispoti, J. C. Jennings Jr., F. J. Millero, J. M. Morrison and C. Sweeney, Seasonal evolution of hydrographic properties in the Ross Sea, Antarctica, 1996-1997. Deep-Sea Res., Part II, 47, 3095-3117, 2000.

Gowing, M. M., D. L. Garrison, H. B. Kunze, C. J. Winchell. Biological components of Ross Sea short-term particle fluxes in the austral summer of 1995-1996. Deep-Sea Res. Pt. I 48, 2645-2671, 2001.

Green, S. E., and R. N. Sambrotto, Phytoplankton community composition and nitrogen and carbon uptake rates off George V coastline, Antarctica, Eos. Trans. AGU, 83(4), Ocean Sciences Meeting Suppl. Abstract OS11L-12.7, 2002.

Grotti, M. F. Soggia, M. L. Abelmoschi, P. Rivaro, E. Magi, and R. Frache, Temporal distribution of trace metals in Antarctic coastal waters, Mar. Chem., 76, 189-209, 2001.

Hamm, C. E. Architecture, ecology and biogeochemistry of Phaeocystis colonies. J. Sea. Res., 43, 307-315, 2000.

Hamm, C. E., M. Reigstad, C. W. Riser, A. Mühlebach, and P. Wassmann. On the trophic fate of Phaeocystis pouchetii. VII. Sterols and fatty acids reveal sedimentation of P. pouchetii derived organic matter via krill fecal strings. Mar. Ecol. Prog. Ser.. 209, 55-69, 2001.

Hansen, B., P. Verity, T. Falkenhaug, K. S. Tande, and F. Norrbin. On the trophic fate of Phaeocystis pouchetii (Hariot). V. Trophic relationships between Phaeocystis and zooplankton: an assessment of methods and size dependence. J. Plankton. Res., 16, 487-511, 1994.

Harrison, P. J., P. W. Boyd, D. E. Varela, and S. Takeda. Comparison of factors controlling phytoplankton productivity in the NE and NW subarctic Pacific. Prog. Oceanogr., 43, 205-234. 1999.

Hart, T., On the phytoplankton of the South-West Atlantic and the Bellinghausen Sea, 1929–31. Discovery Reports, 8, 1–268, 1934.

Haslam, E. Shikimic acid: Metabolism and metabolites, New York, 387pp, 1993.

Hecq, J. H., L. Guglielmo, A. Goffart, G. Catalano, and H. Goosse. A modeling approach to the Ross Sea Plankton Ecosystem. p. 395-411. In F. M. Faranda, L. Guglielmo and A. Ianora [eds.], Ross Sea Ecology. Springer, 2000.

Hedges, J. I., J. A. Baldock, Y. Gelinas, C. Lee, M. L. Peterson, S. G. Wakeham, The biochemical and elemental compositions of marine plankton: A NMR perspective, Mar. Chem., 78, 47-63, 2002.

Hilst, C. M., van., and W. O. Smith. Jr. Photosynthesis/irradiance relationships in the Ross Sea, Antarctica, and their control by phytoplankton assemblage composition and environmental factors. Mar. Ecol. Prog. Ser., 226, 1-12, 2002.

Holling, C. S. Some characteristics of simple types of predation and parasitism. Can. Ent., 91, 385-398, 1959.

Holm-Hansen, O. and B. G. Mitchell. Spatial and temporal distribution of phytoplankton and primary production in the western Bransfield Strait region. Deep-Sea Res. 38, 961-980, 1991.

Hopkins, T. L., T. M. Landcraft, J. J. Torres, and J. Donnelly, Community structure and trophic ecology of zooplankton in the Scotia Sea marginal ice zone in winter (1988), Deep Sea Res. Part I, 40, 81-105, 1993.

Hudson, R. J. M., D. T. Covault, and F. M. M. Morel, Investigations of iron coordination and redox reactions in seawater using Fe-59 radiometry and ion-pair solvent extraction of amphiphilic iron complexes, Mar. Chem., 38, 209-235, 1992.

Huntley, M., K. S. Tande, and H. C. Eilertsen. On the trophic fate of Phaeocystis pouchetii (Hariot). II. Grazing rates of Calanus hyperboreus (Kroyer) on diatoms and different sized categories of P. pouchetii. J. Exp. Mar. Biol. Ecol., 110, 197-212, 1987.

Huntley, M. and M. Zhou. US JGOFS Data System: Southern Ocean Zooplankton displacement volumes from MOCNESS tows. U.S. JGOFS. iPub: July 2000. http://usjgofs.whoi.edu/jg/serv/jgofs/southern/nbp96_4A/dv_mocness.html0, and http://usjgofs.whoi.edu/jg/serv/jgofs/southern/nbp97_1/dv_mocness.html0

Hutchins, D. A., W-X. Wang, and N. S. Fisher, Copepod grazing and the biogeochemical fate of iron, Limnol. Oceangr., 40, 989-994, 1995.

Hutchins, D. A., A. E. Witter, A. Butler, and G. W. Luther III, 1999, Competition among marine phytoplankton for different chelated iron species, Nature, 400, 858-861.

IPCC., Climate Change 2001, The Scientific Basis, 2001.

Jacobs, S. S. and C. F. Giulivi, 1999, Thermocline data and ocean circulation on the Ross Sea continental shelf, In Oceanography of the Ross Sea, Antarctica. G. Spezie and G. M. R. Manzella (eds). Springer-Verlag.

Jacobs, S. S., C. F. Giulivi, and P. A. Mele, Freshening of the Ross Sea during the late 20th century, Science, 297, 386-389, 2002.

Johnson, G., O. Samset, L. Granskog, and E. Satshaug, In vivo absorption characteristics of 10 classes of bloom forming phytoplankton: Taxonomic characteristics and responses to photoadaptation by means of discriminant and HPLL analysis, Mar. Ecol. Prog. Ser., 105, 149-157, 1994.

Johnson, K. S., K. H. Coale, V. A. Elrod, and N. W. Tindale, Iron photochemistry in seawater from the equatorial Pacific, Mar. Chem., 46, 319-334, 1994.

Johnson, K. S., R. M. Gordon, and K. H. Coale, What controls dissolved iron concentrations in the world ocean? Mar. Chem., 57, 137-161, 1997.

Kang, S. H., and S. H. Lee, Antarctic phytoplankton assemblage in the western Bransfield Strait region, Mar. Ecol. Prog. Ser., 129, 253-267, 1995.

Kang, S. H., J. S. Kang, S. H. Lee, K. H. Chung, D. Kim, and M. G. Park, Antarctic phytoplankton assemblages in the marginal ice zone of the northwestern Weddell Sea, J. Plankt. Res., 23, 353-352. 2001.

Kalnay, E., et al., The NCEP/NCAR 40-year reanalysis project, Bull. Am. Meteorol. Soc., 77, 437-471, 1996.

Karentz, D., F. S. McEuen, M. C. Land, and W. C. Dunlap, Survey of mycosporine-like amino acid compounds in Antarctic marine organisms: potential for protection from ultraviolet exposure, Mar. Biol., 108, 157-166, 1991.

Kishino, M., M. Takahashi, N. Okami, and S. Ichimura, Estimation of the spectral absorption coefficients of phytoplankton in the sea, Bull. Mar. Sci., 37, 634-642, 1985.

Kirk, J. T. O., Light and photosynthesis in aquatic ecosystems, 2nd edition, Cambridge, 509pp, 1994.

Knox, G. A. Zooplankton. p. 67-80. In G. A. Knox [ed.], The Biology of the Southern Ocean. Cambridge University Press, Cambridge, 1994.

Lancelot, C. and V. Rousseau. Ecology of Phaeocystis ecosystems: the key role of colony forms. In Green, J. and B. S. C. Leadbeter [eds]. The haptophyte algae. Clarendon Press. Oxford, 1994.

Lancelot, C., E. Hannon, S. Becquevort, C. Veth, H. J. W. De Baar. Modeling phytoplankton blooms and carbon export production in the Southern Ocean: dominant controls by light and iron in the Atlantic sector in Austral spring 1992. Deep-Sea Res. Pt. I. **47**, 1621-1662, 2000.

Landry, M. R., et al. Iron and grazing constraints on primary production in the central equatorial Pacific: An EqPac synthesis. Limnol. Oceanogr. 42, 405-418. 1997.

Lebour, M. V. The food of planktonic organisms. J. Mar. Bio. Assoc. U.K. 12, 644-677, 1922.

Le Quere, C., et al., Two decades of ocean CO2 sink and variability, Tellus, Ser. B, 55, 649-656. 2003.

Liss, P. S., and L. Mervilat, Air-sea gas exchange rates: Introduction and synthesis, in: The role of air-sea exchange in geochemical cycling, pp. 113-145, 1986.

Liss, P. S., G. Malin, S. M. Turner, and P. M. Holligan. Dimethyl sulphide and Phaeocystis: A review. J. Mar. Sys., 5, 41-53, 1994.

Longhurst, A., S. Sathyendranath, T. Platt, and C. Caverhill, An estimate of global primary production in the ocean from satellite radiometer data, J. Plankton Res., 17, 1245-1271. 1995.

Maldonado, M. T., P. W. Boyd, P. J. Harrison, and N. M. Price. Co-limitation of phytoplankton growth by light and Fe during winder in the NE subarctic Pacific Ocean. Deep-Sea Res. Pt. II. 46, 2475-2485, 1999.

Maldonado, M. T. and N. M. Price, Utilization of iron bound to strong organic ligands by plankton communities in the subarctic Pacific Ocean. Deep Sea Res. Part II, 46, 2447-2473, 1999.

Maldonado, M. T., R. F. Strzepek, S. Sander, and P. W. Boyd., Acquisition of iron bound to strong organic complexes, with different Fe binding groups and photochemical reactivities, by plankton communities in Fe-limited subantarctic waters. Global Biogeochem. Cy. 19, GB4S23, 2005.

Maldonado, M. T., A. E. Allen, J. C. Chong, K. Lin, D. Leus, N. Karpenko, and S. Harris. Copper dependent iron transport in coastal and oceanic diatoms. Limnol. Oceanogr., in press. 2006.

Marchant, H. J., A. T. Davidson, and G. J. Kelly, UV-B protecting compounds in the marine alga *Phaeocystis pouchetii* from Antarctica, Mar. Biol., 109, 391-395, 1991.

Markels, M. J., and R. T. Barber, The sequestration of carbon to the deep ocean by fertilization, ACS Symposium on CO2 Capture, Utilization, and Sequestration., 2000.

Martin, J. H., Glacial-Interglacial CO2 Change: the iron hypothesis, Paleoceanography, 5, 1-13, 1990.

Martin, J. H., S. E. Fitzwater, and R. M. Gordon, Iron deficiency limits plankton growth in Antarctic waters, Global Biogeochem. Cycles, 4, 5-12, 1990.

Martinez, J. S., M. G. Haygood, and A. Butler, Identification of a natural desferroxamine siderophore produced by a marine bacterium, Limnol. Oceangr., 46, 420-424, 2001.

McCormack, P., P. J. Worsfold, and M. Gledhill, Separation and detection of siderophores produced by marine bacterioplankton using high-performance liquid chromatography with electrospray ionization mass spectrometry, Anal. Chem., 75, 2647-2652, 2003.

Mellor, G. L., and T. Yamada, Development of a turbulence closure model for geophysical fluid problems, Rev. Geophys., 20, 851-875, 1982.

Millero, F. J., S. Sotolongo, and M. Izaguirre, The oxidation kinetics of Fe(II) in seawater, Geochim. Cosmochim. Acta, 51, 793-801, 1987.

Millero, F. J., K. Lee, and M. Roche. Distribution of alkalinity in the surface waters of the major oceans. Mar. Chem.. 60, 111-130. 1998.

Miller, W. L., D. Whitney King, J. Lin, and D. R. Kester, Photochemical redox cycing of iron in coastal seawater, Mar. Chem. 50, 63-77, 1995.

Mitchell, B. G., and D. A. Kiefer, Variability in the pigment specific fluorescence and absorption spectra in the northeastern Pacific Ocean, Deep Sea Res. Part I., 35, 665-689, 1988.

Moisan, T. A., and B. G. Mitchell. Photophysiological acclimation of Phaeocystis antarctica (Karsten) under light limitation. Limnol. Oceanogr., 44, 247-258, 1999.

Moisan, T. A., and B. G. Mitchell, UV absorption by mycosporine-like amino acids in *Phaeocystis antarctica* Karsten induced by photosynthetically available radiation, Mar. Biol., 138, 217-227, 2001.

Moore, J. K., and M. R. Abbott. Phytoplankton chlorophyll distributions and primary production in the Southern Ocean, J. Geophys. Res., 105, 28709-28722. 2000.

Moore, J. K., M. R. Abbott, J. G. Rochman, and D. M. Nelson. The Southern Ocean at the last glacial maximum: A strong sink for atmospheric carbon dioxide. Global Biogeochem. Cy., 14, 455-475, 2000.

Moore, J. K., S. C. Doney, J. A. Kleypas, D. M. Glover, and I. Y. Fung, An intermediate complexity marine ecosystem model for the global domain, Deep-Sea Res., Part II, 49, 406-462, 2002.

Monod, J., Recherches sur la croissance des cultures bacteriennes, 210pp., Herman, Paris, 1942.

Morel, A., and A. Bricaud, Theoretical results concerning light absorption in a discrete medium, and application to the specific absorption of phytoplankton, Deep Sea Res., Part I., 28, 1375-1393, 1981.

Morel, F. M. M. and N. M. Price, The biogeochemical cycles of trace metals in the oceans, Science, 300, 944-947, 2003.

Najjar, R. G. and J. C. Orr, Biotic-HOWTO. Internal OCMIP Report, LSCE/CEA Saclay, Gif-sur-Yvette, France, 15 pp., http://www.ipsl.jussieu.fr/OCMIP, 1999.

Nelson, D. M., D. J. DeMaster, R. B. Dunbar, W. O. Smith, Jr., Cycling of organic carbon and biogenic silica in the Southern Ocean: Estimates of water column and sedimentary fluxes on the Ross Sea continental shelf, J. Geophys. Res., 101, 18,519-18,532, 1996.

Nolting, R. F., L. J. A. Gerringa, M. J. W. Swagerman, K. R. Timmermans, and H. J. W. de Baar, Fe(III) speciation in the high nutrient, low chlorophyll Pacific region of the Southern Ocean, Mar. Chem., 62, 335-352, 1998.

O'Reilly, J. E., S. Maritorena, B. G. Mitchell, D. A. Siegal, K. L. Carder, S. A. Garver, M. Kahru, and C. McClain, Ocean color chlorophyll algorithms for SeaWiFS, J. Geophys Res., 103, 24937-24953, 1998.

Orr, J. C., et al., Estimates of anthropogenic carbon uptake from four three-dimensional global ocean models, Global Biogeochem. Cycles. 15, 43-60, 2001.

Peng, T-H. and W. S. Broecker, Factors limiting the reduction of atmospheric CO2 by iron fertilization, Limnol. Oceanogr., 36, 1919-1927, 1991.

Petit, J.R., et al., Climate and atmospheric history of the past 420000 years from the Vostok ice core, Antarctica, Nature, 399, 429-36. 1999.

Pitchford, J. W., and J. Brindley. Iron limitation, grazing pressure and oceanic high nutrient-low chlorophyll (HNLC) regions. J. Plankton Res., 21, 525-547, 1999.

Pondaven, P., D. Ruiz-Pino, J. N. Druon, C. Fravalo, P. Tréguer. Factors controlling silicon and nitrogen biogeochemical cycles in high nutrient, low chlorophyll systems (the Southern Ocean and the North Pacific): Comparison with a mesotrophic system (the North Atlantic). Deep-Sea Res. I. 46, 1923-1968, 1999.

Poorvin, L., J. M. Rinta-Kanto, D. A. Hutchins, and S. W. Wilhelm,, Viral release of iron and it's bioavailability to marine phytoplankton, Limnol. Oceanogr., 49, 1734-1741, 2004.

Price, N. M., G. I. Harrison, J. G. Hering, R. J. Hudson, P. M. V. Nirel, B. Palenik, and F. M. M. Morel, Preparation and chemistry of the artificial algal culture medium Aquil, Bio. Oceanogr., 6, 443-461, 1988/1989.

Raven, J. A., A cost-benefit analysis of photon absorption by photosynthetic unicells, New. Phytol., 98, 593-625, 1984.

Raven, J. A., The iron and molybdenum use efficiencies of plant growth with different energy, carbon and nitrogen sources, New Phytol., 109, 279-287, 1988.

Raven, J. A., Predictions of Mn and Fe use efficiencies of phototrophic growth as a function of light availability for growth and of C assimilation pathway, New. Phytol., 116, 1-18, 1990.

Raven, J. A., Responses of aquatic photosynthetic organisms to increased solar UVB, J. Photochem. Photobiol. B., 9, 239-244, 1991.

Redfield, A. C., On the proportions of organic derivations in sea water and their relation to the composition of plankton, James Johnston Memorial Volume, pp. 176-192, Liverpool, 1934.

Redfield, A., B. Ketchum, and F. Richards. P. 224-228. In N. Hill [ed.], The Sea, volume 2. Interscience. New York, 1963.

Reynolds, R. A., D. Stramski, and B. G. Mitchell, A chlorophyll-dependent semianalytical reflectance model derived from field measurements of absorption and backscattering coefficients within the Southern Ocean, J. Geophys. Res., 106, 7125-7138, 2001.

Riegger, L., and D. H. Robinson, Photoinduction of UV-absorbing compounds in Antarctic diatoms and *Phaeocystis antarctica*, Mar. Ecol. Prog. Ser., 160, 13-25, 1997.

Rijkenberg, M. J. A., A. C. Fisher, J. J. Kroon, L. J. A. Gerringa, K. R. Timmermans, H. Th. Wolterbeek, and H. J. W. de Baar, The infuence of UV irradiation on the photoreduction of iron in the Southern Ocean, Mar. Chem., 93, 119-129, 2005.

Robinson, C. S., D. Archer, and P. J. L. Williams, Microbial dynamics in coastal waters of East Antarctica: plankton production and respiration, Mar. Ecol. Prog. Ser., 180, 23-36, 1999.

Robinson, D. H., K. R. Arrigo, M. P. Lizotte. Evaluating phytoplankton productivity in waters dominated by Phaeocystis antarctica. In Biogeochemical Cycles in the Ross Sea, G. R. DiTullio and R. B. Dunbar (Eds.). Antarctic Research Series 2003.

Ross, J. C. Sir, A voyage of discovery and research in the southern and Antarctic regions, during the years 1839-1843, J Murray, London, 1847.

Rousseau, V., D. Vaulot, R. Casotti, V. Cariou, J. Lenz, J. Gunkel, and M. Baumann. The life cycle of *Phaeocystis* (Prymnesiphyceae): evidence and hypotheses, J. Mar. Sys., 5, 23-39, 1994.

Ruben, S, M. D. Kamen, W. Z. Hassin, and D. C. DeVault, Photosynthesis with radiocarbon, Science, 90, 570-571, 1939.

Rue, E. L. and K. W. Bruland, The role of organic complexation on ambient iron chemistry in the equatorial Pacific Ocean and the response of a mesoscale iron addition experiment, Limnol. Oceanogr., 42, 901-910, 1997.

Ryther, J. H. Photosynthesis in the Ocean as a function of light intensity. Limnol. Oceanogr., 1, 61-70. 1956.

Sabine, C. L., et al., The Oceanic Sink for Anthropogenic CO2, Science, 305, 362-6. 2004.

Sarmiento, J. L., J. R. Toggweiler, and R. Najjar, Ocean Carbon-Cycle dynamics and atmospheric pCO2, Phil. Trans. Royal. Soc. A., 325, 3-21. 1988.

Sarmiento, J. L. and J. C. Orr, Three-dimensional simulations of the impact of Southern Ocean nutrient depletion on atmospheric CO2 and ocean chemistry, Limnol. Oceanogr., 36, 1928-1950, 1991.

Sarmiento, J. L., T. M. C. Hughes, R. J. Stouffer, and S. Manabe, Simulated response of the ocean carbon cycle to anthropogenic carbon warming, Nature, 393, 245-249, 1998.

Sarmiento, J. L., N. Gruber, M. A. Brzezinski, and J. P. Dunne, High latitude control of thermocline nutrients and low latitude productivity, Nature, 427, 56-60, 2004.

Sarthou, G., C. Jeandel, L. Brisset, D. Amouroux, T. Besson, and O. F. X. Donard. Fe and H2O2 distributions in the upper water column in the Indian sector of the Southern Ocean. Earth. Plan. Sci. Lett., 147, 83-92. 1997.

Sathyendranath, S., L. Lazzara, and L. Prieur, Variations in the spectral values of specific absorption of phytoplankton, Limnol. Oceanogr., 32, 403-415, 1987.

Schmidt, M. A., Y. H. Zhang, and D. A. Hutchins, Assimilation of Fe and carbon by marine copepods from Fe-limited and Fe-replete diatom prey. J. Plankt. Res. 21, 1753-1764, 1999.

Sedwick, P. N. and G. R. DiTullio, Regulation of algal blooms in Antarctic shelf waters by the release of iron from melting sea ice, Geophys. Res. Lett., 24, 2515-2518, 1997.

Sedwick, P. N., G. R. DiTullio, D. J. Mackey, Iron and manganese in the Ross Sea, Antarctica: Seasonal iron limitation in Antarctic shelf waters, J. Geophys. Res., 105, 11321-11336, 2000.

Shaked, Y., A. B. Kustka, and F. M. M. Morel, A general kinetic model for iron acquisition by eukaryotic phytoplankton, Limnol. Oceanogr., 50, 872-882, 2005.

Shick, J. M., S. Romaine-Lioud, C. Ferrier-Pages, and J-P. Gattuso, Ultraviolet –B radiation stimultates shikimate pathway dependent accumulation of mycosporine-like amino acids in the coral *Stylophora pistilla* despite decreases in its population of symbiotic dinoflagellates, Limnol. Oceanogr., 44, 1667-1682, 1999.

Shick, J. M., and W. C. Dunlap, Mycosporine-like amino acids and related gradusols: Biosynthesis, accumulation and UV-protective functions in aquatic organisms, Ann. Rev. Physiol., 64, 223-262, 2002.

Smith Jr., W. O. and D. M. Nelson, Importance of ice-edge phytoplankton production in the Southern Ocean, BioScience, 36, 251-256, 1986.

Smith, W. O., Jr. and L. I. Gordon, Hyperproductivity of the Ross Sea (Antarctica) Polynya during austral spring, Geophys. Res. Lett., 24, 233-236, 1997.

Smith, W. O., J. Marra, M. R. Hiscock, and R. T. Barber, The seasonal cycle of phytoplankton biomass and primary productivity in the Ross Sea, Antarctica, Deep-Sea Res., Part II, 47, 3119-3140, 2000.

Soria-Dengg, S. and U. Horstmann, Ferrioxamines B and E as iron sources for the marine diatom Phaeodactylum tricornutum, Mar. Ecol. Prog. Ser., 127, 269-277, 1995.

Strom, S. L., M. A. Brainard, J. L. Holmes, and M. B. Olson, Phytoplankton blooms are strongly impacted by microzooplankton grazing in coastal North Pacific waters. Mar Bio., 138, 355-368, 2001.

Stuart, V., S. Sathyendranath, E. J. H. Head, T. Platt, B. Irwin and H. Maas, Bio-optical characteristics of diatom and prymnesiophytes populations in the Labrador Sea. Mar. Ecol. Prog. Ser., 201, 91-106, 2001.

Sullivan, C. W., K. R. Arrigo, C. R. McClain, J. C. Comiso, and J. Firestone, Distributions of phytoplankton blooms in the Southern Ocean, Science, 262, 1832-1837, 1993.

Sunda, W. G., What controls dissolved iron concentrations in the world ocean: A comment, Mar. Chem., 57, 169-172, 1997.

Sunda, W. G., and S. A. Huntsman, Iron uptake and growth limitation in oceanic and coastal phytoplankton, Mar. Chem., 50, 189-206, 1995.

Sunda, W. G., and S. A. Huntsman, Interrelated influence of iron, light and cell size on marine phytoplankton growth, Nature, 390, 389-392, 1997.

Sverdrup, H. U. On the conditions for the vertical blooming of phytoplankton. J. Cons. Cons. Int. Explor. Mer. 18, 287-295, 1953.

Sweeney, C., W. O. Smith, B. Hales, R. B. Bidigare, C. A. Carlson, L. A. Codispoti, L. I. Gordon, D. A. Hansell, F. J. Millero, M-O Park, and T. Takahashi, Nutrient and carbon removal ratios and fluxes in the Ross Sea, Antarctica, Deep-Sea Res., Part II, 47, 3395-3422, 2000a.

Sweeney, C., D. A. Hansell, C. A. Carlson, L. A. Codispoti, L. I. Gordon, J. Marra, F.J. Millero, W.O. Smith and T. Takahashi, Biogeochemical regimes, net community production and carbon export in the Ross Sea, Antarctica, Deep-Sea Res., Part II, 47, 3369-3394, 2000b.

Sweeney, C., The annual cycle of surface water CO2 and O2 in the Ross Sea: A model for gas exchange on the continental shelves of Antarctica, in Biogeochemistry of the Ross Sea, R. Dunbar and G. Di Tullio (Eds), Ant. Res. Ser., 78, 295-312, 2003.

Tagliabue, A., and K. R. Arrigo, Anomalously low zooplankton abundance in the Ross Sea: An alternative explanation, Limnol. Oceanogr., 48, 686-699, 2003.

Tagliabue, A., and K. R. Arrigo, Iron in the Ross Sea: 1. Impact of CO_2 fluxes via variation in phytoplankton functional group and non-Redfield stoichiometry, J. Geophys. Res., 110, C03009. doi:10.1029/2004JC002531, 2005.

Tagliabue, A., and K. R. Arrigo, Processes governing the supply of iron to phytoplankton in stratified seas, J. Geophys. Res., 111, doi:10.1029/2005JC003363, 2006.

Takahashi, T., S. C. Sutherland, C. Sweeney, A. Poisson, N. Metzl, B. Tilbrook, N. Bates, R. Wanninkhof, R. A. Feely, C. Sabine, et al., Global sea-air CO2 flux based on climatological surface ocean pCO2, and seasonal biological and temperature effects, Deep-Sea Res., Part II, 49, 1601-1622, 2002.

Takeda, S. Influence of iron availability on nutrient consumption ratio of diatoms in oceanic waters. Nature, 393, 774-777. 1998.

Timmermans, K. R., L. J. A. Gerringa, H. J. W. de Baar, B. van der Wagt, M. J. W. Veldhuis, J. T. M. de Jong, and P. L. Croot. Growth rates of larger and small Southern Ocean diatoms in relation to the availability of iron in natural seawater. Limnol. Oceanogr., 46, 260-266. 2001.

Timmermans, K. R., B. van der Wagt, and H. J. W. de Baar. Growth rates, half saturation constants, and silicate, nitrate, and phosphate depletion in relation to iron availability of four large, open ocean diatoms from the Southern Ocean. Limnol. Oceanogr., 49, 2141-2151. 2004

Toggweiler, J. R., Variation of atmospheric CO_2 by ventilation of the ocean's deepest water, Paleoceanography, 14, 571-588, 1999.

Tsuda, A. *et al.* A mesoscale iron enrichment in the western subarctic Pacific induces a large centric diatom bloom. Science, 300, 958-961. 2003.

Turner, J. T., and P. A. Tester. Toxic marine phytoplankton, zooplankton grazers, and pelagic food webs. Limnol. Oceanogr., 42, 1203-1214, 1997.

Twining, B. S., S. B. Baines, N. S. Fisher, and M. R. Landry, Fe;C ratios within the plankton community during the Southern Ocean Iron Experiment (SOFeX), Eos. Trans. AGU, 82(47) Fall Meeting Suppl., Abstract OS11A-0205, 2002.

Tyrrell, T., The relative influences of nitrogen and phosphorous on oceanic primary production, Nature, 400, 525-538, 1999.

Verity. P. G. Grazing experiments and model simulations of the role of zooplankton in Phaeocystis food webs. J. Sea. Res., 43, 317-343, 2000.

Wanninkhof, R., Relationship between wind-speed and gas-exchange over the ocean, J. Geophys. Res., 97, 7373-7382, 1992.

Ward, P., A. Atkinson, A. W. A. Murray, A. G. Wood, R. Williams, and S. A. Poulet. The summer zooplankton community at South Georgia: biomass, vertical migration and grazing. Polar Biol., 15, 195-208, 1995.

Watson, A.J ., D. C. E. Bakker, A. J. Ridgwell, P. W. Boyd, and C. S. Law, Effect of iron supply on Southern Ocean CO2 uptake and implications for glacial atmospheric CO_2, Nature, 407, 730-733, 2000.

Weber, L., C. Voelker, M. Schartau, and D. A. Wolf-Gladrow, Modeling the speciation and biogeochemistry of iron at the Bermuda Atlantic Time-series study site, Global Biogeochem., Cy., 19, GB1019, 2005.

Weiss, R. F. and B. A. Price, Nitrous Oxide solubility in water and seawater, Mar. Chem., 8, 347-359, 1980.

Wells, M. L., N. M. Price, and K. W. Bruland, Iron chemistry in seawater and its relationship to phytoplankton: a workshop report, Mar. Chem., 48, 157-182, 1995.

Wilhelm, S. T. and C. G. Trick, Iron-limted growth of cyanobacteria: Multiple siderophore production is a common response, Limnol. Oceangr., 39, 1979-1984, 1994.

Witter, A. E. and G. W. Luther III, Variation in Fe-organic complexation with depth in the Northwestern Atlantic Ocean as determined using a kinetic approach. Mar. Chem., 62, 241-258., 1998.

Witter, A. E., D. A. Hutchins, A. Butler, and G. W. Luther III, Determination of conditional stability constants and kinetic constants for strong model Fe-binding ligands in seawater, Mar. Chem., 69, 1-17, 2000.

Worthen, D. L., and K. R. Arrigo, A coupled ocean-ecosystem model of the Ross Sea. Part 1: Interannual variability of primary production and phytoplankton community structure, In Biogeochemistry of the Ross Sea, G. R. DiTullio and R. B. Dunbar (Eds.), Ant. Res. Ser., 78, 93-106, 2003.

Wright, S. W., D. P. Thomas, H. J. Marchant, H. W. Higgins, M. D. Mackay, and D. J. Mackay, Analysis of phytoplankton of the Australian sector of the Southern Ocean: Comparisons or microscopy and size frequency data with interpretations of pigment HPLC data using the CHEMTAX matrix fractionation program, Mar. Ecol. Prog. Ser., 144, 285-298, 1996.

Zwally, H. J., C. Parkinson, F. Carsley, P. Gloersen, W. J. Campbell, and R. O. Ramseier, Antarctic sea ice variations 1973-1975, in NASA Weather Clim. Rev. Pap., 56, 335-340, 1979.